Optimal Design of Microstrip Antennas and Arrays Using Differential Evolution Algorithm and Its Variants

Thesis submitted by

Arindam Deb

Doctor of Philosophy (Engineering)

Department of Electronics and Telecommunication Engineering
Faculty Council of Engineering and Technology
Jadavpur University
Kolkata, India

2016

JADAVPUR UNIVERSITY

KOLKATA – 700032, INDIA

INDEX NO. 125/11/E

1. TITLE OF THE THESIS:

Optimal Design of Microstrip Antennas and Arrays Using Differential Evolution Algorithm and Its Variants

2. NAME, DESIGNATION & INSTITUTION OF SUPERVISORS:

Dr. Bhaskar Gupta

Professor

Department of Electronics and Telecommunication Engineering

Jadavpur University, Kolkata – 700032, India

Dr. Jibendu Sekhar Roy

Professor

School of Electronics Engineering

KIIT University, Bhubaneswar – 751024, India

3. LIST OF PUBLICATIONS

List of Publications in National / International Journals

- **Arindam Deb**, J. S. Roy and B. Gupta, 'Performance Comparison of Differential Evolution, Particle Swarm Optimization and Genetic Algorithm in the Design of Circularly Polarized Microstrip Antennas', *IEEE Transactions on Antennas and Propagation* , vol. 62, no. 8, pp. 3920-3928, 2014.

- **Arindam Deb**, J. S. Roy and B. Gupta, 'Design of Short Circuited Microstrip Antenna Using Differential Evolution Algorithm', *Microwave Review*, vol.18, no.1. pp 7-10, 2012.

- **Arindam Deb**, J. S. Roy and B. Gupta ,'Design of Microstrip antennas Using Differential Evolution Algorithm', *International Journal of Information Systems and Communications*, vol. 1 , no. 1, pp 1-14,2011.

Paper accepted

- **Arindam Deb**, J. S. Roy and B. Gupta, 'Performance Comparison of Differential Evolution Variants and Hybrid Algorithms in the Design of Microstrip Antennas and Arrays', accepted by *IEEE Antennas and Propagation Magazine.*

4. List of Patents: Nil

5. List of Presentations in National / International Conferences/Workshops

- **Arindam Deb**, J.S. Roy and B. Gupta**,'** Design of Aperture Coupled Microstrip Antenna for WLAN using Differential Evolution Algorithm', *Proceedings of International Symposium on Microwave and Optical Technology (ISMOT) 2011*, Prague, Czech Republic.

- **Arindam Deb**, B. Gupta and J.S. Roy,**'** Performance Comparison of Differential Evolution, Genetic Algorithm and Particle Swarm Optimization in impedance matching of Aperture Coupled Microstrip Antennas', *IEEE proceedings of Mediterranean Microwave Symposium (MMS) 2011*, Hammemet, Tunisia.

- **Arindam Deb**, J.S. Roy and B. Gupta,' Design of Dual Frequency Microstrip Antenna using Differential Evolution algorithm', *IEEE Proceedings of International Symposium on Microwave, Antenna, Propagation and EMC Technologies for Wireless Communication (MAPE) 2011*, Beijing, China.

- **Arindam Deb**, J.S. Roy and B. Gupta,' Design of Probe Fed Microstrip Antenna using Differential Evolution algorithm', *IEEE Proceedings of International Symposium on Microwave, Antenna, Propagation and EMC Technologies for Wireless Communication (MAPE) 2011*, Beijing, China.

- **Arindam Deb**, J.S. Roy and B. Gupta ,' Design of Cross Slot coupled Microstrip Antenna using Self Adaptive Differential Evolution Algorithm', *IEEE Proceedings of Applied Electromagnetic Conference 2011*, Kolkata, India.

- **Arindam Deb**, B. Gupta and J.S.Roy,'Design of Thinned Antenna Arrays Using Particle Swarm Optimization with Differentially Perturbed Velocity', *IEEE Proceedings of International Conference on Communications, Devices and Intelligent Systems,28-29 December,2012*, Kolkata, India.

- **Arindam Deb**, J.S. Roy and B. Gupta,' Automated Design of Triple-Band Microstrip Slot Antenna using Real-Boolean Improved Differential Evolution Algorithm', *The Institution of Engineers (India) ,All India Seminar on 'Emerging Trends in Telecommunication',September, 2016*, Kolkata, India.

JADAVPUR UNIVERSITY
KOLKATA – 700032, INDIA

FACULTY OF ENGINEERING & TECHNOLOGY

CERTIFICATE FROM THE SUPERVISORS

This is to certify that the thesis entitled **"Optimal Design of Microstrip Antennas and Arrays using Differential Evolution Algorithm and its Variants"** submitted by **Shri Arindam Deb**, who got his name registered on 31.01.2011 for the award of **Ph.D. (Engg.)** degree of Jadavpur University is absolutely based upon his own work under the supervision of **Dr. Bhaskar Gupta**, Professor, Department of Electronics and Telecommunication Engineering, Jadavpur University and **Dr. Jibendu Sekhar Roy**, Professor, School of Electronics Engineering, KIIT University, Bhubaneswar, and that neither his thesis nor any part of the thesis has been submitted for any degree/diploma or any other academic award anywhere before.

Dr. Bhaskar Gupta
Professor
Dept. of Electronics
& Telecommunication Engineering
Jadavpur University
Kolkata – 700032, India

Dr. Jibendu Sekhar Roy
Professor
School of Electronics Engineering
KIIT University
Bhubaneswar – 751024
India

Acknowledgement

I would like to thank the Almighty for his blessings throughout my career. Without his blessings, it would not have been possible for me to reach so far in my education and professional career. I pray that his blessings remain with me for the rest of my life.

I am deeply indebted to my Ph D supervisor, Prof. Bhaskar Gupta (Department of Electronics and Telecommunication Engineering, Jadavpur University, Kolkata) for his guidance, valuable suggestions, and insights throughout my research tenure. He has taught me to keep an open mind and analytically or logically come up with explanations for my research outputs. He has helped me to explore intricate areas corresponding to my research and venture new avenues. I am also grateful to him for teaching me the art of technical writing, explicitly mentioning the contributions of my research and their significance.

I am also deeply indebted to my Ph D supervisor, Prof. Jibendu Sekhar Roy (School of Electronics Engineering, KIIT University, Bhubaneswar) for his time, valuable suggestions, guidance and inputs corresponding to my research from time to time. He has taught me to be methodical, organized and analytical in different phases of my research.

I am grateful to both my PhD supervisors for providing me mental support during the years of research. They have been a constant source of inspiration to me. They have taught me to be methodical and patient. Their moral and mental support all these years helped me complete my research and dissertation.

I would also like to thank my colleagues at the Microstrip Laboratory, Department of Electronics and Telecommunication Engineering, Jadavpur University namely Mr. Kaushik Patra, Mr. Buddhadev Pradhan, Mr. Ardhendu Kundu , Ms. Amrita Chakraborty, Mr. Sudipta Maity, Dr. Sayantan Dhar, Mr. Sharan Bassapa Belamgi, Dr. Rajendra Prasad Ghosh, Mr Suman Pradhan Ms. Rinki Ghoshal, Ms. Ayona Chakraborti and Mr. Nipun Roy for their support and help throughout my research work. I would like to specially thank Mr. Kaushik Patra for his much needed help in doing fabrication and measurements at the Microstrip Antenna laboratory.

I express my sinceregratitude to my father, Sri. Deba Prosad Deb and mother, Smt. Mridula Deb for their blessings, encouragement, and understanding all these years. I express my heartfelt thanks to my wife, Smt. Debolina Deb for providing me with mental and moral support during

the days of my research after marriage. I also thank my father-in-law, Sri Debasish Brahma and mother-in-law, Smt. Saswati Brahma for their understanding and support as well. To conclude, I express my sincerest gratitude to all my friends, colleagues, relatives and seniors for their good wishes and blessings throughout my career.

Contents

Chapter 1

Introduction

Antenna engineering has emerged as a popular area of study among communication engineers in recent times. Proper design of an antenna to meet the requirements for a particular mode of communication, its shape and size to fit in the available area in the communication circuit or module is extremely important and crucial for antenna designers. Most of the antennas used in portable communication devices nowadays are microstrip antenna or their variants. Microstrip antenna consists of a metallic strip fabricated on a layer of dielectric supported on a ground plane. Microstrip antenna provides several advantages like conformability to planar and non planar surfaces, robustness and its ease of fabrication with different MICs or MMICs. However it also has several disadvantages in terms of narrow impedance bandwidth, low gain, low polarization purity and possible loss of power due to dielectric loss, conductor loss and surface wave losses. Although design equations are available for microstrip antennas having regular shapes, most of them are based on empirical formulas. It is often observed that an attempt to improve one aspect of the microstrip antenna may lead to deterioration in performance with respect to some other aspect. For example, an attempt to increase the impedance bandwidth of the microstrip antenna may lead to decrease in its broadside gain. Under such circumstances, optimization of microstrip antennas required for specific applications is necessary followed by its validation by fabrication and testing.

Optimization techniques can be broadly classified into gradient descent techniques and bio-inspired techniques. Gradient descent techniques are applicable only for well defined, differentiable, continuous functions and have low robustness compared to bio-inspired optimization techniques. Different bio-inspired optimization techniques have been proposed till date after observations based on Darwin's theory, search of food by ants and swarms etc. Some of the popular bio-inspired optimization techniques include genetic algorithm, particle swarm optimization and differential evolution algorithm. All these algorithms have been successfully applied for optimization of antennas in the past. Most of the optimization work carried out on microstrip antennas concentrated on optimizing the impedance properties of the antenna in the

initial days. However, all the present day designs include simultaneous and multi-objective optimizations concerning both impedance and pattern properties of the antenna. In addition, continuous attempts are being carried out to make the bio-inspired optimization techniques more robust and have improved statistical performance compared to their conventional versions.

Bio-inspired optimization techniques are natural choice for antenna design problems nowadays. However, all the bio-inspired optimization techniques are not equally applicable for all types of antenna optimizations problems, antenna geometries and feeding techniques. The research work presented in this thesis is on optimal design of microstrip antennas and arrays using differential evolution algorithm and its variants. The research work initially concentrated on three most popular optimization techniques namely real coded genetic algorithm, particle swarm optimization and differential evolution algorithm for the design of circularly polarized microstrip antennas with different feeding techniques, theoretical and practical array designs. The reason for choosing circularly polarized microstrip antenna is its ability to receive signal with any arbitrary polarization and the design problem includes multiple objectives to be satisfied at the same time. The design and optimization of circularly polarized microstrip antennas, theoretical and practical arrays are considered to be appropriate test bench problems for evaluating the statistical performance of the bio-inspired optimization algorithms. Once the algorithm with superior statistical performance is identified (the differential evolution algorithm), similar test bench problems are used to evaluate the advanced versions of the algorithm. Once the advanced version is identified, it will be used for practical design and optimization of multiband and circularly polarized microstrip antennas for wireless local area network and vehicular communication applications. The antennas thus designed using the best suited optimization algorithm are fabricated and experimental studies of their impedance and pattern characteristics are performed.

The organization of this thesis is as follows:

Chapter 1 is the introduction to the research work presented in the thesis with a brief overview of each chapter.

Chapter 2 is the literature review and survey conducted on origin and significant advances in the microstrip antenna technology during the course of the research work.

Chapter 3 is the literature review and survey conducted on development of bio-inspired optimization algorithms, their improved versions and application to antenna and array design problems during the course of the research work.

Chapter 4 gives the performance comparison of genetic algorithm, particle swarm optimization differential evolution algorithms and their improved versions in the design of circularly polarized microstrip antennas (with probe feed, transmission line feed and cross aperture coupled feed), linear array of unequally spaced elements and a 4-element Yagi-Uda antenna array. The optimization objectives for the circularly polarized microstrip antennas are to provide improved impedance matching within a predefined frequency range, minimize axial ratio and maximize the gain at the centre frequency. The optimally designed microstrip antennas are fabricated and measured results are presented along with the simulated data. The optimization objectives for the linear array of unequally spaced isotropic elements are the minimization of beam width between first nulls, minimization of maximum side lobe level and minimization of inter-element spacing between the elements to reduce the overall size of the array. Optimization of impedance properties is not carried out since isotropic antenna elements are considered. However both impedance and pattern properties are optimized in case of the 4-element Yagi-Uda antenna array. The optimization objectives in this case are to minimize the half power beam widths and side lobe levels for both E-plane and H-plane, and improve the voltage standing wave ratio at the design frequency. All the cost functions in these optimization case studies are adaptive in nature involving dynamic weights. Performance comparison of the algorithms considered in this chapter is done for the first time with such types of cost function in the domain of antenna and array design and optimization. Differential evolution algorithm showed very promising performance for the numerical antenna benchmark problems in this chapter. This study leads to the next chapter where applicability of more advanced and improved schemes of differential evolution (both adaptive and non adaptive) algorithms are studied with respect to similar antenna numerical benchmark problems.

Chapter 5 gives the performance comparison of the differential evolution variants and hybrid algorithms in the design of same circularly polarized microstrip antennas, linear array of unequally spaced isotropic antenna elements and 4-element Yagi-Uda antenna array as in chapter 4. Although same cost functions are used in case of the theoretical and practical arrays, the cost

functions are slightly modified in case of circularly polarized microstrip antennas. The optimization objectives for the circularly polarized microstrip antennas are to maximize the axial ratio bandwidth within a predefined frequency range, improving impedance matching within the axial ratio bandwidth and maximization of realized gain at the center frequency. The optimal microstrip antennas are fabricated and measured results are presented along with the simulated data. The relative performance of the algorithms varied for different optimization case studies. Some algorithms showed consistently good convergence rate and some others showed good exploration and exploitation of search space. Some algorithms failed to show strong robustness. Algorithms which exhibited robustness and fast convergence rate are subsequently used to design different microstrip antennas with compactness, dual band characteristics and circular polarization in both bands.

Chapter 6 provides the performance comparison of a novel self adaptive Real-Boolean differential evolution algorithm and non adaptive Real-Boolean differential evolution algorithm in the design of thinned antenna arrays. Boolean optimization algorithms are still in vogue with respect to thinned antenna arrays and automated pixel antenna geometry although interest in applying them seems to be dwindling. Since differential evolution algorithms had already shown promising performance with respect to antenna and array design problems in earlier chapters, an attempt has been made in this chapter to develop a novel self adaptive Real-Boolean differential evolution algorithm with dynamic population size. The statistical performance of this algorithm is compared with that of the existing non-adaptive Real-Boolean differential evolution algorithm with respect to numerical benchmark problems based on design of thinned antenna arrays using different optimization objectives and cost functions. Three types of thinned antenna array designs are considered involving linear thinned arrays with constant inter-element spacing, thinned planar arrays with constant inter-element spacing and thinned linear arrays with different inter-element spacing. In each of these design cases, two types of optimization objectives are used. In the first type, optimization of side lobe level is done. In the second type, the side lobe levels along with the number of active elements in the array and minimization of inter-element spacing are optimized. Care has been taken to ensure that the beam width of the designed array remains as close as possible to that of a fully filled array after satisfying the optimization objectives. For each type of optimization, two types of cost functions are formulated, one involving constant weights and the other involving dynamic and adaptive weights. The novel self

adaptive Real-Boolean differential evolution algorithm is seen to perform statistically better or at least at par with non-adaptive scheme with different numerical benchmark problems considered in this chapter. Hence this algorithm is used to design dual band automated antenna based on pixel geometry in the next chapter.

Chapter 7 provides several designs of microstrip antennas for WLAN and vehicular applications using suitable differential evolution algorithms based on the performances of the algorithms studied in the previous chapters. Six microstrip antennas are designed and optimized. Some of these antennas are fabricated; their measured results are presented along with the simulated data. Microstrip antenna 1 is a short circuited microstrip antenna designed to operate at the GPS L1 band. Microstrip antenna 2 is a probe fed dual band microstrip with corner truncations and parasitic loadings designed for vehicular applications. This antenna works at 1.575 GHz and 5.88 GHz and is applicable for GPS and Direct Short Range Communication (DSRC) between vehicles. It radiates right handed circularly polarized waves in the first band and linearly polarized waves at the second band. Microstrip antenna 3 is a slightly modified version of microstrip antenna 2 designed to operate at the same frequencies and radiate circularly polarized waves in both the bands. Microstrip antenna 4 is a probe fed dual band slotted microstrip antenna designed to operate at 2.45 GHz and 3.65 GHz with right handed circular polarization at both bands. Microstrip antenna 5 is a dual band grounded slot circularly polarized antenna based on pixel geometry designed to operate at 2.45 GHz and 5.15 GHz. Microstrip antenna 6 is a triple band linearly polarized grounded slot antenna based on pixel geometry designed to operate at 2.46 GHz, 3.65 GHz and 5.85 GHz. All these antennas are designed using appropriate differential evolution algorithm coded in MATLAB and coupled with Method of Moments based electromagnetic simulation software IE3D.

Chapter 8 concludes the thesis and summarizes the research work presented. Suggestions on further extension of the work presented in this thesis are also mentioned.

Chapter 2

Literature Review on Microstrip Antennas

2.1 Introduction

Wireless communication [1] has affected our lives in many ways. It is one of the most preferred means of communication nowadays because of low tariff rates, portability of mobile equipments, constant connectivity and high speed data transfer. It has found applications in different aspects of life including data communication, education, health care and entertainment. However, wireless communication would have not been possible without the formulation of Maxwell-Heaviside's equations, retarded potentials and subsequent invention of antennas.

Antenna is a transducer which can convert electric signal into electromagnetic signal. Initial demonstration and conceptualization of antennas is attributed to Dr. J. C. Bose and Dr. Henriech Hertz between 1880-1890. Since then, scientists and physicists have developed and studied different types of antennas till date. In earlier days, the most widely used antennas were the wire antennas and arrays[2] (quarter wave monopole antenna, half wave dipole antenna, turnstile antenna, V-antenna, rhombic antenna, loop antenna, helical antennas, Yagi-Uda antennas, log periodic dipole antenna arrays to name a few). In the era next to development of wire antennas, the technical community experienced development of aperture antennas [2] (horn antenna, dish antennas etc). Some of these antennas are shown below in Fig. 2.1, Fig. 2.2 and Fig. 2.3.

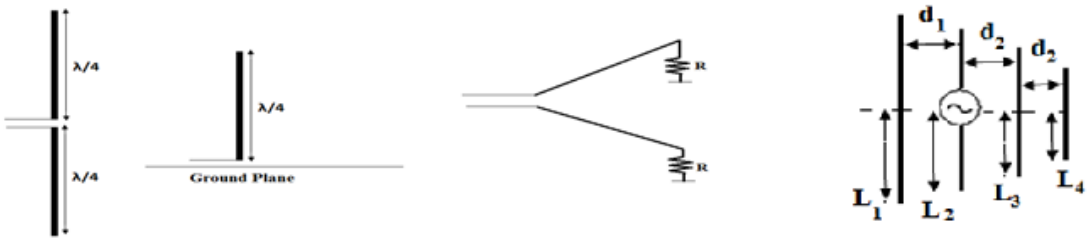

(a) (b) (c) (d)

Fig. 2.1 (a) Half-wave dipole antenna (b) Quarter wave monopole antenna (c) V-antenna (d) Yagi-Uda antenna

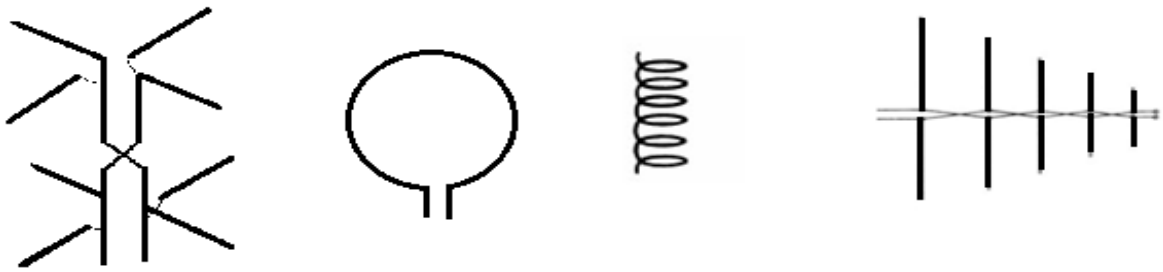

(a) (b) (c) (d)

Fig 2.2 (a) Turnstile antenna (b) Loop antenna (c) Helix antenna (d) Log-periodic dipole antenna array

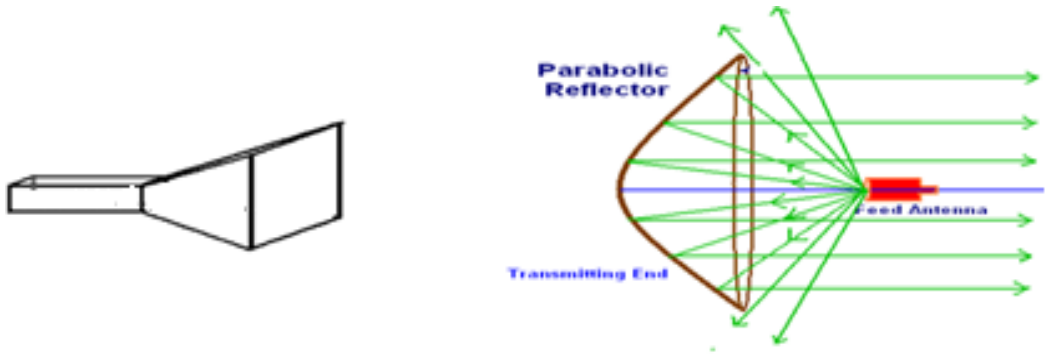

(a) (b)

Fig. 2.3 (a) Horn antenna (b) Parabolic reflector dish antenna

At the same time, there were big leaps in VLSI technology and subsequently in the domains of MIC and MMIC designs. Planar or microstrip antennas came into realization which could be easily integrated with MIC and MMIC boards and within available circuit area. The microstrip antenna [3] is a strip of metal placed above a layer of low loss dielectric supported at the back by a large ground plane as shown in Fig. 2.4. The microstrip antenna has several other advantages compared to conventional non-planar antennas available. It is robust, low cost, easy to fabricate and can operate at multiple frequency bands. This features made microstrip antenna very popular among antenna engineers which ensued in rapid advancement and development in microstrip antenna technology. However, the conventional microstrip antenna also has several disadvantages like narrow impedance bandwidth, low gain, poor polarization purity and possible loss of efficiency due to dielectric loss, copper loss and presence of surface waves.

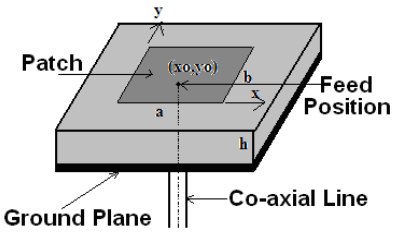

Fig 2.4 Probe fed circularly polarized microstrip antenna

Continuous efforts are being made by researchers around the world to overcome these disadvantages and make the microstrip antenna more suited for modern day wireless communication systems. A review on the history and advances made in the microstrip antenna technology is done to apprise the reader regarding its origin and applicability in recent times. This chapter is organized as follows. Section I is the introduction to the chapter. Section II describes microstrip antenna in general starting from its conceptualization to some advancements. Section III is a review on some fundamental methods of miniaturizing the microstrip antenna to fit into the available chip area. Section IV reviews fundamental techniques of developing multi-band antennas. Section V reviews papers on multi band circularly polarized microstrip antennas. Section VI concludes the chapter.

2.2. Linearly and Circularly Polarized Microstrip Antennas

The initiation of the microstrip technology is attributed to [4] where an X-band antenna array of 300 elements of high resolution, shaped vertical pattern and a very narrow horizontal beam width is presented. Since the system is extremely bulky, the authors conceptualized a microstrip feeding system and reported it for the first time. Indeed the name used i.e. ‘Microstrip microwave antenna’ is a misnomer in the sense that no actual microstrip antenna is used; instead a microstrip power divider cum feeding network was used. However the initiation of microstrip technology triggered interest in radiation from such systems and its possibility to be used as an antenna. These possibilities are referenced in [5]-[6]. These concepts lay dormant for some time till 1969 when in [7], radiations from disc and transmission line shaped microstrip resonators were reported and laid the foundation for microstrip antennas. Further work was continued in [8] where a wraparound microstrip radiator was reported with corporate feed network arrangement. Advantages of the microstrip structure and concepts of microstrip phased arrays were also

discussed. Theoretical investigations on microstrip antenna elements were reported in [9] where the microstrip antenna element was a rectangular transmission line resonator radiating EM waves from its open ends (radiating edges). Formulation of antenna input impedance taking in to account mutual coupling between the two radiating edges and closed form expressions for radiated far fields were also given. Cavity model analysis technique for microstrip antennas was proposed in [10] where the antenna was modeled as a cavity with electric walls at the top and bottom and surrounded by magnetic walls along the edges. New closed form expressions for input impedance and far fields were derived based on these assumptions. This technique proved to be applicable to a large variety of microstrip antennas with different shapes. Measured data matched very closely with the theoretical results obtained using this technique. A brief survey on microstrip antenna technology till 1981 is available in [11] summarizing analytical techniques for characterizing microstrip antenna, substrate materials available for fabrication, design needs and discussion on microstrip dipoles and conformal antennas. Improved modeling and analysis of microstrip antennas was proposed in [12] with proper probe feed modeling and discussion on multi-port network modeling technique.

Most of the literatures reviewed till now are on microstrip antenna structures radiating linearly polarized waves. However there are applications where circularly polarized antennas are required. Capability and geometry of microstrip structures for radiating circularly polarized waves are available in [13]-[14] as early references. Elliptical shaped microstrip antenna capable of radiating Right Handed Circularly Polarized (RHCP) and Left Handed Circularly Polarized (LHCP) waves with probe feed and low ellipticity was proposed in [15]. Circularly polarized series fed S-band antenna using strip dipoles and slots having wide axial ratio band width was also proposed in [16]. Crank type circularly polarized microstrip antenna radiating circularly polarized waves at 12 GHz was reported in [17]. Microstrip series fed linear array based on rampart line geometry with polarization control of the main beam was proposed in [18]. Rectangular microstrip antennas with nearly square geometry, corner truncations and diagonal slots with probe feed were presented in [19]. These structures were shown to radiate circularly polarized waves in the broadside direction provided dimensions and feed locations were appropriately chosen. The analysis of these antennas was done by using Green's function approach in combination with desegmentation technique. However the bandwidth of these antennas was reported to be very narrow. Almost at the same time another work on generating

circularly polarized waves from an array of linear microstrip radiators with suitable phase and angular arrangements was reported in [20]. In this case the bandwidth was relatively wide compared to the antennas reported in [19].

Most of the antennas reviewed till now are based on transmission line feeding approach or probe feeding approach which result in narrow impedance bandwidth. Indirect feeding method using aperture coupled feed mechanism resulting in wider impedance bandwidth was reported in [21]. A rectangular microstrip antenna was excited by a microstrip line through an aperture in the ground plane. The antenna was fabricated on a substrate with low dielectric constant and the feed line was fabricated on a substrate with high dielectric constant. The antenna parameters were computed using the MoM techniques. The same antenna geometry was analyzed by an easier process in [22] by combining cavity model analysis technique with small-hole coupling theory [13]. An alternative approach to determine the characteristics of this antenna using transmission line modeling method and easier cavity formulation was reported in [23]-[24] respectively. This geometry was also capable of radiating dual or circularly polarized waves in the broadside direction as reported in [25]. It used square microstrip radiator along with dual apertures in the ground plane and dual feed lines. Numerous research results on radiating circular polarization from differently shaped microstrip elements were presented in [26]-[29].

Slanted slot coupled microstrip antennas for radiating CP waves were analyzed and presented in [30]. The antennas were analyzed accurately using cavity model method and magnetic current formulation at the slots. Transmission line analysis of non linear slot fed antennas were carried out and reported in [31] where wider impedance bandwidth was observed. Designs of wideband circularly polarized aperture coupled microstrip antennas were presented in [32]. Cross slots were used in the ground plane for aperture coupling. Design of series and parallel feeding techniques were described. An alternative simple feeding structure employing single feed line and four coupling points in the same antenna was reported in [33] and analyzed by integral equation method in combination with transmission line analysis. Proper variations in the designs of the slot often result in improved impedance bandwidth. An inclined nonlinear slot, V-shaped at both ends served the same purpose in an aperture coupled antenna as reported in [34]. The rise in interest and applicability of aperture coupled microstrip antennas triggered need for more accurate and computationally efficient computation. Such an efficient analysis technique for

these antennas taking into account the higher order modes was reported in [35]. Two computer programs one for analysis and another for design and optimization were used. Improved transmission line and cavity model analysis for cross aperture coupled circularly polarized antennas were also proposed in [36]-[37] respectively.

Circularly polarized microstrip antennas with two different geometries were proposed in [38]. The antennas were circular microstrip antennas with tuning stub. Two different geometries were presented one with probe feed and the other one with transmission line feed and quarter wave impedance matching section. The second antenna was compact in size compared to the first one and it employed two cross slots of equal length. Design and performance of circularly polarized microstrip antennas on two different biased substrates were presented in [39]. Use of ferrite materials with high saturation magnetization was recommended. Aperture coupled annular ring microstrip antenna was presented in [40]. The performance analysis of this antenna was done by Method of Moments (MoM) technique. The antenna orthogonal modes were excited with proper phase difference and an annular slot was used for aperture coupling. Wide band E-shaped microstrip antenna was proposed in [41]. The antenna used unequal lengths of parallel slots in a rectangular microstrip antenna to provide appropriate phase difference between the orthogonal modes in the patch were excited by the probe at optimal feed location. The circularly polarized antennas described in the reviewed literature were fabricated and the measured results are compared with the simulated or computed results for validation. This would have required accurate testing and measurement of the antenna characteristics which was described in [42].However the measurement procedures for the antennas reviewed till now were not explicitly explained by the authors.

2.3 Compact Microstrip Antennas

Compactness of microstrip antenna without disturbing the gain and bandwidth to a large extent has been one of the challenging tasks for antenna engineers. This is required to easily fit the antenna into the available module space of the required communication system. Many designs and studies have been performed over the years on this topic. Some fundamental papers are reviewed which triggered advances in this research area. In most of the cases the compactness of the antenna is achieved by reactively loading the antenna so that its resonant frequency can be

tuned down. The reactive loading is mostly done by inserting slots in the patch or inserting shorting posts /walls between the ground plane and the patch.

A compact circular microstrip antenna was reported in [43]. It incorporated a shorting post between the ground plane and the patch and located quite close to the probe feed. Significant reduction in size was observed. Although this antenna was analyzed by a very rigorous full wave method, the detailed insight and analysis came later in [44] where antenna eigenmodes and eigenvalues were used to describe the antenna performance. A dual frequency microstrip antenna with compact size was reported in [45] where a shorting pin was inserted between the ground plane and the patch. The shorting pin was located very close to the probe feed along the center line of the patch. The frequency ratio of this antenna was reported to be tunable between 2.0 to 3.2. Similarly compactness of a probe fed triangular microstrip antenna using shorting pin was also reported in [46]. Compact microstrip array of shorted patches radiating circularly polarized waves was proposed in [47]. A shorted compact multiband antenna for wireless communication was reported in [48]. A novel compact microstrip antenna was presented in [49] where the non radiating edges of the patch were modified to take a V shape. The antenna was analyzed by the multiport network modeling technique. The deformation of the non radiating edges caused the resonating mode currents travel a longer path to travel from one radiating edge to the other. A compact circularly polarized antenna was proposed in [50] where the size reduction was almost half of the original antenna. It used a corner truncated circularly polarized probe fed patch with 4 L-shaped symmetrically placed slots to bring in the compactness. A novel miniaturized stacked folded microstrip antenna using L-probe feed was proposed in [51]. The size reduction of this antenna was close to 81.5% compared to conventional half wavelength long patch antennas. Most of the compact antennas reviewed till now have very narrow band width. A compact UWB slotted circularly polarized antenna was reported in [52]. A compact symmetric slit microstrip antenna for circular polarization was presented in [53]. The slits were cut on a square microstrip antenna along the diagonals through the vertices. Compact cross shaped circularly polarized microstrip antenna was proposed in [54] where again a probe fed square microstrip antenna was used and the required phase difference between the orthogonal modes and compactness was simultaneously achieved by cutting slots of appropriate shape and size on the surface of the patch.

2.4 Multi-band Microstrip Antennas

Multi-band antennas provide the advantage of using a common antenna module for multiple communication applications from a single device. Dual –band microstrip antennas have been proposed by many researchers in the past followed by advancements to extend the dual-band nature to multiple bands. Some fundamental papers are reviewed hereunder on the conceptualization and development of multi-band antennas in the field of microstrip technology.

Dual frequency circularly polarized printed antenna composed of strip dipoles and slots was proposed very early in [55]. The antenna was fed by a microstrip transmission line. Dual frequency behavior of a compact rectangular microstrip antenna with a slot in the center and using probe feed was presented in [56]. The antenna was matched both for the TM_{10} and TM_{01} modes and radiated in the broadside direction. A dual band tunable microstrip antenna was proposed in [57]. The dual band response was obtained by a loading a probe fed rectangular microstrip antenna with a cross line soldered to one end of the ground plane. Broadband dual frequency dual port microstrip antenna was proposed in [58]. The antenna geometry was obtained by merging two circular patches of same radius but their centers distanced by a very small gap. A dual frequency patch antenna using slots very close to the radiating edges was proposed in [59] and several experimental results were provided. The slots and the probe feed matched the antenna for the TM_{10} and TM_{30} modes having identical broadside radiation patterns under such conditions. Similarly a dual frequency probe fed microstrip antenna with a cross slot was reported in [60]. The frequency ratio was mainly controlled by the aspect ratio of the patch. Two novel triple band microstrip antennas using composite resonator structures were presented in [61]. Stepped impedance and quarter wave transformers were used for implementing the composite design.

2.5 Dual Band Circularly Polarized Microstrip Antennas

All the antennas reviewed in the previous section are linearly polarized in nature. It is also possible to achieve circular polarization characteristic at dual frequencies in the broad side direction. The dual frequency behavior of circularly polarized microstrip antennas is normally implemented in two different ways. Two independent circularly polarized resonators are coupled together and fed commonly or two orthogonal modes are identified with phase quadrature at the

dual frequencies and impedance matching is performed. However very few papers with microstrip antenna configuration are available for this purpose since it is extremely difficult to maintain broadside circular polarization characteristics, gain and impedance matching at different combination of dual frequencies (depending of wireless applications) with all types of substrates.

The first dual band circularly polarized microstrip antenna was proposed in [62]. The antenna used probe feed and single layer of substrate. A spur line band stop filter was incorporated along one of the edges of the patch along with perturbation segment technique. Dual band circularly polarized stacked aperture coupled patch antenna configuration was presented in [63]. However the feed network to excite the stacked patches using cross slots was complicated and consumed huge amount of substrate area. Single feed dual band circularly polarized circular microstrip antenna was proposed in [64]. There were two pairs of arc shaped slots along the boundary of the patch with one of them protruding by a small length. The antenna exhibited Circularly Polarized (CP) nature for TM_{11} and TM_{12} modes. Dual band circularly polarized square microstrip antennas were also presented in [65] where the four sides of the patch were reactively loaded with slots so that it resonated at TM_{10} and TM_{01} modes at the lower frequency and TM_{30} and TM_{03} modes at the higher frequency. The phase difference between the orthogonal modes at the resonant frequencies was introduced by a narrow slot at the center of the square patch. Two stacked corner truncated patches for CP were proposed in [66] for dual frequency operation. The lower patch was of smaller size and resonated at the higher frequency and upper patch was of larger size and resonated at the lower frequency. An air gap was introduced between the two patches as reported in [66]. Two circular microstrip antenna configurations exhibiting dual band and broad band circularly polarized behavior was reported in [67]. Circular holes of appropriate dimensions were inserted at proper locations to excite orthogonal modes with equal amplitudes and having 90^o phase difference between them. However, a quarter wave transformer was required for impedance matching of the antenna. Compact dual band circularly polarized microstrip antenna similar to [66] was proposed in [68]. Here also, two stacked corner truncated patch antennas were used exhibiting dual band circularly polarized behavior. The lower patch with larger dimensions operated in the lower band whereas the upper patch with smaller dimensions operated in the higher band. A dual band circularly polarized antenna for satellite applications was proposed in [69] where an X-band microstrip antenna was inserted in the L-

band microstrip antenna and fed by aperture coupling through perpendicular slots in the ground plane. Power was fed to the slots through an impedance matching cum power divider circuit. A novel microstrip antenna structure exhibiting dual frequency circularly polarized behavior was reported in [70]. The antenna was etched by a two turn complementary split resonator slots resulting in such characteristics. Another dual band circularly polarized S-shaped slotted antenna with aperture coupled feed was proposed in [71] with a small frequency ratio of 1.28. It was suggested to be suitable for CP array designs as well. Probe fed stacked patches with each of them having asymmetric U-slots was investigated in [72]. In this case, each U-slotted patch resonated separately at their operating bands radiating CP waves in the broadside direction. An innovative way of exhibiting dual band CP behavior was suggested in [73]. Two separate CP resonators were used; a microstrip patch embedded inside a square ring antenna. The ring antenna was fed through a diamond shaped slot by a serial feed line. The same feed line also coupled power to the embedded microstrip patch through a cross slot. Another corner truncated patch antenna fed by a meandering probe and employing L-shaped reactive stubs was presented in [74]. The antenna exhibited very high gains at the dual bands, wide impedance bandwidths, and large front to back lobe ratio but very narrow axial ratio bandwidths.

2.6 Conclusion

Origin, conceptualization and significant advances in the field of linearly and circularly polarized microstrip antennas have been reviewed. The antenna performance parameters are observed to be extremely sensitive to its dimensions. Although closed form expressions for impedance and radiation characteristics are available for well known or established microstrip geometries, such formulations are extremely rare for linearly and circularly polarized multi-band and compact microstrip antennas. The antenna performance is believed to be highly non linear function of its design parameters. Most of the antenna designs reviewed is arrived at only by iterative procedures and parametric studies of incepted geometries by using commercial electromagnetic simulation software. All these reported designs may not be optimal ones. Optimal design of antenna with satisfactory performance characteristics can be achieved only by applying suitable bio-inspired optimization algorithms capable of handling non linear and discontinuous multi-variable functions in conjunction with numerical electromagnetic simulation techniques. The

widely appreciated and advanced bio-inspired optimization algorithms and their application to antenna design are reviewed in the next chapter.

Chapter 3

Literature Review on Bio-inspired Optimization Algorithms and their Application to Optimal Antenna and Array Designs

3.1 Introduction

Optimization techniques can be broadly classified into gradient descent techniques and bio-inspired optimization techniques. Gradient descent techniques are fast but are more prone to getting trapped in local minima compared to bio-inspired optimization techniques. Besides, the gradient descent techniques fail to reach the global optimal point when functions with discontinuities are used. On the other hand, bio-inspired optimization techniques are more applicable to functions with and without discontinuities. Bio-inspired optimization techniques imitate the behavior of nature, living organisms and groups for developing in to fitter individual, searching optimal location for good habitat and ample food for survival. Different researchers over the past have developed algorithms to imitate such behavior and apply them for arriving at optimal engineering solutions. The most conventional and widely used bio-inspired algorithms are genetic algorithms, particle swarm optimization and differential evolution algorithm. Although these algorithms have been seen to perform well and give satisfactory solutions for different engineering optimization problems, still their applicability to all sorts of problems are not guaranteed. These algorithms are also susceptible to getting trapped in local minima and chances of such situation depend on the choice of optimization algorithm pertaining to the optimization problem at hand and the values of control parameters involved. The behavior of these algorithms is stochastic in nature and optimal performance of these algorithms depends on the optimal choice of control parameters and the initial population of chromosomes, particles or vectors. The optimal choice of control parameters is problem dependent and need to be chosen very carefully to ensure that the algorithm converges to the global optima within the stipulated number of generations. Research is being continually carried on to improve these algorithms and come up with their advanced versions which are more applicable in a general sense over different optimization problems. Self adaptive versions of these algorithms where no user

decision of control parameter values are required are also being developed and proposed. Hybridization of different optimization schemes in search of improved algorithm performance are also carried out by researchers around the world.

Dimensions of antennas in terms of electrical length are very critical and sensitive to the antenna performance at desired operating frequency. Shape of the antenna is also important in deciding the type of antenna performance required in terms of antenna bandwidths and radiation properties. It is often observed that an attempt to improve one antenna performance parameter may lead to deterioration in performance with respect to some other parameter. For example, an attempt to increase impedance bandwidth of microstrip antenna by changing substrate height may lead to decrease in broad side gain due to effect of surface waves. Hence, choice of optimal antenna dimensions to reach a compromised antenna performance (where all antenna performance parameters are satisfied to a defined threshold level) is important and this can be achieved with the help of bio-inspired optimization and properly defined cost functions. Two types of optimization procedures are available in literature. In type 1, the geometry or the shape of the antenna is known and only dimensions are to be determined or optimized using algorithms. In type 2, the shape of the antenna is also unknown; hence both the shape and size of the antenna are optimized using the algorithms. Both types of optimizations have been carried out by bio-inspired optimization algorithms like genetic algorithm, particle swarm optimization and differential evolution algorithm.

Literature survey has been carried out on the bio-inspired optimization algorithms, and their modified versions, their application to antenna design and optimization. The purpose of this survey is to apprise the reader regarding the advances in bio-inspired optimization algorithms and development of new antennas structures with these algorithms. The organization of this review chapter is as follows. Section I is the introduction to the chapter. Section II is a review on genetic algorithms and their application to antenna design. Section III is a review on particle swarm optimization algorithms and their application to antenna design. Section IV is a review on differential evolution algorithms and their application to antenna design. Section V is the conclusion briefing the reader the inferences drawn from the conducted survey.

3.2 Genetic Algorithms and their Application to Antenna Design

Genetic Algorithm (GA) emulates Darwin's theory of evolution of a species into the fittest individual for survival in changing environment over a period of time. This biological change occurs in genes in the DNA of the species over a period of time. Genetic algorithm proposed by Holland in [75] models possible engineering solutions for a particular problem as a set of binary chromosomes or strings. Each position in a chromosome is called a gene and can take binary values of 0 or 1. The set of possible or assumed solutions is termed as the initial population. The genetic algorithm goes through several cycles wherein the combination of genes in each chromosome changes until the maximum cycles are exhausted or an acceptable solution is reached. Each cycle has several stages like selection, crossover, mutation and elimination. A detailed overview of binary GA and their application to different electromagnetic optimization problems are given in [76]-[78]. A MATLAB code for binary GA is given in [77] and it was applied to optimization of antenna, arrays and radar back scattering patterns. The performance of the GA was compared with that of quasi-Newton method. Discussion on algorithm control parameters and trade-offs associated with number of bits in a chromosome, initial population, selection, mating and mutation of chromosomes were also discussed. The advantage of using GA lies in avoidance of gradient calculations. However the convergence speed was reported to be slow and the GA was outperformed by quasi-Newton algorithm when smaller numbers of parameters were to be optimized. The tutorial in [78] is more detailed describing all types of chromosome and parameter coding, selection strategies, mating procedures and population selection for next generation so that possible good solutions are not missed out in intermediate stages of the algorithm before convergence takes place. The understanding of the reader is facilitated by a number of figures and charts. GA was successfully applied to design and optimize broad band multi-layer microwave absorbers, thinned and non –uniform arrays with low side lobes, shaped beam arrays, natural resonance extraction and broad band patch antenna design. The performance of the GA is optimal when its control parameters are tuned for highest algorithm efficiency. One way of doing these is to tune the chosen GA by a meta-level GA with strategy adaptive procedures as proposed in [79]. However the process has limitation in terms of CPU time required to tune the GA and the results demonstrated were based on unconstrained optimization problems. Recombination parameters (such as multi-point crossover), inversion and crowding factor were not taken in to account.

The GA was applied to a wide class of antenna optimization problems encompassing design of isotropic antenna arrays, wire antennas and planar antennas. GA was applied to design and optimization of thinned antenna arrays in [80]. Thinning of both linear and planar isotropic antenna arrays were done to reduce maximum side lobe level for a given beam width. Optimization case studies with different scan angles were reported. The authors observed that the convergence of the GA was slow and would be impractical for use in adaptive nulling applications. However the performance of the GA optimized thinned arrays reported in this work were quite good. In recent times, optimization of thinned arrays are also reported using alternative optimization algorithms like ant-colony optimization [81] and pattern search algorithm [82] where the converge is seen to be comparatively fast. Very recently, a modified compact GA [83] had been proposed for optimization of thinned array problems incorporating suitable learning schemes along with multiple probability vectors. This technique claimed to use much lower computational cost in arriving at the optimal solution compared to any other optimization algorithm used till date.

Real coded GA was also used for design of wire antennas with different impedance and radiation property specification as reported in [84]-[89]. Wire antenna designs by coupling commercially available Numerical Electromagnetic Simulator 2 (NEC 2) with real coded GA have been demonstrated. Several designs using loaded monopole, modified Yagi antennas and automated crooked wire antenna (radiating circularly polarized waves over the entire hemisphere above a ground plane) have been successfully performed. Different aspects of real coded GA with different crossover and mutation schemes were well explained in [85]. Multi-objective optimization of Yagi-Uda antennas were also reported in [86]-[87]. In both cases, NEC2 have been used for cost function evaluation. More desirable performance of optimally designed Yagi-Uda antennas using GA was reported in [86] compared to earlier literatures in this regard. The antenna element spacing and lengths were optimized for high gain, impedance matching and low side lobes. Four, six and fifteen element Yagi-Uda antennas were designed. Pareto-GA was used for getting Pareto-optimal solutions for Yagi-Uda antenna array with different element numbers in [87]. Trade-offs between achieving impedance match at the operating frequency, high gain and low side lobe levels were observed. Pareto-GA provides the optimizer with all possible variations of objectives in the problem hyperspace from where he can choose the required set of performance parameters and extract corresponding antenna dimensions. An improvement over

the Yagi-Uda antenna called the three dimensional fish bone antenna was reported in [88]. It consisted of a number of dipoles along the transmission line feed network. The dipoles have varying lengths and inter-element spacing. They were also allowed to tilt in haphazard directions to achieve desired radiation pattern, high gain and impedance match. The designs were performed by using GA coupled with NEC and cluster parallel computing system. It was reported that using a higher population size and supercomputer might result in improved designs than that reported. Although most of the wire antenna designs were performed using NEC for cost or fitness function evaluation, one can also directly used the Pocklington's or Hallen's integral equation approach. The approach for formulating such fitness function in case of Yagi-Uda antenna arrays using Hallen's integral equation approach was given and explained in [89].

Microstrip antennas have become popular in the field of antenna engineering because of their robust nature and ease of integration with MICs and MMICs. Design and optimization of various types of microstrip antennas satisfying different performance criteria using GA with electromagnetic simulation tools are reported in [90]-[99]. Design and optimization of microstrip antennas by coupling GA with Finite Difference Time Domain (FDTD) method had been demonstrated in [90]. Since cost function evaluation through FDTD was time consuming, a neural network was employed simultaneously to get trained and predict the output without using any additional calls to FDTD. Automated design of multi-band microstrip antennas employing GA and a full-wave periodic patch code based on Electric Field Integral Equation (EFIE) formulation was reported in [91]. However, the antennas were reported to be fabricated on FR-4 substrate which is usually lossy in nature and easy to match at desired frequencies. Optimization with respect to only impedance matching was performed and no consideration about radiation pattern and gain was reported. Another automated procedure of microstrip antenna design by overlapping ellipses arbitrarily with different sizes was reported in [92]. Designs of both broad band and multiband antennas have been performed. The design and optimization was done by real coded GA whereas the cost function evaluation was done by using Q-FDTD analysis of the structure. However, in this case also, only optimization of impedance properties was and the substrate used was FR-4. A partially automated design for a circularly polarized proximity coupled feed microstrip antenna was reported in [93] where the computational time was greatly reduced due to the use of a fast multi-structure method of moment analysis technique for cost function evaluation. Although the previous GA optimizations focused only on impedance

matching, this antenna design was optimized for both impedance bandwidth and axial ratio in the broad side direction. A low loss substrate of dielectric constant 2.2 was used. Design of a linearly polarized aperture coupled microstrip antenna was reported in [94]. Optimizations of microstrip antennas with and without superstrate and using magnetized ferrite substrate were performed in [95]-[96]. Fitness function evaluations were done by cavity model analysis of the antennas. Resonant frequencies and the corresponding antenna gains were optimized. Triple-frequency Sierpinski gasket fractal microstrip antenna was optimized using real coded GA in [97] in two ways, one using Adewuya mating with Gaussian mutation and the other one using Wright's heuristic crossover with non-uniform mutation. Only return losses at the design frequencies were optimized in this case. Design cases for microstrip antennas with harmonic suppression were presented in [98] where optimizations were reportedly performed by real coded GA with integral equation solver and adaptive surface meshing.

Since GA converges slowly and is expected to provide better results only when evolving with large population size, the computation cost increases tremendously. Also the robustness of GA to optimization of all electromagnetic problems is not guaranteed. Hence continuous improvements and modifications are done in real coded GA scheme to fasten the convergence speed and increase its robustness. Vector-GA for efficient multi-variable and multi-dimensional search was proposed in [99]. Chromosomes were treated as vectors and vector operators were employed for the new GA procedure. Vector-GA procedure outperformed the conventional real coded GA in terms of high convergence speed and fitness values. Hybrid optimization algorithms based on GA with variable population size and Particle Swarm Optimization were proposed in [100]. Real coded genetic algorithm based on quantum mechanics was proposed in [101] as a new evolutionary computation method termed as Quantum GA (QGA).It was proposed informally that quantum GA could perform better than the conventional GA within small domains. Improved version of quantum GA was proposed in [102] where the concepts of real coded GA employing arithmetic crossover and quantum door revolution were merged to perform beam forming of adaptive antenna arrays. Improved genetic algorithm employing strategies like section based crossover and self-supervised mutation proposed in [103], was applied for linear aperiodic array synthesis and optimization problems. In most of the optimization case studies of antenna arrays using GA, isotropic antenna elements were considered and no effect of mutual coupling, edge diffractions and design aspects of feed network were taken into account. Recently

GA along with sequential programming is used to design mobile base station arrays using practical antenna elements where all these issues are addressed [104].

3.3 Particle Swarm Optimization Algorithms and their Application to Antenna Design

The concept of Particle Swarm Optimization algorithm is inspired from the behavior of a swarm of bees in search for the flower with maximum nectar. These behavior of swarm and its conceptualization as an optimization algorithm was first reported in [105]. The applicability of this optimization algorithm was tested on a number of non linear functions and for training neural networks. Each bee in the swarm communicates its local best position depending on the amount of nectar found. A global best position is determined from the local best positions communicated by all the bees in the swarm. Thereafter, each bee assumes that the optimal nectar location lies somewhere in between the direction of its local best position and global best position. Each of the bees change their flying directions and repeats the process after regular time intervals until they all converge or reach a common point of optimal nectar location. The update of local best positions of all the bees and corresponding global best location is similar to the crossover and mutation operation in genetic algorithm. The garden of flowers may be considered as the solution space for the optimization problem, position of maximum nectar as the optimal solution in the problem hyperspace and the bees as the search agents in search of global optima. The particle swarm optimization is seen to converge faster than the GA from different reported case studies. Since its conceptualization, the PSO algorithm has been widely applied to different complex optimization problems, undergone various modifications and improvements. An overview of PSO, its development, modifications, new versions and applications are given in [106] providing discussion on topics like original PSO algorithm, its control parameters, fully informed PSO, population topology, PSO variants (binary PSO, hybrid and adaptive PSO and bare-bones PSO). Application of PSO algorithm to electromagnetic optimization problems was proposed in [107]. Discussion on suitable choice of parameter values were provided along with that of boundary conditions. Invisible wall boundary condition was seen to outperform absorbing and reflecting wall boundary conditions. This boundary condition along with suitable control parameter values of the algorithm were used for the optimization of a profile-corrugated horn antenna. However use of invisible wall boundary condition may give solutions outside the problem hyperspace and is not applicable for constrained optimization problems. For such

optimization problems, suitable boundary conditions are required. More varieties of such boundary conditions including damping wall, invisible/reflecting and invisible/damping boundary conditions and their applications were reported in [108]. A review article on PSO and its application to engineering electromagnetic is available [109]. Different advances in the development of the PSO algorithm are reviewed. PSO is coupled with electromagnetic simulators to design dual band patch antenna, artificial ground plane for surface wave and an aperiodic microstrip antenna array with corporate feed network. Performance comparison of real coded GA, PSO and a GA-PSO hybrid was performed for the design of a profile corrugated horn antenna in [110]. It was found that the PSO not only outperformed GA but also the GA-PSO hybrid.

PSO algorithm was applied to various types of antenna optimization problems incorporating designs of isotropic antenna arrays, thinned arrays, wire antennas and microstrip radiators. Performance study of genetic algorithm and particle swarm optimization was done with respect to the design of a phased antenna array involving far field side lobe notch as reported in [111]. Designs have been performed using amplitude only, phase only and complex tapering. Both GA and PSO performed well. In some cases GA outperformed PSO and vice versa for some other cases. The authors of [111] observed that the computational cost was basically dependent on cost function evaluation rather than on the optimization algorithms themselves. PSO was appreciated for its simpler coding and less book-keeping requirements. The application of real coded PSO and binary PSO was also demonstrated in [112]. Real coded PSO was applied to aperiodic antenna array synthesis whereas the binary PSO was applied for synthesis of thinned antenna arrays. The optimal results obtained were compared with those already reported in literature during that time. The applicability and study on the PSO algorithms was extended for multi-objective optimization to generate and study the Pareto-optimal front. A modified PSO which combined particle velocity clipping procedure with time varying maximum velocity factor was used for thinning of concentric circular arrays of isotropic elements in [113]. The algorithm converged fast, optimized peak side lobe level, number of turned-on/active elements maintaining the specified half power beam width. Although optimization of thinned antenna arrays had been reported widely using isotropic elements, their real time implementation was not stressed upon. Real time optimization of thinned antenna arrays was proposed for the first time in [114] using GA, binary PSO and a modified binary PSO on TMS320C6416T DSP chip. The computational

time and hardware requirement were the primary performance criteria to judge the efficiency and applicability of these algorithms. Modified binary PSO proposed here was shown to require much lower computation cost compared to the other two algorithms. Chaotic binary PSO was proposed in [115] employing non-linear inertia weight and chaotic mutation for thinning of large antenna arrays. The performance of this new PSO technique was compared with those of ant colony optimization, genetic algorithm, binary PSO and Boolean differential evolution algorithm.

A miniaturized 3-element Yagi-Uda antenna was reported in [116] with optimized gain, front-to-back lobe ratio and VSWR at the design frequency. Each element in the Yagi-Uda array is arbitrarily shaped wire formed by grid search using grids of optimal lengths. The grid inter-element spacing was also optimized. The optimization was performed by PSO and GA and the optimal results were compared to prove that PSO had performed comparatively better. PSO was also applied for optimization of 10 and 20 element log periodic wire antenna arrays in [117]. The optimization was accomplished by coupling PSO with appropriate cost/fitness function which was again evaluated by NEC. The contour graphs of radiation properties of PSO optimized log dipole arrays were obtained to provide the readers with a more clear design idea. A hybridized PSO-GA algorithm was proposed in [118] with variable population size which was shown to outperform conventional GA and PSO according to the benchmark problems used in the paper.

PSO algorithms were also widely used for design and optimization of planar antenna structures. PSO was applied for design of wideband and dual-band probe fed E-shaped microstrip antennas in combination with FDTD method for fitness function evaluation as reported in [119]. Parallel computing clusters were employed for the optimization set-up. PSO algorithm incorporated invisible boundary condition and Repeated Position Checking (RPC) scheme to minimize the number of fitness function evaluations and computation time. PSO was applied for hybridized fractal antennas suitable for GSM and Wi-Fi applications in [120]. Design of UWB antenna using spline based shaping approach and optimized using PSO was reported in [121].

PSO has undergone several modifications over the years in an attempt to increase its applicability, robustness and statistical performance compared to other evolutionary algorithms. The Comprehensive Particle Swarm Optimization (CLPSO) was proposed in [122]. The conventional particle swarm optimization sometimes suffers from premature convergence. To

tackle this problem, the self adjustable comprehensive learning particle swarm optimization algorithm came into picture. In this case the velocity update of a particle in a swarm was done without taking into account the effect of global best position. The velocity update in the CLPSO was done based on local best positions of different particles in the swarm. A modified version of this algorithm called Improved Comprehensive Learning Particle Swarm Optimization was proposed in [123]. The core difference between the CLPSO and the ICLPSO is the change in the velocity update procedure. The information regarding the previous velocity along a particular dimension for the particles in the swarms are preserved to some extent in CLPSO whereas in the case of improved comprehensive learning particle swarm optimization, it is believed that as long as the velocity of a particle is updated using other particles' local best positions, diversity remains preserved and hence information regarding the previous velocity of the particle along various dimensions can be done away with. Quantum PSO (QPSO) based on quantum mechanics was proposed in [124] and was shown to outperform classical PSO for array synthesis problems. It was further used to successfully model cylindrical DRAs with infinitesimal dipoles and lumped circuit components. Convergence control procedures of PSO and DE and their hybridization perspectives were discussed in [125]. Boolean PSO proposed in [126] , was used to design a dual band, dual polarized microstrip antenna in conjunction with MoM for fitness function evaluation. The fitness function used fuzzy rules which helped in easily arriving at the design specifications. Hybrid real-binary PSO (HPSO) was proposed in [127] where the particle positions were represented by both real and binary values. This scheme was used for optimization of non-uniform antenna array, multi-layered planar radar absorbing material and a dual band handset antenna. Very recently, Position Mutated Hierarchical Particle Swarm Optimization (PMn-HPSO) was proposed in [128]. The velocity update scheme was modified from that of the conventional particle swarm optimization algorithm. In the new velocity update scheme, no information or memory of the previous velocity was used. However the information regarding the local best positions and the global best positions were used in the velocity update procedure. When the particle becomes stagnant in the search space in some dimension with velocity equal to zero, it is reinitialized to a new value so that the particle search process may continue from that particular position.

3.4 Differential Evolution Optimization Algorithms and their Application to Antenna Design

Differential Evolution (DE) proposed in [129], claimed to be much more efficient, robust, easy to use and suited for parallel computing platforms compared to the already existing evolutionary algorithms. Originally, differential evolution algorithm works with real coded chromosomes or vectors. Differential evolution involves steps like population initialization, mutation, crossover and selection. Differential evolution uses less number of control parameters and can be efficiently used for optimization of non-linear and non-differentiable functions. In fact, DE was proven to be statistically superior compared to other evolutionary algorithms based on 25 numerical benchmark problems as reported in [130]. However, differential evolution is considered to be optimally tuned only when proper set of control parameters (initial population size, scaling factor and crossover probability) are chosen. A preliminary study on proper choice of control parameters of the DE algorithm proposed in [129] was reported in [131] .The study was based on unimodal and multimodal benchmark functions like sphere, Rosenbreck, modified Rosenbreck and Rastrigins functions. Convergence speed of DE algorithm was again proven to be superior compared to modern day GA algorithms (PGA, Grefensstette and Eshelman) in [132]. However in this case, the comparisons were based on De Jong's test functions. Since then, differential evolution algorithms have been widely used for different engineering optimization problems including those related to electromagnetics. Brief history of the origin of differential evolution, its advancement, misconceptions and misconducts, dynamic DE , retrospection of its application to electromagnetic optimization problems (before and around 2008) and finally development of a novel superior hybrid PSO-EA-DEPSO (combining evolutionary algorithm, PSO and differential evolution) can be found in [133]. The book [133] serves as a good starting for researchers looking to learn DE from scratch, and how to apply them from simple to complex electromagnetic optimization problems.

Differential evolution algorithms have been widely used for antenna design and optimization problems including arrays, wire and planar antennas. Performance comparison of real coded standard GA, classical PSO and DE had been carried out and reported in [134] with respect to the design and optimization of scannable circular antenna arrays. It was conjectured by the

authors, than newer evolutionary approaches like PSO and DE were far superior compared to standard GA.

Design of a folded wire antenna with matching network and optimized by bi-swarm differential evolution algorithm was reported in [135]. Bi-swarm differential evolution worked by dividing the population into two swarms, one emphasizing on assimilation speed and the other on randomicity. The cost function evaluation of the folded dipole antenna was done by the Galerkin's method. A crooked wire monopole antenna radiating left handed circularly polarized waves was reported in [136]. The antenna was optimized using DE. Although the gain and CP beam width were reported to be quite high, the impedance matching was not satisfactory. However, the authors suggested use of additional matching network to achieve impedance matching.

Apart from its application to electromagnetic optimization problems, the basic DE algorithm has been analyzed and improved in several ways by different researchers around the world at the same time. Such analyses and advances are surveyed and reviewed in [137] (control parameter and their adaptation in DE, constrained single objective optimization by DE, opposition based DE, multi-objective optimization using DE, application of DE to array antennas and imaging, power system optimization by DE, self adaptive DE using chaotic local search, adaptive DE with opposition based mechanisms, offline and online optimization by DE for fed-batch fermentation process and hybrid differential evolutions).Often the choice of strategies and correct values of control parameters in DE can play crucial roles in converging to the global optimal for a particular optimization problem. Also, the optimal values of control parameters and strategies required may change with generations of the algorithm. This realization among previous researchers prompted development of Self- Adaptive Differential Evolution algorithms (SADE). An early version of SADE was reported in [138] where self adaptations were mainly done for strategies involved and crossover probabilities. These self adaptations were done on success probability of the trial vectors to move to the next generation. More improved work on self adaptation was reported in [139] where self adaptation was performed mainly for scaling factor and crossover probability. Each vector in the population had its own individual crossover probability and scaling factor based on which corresponding donor and trial vectors were generated. The crossover probabilities and scaling factors associated with the population vectors

evolved gradually with better individuals over number of generations. Another version of SADE referred as JADE was proposed in [140] and it used new mutation strategy (DE/rand-to-*p*best) and an optional external archive. The algorithm balanced between exploration and exploitation at different stages of the algorithm. The self adaptation and update of scaling factor (F)and crossover probability (CR) were done for every individual based on success history of (F, CR) combinations. A version similar to JADE was applied to real valued antenna design and optimization problems in [141]. Design and optimization of linear isotropic antenna arrays, E-shaped patch antenna and microstrip band pass filters were performed. The performance of the SADE was compared with conventional PSOs with respect to these optimization problems. Differential evolution with neighborhood based mutation operator was proposed in [142]. It was also referred to as Differential Evolution with global and Local Neighborhood search (DEGL). In this algorithm, two terms namely global and local neighborhoods were introduced. Global neighborhood referred to the entire population during any generation of the algorithm. The candidates were assumed to be organized in a ring topology. For each candidate, a local neighborhood of size was also defined. A local donor vector and a global donor vector were created from the two neighborhoods which were combined to yield the actual donor vector using appropriate weight factor. DEGL was applied to synthesis of thinned circular arrays in [143]. The Biogeography based Optimization (BBO) algorithm was first proposed in [144]. The BBO was hybridized with the original DE (Hybridized Biogeography based Optimization with Differential Evolution (BBO-DE)) and applied to economic load dispatch problems in power systems in [145]. Biogeography based optimization was also used for optimization of thinned antenna arrays as in [146]. Boolean DE was proposed and applied for optimization of thinned planar antenna arrays in [147] and it was shown to outperform binary DE. Unlike real coded DE where high value of CR close to 1 is preferable, CR value was kept as low as 0.2 in Boolean DE. Boolean DE used Boolean operators instead of arithmetic operators for donor vector generation. Synthesis and optimization of aperiodic linear antenna array using a hybrid self adaptive differential evolution algorithm was reported in [148]. This self adaptive algorithm was actually a combination of JADE and local search algorithm. Improved Differential Evolution (IDE) [149] was simple modification of DE/rand/1. It improved upon donor vector generation strategy by replacing one arbitrary candidate by the sup-optimal candidate vector in the difference vector for donor generation. The sub-optimal candidate was the one having the second lowest cost function

in the existing population. The sub-optimal candidate was updated not only at the end of each generation but also after the trial vector evaluation of each candidate.

Another brief review on DE, its modified and hybridized versions, dynamic DE, ideas on control parameter settings and their applicability to electromagnetic optimization problems is provided in [150]. It is concluded from [150] that it cannot be strongly claimed that DE is superior compared to other evolutionary algorithm for all optimization problems, However it is generally observed to perform with good reliability in case of electromagnetic optimization problems. Composite DE (CoDE) was proposed in [151]. It used a combination of several trial vector generation strategies and possible control parameter values. The performance of this algorithm was tested in comparison with some improved versions of DE with respect to standard numerical benchmark problems and was considered to be superior in a general sense over conventional DE algorithms. However the required computation cost was high for this algorithm. Modified Differential Evolution with p-Best Crossover Strategy (MDE-pBX) was conceived in [152]. It altered the generation process of donor vectors and crossover strategy of DE/rand/1 to increase the diversity of the solutions and to make the algorithm more explorative in nature. For each candidate vector, an arbitrary group of 'q' vectors was created (chosen randomly from the total population excluding the present candidate vector) from which the donor vector was generated. The p-best crossover strategy used binomial crossover between the donor vector and an arbitrarily chosen vector from among top p-candidate vectors of the population (sorted in ascending order of their cost values) to generate the trial vector. Adaptive Differential Evolution with Optimization State Estimation (ADE) was proposed in [153]. It identified each run of the algorithm as exploration state and exploitation state (by studying the population distribution) and accordingly adapted the scaling factor and crossover probability. A hybrid real-binary differential evolution algorithm was applied for optimization of unequally spaced thinned array and automated UWB antenna in [154]. Similar approach was also used for optimization of automated triple band antenna in [155]. Harmonic Search Differential Evolution (HSDE) was recently proposed in [156]. The idea behind this novel DE optimization scheme was to enhance its explorative capability by merging conventional DE with harmonic search algorithm [157]. Modified Differential Evolution (MDE) was proposed in [158]. It incorporated two basic modifications namely best of random mutation and randomized local search. Differential Evolution with an individual dependent mechanism (DE-IDP-IDM) was proposed in [159]. In

this novel self adaptive DE algorithm, the cost values of the individuals in the population were used for identifying them into groups of superior set and inferior set. Hence forth, depending on the classification of the individuals and differences of the cost values, the individuals were assigned their own control parameter values and mutation strategies. A recent differential evolution scheme with dynamic control parameter adaptation was proposed in [160] and it used success history of defined combinations of control parameters over an epoch for parameter update. However it used large population size. Very recently, differential evolution with auto enhanced population diversity is proposed in [161]. This algorithm addresses the issues of population premature convergence and stagnation during optimization runs and accordingly diversifies the population to resolve the problem. Diversity based multi-population differential evolution is also proposed in [162] for large scale optimization problems and relies on exchange of information between sub-populations.

3.5 Conclusion

Different bio-inspired evolutionary optimization algorithms including genetic algorithm, particle swarm optimization and differential evolution have been proposed and applied to different antenna design and array synthesis problems as surveyed. However the applicability of the evolutionary algorithms varies depending on the optimization problem at hand and formulation of the cost function or the fitness function. The optimal performance of any optimization algorithm for a particular optimization problem also depends on the proper tuning of its control parameters and choice of strategies involved. Much have been published providing guidelines for choosing such control parameter values and strategies. These algorithms have been modified, improved or made self adaptive to increase their applicability and reduce overall computational cost involved in the process. However the superiority of most of these algorithms has been claimed over only limited number of existing evolutionary algorithms only. Moreover, these algorithms assumed cost functions or fitness functions having multiple objectives, mostly combined by fixed weights. Very rare attempts have been made to study the applicability of these algorithms in situations where dynamically adaptive cost functions or fitness functions can be used. As surveyed, these algorithms are widely applied for array synthesis problems mostly assuming isotropic antenna arrays. Very little amount of literatures is available using evolutionary optimization algorithms where practical antenna elements are considered and the

design of feed network is also taken in to account. Design of planar and microstrip antennas have also been reported in surveyed literature. It is observed that initially, most of the design optimizations are done taking in to account only the antenna impedance properties. Later on, researchers have started multi-objective optimization of antenna taking in to account both its impedance and pattern properties. However most of the optimally designed antennas are linearly polarized. Limited literature is available with respect to the applicability of these evolutionary algorithms for design of circularly polarized antennas.

Chapter 4

Performance Comparison of Genetic Algorithms, Particle Swarm Optimization Techniques and Differential Evolution Algorithms in the Optimization of Microstrip Antennas and Arrays

4.1 Introduction

The differential evolution optimization algorithm, which works on the stochastic vector-based population approach, was proposed in [129]. It was proven superior with respect to the optimization of 34 widely used numerical benchmark problems and was regarded the fastest on a general basis over particle swarm optimization and the evolutionary algorithms in [130]. Since then, Differential Evolution (DE) has found wide applications in engineering designs in various fields [134],[142],[143],[150]. Earlier Genetic Algorithms (GA) [76], Particle Swarm Optimization (PSO) techniques, and some of their variants [107],[108],[122],[124] have been widely used to design antennas and arrays using analytical methods or full wave simulation techniques [78],[85],[98],[102],[103],[110],[111],[114],[119],[120],[121],[123],[125],[128]. The performance of any optimization algorithm depends on the optimization problem hyperspace and proper tuning of control parameters involved in the algorithm. Antenna design often requires multiple objectives to be optimized at the same times for example gain and bandwidth of the microstrip antenna about the center frequency. The performance evaluation of GA, PSO and DE are necessary with respect to antenna design problems in such types of situations. One way is to combine several objectives by a weighted sum approach. Although this was done in antenna design problems earlier [143], it was mostly restricted to a maximum of two objectives, and the weights assigned to each objective were fixed. In this chapter, performance comparison of DE is made with respect to that of PSO and GA under a multi-objective situation along with their advanced versions, such as improved GA, quantum GA, improved comprehensive learning PSO and position mutated hierarchical PSO and DE with a neighborhood based mutation operator (using a global and local neighborhood search). Although similar comparisons were reported in [111], [114], and [134], it was not extended to any advanced optimization schemes. Such an extensive comparison with respect to antenna design was not reported earlier. It is also ensured

that the comparison is made with all algorithms working nearly at their best by tuning all control parameters using a meta-level position mutated hierarchical PSO algorithm, which is one of the novelties introduced here. This is an improvisation over [79], where meta-GA was used for the same purpose. Meta-position mutated PSO does not require control parameter tuning, converges fast and, hence, is time-economic. Earlier comparisons relied on already established literature for control parameter values, and the cost function was mostly related to theoretical array designs using fixed weights. The benchmark design problems considered here is that of a right-handed circularly polarized microstrip antennas(using different feeding techniques like probe feed, transmission line feed and cross aperture coupled feed) with impedance matching over a predefined frequency range, good axial ratio and high gain at the specified center frequency. The other benchmark design problems include synthesis of linear array of unequally spaced isotropic antenna elements optimized to achieve minimum beam width, minimum side-lobe level and as little length of the array as possible (no impedance matching criteria and mutual coupling between antenna elements are considered) and design of a 4-element Yagi-Uda antenna array with similar design objectives taking into account impedance matching at the design frequency and mutual coupling between the dipole antennas. The half power beam widths and the maximum side lobe levels are optimized in both E-plane and H-plane for the Yagi-Uda antenna array. All these objectives and cost functions are combined into a single objective by assigning dynamic weights to each of them. The weights are updated in each generation according to a fuzzy inference scheme to ensure all objective costs satisfy at least their threshold values in minimum runs of the algorithm.

The chapter is organized as follows. Section II provides a brief overview and references for the algorithms evaluated in this chapter. Section III describes tuning of control parameters of different optimization algorithms for optimal performance. Sections IV–VI explain the formulation of cost function, analysis of the solutions, performances of the bio-inspired algorithms with respect to design of right-handed circularly polarized microstrip antenna for three different feeding techniques, namely probe feed, transmission line feed, and cross-aperture coupled feed respectively. Sections VII-VIII explain the performances of the bio-inspired optimization algorithms in the design of linear array of unequally spaced isotropic antenna elements and also the 4-element Yagi-Uda antenna array respectively. Section IX summarizes the results.

4.2 Bio-inspired Optimization Algorithms

4.2.1Real Coded Genetic Algorithm and Quantum Genetic Algorithm

Genetic algorithm is used with binary coded chromosomes as well as real coded chromosomes. However the real coded chromosome techniques are in vogue now because of its accuracy in reaching the global optima or very near to it during a successful run. Quantum Genetic Algorithm (QGA), an improved version of the real coded GA was proposed in [102]. A brief overview of the steps involved in the Quantum Genetic Algorithm is given below. All the steps in QGA are same as that of the real coded GA except the one using quantum door revolution.

Encoding and initializing the population: The first stage in the initiation of the algorithm is the encoding procedure. Here a population of chromosomes are used which represents the candidates to be used for the optimization process. Each chromosome comprises of a set of genes. The genes represent the parameter values or the different dimension values of the antenna to be optimized. The population size is represented by P which is actually the number of chromosomes. The number of genes in each chromosome is represented by D. To maintain diversity and ensure better chances of reaching the global optima, P should be several times that of D. Normally the value of each gene is supposed to be either ‘0’ or ‘1’ as is evident in case of binary GA. However it will lead to a lengthy chromosome and huge population size need to be used which will not only take high computation time but may also reduce the convergence rate of the algorithm. Using a series of binary digits and a fixed length of chromosome, does not ensure that we reach parameter values corresponding to the global optima, but we reach values which are close to the global optima. To overcome this disadvantage of the binary GA , real coded GA scheme is used. Each gene value of a chromosome represents a possible dimension value of the antenna. These values will keep on changing as the GA run through the sequence of selection, crossover, mutation, quantum door revolution and migration to next iteration over the stipulated number of generations.

Cost evaluation of the chromosomes in the population: Each chromosome with its respective gene values representing different dimensions of an antenna is evaluated for its cost. The objective is to reach a combination of gene values with the lowest possible cost value. The cost

value for each optimization problem should be defined accordingly depending on the performance of the antenna required.

Selection: The purpose of this step is to select those chromosomes in the population which are supposed to participate in a simulated mating process in order to produce better offspring in terms of relatively lower cost values. The individuals with lower cost values in the present generation are considered to be superior individuals and are preferred for taking part in the mating or crossover operation. It is believed that good parents have more probability of producing better children or offspring. In order to speed up the convergence rate in case of quantum genetic algorithm, a certain percentage of the superior individuals in the present population are preferred for taking part in the crossover operation which is described next.

Crossover: Crossover operation is a mathematical equivalent of the biological mating process of two individuals. Two parents from the present generation take part in the crossover operation. They produce two offspring. The cost values of these offspring are evaluated. There are different types of crossover mechanisms pertaining to binary GA and real coded GA. In the Quantum Genetic Algorithm, the mathematical crossover technique is used to give birth to new individuals or children. In arithmetic crossover technique, the values of the real coded gene corresponding to a particular gene position for the parents are noted. Let ‘a’ be the smaller value and ‘b’ is the higher value among the two values noted. The corresponding gene value of the child or offspring is calculated as:

$$c = a + rand * (b - a) \tag{4.1}$$

In the formula above, ‘rand’ is a random value with uniform distribution between 0 and 1. The same procedure is repeated to get the gene values of the other child. It is expected that the arithmetic crossover will produce children having characteristic and traits from both the parents. Other children are also produced in the same manner.

Variation or mutation operation: In the variation or mutation operation, some genes from some chromosomes are randomly mutated or changed to incorporate the diversity factor in the

population. In binary GA the chromosomes are encoded as strings of zeros and ones. For random positions in some chromosomes depending on mutation probability (which is usually quite low), the binary values are reversed i.e. one is converted to zero and vice versa. However in case of real coded GA, the process is not so simple because the genes are encoded with real numbers. The mutation operation is done on the children produced by the parents. The cost values of the offspring are evaluated for comparing them with those of their parents. In case of Quantum Genetic Algorithm, the Multiple Disequilibrium Variation method is used for implementing the mutation step.

In the Multiple Disequilibrium Variation or mutation technique, several gene positions from a chromosome are chosen randomly and random real numbers are used to obtain those places in the selected chromosomes. The random real number in the selected gene position may be higher or lower than the old value (but within limits as specified by the programmer) and will be determined by computer randomly. A new chromosome will be obtained after these operations.

Real quantum door rotation step: Quantum door rotation is a method for evolving the present population to the next generation. Each gene value in the chromosome is converted into a string of equivalent angle values. Let us assume that for a particular gene position, the lower and upper limits of the dimension value be ‘a’ and ‘b’ respectively. Let us also assume that the actual value of the gene in that position is ‘c’ which is between the limits ‘a’ and ‘b’ specified by the programmer. This gene is converted into an equivalent angle value by the following equation:

$$\theta = arctan(b - c)/(c - a) \qquad (4.2)$$

In this manner, all the genes in all the chromosomes are converted into respective angle values. Let the angle value for a particular gene position in the best individual in the population is represented by θ_{best}. The gene values for other chromosomes in the same position are modified as:

If $\theta > \theta best$ (4.3)

$\Theta = \theta - \Delta\theta$

Else

$\Theta=\theta+\Delta\theta$

end

The other gene values for the chromosomes are altered and modified similarly.

After many experiments, the value of 0.01π was suggested as reference value in [102]. Using a reverse procedure, a chromosome with encoded angle values can be converted back into a string of real coded gene values.

When the operations of selection, crossover, variation and quantum door revolving are finished, a new population of children in the new generation is produced. Because a part of chromosomes of father generation evolve to the son generation directly, the number of father-generation population is less than that of son-generation population. The cost value of each chromosome of son-generation is computed and compared with the conditions which are set in the initial stage. If the conditions are satisfied, it is assumed that the best individual has been obtained and the calculations should be stopped. If not, P chromosomes from the new-generation of children are selected according to their cost values, and the operations of selection, crossover, variation, quantum door revolution are repeated.

4.2.2 Improved Genetic Algorithm

The genetic algorithms both with binary coded genes and real value coded genes have been widely used to solve optimization and design problems for antennas and antenna arrays. Though it is observed that genetic algorithm can be applied to non-convex optimization problems, its robustness and convergence rate remains a problem. Most of the genetic algorithms till date suffer from poor robustness and slow convergence rate. To improve the statistical performance of the genetic algorithms with respect to issues mentioned, the Improved Genetic Algorithm (IGA) was proposed in [103]. The improved genetic algorithm uses three main strategies comprising multi-section based real encoding scheme, a section-based crossover process, and a self-supervised mutation process. A brief overview of these strategies is given below:

Encoding and initializing the population: The first stage in the initiation of the algorithm is the encoding procedure. Here a population of chromosomes is used which represent the initial candidates to be used for the optimization process. Each chromosome comprises a set of genes. The genes represent the parameter values or the different dimension values of the antenna to be optimized. The population size is represented by P which is actually the number of chromosomes. The number of genes in each chromosome is represented by D. To maintain diversity and ensure better chances of reaching the global optima, P should be several times D. Normally the value of each gene is supposed to be either '0' or '1' as is evident in case of binary GA. However it will lead to a lengthy chromosome and huge population size is needed to be used which will not only take high computation time but may also reduce the convergence rate of the algorithm. To overcome this disadvantage of the binary GA , real coded GA scheme is used. Each gene value of a chromosome represents a possible dimension value of the antenna. These values will keep on changing as the GA runs through the sequence of GA operators over the stipulated number of generations.

Section-Based Crossover: The next stage is the crossover operation which is a mathematical simulation of the mating of two chromosomes. The selected chromosomes with preferably low cost or high fitness are termed as parents and the new chromosomes that result from the crossover operation are termed as children or offspring. The parents which are to participate in the crossover operation are chosen from the entire population using the Roulette Wheel Selection Method. In the IGA, various crossover strategies are followed based on a crossover probability, P_c where P_c lies between 0 and 1. Mainly three crossover methods are used, namely uniform crossover, single-point crossover and multi-point crossover. These crossover methods are randomly applied on each generation of the optimization algorithm. A control parameter, 'm_c' is used to determine which crossover strategy is to be used. The parameter 'm_c' can have any value from the set {0, 1, 2}. The value of 'm_c' is chosen randomly from this set. If m_c=0, then uniform crossover method is used (where the crossover is performed over all the genes in entire chromosome using a randomly generated mask). This mask is a string of random binary bits having the same length as that of the chromosome. The corresponding offspring are produced according to the information in the mask. However, if m_c= 1 or 2, then single point or two point

crossover methods are used. In single-point crossover, one gene position is randomly chosen as the cut-point from the parents. Only the genes located in the right of the cut-point are exchanged and the others are kept same. In case of two-point crossover, two gene positions are chosen as cut-points. Only the genes between the two cut points are exchanged and others are kept same. The positions of the new cut-point genes g_{c1}, and g_{c2}, are obtained by taking a linear combination of the positions of the old cut-point genes, $g_{p1}$and g_{p2}, the upper and lower bounds of the real coded gene value (g_L and g_U) and a randomly generated value, c.

$$g_{c1} = \min[\, g_l + c(g_u - g_l), \frac{(g_{p1}+g_{p2})}{2} + c\,\frac{(g_{p1}-g_{p2})}{2}] \quad (4.4a)$$

$$g_{c2} = \max[\, g_l + (1-c)(g_u - g_l), \frac{(g_{p2}+g_{p1})}{2} + (1-c)\,\frac{(g_{p2}-g_{p1})}{2}] \quad (4.4b)$$

'c' is randomly generated within [0, 1]. This ensures that g_{c1} and g_{c2} are confined to be within the upper and lower bounds.

Self-Supervised Mutation: Once the offspring or children are produced from the crossover operation, the next stage is the mutation operation which is performed with a mutation probability (P_m) and is aimed at maintaining diversity in the population. It is observed that in case of stochastic mutation process, the algorithm may overlook better solutions and waste much time on exploiting searching areas with low fitness chromosomes. To rectify this problem, a self-supervised mutation is proposed in this improved genetic algorithm which is the core idea behind this novel algorithm. Opposed to the conventional mutation strategies, this mutation process can be applied to the selected gene for one or more times in each generation. Each update of a gene during the mutation process is termed as a search. In the self-supervised mutation process, the results of the previous searches are used to direct the direction of adjustment of the gene value and the step size of the next search. In the beginning of the mutation process, a search is performed on the gene in an arbitrary direction. If a better solution or a chromosome with lower cost is obtained in that direction, the mutation will be repeated again in the same direction.

However, the step size of the search is gradually reduced as per a defined reducing rate. The search in the same direction will stop when there is no significant improvement in cost values. This process will have less chance of missing out the good solutions and fitter individuals and lesser time will be wasted in searching around the bad solution space. Let the gene to be mutated be denoted as g_i , the new gene after one search is calculated as g_i' given by

$$g_i' = g_i + M_i(g_{ui} - g_i), if\, g_i \geq 0, 0 < M \leq 1 \quad (4.5a)$$

$$g_i' = g_i + M_i(g_{li} - g_i), if\, g_i < 0, 0 < M \leq 1 \quad (4.5b)$$

$$g_i' = g_i + M_i(g_i - g_{li}), if\, g_i \geq 0, -1 < M \leq 0 \quad (4.5c)$$

$$g_i' = g_i + M_i(g_i - g_{ui}), if\, g_i < 0, -1 < M \leq 0 \quad (4.5d)$$

where g_{li} and g_{ui} are the lower and upper bounds of g_i respectively. M_i is a real number within the range of [-1,1], which is randomly initialized at the beginning of the mutation. After each search, M_i is decreased by multiplying a factor r_{dec} to it as

$$M_i' = M_i.r_{dec}, \;\; if fit_n - fit_o > e and fit_o > fit_a \quad (4.6)$$

where M_i' is the new value of M_i ,r_{dec} is the decreasing rate used for reducing the step size of subsequent searches in the self supervised mutation, satisfying $0<r_{dec}<1$, fit_o and fit_n are the original and the new fitness values, respectively, fit_a is the mean fitness value of the offspring starting from the crossover stage, and 'e' is the minimum acceptable improvement in fitness values or cost values. The conditions fit_n-fit_o>e and fit_o>fit_a, are used to take in to consideration certain issues. Firstly, it is observed that, when fit_n is slightly better than fit_o, there is hardly any possibility to get a comparatively much better individual from further searches. It is therefore reasonable to terminate the supervised mutation process at this point so as to save computation time. Secondly, it is also observed that the cost function or fitness function evaluation of additional individuals generated in each mutation search step augments the computation time. It

is reasonable to assume that fitter individuals with higher fitness have a higher probability to produce better quality offspring. To reduce computational cost, the search and computational process are performed only on fitter individuals whose fitness values are larger than the mean value. After updating M_i and g_i, a new search will start with M_i' and g_i' . The mutation search on g_i is considered to be complete when the conditions in (3.6) are no longer true.

4.2.3 Particle Swarm Optimization

The Particle Swarm Optimization (PSO) and its application to electromagnetic optimization problems werereported in [107]. A brief description and outline of the algorithm is given below:

1. An initial population of swarm is generated. Let the population size be P. Each swarm has 'N' dimensions. Each dimension in the swarm particle represents a particular antenna dimension or parameter. Each dimension can have values between the limits specified by the programmer. Each dimension has its own lower and upper value limits which can be designated as $X_{min,n}$ and $X_{max,n}$, respectively, where n ranges from 1 to N. In addition each dimension for each swarm is initialized with a velocity to initiate the search process of the fitter individuals in the solution hyperspace. The cost values of each particle in the initial population are evaluated before starting the optimization process. Each swarm is represented as $X_G(i,j)$ where G represents the generation number, i represents the i^{th} swarm in the population and j denotes the j^{th} dimension of the swarm particle. Each swarm has a velocity string associated with it and is represented by $V_G(i,j)$. 'G','i' and 'j'have the same meaning as in X_G (i,j). With each swarm particle, is associated one local best particle (L_best). The local best particle is the fittest combination of dimensional values that a particle has come across while searching for the optimal solution in the solution hyperspace. With each generation, there is associated one swarm particle known as the global best (G_best). The global best particle is the fittest particle among all local best particles. In the start of the optimization process, the initial combination of dimensional values for each swarm particle is considered to be their local best since no search is performed till then. The global best particle is identified from among the local best particles. The following steps (2-4) are repeated until the maximum numbers of generations are over or the termination criterion is met.

2. Each particle travels through the solution space within the limits of each dimension already specified by the programmer. If the particle tries to go out of the limits specified by the programmer, suitable boundary conditions [108] are applied to bring the particle back into the defined search space. The boundary condition to be used varies with each optimization problem. The boundary condition best suited for using PSO in a particular optimization problem has to be determined by using repeated trials. The algorithm simulates the movement of each particle in the swarm one by one, by a very small distance along every dimension.

3. The local best position corresponding to each particle in the swarm and the corresponding global best position for each generation is continuously updated. The current cost of a particle is compared with the cost of its local best particle. If the current cost is lower than that of the previous local best, the local best particle is updated with its dimensional values same as that of the current particle. This process is repeated for each particle in the swarm to update their local best positions. Once the local best positions are updated in each generation, the global best position for that particular generation is also updated.

4. The velocity of each particle in the swarm is updated and the velocity update procedure is the key to the wide range of applicability of PSO algorithm to engineering optimization problems. The velocity of each particle can be in a random direction with a particular magnitude. The velocity of the particle is assumed to have components in each of the N-dimensions of the swarm performing search in the search space. That's why with every $X_G(i,j)$ is associated one velocity vector $V_G(i,j)$. The velocity components along the N-dimensions are updated according to the equation given below. It may be noted that the updated velocity of the particle in the swarm depends on the relative location of its local best and global best in the search space.

$$V_{G+1}(i,j) = w * V_G(i,j) + C_1 * rand * \left(X_{G,local\_best}(i,j) - X_G(i,j)\right) + C_2 * rand * (Global_{best}(j) - X_G(i,j)) \quad (4.7)$$

5. The velocity update calculation is done for each of the N dimensions in an N-dimensional optimization. $C_1$and C_2 are constants or scaling factors that determine how much the new

velocity of the particle is biased towards the direction of local best position of the particle and the overall global best position respectively. The constants C_1 and C_2 are normally referred to as the cognitive and social rates, respectively. C_1 determines how much the particle is affected by the memory of its best location, and C_2 determines how much the particle is affected by the rest of the swarm. The random number function rand () returns a number between 0.0 and 1.0. The same random number value may be used in the above equation where rand () is referred twice. However in most cases two different values of random numbers obtained using two independent function calls to rand () are used. This perturbs the cognitive and social rates which in turn simulates the possibility of wanton movement of the swarm. 'w' is the inertia factor that determines how much effect of the previous velocity will be retained in the new velocity of the particle. The introduction of these three factors namely the inertial factor, social and cognitive rates with proper values helps in maintaining a balance between exploration and exploitation performed by the swarm in the optimization algorithm.

6. Initially the particles in the swarm are supposed to be scattered all over the solution space. The particles which are further away from the global and respective local best try to move faster and quicker to locations which result in lower cost values. In attempting to do so, the particles need to fly over a trajectory, in the midst of which they may come across locations in the search space yielding lower cost values than those of the already available local best. This will lead to update of local best positions for the particles. It is also possible that the global best location also gets updated in the process. Once the local best and global best positions are relocated, the particles in the swarm change their trajectories according to the revised locations. This process continues with each generation until all the particles converge to the optimal location or solution in the search space.

7. The trajectory along which the particles move is defined by the relative displacements occurring along each dimension of the particle according to its updated velocity. In other words, the particles move from the old location to a new location. The coordinates of the new location can be obtained through a position update algorithm as given below:

$$X_{G+1}(i,j) = X_G(i,j) + \Delta t * V_G(i,j) \quad (4.8)$$

4.2.4 Comprehensive Particle Swarm Optimization (CLPSO)

The Comprehensive Particle Swarm Optimization (CLPSO) was proposed in [122]. The conventional particle swarm optimization sometimes suffers from premature convergence. To tackle this problem, the self adjustable comprehensive learning particle swarm optimization algorithm came into picture. A brief overview of the CLPSO optimization technique is given here [122].

The underlying idea of the comprehensive learning particle swarm optimization is the modification of the velocity update rule of conventional PSO. In this case the velocity update of a particle in a swarm is done without taking into account the effect of global best position. The velocity update in the CLPSO is done based on local best positions of different particles in the swarm. Moreover, the velocity updates along N-dimensions may use local best coordinates from different particles instead of one.

The velocity update equation in case of CLPSO is given below:

$$V_{G+1}(i,j) = w * V_G(i,j) + c * rand * (Local\_best(f_i(D), j) - X_G(i,j)) \quad (4.9)$$

'rand' refers to a random number between 0 and 1. The local best position used in the velocity update equation does not belong to the same particle whose velocity components are being updated. The index of the particle whose local best information is used in the equation above has the index given by fi(D). Further the velocity update is based on a probability 'P_c' defined in [122]. Different particles in the swarm have different values of 'P_c' and this value is kept same throughout the algorithm. The 'P_c' values are arbitrarily set at the start of the algorithm. It is reported that the CLPSO performs well compared to other versions of PSO in case of many multimodal problems. However there are exceptions like Griewanks function and rotated Griewanks function where the performance of CLPSO is found to be not so good. The weakness of the CLPSO lies in the following:

1. The local best of the fi(D) particle is used in the velocity update procedure mentioned above. Normally, the fi(D) particle is chosen after a binary tournament selection from two other particles in the swarm . fi(D) is the index of the winner particle. However, it is proposed that choosing the fi(D) as the loser particle may sometimes help the particle in the CLPSO swarm come out of local minima traps.

2. Each particle in the CLSPO swarm has a probability P_c assigned to it in the beginning of the optimization procedure. This value is kept same throughout the algorithm. However, it is proposed that a dynamic value of P_c for every particle depending on its trajectory in the search space and current location may be helpful in improving the robustness and statistical performance of the algorithm.

3. There is no provision in the CLPSO algorithm to reach the optimal solution if all the particles get trapped in to local minima.

4.2.5 Improved Comprehensive Learning Particle Swarm Optimization (ICLPSO)

To overcome the potential disadvantages of CLPSO, a modified version called Improved Comprehensive Learning Particle Swarm Optimization was proposed in [123]. However the core difference between the CLPSO and the ICLPSO is the change in the velocity update procedure. The information regarding the previous velocity along a particular dimension for the particles in the swarms are preserved to some extent in the comprehensive learning particle swarm optimization. This is done mainly to preserve the diversity of the population of the swarm. However in the optimization strategy of the improved comprehensive learning particle swarm optimization, it is proposed that as long as the velocity of a particle is updated using other particles' local best positions, diversity remains preserved and hence information regarding the previous velocity of the particle along various dimensions can be done away with. It is also proposed that one may assume that the optimal solution or the global best position may lie along one of the particles' local best positions. Hence the velocity update equation is modified as shown below:

$$V_{G+1}(i,j) = [1 - as(i) + 2 * as(i) * rand] * (Local\_best(f_i(D), j) - X(i,j)) \quad (4.10)$$

where as(i) is a number between 0 and 1 corresponding to a sequence index s(i). s(i) is the sequence or rank of the particles whose corresponding local best position cost values are arranged from low to high. It is reasonable enough to search the area around the particles with lower costs (corresponding to their local bests) more compared to ones with higher cost values. Hence, an empirical formula for as(i) is developed as given below:

$$a_{s(i)} = 0.7 - \frac{s(i)}{4*P} \tag{4.11}$$

Whenever a particular dimension value for any particle tries to go out of its limits specified by the programmer, hybrid periodic boundary conditions are used to restrict its value within the limits. Moreover to overcome the disadvantages of the actual comprehensive learning particle swarm optimization, three strategies are introduced to the improved version of the CLPSO.

Strategy1: A loser group of size 'n' is defined. The loser group of size 'n' comprises of the best 'n' particles of the swarm. These 'n' particles learn from the loser candidate of a binary tournament while updating their velocity along different directions. The size 'n' required for different optimization problems may vary and need to be tuned accordingly for proper performance of the optimization technique.

Strategy 2: A dynamic value of P_c (which is mentioned in the actual comprehensive learning particle swarm optimization strategy) is introduced here. It is reasoned that a better particle should actually learn from its own local best position whereas a worse particle should learn from other's local best position. Accordingly, the P_c for each particle in the swarm with index 'i' is defined as

$$Pc_i = Pco_{s(i)} \tag{4.12a}$$

$$Pco_{s(i)} = 0.05 + 0.25 * (\frac{i}{P})^{10} \tag{4.12b}$$

If the global best position does not improve in each generation, then the $Pco_{s(i)}$ value is further augmented as shown below:

$$Pco_{(i)} = Pco_{(i)} + 0.00005 * i^{0.5} \quad (4.13)$$

Strategy 3: If most of the particles tend to converge to local minima, after a certain number of generations, strategy 3 is adopted to make them explore some new area and provide a possibility to come out of the local minima trap. If random mutations are performed on some particle's current positions, it may not be of much help since their local best position information may draw them back to previous positions within few generations. One can try to make variations in the particles' positions in their corresponding local minima. However, this strategy risks losing vital information from those of the better particles. To reduce the risk, the variation of the local best positions is done for a certain number of worse particles only. In [123], the number of worse particles is chosen to be 6 with a variation probability of 0.04.

4.2.6 Position Mutated Hierarchical Particle Swarm Optimization

The Hierarchical Particle Swarm Optimization (HPSO) was proposed in [128]. A brief overview of the algorithm is presented here. In this case also, the velocity update scheme is modified from that of the conventional particle swarm optimization algorithm. In the new velocity update scheme, no information or memory of the previous velocity is used. However the information regarding the local best positions and the global best positions are used in the velocity update procedure. When the particle becomes stagnant in the search space in some dimension with velocity equal to zero, it is reinitialized to a new value so that the particle search process may continue from that particular position. This strategy of the re-initialization of the particle velocity along some dimension is supposed to enhance the explorative nature of the algorithm. All the random numbers mentioned in the equations below are mutually exclusive.

$$V_{G+1}(i,j) = C_1 * rand * \left(X_{G,local\_best}(i,j) - X_G(i,j)\right) + C_2 * rand * (Global_{best}(j) - X_G(i,j)) \quad (4.14)$$

$$if\ V_{G+1}(i,j) = 0\ \ then V_{G+1}(i,j) = 2 * (rand - 0.5)V_r \quad (4.15)$$

However it is observed that the HPSO algorithm is not efficient enough to escape out of local minima and hence further improvements to this algorithm is introduced. Instead of keeping social and cognitive rates constant, they are made varying with number of generations. C_1 is linearly varied from 2.5 to 0.5 whereas C_2 is linearly increased from 0.5 to 2.5 with increasing number of iterations or generations. The most important modification to the HPSO algorithm is done by introducing position mutation [128]. Four types of position mutation schemes are possible. In the first position mutation scheme (PM_1), one particle is chosen at random and any one dimensional value of that particle is changed within the limits of that dimension. In the second position mutation scheme (PM_2), any one particle from the swarm can be chosen at random and all the dimensional values are changed randomly within limits. In the third position mutation scheme (PM_3), all the dimensional values are assigned same mutated values for the particle chosen for mutation. In the fourth position mutation scheme (PM_4), the dimensional values of the chosen particle are mutated either according to PM_1 strategy or PM_3 strategy. The decision to choose from PM_1 and PM_3 is done by generating a random value with uniform distribution between 0 and 1. PM_1 is chosen if the randomly generated number is greater than or equal to 0.5. PM_3 is chosen otherwise. It is normally observed that the fourth position mutation strategy is statistically more superior in performance compared to other position mutation strategies. As far as the boundary conditions are concerned, velocity clipping and position clipping procedures are applied. If the velocity for a particular particle along a dimension becomes zero, it is reinitialized to a velocity V_r which varies linearly over generations from V_{max} to $0.1V_{max}$.

4.2.7 Differential Evolution Algorithm with Random Scale Factor (DE/rand/1)

Differential Evolution (DE), [129] works by having a population of candidate vectors. These candidates explore the search-space by using simple mathematical formula to alter their positions by combining the positions of other candidates from the population. If the new position of the candidates provides some improvement, it is accepted and becomes part of the new population; otherwise the new position is discarded. The process is repeated until the goal is met or the

maximum number of iterations specified by the programmer has been tried. A brief outline of the algorithm is given below:

1. An initial population of target or parent vectors is generated. Let the population size be P. Each vector contains 'n' number of genes. Each gene represents a particular antenna dimension or parameter. Each gene can have values between the limits specified by the programmer. The cost values of each vector in the initial population are evaluated before starting the optimization process. Each gene is represented as $X_G(i,j)$ where G represents the generation number, i represents the i^{th} parent vector and j denotes the j^{th} gene of the parent vector. The following steps (2-4) are repeated until the maximum numbers of generations are over or the termination criterion is met.

2. For the i^{th} vector, three other vectors are chosen, different from 'i' and mutually exclusive in nature. An intermediate vector called the donor vector corresponding to $X_G(i, 1…….n)$ is formed according to the following equation and denoted as $V_G(i, 1…..n)$:

$$V_G(i,j) = X_G(n1,j) + F.(\left(X_G(n2,j) - X_G(n3,j)\right)) \quad (4.16)$$

where F is the scaling factor, its value being a random variable (with uniform distribution between 0 and 2).

3. The donor vector undergoes a binary crossover operation with the parent vector based on a crossover probability CR. This results in a corresponding trial vector $T_G(i,1…….n)$. A random number (y) is generated based on uniform probability distribution for every gene of the vector. 'j_{rand}' is a random whole number between 1 and n.

$$T_G(i,j) = V_G(i,j) if y \leq CR or j = j_{rand}$$
$$T_G(i,j) = X_G(i,j) otherwise \quad (4.17)$$

4. The trial vector is evaluated for its cost. If the trial vector has a lower cost than the corresponding parent vector $X_G(i,1……n)$, then the trial vector will replace the parent vector in the next generation.

4.2.8 Differential Evolution with Global and Local Neighborhood Search (DEGL)

Differential Evolution with Global and Local Neighborhood Search (DEGL) was proposed in [142]. Two terms namely global and local neighborhoods are introduced. Global neighborhood refers to the entire population during any generation of the algorithm. The candidates are assumed to be organized in a ring topology. For each candidate, a local neighborhood of size 'k' is defined. For each candidate vector, a local donor vector and a global donor vector are created from the two neighborhoods which are combined to yield the actual donor vector using a weight factor 'w' (determined by self adaptive algorithm [142]) which varies between 0 and 1.Once the actual donor vector is created, the rest of the DEGL optimization process i.e. generation of trial vectors and choosing parents for the next generation are same as DE/rand/1. The value of the weight factor is restricted between 0.05 and 0.95. A brief outline of the algorithm is given below:

1. An initial population of target or parent vectors is generated. Let the population size be P. Each vector contains 'n' number of genes. Each gene represents a particular antenna dimension or parameter. Each gene can have values between the limits specified by the programmer. The cost values of each vector in the initial population are evaluated before starting the optimization process. Each gene is represented as $X_G(i,j)$ where G represents the generation number, i represents the i^{th} parent vector and j denotes the j^{th} gene of the parent vector.

2. A neighborhood of radius 'k' is assumed around all individual vectors. All the individuals in the population are assumed to be arranged in a ring topology according to their indices. The value of 'k' can range from 0 to (P-1)/2. Since the cost of all the individual vectors are already evaluated, we identify the best vector in the neighborhood ($X_{local\_best}(i, 1…n)$)and globally best vector ($X_{global\_best}(i,1…n)$). The following steps (3-6) are repeated until the maximum numbers of generations are over or the termination criterion is met.

3. For the i^{th} vector, the donor vector is formed as a combination of local donor vector and global donor vector. The local donor vector formation involves the best vector in the neighborhood of the i^{th} vector and two other random vectors from the same neighborhood. Let these random vectors in the same neighborhood have indices 'p' and 'q'.

$$L_G(i,j) = X_G(i,j) + \alpha(X_G(Local\_best,j) - X_G(i,j) + \beta(X_G(p,j) - X_G(q,j)) \quad (4.18)$$

4. The global donor vector formation involves the global best vector and two other random vectors from the entire population. Let the random vectors have indices 'r' and 's'

$$G_G(i,j) = X_G(i,j) + \alpha(X_G(Global\_best,j) - X_G(i,j) + \beta(X_G(r,j) - X_G(s,j)) \quad (4.19)$$

5. The net donor vector is formed as a combination of local donor vector and global donor vector

$$V_G(i,j) = w.L_G + (1-w).G_G \quad (4.20)$$

where α and β are random variables (with uniform distribution between 0 and 1).

The weight 'w' should maintain a balance between the contributions from local donor vector and global donor vector. Each population vector has its own weighing factor $W_G(i)$.The value of the weighing factor is dynamically updated as given below:

$$w_G^{'}(i) = w_G(i) + F.\left(w_G(global_{best}) - w_G\ (i)\right) + F.(w_G(r1 - w_G(r2)) \quad (4.21)$$

6. The donor vector undergoes a binary crossover operation with the parent vector based on a crossover probability CR. This results in a corresponding trial vector $T_G(i,1…….n)$. A random number (y) is generated based on uniform probability distribution for every gene of the vector.

$$T_G(i,j) = V_G(i,j) if\ y \le CR\ or\ j = j_{rand}$$
$$T_G(i,j) = X_G(i,j) otherwise \quad (4.22)$$

7. The trial vector is evaluated for its cost. If the trial vector has a lower cost than the corresponding parent vector $X_G(i,1……n)$, the trial vector replaces the parent vector in the next generation.

4.3 Tuning of Optimization Algorithms

All the optimization algorithms for optimizing RHCP microstrip antennas with different feeding techniques are tuned for their optimal performance by using a meta-level position mutated hierarchical particle swarm optimization, as shown in Fig. 4.1. The population size for position mutated PSO is kept at 20. Algorithm-x (ALGx) refers to a particular optimization algorithm corresponding to a problem to be tuned. The meta-optimizer minimizes the mean cost of " N "

runs of the actual algorithm with different control parameter settings. The actual algorithm, in turn, optimizes the different dimensions of the RHCP microstrip antenna with a specified feed type. The number used in our case is N=20. The optimized mean cost over N runs obtained from the meta-PSO may not represent the true mean but the sample mean of the population. Hence, each optimized control parameter setting for an algorithm is re-verified by 50 runs of the algorithm with the same set of control parameters. PMn–HPSO (with position and velocity clipping boundary condition) does not require control parameter tuning [128].

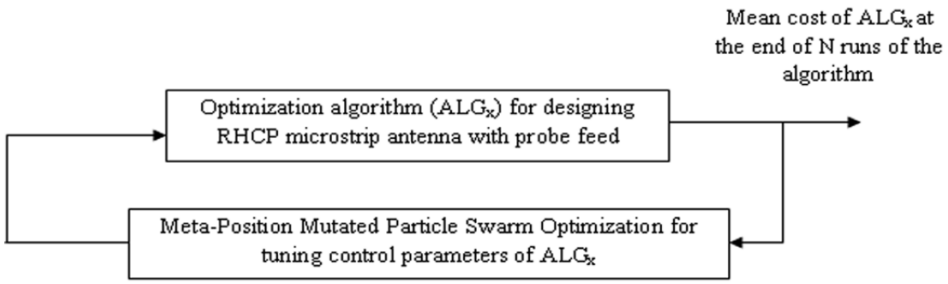

Fig. 4.1 Tuning process for optimization algorithms.

A meta-DEGL algorithm is used to find out the optimal value of control parameters in case of the optimization of unequally spaced linear array of isotropic elements in a similar way as mentioned above. A separate meta-DEGL scheme is used for this array since the parts of the algorithm performance results obtained will be used in the comparisons in the next chapter where all optimizations are exclusively based on DE algorithms. The DEGL algorithm is chosen for meta-optimization since it has shown very fast convergence for different numerical benchmark functions earlier [108]. The meta-DEGL algorithm uses F as a random variable, CR as 0.7 and a neighborhood radius of 20%. The meta–DEGL attempts to minimize the mean and standard deviation of 20 runs of the required algorithm with different values of control parameters. Statistical data from the values of control parameters near the optimal control parameter solution provided by the meta-optimizer are also computed to ensure and finalize the control parameter values of the algorithm which are best suited for the optimization problem.

The cost function evaluation for the 4 element Yagi-Uda antenna is very time consuming. Meta-optimization of the control parameters for the different optimization algorithms considered in

this chapter would have required extremely high computation time. Hence, the control parameters best suited for the optimization algorithms for this problem are determined by repeated trial and error procedure with values in close range around the ones mentioned in [129],[150],[142],[134],[107],[108],[102],[103],[123],[128].

4.4 Probe Fed Right Handed Circularly Polarized Microstrip Antenna

4.4.1 Theory

One of the simplest ways of exciting a microstrip antenna is to use the probe-feeding technique [3] shown in Fig.4.2. Five parameters are available for optimization in this case, (a) the length and (b) the width of the patch, coordinates of probe feed (x_o,y_o), and the height of the substrate (h). The substrate used has a dielectric constant of 2.5.

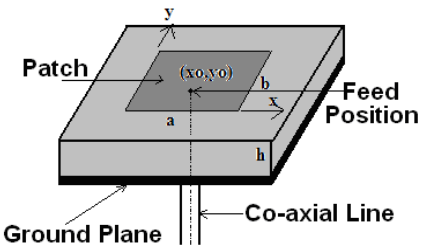

Fig 4.2 Probe fed circularly polarized microstrip antenna

The present optimization problem is of multi objective nature where several criteria for a right handed circularly polarized antenna are to be satisfied. The first objective requires that the antenna should be impedance matched over a certain frequency range chosen from 2.25 to 2.55 GHz with a substrate height varying between 0.5 and 6.0 mm. The corresponding cost function for impedance matching can be written as:

$$Cost_1 = \frac{1}{n}\sum_{f_L}^{f_U} |\tau_i| \qquad (4.23)$$

Where τ_i is the reflection coefficient at the i^{th} frequency, and n is the number of frequency points within the frequency range.

Circular polarization at the center frequency of the antenna in the bore sight direction requires that the electric field phasor in the far field at the bore sight direction due to the radiation from the antenna should have two mutually perpendicular components (E_{xo} and E_{yo}), both equal in amplitude but having phase difference $\pi/2$ between them [3]. Hence, the corresponding costs can be defined as:

$$Cost_2 = |\frac{E_{xo}}{E_{yo}} - 1|^2 \quad (4.24)$$

$$Cost_3 = |\angle E_{xo} - \angle E_{yo} - \frac{\pi}{2}| \quad (4.25)$$

The fourth objective that is to be satisfied is the one for gain of the antenna in the bore sight direction at the center frequency. The gain is a calculated by evaluating the directivity and efficiency of microstrip antenna as in [3].

$$Cost_4 = \frac{1}{Gain} \quad (4.26)$$

All the individual costs described above are combined into a single cost by assigning dynamically varying weights to each of them.

$$Cost = w_1.Cost_1 + w_2.Cost_2 + w_3.Cost_3 + w_4.Cost_4 \quad (4.27)$$

Equal distribution of weights causes the optimization algorithm to randomly prefer one or some of the objectives and neglect others. Biased weight distribution does not always guarantee that all the objectives will satisfy at least to a threshold level. A fuzzy-rule based model for weight distribution is used here which will cause the corresponding weights for each objective to dynamically vary in each generation according to certain fuzzy rules . The weights are assigned initial values randomly between 0 and 1 to start the algorithm. Whenever any one of the objectives goes above a threshold value, the dynamic weight allocated to it is simultaneously augmented to temporarily provide more preference to it. The thresholds for the probe-fed RHCP antennas are an average $S_{11}$of -10 dB (maximum) over the entire frequency range, an axial ratio of 2 dB (maximum), and a gain of 5 dBi (minimum) at the center frequency respectively.

4.4.2 Experimental Results

The optimization of the probe fed patch antenna is carried out with the objectives discussed above. The substrate height is allowed to vary from 0.5 to 6.0 mm. The dimensions of the antenna are optimized using the mentioned eight optimization schemes in Section II. The algorithms are run for 50 independent trials, and their statistical performance measures are estimated and indicated in Table 3.2. The control parameters for the algorithms are given in Table 3.1. All the algorithms use the same initial population. The best algorithm adjudged from the statistical performance table will be further used to design and simulate the antenna with available substrate of same dielectric constant and thickness of 0.76mm for testing and validation.

Table 4.1. Control parameter settings of the bio-inspired optimization algorithms for the optimization of probe fed RHCP microstrip antenna

Optimization algorithms	Control Parameter Settings
Real coded genetic algorithm (Real GA)	Crossover probability=1 Mutation probability=0.1
Quantum genetic algorithm (QGA)	Crossover probability=1 Mutation probability=0.04
Improved genetic algorithm (IGA)	Crossover probability=1 Mutation Probability=0.05
Particle swarm optimization(PSO)	C_1=1.8458 C_2=1.6865 Damping boundary conditions are used. Linearly decreasing inertial weight used.
Improved Comprehensive learning particle swarm optimization (CLPSO)	Loser group size =6 Hybrid periodic boundary conditions are used. Other parameters same as in [123].
Position mutated hierarchical particle swarm optimization (PMn-HPSO)	Parameters same as in [128].

Optimization algorithms	Control Parameter Settings
Differential evolution with random scale factor (DE/rand/1)	F=random number between 0 and 2 with uniform probability density function distribution. CR=0.98
Differential evolution with global and local neighborhood search (DEGL)	Crossover probability=0.60 Neighborhood size~40%.

The statistical performances of the algorithms are given in Table 4.2.

Table 4.2. Statistical performances of the bio-inspired algorithms in the optimization of probe fed RHCP microstrip antenna.

Optimization algorithms	Mean cost value	Best cost value	Worst cost value	Standard deviation	Robustness (%)	Convergence rate(iterations)
Real GA	0.1054	0.1004	0.1102	0.0024	100	24
QGA	0.1402	0.1103	0.2071	0.0219	72	71
IGA	0.1237	0.1080	0.1981	0.0186	92	49
PSO	0.0979	0.0967	0.1037	0.0022	100	17
CLPSO	0.1203	0.1056	0.1535	0.0121	92	90
PMn-HPSO	0.1076	0.0967	0.1151	0.0028	100	23
DE/rand/1	0.0967	0.0966	0.0972	1.16e-4	100	28
DEGL	0.0966	0.0966	0.0967	1.36e-5	94	11

The conventional real coded GA and PSO with properly tuned control parameters outperform their advanced schemes in this optimization problem. Real coded GA, QGA, and IGA have crossover probability 1.0 and mutation probabilities 0.1, 0.04, and 0.05, respectively. Out of all, DEGL (crossover probability 0.60) emerges as statistically superior having the lowest mean and standard deviation. DE/rand/1 (crossover probability = 0.98) is outperformed in terms of standard deviation and convergence rate but has higher robustness compared with DEGL. PSO

(using decreasing inertial weight from 0.9–0.4, social and cognitive rates 1.8458 and 1.6865 with damping wall boundary conditions) has the second fastest convergence rate and outperforms improved CLPSO (using loser group size of 6 and mutation probability 0.04 with hybrid periodic boundary conditions) as well as PMn–HPSO (using mutation strategy 4 as in [128]). QGA optimization gives the highest mean, standard deviation, and comparatively low robustness. DEGL (crossover probability 0.84) is seen to have the fastest convergence rate. The convergence graphs of all the optimization algorithms are depicted in Fig. 4.3.

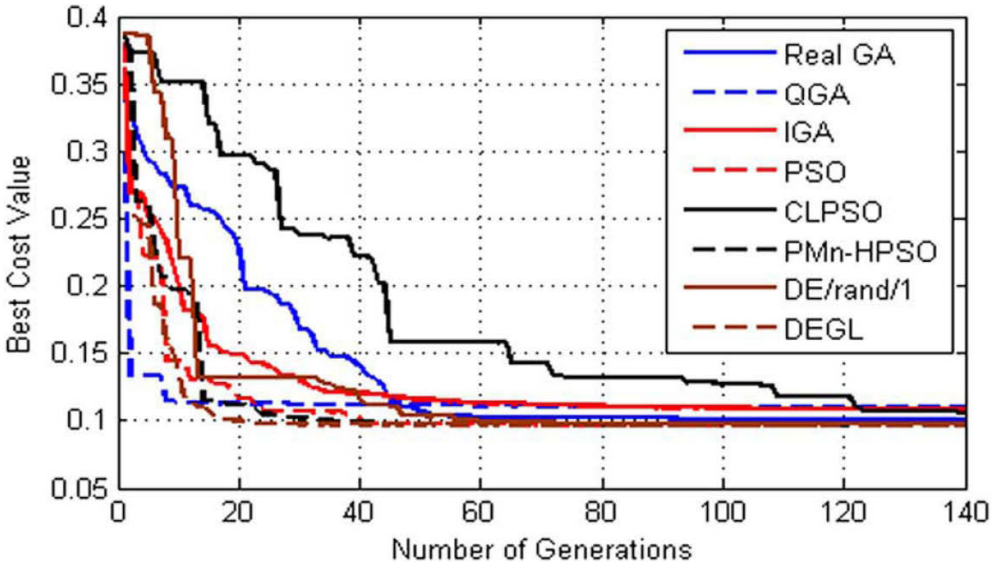

Fig 4.3 Best convergence plots for the optimization algorithms in the optimization of RHCP probe fed microstrip antenna

The mean cost convergence curves are shown below in Fig. 4.4:

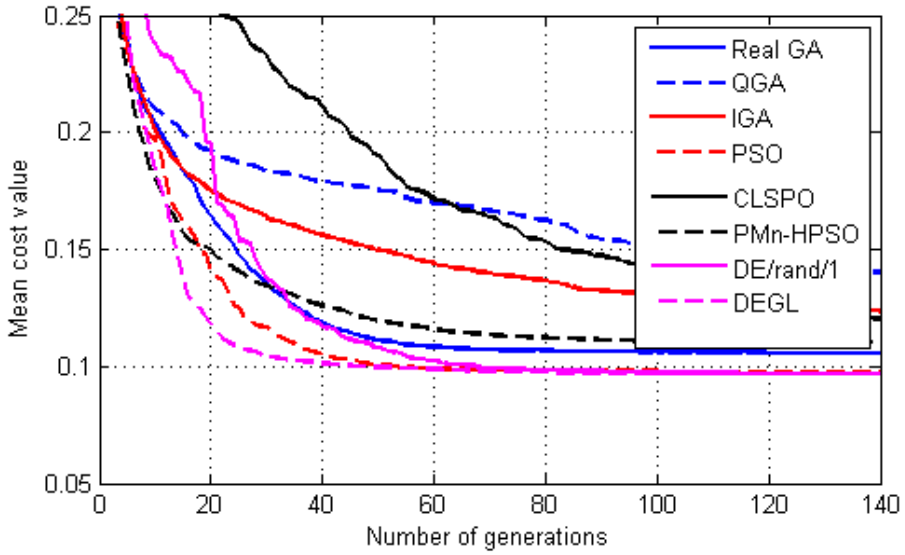

Fig 4.4 Mean convergence plots for the bio-inspired optimization algorithms in the optimization of RHCP probe fed microstrip antenna

Performance measures of the antennas obtained from the best run of each algorithm are given in Table 3.2. The optimized antenna from DEGL has a= 34.76 mm, b=38.20 mm, h= 5.15 mm, and the probe feed is located at (11.96 mm, 9.59 mm) from the lower left vertex. It shows an impedance bandwidth of 252 MHz, with the axial ratio and gain being 1.49 dB and 5.67 dBi at the center frequency, respectively. The lowest axial ratio is obtained with CLPSO, although it has lower impedance bandwidth.

The antenna performances obtained from the best run of reach algorithm are given in Table 4.3.

Table 4.3. Performances of the optimized probe fed RHCP microstrip antennas obtained from the best run of each bio-inspired optimization algorithm.

Optimization algorithms	Impedance Bandwidth(MHz)	Mean S_{11}in the frequency range (dB)	Axial ratio at 2.4 GHz (dB)	Gain at 2.4 GHz (dBi)
Real GA	234.34	-13.39	1.4840	5.72
QGA	201.74	-11.47	1.7169	5.82
IGA	201.58	-11.53	1.6525	5.83

Optimization algorithms	Impedance Bandwidth(MHz)	Mean S_{11}in the frequency range (dB)	Axial ratio at 2.4 GHz (dB)	Gain at 2.4 GHz (dBi)
PSO	252.03	-14.35	1.4920	5.67
CLPSO	222.44	-13.30	1.3806	5.74
PMn-HPSO	252.03	-14.35	1.4920	5.67
DE/rand/1	252.03	-14.35	1.4920	5.67
DEGL	252.03	-14.35	1.4920	5.67

Depending on the above statistical measures, we consider DEGL to be the best optimization algorithm for this problem, and it is used to optimize a similar antenna with our available substrate having dielectric constant 2.5 and substrate height 0.76 mm. It has dimensions a=38.52 mm, b=38.99 mm, and probe feed at (13.66 mm, 13.94 mm) from the lower left vertex. Simulation results indicate an impedance bandwidth of 38.40 MHz, an axial ratio of 1 dB, and a gain of 5.41 dBi. It is fabricated, and the measured impedance bandwidth and axial ratio are 37.30 MHz and 1.06 dB, respectively. Gain is 5.3 dBi at the center frequency. The S_{11} and axial ratio variations with frequency for the fabricated antenna (simulated and measured data) are shown in Fig.4.5 and Fig. 4.6 respectively. The fabricated prototype of the probe fed microstrip antenna is shown in Fig. 4.7.

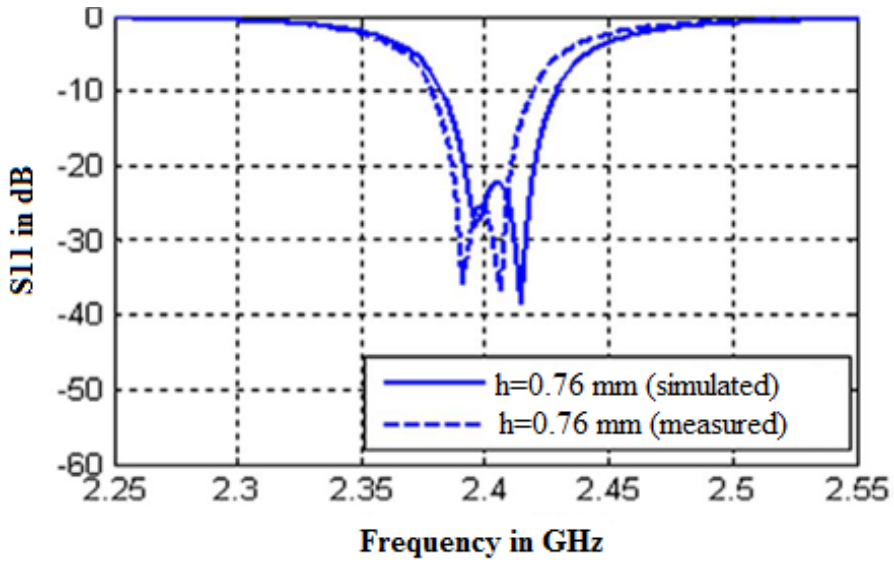

Fig 4.5 Simulated and measured S_{11} versus frequency plot for the probe fed RHCP microstrip antenna with substrate height of 0.76 mm

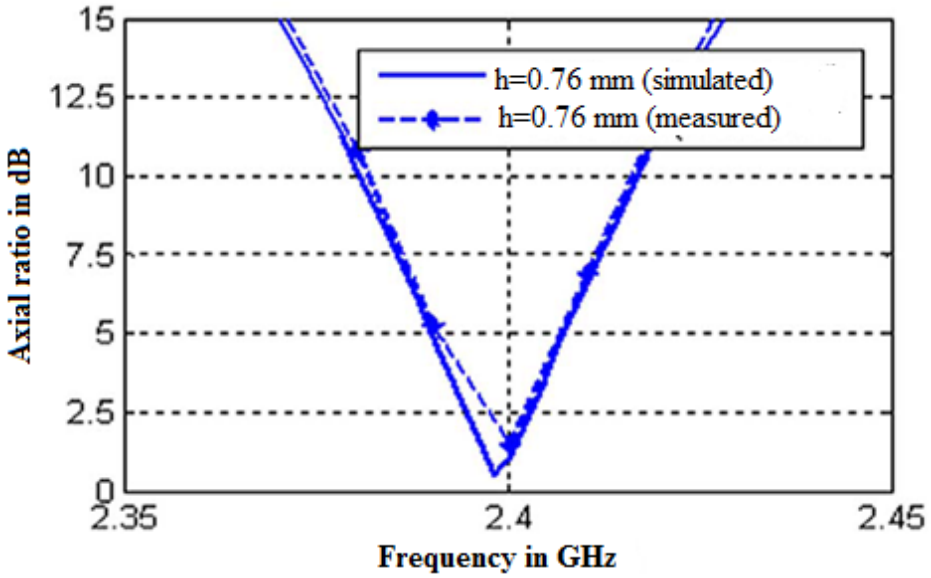

Fig. 4.6 Simulated and measured axial ratio versus frequency plot for the probe fed RHCP microstrip antenna with substrate height of 0.76 mm

The fabricated prototype of the antenna is given in Fig. 4.7.

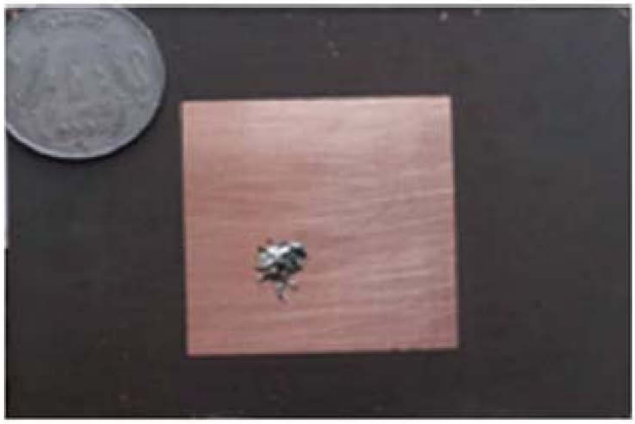

Fig 4.7 Fabricated prototype of the probe fed RHCP microstrip antenna from the best run of DEGL algorithm.

4.5 Transmission Line Fed Microstrip Antenna for Circular Polarization

4.5.1 Theory

Another simple way of exciting a microstrip antenna is through the use of transmission line-feeding network in Fig. 4.8. Different transmission linefeed networks involving power dividers [3] are available in literature, but most of them require the design of the antenna with 2-port feed networks. The feed network employs five transmission line sections. Section-n has length L_n and width W_n. Each of the discontinuities is taken into consideration using the multiport network modeling technique (MNM) and the usual cavity model of the patch as in the previous section. The parameters to be independently optimized for the antenna are: a, b, L_1, L_2, L_5, W_1-W_5 and h. From the diagram, L_3 and L_4 are given as:

$$L_3 = (L_1 - W_2) + \frac{a}{2} + \frac{W_4}{2} \quad (4.28a)$$

$$L_4 = \left(L_2 + \frac{W_1}{2}\right) - \left(\frac{b}{2} + W_3\right) \quad (4.28b)$$

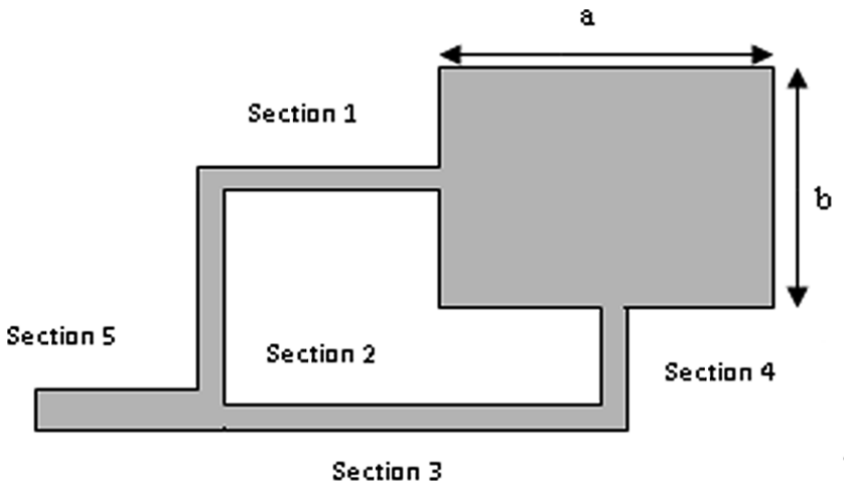

Fig 4.8 Transmission line fed circularly polarized microstrip antenna

The antenna structure shown in the figure above is analyzed using multiport network modeling approach [3] so that the microstrip line discontinuity effects can be taken in to account. The feed line network has five straight microstrip line segments numbered from one to five as shown in the figure above. Each segment has its own length and width to be optimized for the objectives described below. For example segment 1 has length L_1 and width W_1 and so on. The dimensions of the nearly square patch antenna are 'a' x'b'.

As already mentioned, the structure is analyzed using the multiport network modeling method and cavity modeling method. Different ports are defined at the microstrip interconnections and junctions in the figure above. The Z-matrix needs to be computed for the multiport network model. The matrix value for any two ports (for example 'i' and 'j') associated with the same microstrip segment can be calculated as [3]:

$$Z_{ij}^{s} = \frac{1}{W_i W_j} \iint_{PW_i PW_j} G^{S}(s, s_o) ds ds_o \qquad (4.29)$$

Z_{ij} represents the (i, j) element of the impedance matrix. W_i and PW_i represent the effective width and physical width of the i^{th} port. Similarly W_j and PW_j represent the effective width and physical width of the j^{th} port. The effective widths are calculated after taking into account the fringing field extensions along the edges of the microstrip structure. It is assumed that the microstrip planar structure is placed on the x-y plane above a substrate of dielectric constant ε

and height ‘h’. The substrate layout is assumed to be infinite along x and y axis and is placed on an infinite ground plane. $G^s(s,s_o)$ represent the Green’s function which has the following form [3]:

$$G_s(x,y|x_o,y_o) = \frac{j\omega\mu h}{ab}\sum_{m=-\infty}^{+\infty}\sum_{n=-\infty}^{+\infty}\frac{\psi^s_{mn}(x,y)\psi^{s*}_{mn}(x_o,y_o)}{k^2_{mn}-k^2} \quad (4.30)$$

where $\psi^s_{mn}(x,y)$ represent the Eigen function of the (m,n) mode of the microstrip segment under consideration and k_{mn} is the corresponding Eigen-value. For a rectangular microstrip segment the Eigen function is given by [3]:

$$G(x,y|x_o,y_o) = \frac{j\omega\mu h}{a'b'}\sum_{m=-\infty}^{+\infty}\sum_{n=-\infty}^{+\infty}\frac{\sigma_m\sigma_n}{k_x^2+k_y^2-k^2}\cos(k_x x)\,cos(k_x x_o)\cos(k_y y)\cos(k_y y_o) \quad (4.31)$$

where the parameter σ_m=1 if m=0 otherwise σ_m=1. This also holds true for σ_n.

Also,

$$k_x = \frac{m\pi}{a'} \quad (4.32a)$$

$$k_y = \frac{n\pi}{b'} \quad (4.32b)$$

$$k^2 = \omega^2\mu_o\varepsilon_o\varepsilon_{eff} \quad (4.32c)$$

‘a’ and b’ are the dimensions (along x-axis and y-axis) of the microstrip segment under consideration.

4.5.2 Experimental Results

The optimization of the transmission line-fed patch antenna was carried out with the objectives explained earlier. The substrate height is allowed to vary from 0.5 to 6.0 mm. The algorithms are run for 50 independent trials and their statistical performance measures are estimated and indicated in Table 4.5. The convergence graphs for the best run of each algorithm are given below in Fig. 4.9:

The initial conditions for the algorithms in this optimization problem are similar to those of the previous one. The best algorithm adjudged from the statistical performance table will be further used to design and simulate the antenna with available substrate of same dielectric constant and thickness of 0.76mm for testing and validation. The threshold values of the transmission line fed RHCP microstrip antennas are an average S_{11} of -8 dB (maximum) over the stipulated frequency band, and an axial ratio and gain of 3 dB (maximum) and 5 dBi (minimum)at the center frequency in the bore sight direction respectively.

The control parameter settings of the optimization algorithms are given in the Table 4.4 below:

Table 4.4. Control parameter settings of the bio-inspired optimization algorithms for the optimization of transmission line fed RHCP microstrip antenna

Optimization algorithms	Control Parameter Settings
Real coded GA	Crossover probability=1 Mutation probability=0.098
Quantum GA	Crossover probability=1 Mutation probability=0.081
Improved GA	Crossover probability=1 Mutation probability=0.046
Particle Swarm Optimization	C_1=2.1236 C_2=1.7022 Linearly deceasing inertial weight Damping wall boundary conditions
Improved comprehensive Learning PSO	Loser group size=4 Hybrid periodic boundary condition[123]
Position mutated hierarchical PSO	Parameters as in [128]
DE/rand/1	Crossover probability=0.99
DEGL	Crossover probability=0.54 Neighborhood size~40%.

The statistical performances of the algorithms are given in Table 4.5.

Table 4.5. Statistical performances of the bio-inspired optimization algorithms in the optimization of transmission line fed RHCP microstrip antenna.

Optimization algorithms	Mean cost value	Best cost value	Worst cost value	Standard deviation	Robustness (%)	Convergence rate(iterations)
Real GA	0.1335	0.1173	0.1936	0.0155	100	35
QGA	0.1583	0.1281	0.2134	0.0214	92	47
IGA	0.1806	0.1259	0.2113	0.0262	76	44
PSO	0.1344	0.1015	0.1909	0.0295	100	52
CLPSO	0.1866	0.1319	0.2541	0.0388	52	78
PMn-HPSO	0.1438	0.1103	0.2349	0.0355	88	65
DE/rand/1	0.1171	0.1081	0.1381	0.0075	100	44
DEGL	0.1168	0.1074	0.1503	0.0095	100	37

The conventional GA and PSO schemes again outperform their advanced schemes as before. Real GA, QGA, and IGA have crossover probability 1.0 and mutation probabilities 0.098, 0.081, and 0.046, respectively. The PSO found to work better is the decreasing inertial weight PSO [107] with damping wall boundary condition having social and cognitive rates tuned to 2.1236 and 1.7022 respectively. CLPSO used a loser group size of 4 with mutation probability 0.05 along with the hybrid periodic boundary condition. The crossover probabilities of DE/rand/1 and DEGL are tuned to 0.99 and 0.54, respectively. Real coded GA has performed statistically better than the conventional PSO as indicated by their mean and standard deviation in Table 3.5. DEGL has the lowest mean cost and highest robustness. It is second best in convergence rate, with real coded GA being the fastest. The performance of DE/rand/1 is very similar to that of DEGL. Considering the above facts, DEGL can be considered statistically most suited for this optimization problem. The best convergence cost convergence graphs of all the optimization algorithms are depicted in Fig. 4.9.

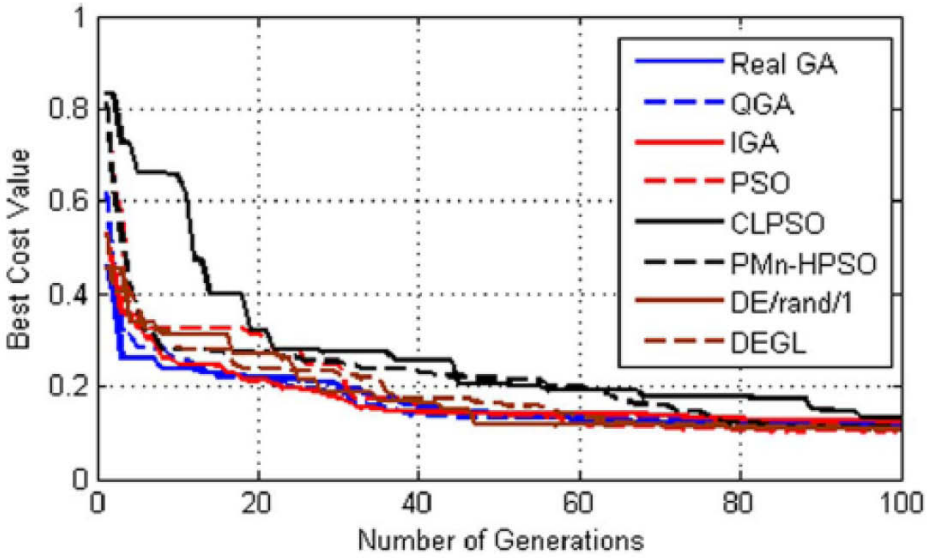

Fig 4.9 Best convergence plots for the bio-inspired optimization algorithms in the design of transmission line fed RHCP microstrip algorithms

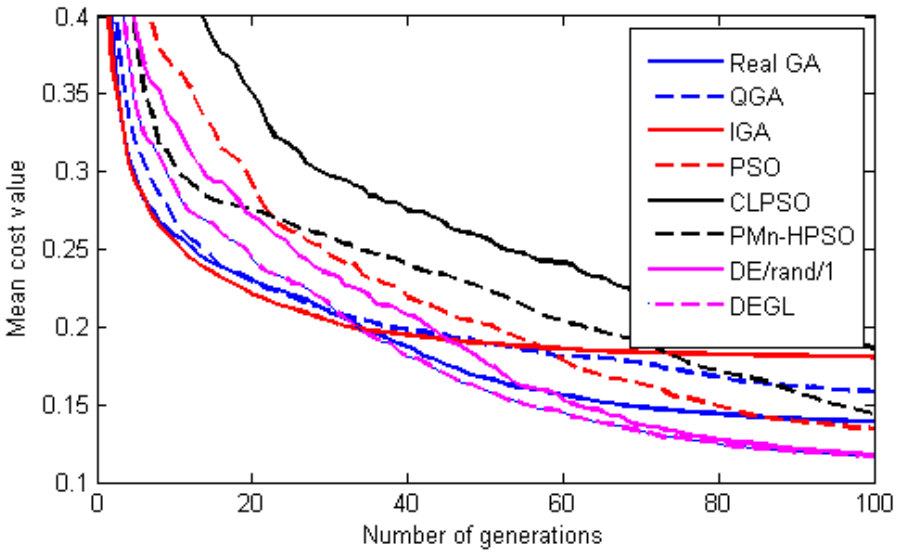

Fig 4.10 Mean convergence plots for the bio-inspired optimization algorithms in the design of transmission line fed RHCP microstrip antenna

The antenna performances obtained from the best run of reach algorithm are given in Table 4.6.

Table 4.6. Performances of the optimized transmission line fed RHCP microstrip antennas obtained from the best run of each bio-inspired optimization algorithm.

Optimization algorithms	Impedance Bandwidth(MHz)	Mean S_{11} in the frequency range (dB)	Axial ratio (2.4 GHz)	Gain (2.4 GHz)(dBi)
Real coded GA	142.50	-8.82	2.37	5.47
QGA	135.00	-8.53	2.95	5.29
IGA	136.50	-8.70	2.68	5.47
PSO	176.00	-10.43	1.88	5.39
CLPSO	128.00	-8.24	2.99	5.10
PMn-HPSO	160.00	-9.51	2.13	5.45
DE/rand/1	164.00	-9.58	1.93	5.41
DEGL	168.00	-9.93	1.95	5.41

DEGL optimized antenna has good impedance matching within the given frequency range, having an impedance bandwidth of 168 MHz, axial ratio of 2.07 dB, and gain equal to 5.41 dBi at 2.4 GHz. The antenna has dimensions (mm) given by (a, b, h)= (35.74, 38.74, 4.00), (L_1,W_1)= (40.52, 0.76), (L_2, W_2)= (39.61, 11.56), (L_3,W_3)= (47.89,7.41), (L_4,W_4)=(14.71,2.12), (L_5,W_5)=(25.38,8.58).Using DEGL with tuned control parameters, we optimized and fabricated the RHCP microstrip antenna with the available substrate as used in the previous section. It has dimensions (mm) (a, b ,h)= (38.73, 39.64, 0.76), (L_1 ,W_1)=(10.92,1.60), (L_2,W_2)=(53.15, 0.50), (L_3, W_3)=(30.86, 1.26), (L_4,W_4)= (37.53, 2.14) and (L_5, W_5)=(16.39, 3.30). The S_{11} and axial ratio variation with frequency for the fabricated antenna (simulated and measured results) are shown in Fig. 4.11 and Fig. 4.12 respectively. Simulation results indicate an impedance bandwidth of 35.87 MHz, axial ratio of 1.2 dB, and gain of 5.3 dBi. The fabricated antenna 0.76 mm has an impedance bandwidth of 38 MHz, and an axial ratio and gain being 2.22 dB and 5.21 dBi at the center frequency. The fabricated prototype of the transmission line-fed microstrip antenna is shown in Fig. 4.13.

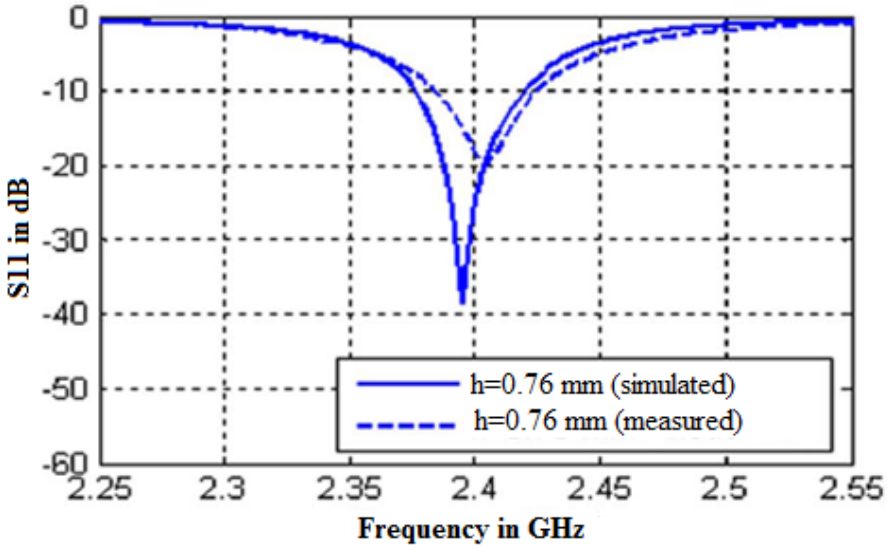

Fig. 4.11 Simulated and measured S_{11} versus frequency plot for the transmission line fed RHCP microstrip antenna with substrate height of 0.76 mm

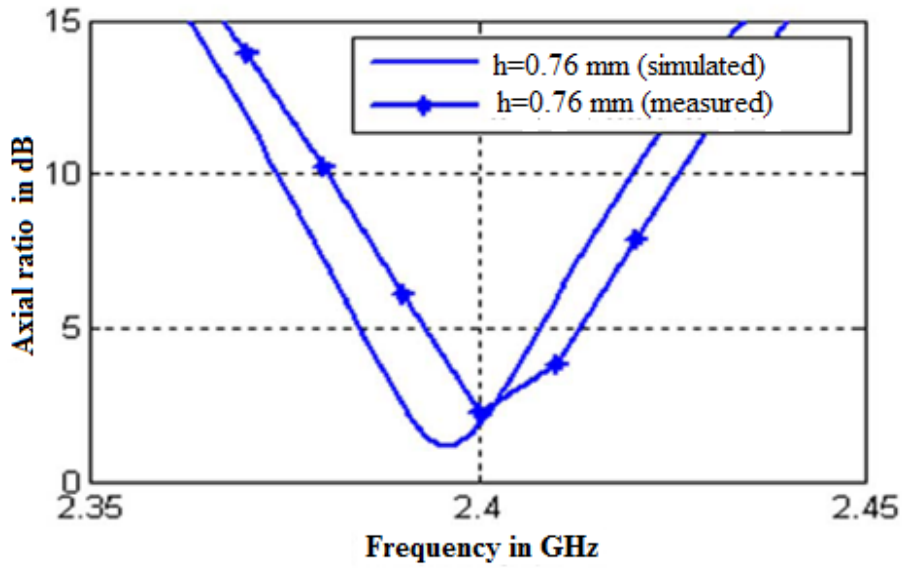

Fig. 4.12 Simulated and measured axial ratio versus frequency plot for the transmission line fed RHCP microstrip antenna with substrate height of 0.76 mm

The fabricated prototype of this antenna is shown in Fig. 4.13 below:

Fig. 4.13 Fabricated prototype of the transmission line fed RHCP microstrip antenna obtained from the best run of DEGL.

4.6 Cross Aperture Coupled Microstrip Antenna for Circular Polarization

4.6.1 Theory

An aperture coupled patch antenna provides a wide range of parameters described below for optimization in terms of impedance bandwidth, axial ratio, and gain. One inherent advantage of using the aperture feeding technique is the separate optimization for the patch structure and the feed line, which often helps in maintaining impedance matching over a wide range of frequencies. Different analytical methods are used for estimating the aperture coupled antenna parameters in the past [21]–[37]. The cost or objective values in our case are derived using the cavity model in [37]. The top and side views of the antenna are shown below in Fig. 4.14. The substrate parameters remain the same as before.

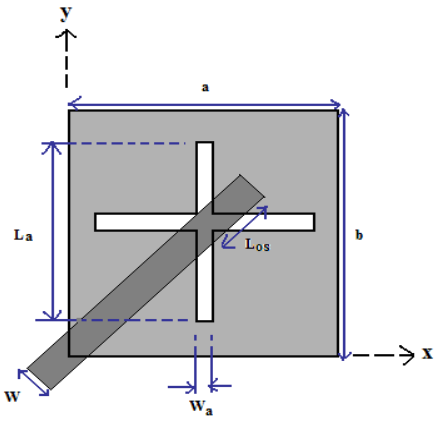

(a) Top view

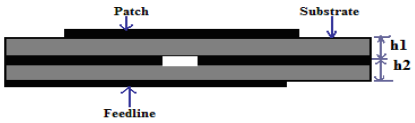

(b)Side view

Fig. 4.14 Cross aperture coupled RHCP microstrip antenna

4.6.2 Experimental Results

The optimization of the cross slotted patch antenna was carried out with the same objectives explained in probe fed rectangular RHCP microstrip antenna. The threshold values of average $S_{11}$and the axial ratio of the cross-aperture coupled RHCP antenna is the same as that of probe-fed antenna, except the gain whose threshold limit is taken to be 6 dBi (minimum) at the center frequency in the bore sight direction. The initial conditions for the algorithms in this optimization problem are similar to those of the previous one. The optimization of the cross slotted patch antenna was carried out with the same objectives explained earlier. The algorithms are run for 50 independent trials. The control parameter settings of the algorithms and their statistical performance measures are estimated and indicated in Table 4.7 and Table 4.8 respectively.

Table 4.7. Control parameter settings of the bio-inspired optimization algorithms for the optimization of aperture coupled RHCP microstrip antenna

Optimization algorithms	Control Parameter Settings
Real coded GA	Crossover probability=1 Mutation probability=0.02
QGA	Crossover probability=1 Mutation probability=0.04
IGA	Crossover probability=1 Mutation probability=0.05
PSO	C_1=1.92 C_2=2.18 Linearly decreasing inertial weight Damping wall boundary conditions
CLPSO	Loser group=4 Other parameters as in [123]
PMn-HPSO	Parameters used as in [128]
DE/rand/1	Crossover probability=0.98
DEGL	Crossover probability=0.69 Neighborhood size~40%.

The statistical performances of the algorithms are given in Table 4.8.

Table 4.8. Statistical performances of the bio-inspired optimization algorithms for the optimization of cross aperture coupled RHCP microstrip antenna.

Optimization algorithms	Mean cost value	Best cost value	Worst cost value	Standard deviation	Robustness (%)	Convergence rate(iterations)
Real GA	0.5542	0.5483	0.5653	0.0074	50	22
QGA	0.5534	0.5483	0.5663	0.0063	96	50
IGA	0.5518	0.5483	0.5653	0.0049	60	31

Optimization algorithms	Mean cost value	Best cost value	Worst cost value	Standard deviation	Robustness (%)	Convergence rate(iterations)
PSO	0.5491	0.5483	0.5569	0.0018	100	42
CLPSO	0.5525	0.5487	0.5623	0.0032	20	87
PMn-HPSO	0.5498	0.5483	0.5653	0.0040	84	47
DE/rand/1	0.5484	0.5483	0.5490	1.86e-04	60	80
DEGL	0.5483	0.5483	0.5484	1.55e-05	96	28

Real coded GA, QGA, and IGA have crossover probability 1.0 as before but mutation probabilities equal to 0.02, 0.04, and 0.05 respectively. Unlike the previous cases, IGA outperforms QGA, and QGA outperforms real GA in terms of mean and standard deviation. The convergence rate is fastest for real GA and robustness is highest for QGA among the three. The PSO found to be suited best is the constriction factor PSO [107] with C_1=1.92 and C_2=2.18 along with damping wall boundary conditions. PSO outperforms PMn-HPSO (using mutation strategy 4) and CLPSO (with loser group size of 4 and mutation probability 0.05). As seen from Table 4.8, the performance of DEGL is statistically best among all in all respects. DE/rand/1 is outperformed by DEGL in terms of convergence rate and robustness. Crossover probabilities of DE/rand/1 and DEGL are tuned to 0.98 and 0.69, respectively. The convergence graphs for the different algorithms obtained from the best run of each algorithm are given in Fig. 4.18 and Fig. 4.19 respectively. Real GA, QGA, IGA, PSO, PM -HPSO and DEGL yielded same antenna performance obtained from their best run as given in Table 4.8. DEGL is justified to be the statistically best algorithm in this case.

The best cost convergence plots are shown in Fig. 4.15below:

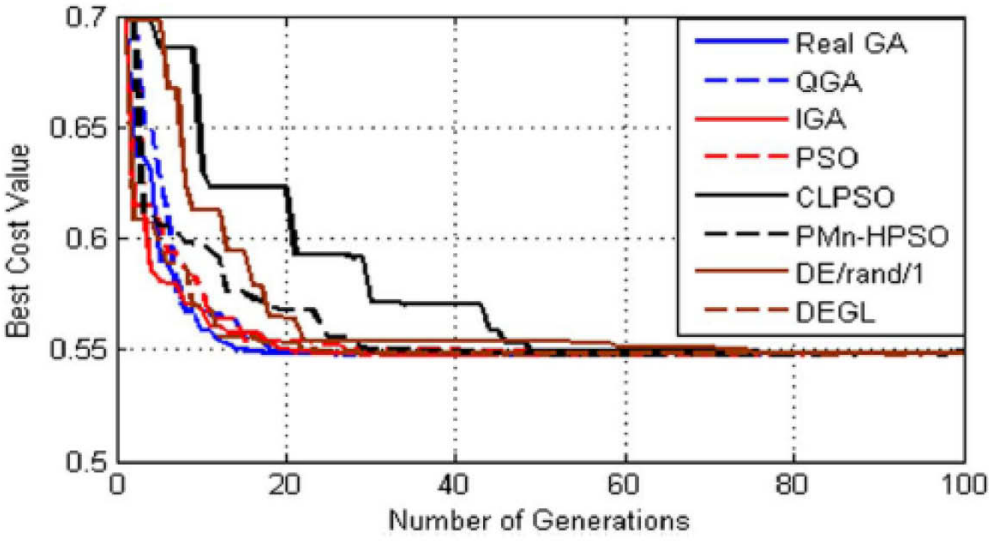

Fig. 4.15 Best convergence plots for the bio-inspired optimization algorithms in the optimization of RHCP cross aperture coupled microstrip antenna

The mean cost convergence plots are shown below in Fig 4.16.

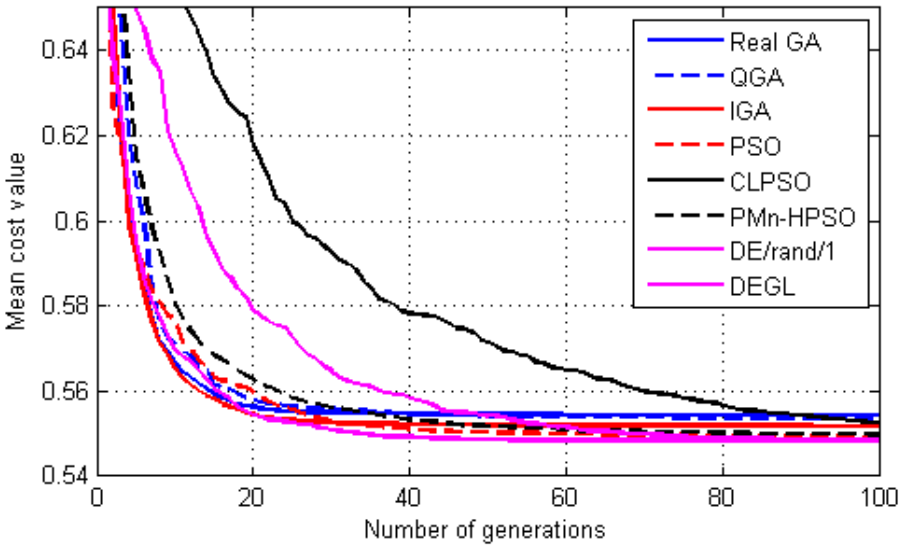

Fig 4.16 Mean convergence plots for bio-inspired optimization algorithms in the optimization of RHCP cross aperture coupled microstrip antenna

The performances of the optimally designed antennas obtained from the best run of each algorithm are given in Table 4.9.

Table 4.9.The optimal cross aperture coupled RHCP microstrip antenna performances obtained from the best run of each bio-inspired optimization algorithm:

Optimization algorithms	Impedance Bandwidth (MHz)	Mean S_{11} in the frequency band (dB)	Axial ratio(2.4GHz) (dB)	Gain (2.4 GHz) (dBi)
Real GA	268.65	-13.90	1.54	6.06
QGA	264.18	-13.90	1.54	6.06
IGA	264.18	-13.90	1.54	6.06
PSO	274.62	-13.90	1.54	6.06
CLPSO	280.00	-13.86	1.62	6.08
PMn-HPSO	276.00	-13.90	1.54	6.06
DE/rand/1	280.00	-13.90	1.54	6.06
DEGL	271.00	-13.90	1.54	6.06

The dimensions of the antenna (in millimeters) obtained from its best run are a=32.40, b=35.34, h=5.37 , L_a=18.90 , W_a=1.01 , W=3.98, and L_{os}=7.87. It shows an impedance bandwidth of 271 MHz, with the axial ratio and gain being 1.54 dB and 6.06 dBi at the center frequency, respectively. DEGL is also used to optimize and fabricate an antenna using the available substrate. The fabricated antenna has dimensions (in millimeters) given as a=37.24, b=37.68, h=0.76 mm, L_a=9.28, W_a=1.33, W=2.87 and L_{os}=16.05. Simulation results indicate an impedance bandwidth of 36.50 MHz, with an axial ratio of 1.7 dB and gain of 5.8 dBi. It has measured impedance bandwidth of 34.17 MHz, with the axial ratio and gain being 1.64 dB and 5.66 dBi at the center frequency of 2.4 GHz. The S_{11} and axial ratio variation with frequency for the fabricated antenna (simulated and measured results) are given in Fig. 4.17 and Fig. 4.18 respectively. The fabricated prototype of the cross-aperture coupled circularly polarized microstrip antenna is shown in Fig. 4.19.

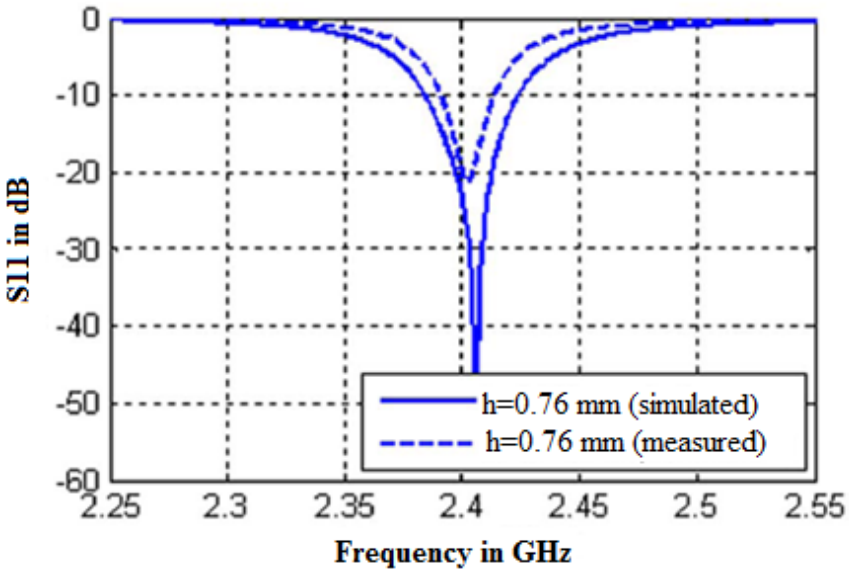

Fig. 4.17 Simulated and measured S_{11} versus frequency for the aperture coupled microstrip antenna with substrate height of 0.76 mm

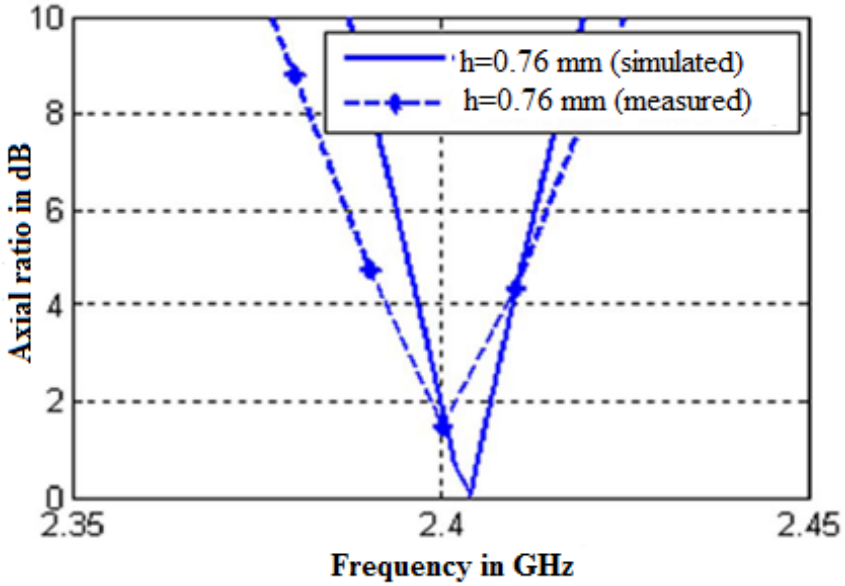

Fig. 4.18 Simulated and measured axial ratio versus frequency for the aperture coupled microstrip antenna with substrate height of 0.76 mm

The fabricated prototype of the cross-aperture coupled circularly polarized microstrip antenna is shown in Fig. 4.19.

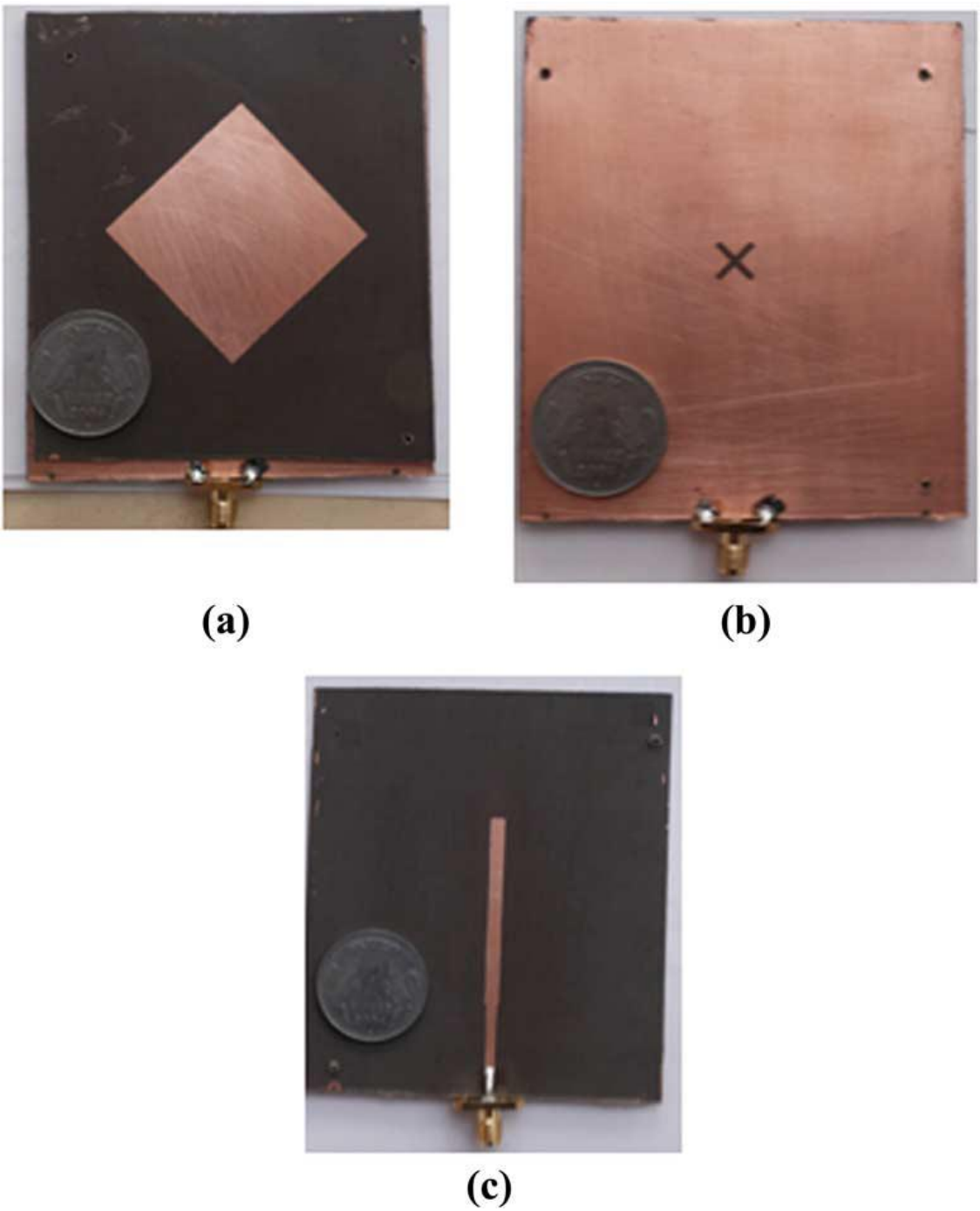

Fig. 4.19 Fabricated prototype of the cross-aperture coupled microstrip antenna from the best run of DEGL algorithm

4.7 Linear Array of Unequally Spaced Isotropic Antenna Elements

4.7.1 Theory

A linear array of unequally spaced linear antenna elements is shown in the Fig. 4.20. The array has unequal inter-element spacing between the adjacent elements. 16 isotropic antenna elements are used in this optimization case study. The arrangement of the array is assumed to be symmetric about the center of the array. Hence only 8 variables or 8 inter-element spacing are to be optimized. The lower and upper boundaries of inter-element spacing are assumed to be 0.5λ and 1λ respectively to avoid mutual coupling and grating lobe effects:

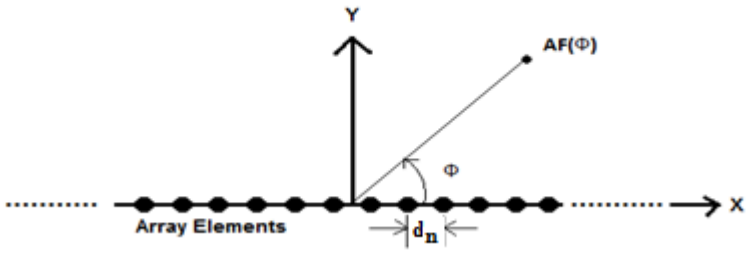

Fig.4.20 Geometry of unequally spaced linear array of isotropic elements

If all the antenna elements are assumed to be isotropic, then the array factor (AF) of the antenna can be written as:

$$AF = \sum_{n=-N}^{n=+N} A_n e^{[jk(dd_n)cos(\phi)+n\alpha]} \quad (4.33)$$

A_n is the excitation amplitude of the n^{th} antenna element (N=8 in (6.1)), k is the wave number, dd_n is the distance of the n^{th} antenna element from the center of the array, α is the progressive phase shift between elements (here α =0) and φ is the scan angle. Normalized power pattern P (φ) can be expressed in terms of array factor as given below:

$$P(\Phi) = 20\ log_{10}(AF(\Phi)/AF(\Phi)max) \quad (4.34)$$

The design objectives are to minimize the beam width between first nulls, maximum value of side-lobe level in the elevation plane of the array and reduce the overall size of the array (by minimizing the mean value of inter-element spacing in the array). However the mutual coupling between antenna elements and impedance matching of the overall array arrangement are not considered. The corresponding costs according to the design objectives mentioned are given below:

$Cost_1$=*BWFN (Beam-width between first nulls)* (4.35)

$Cost_2$=*max(SLL)* (4.36)

$Cost_3$=*mean(inter-element spacing)*=$(1/N)\sum_{i=1}^{i=N} d_i$ (4.37)

The overall cost function can be written as:

$Cost=w_1.Cost_1+w_2.Cost_2+w_3.Cost_3$ (4.38)

The threshold values of beam width between first nulls (maximum), maximum side-lobe level and mean of first 8 inter-element spacing (maximum) are 15 degrees,-18 dB and 0.70λ respectively.

4.7.2 Experimental Results

Table 4.10. Control parameter settings of the bio-inspired optimization algorithms for the optimization of unequally spaced linear antenna array

Optimization algorithms	Control Parameter Settings
Real coded genetic algorithm (Real GA)	Crossover probability=1 Mutation probability=0.16
Quantum genetic algorithm (QGA)	Crossover probability=1 Mutation probability=0.18
Improved genetic algorithm (IGA)	Crossover probability=1 Mutation Probability=0.16
Particle swarm optimization(PSO)	C_1=1.4 C_2=2.0 Damping boundary conditions are used. Linearly decreasing inertial weight used.

Optimization algorithms	Control Parameter Settings
Improved Comprehensive learning particle swarm optimization (CLPSO)	Loser group size =6 Damping boundary conditions are used. P_c as in [122], mutation on worst 8 particles.
Position mutated hierarchical particle swarm optimization (PMn-HPSO)	Parameters same as in [128].
Differential evolution with random scale factor (DE/rand/1)	F=random number between 0 and 2 with uniform probability density function distribution. CR=0.99
Differential evolution with global and local neighborhood search (DEGL)	Crossover probability=0.60 Neighborhood radius=20%

The statistical performances of the different bio-inspired optimization algorithms are given below in Table 4.11.

Table 4.11. Statistical performances of the bio-inspired optimization algorithms in the optimization of linear array of unequally spaced isotropic antenna elements.

Optimization algorithms	Mean cost value	Best cost value	Worst cost value	Standard deviation	Robustness (%)	Convergence rate(iterations)
Real GA	0.1690	0.1682	0.1705	8.05e-04	100	13
QGA	0.1689	0.1681	0.1727	9.83e-04	96	13
IGA	0.1702	0.1689	0.1727	7.94e-04	96	75
PSO	0.1677	0.1670	0.1689	4.21e-04	100	15
CLPSO	0.1676	0.1671	0.1693	4.10e-04	100	14
PMn-HPSO	0.1688	0.1679	0.1720	0.0010	96	22
DE/rand/1	0.1672	0.1670	0.1675	1.56e-04	100	18
DEGL	0.1676	0.1671	0.1682	2.53e-04	100	10

The statistical performance of the optimization algorithms are given in the table above. Although all these optimization algorithms have been applied to array design and optimization problems earlier, their performance was studied based on a fixed and static cost function. The table above presents the statistical performance comparison based on a dynamic cost function. The algorithms which show 100% robustness are real coded genetic algorithm, particle swarm optimization, improved comprehensive learning particle swarm optimization differential evolution with random scale factor and DEGL. The robustness of the other algorithms is slightly less than 100%. Among the algorithms showing 100% robustness, fastest convergence is shown by the DEGL based on the control parameters indicated earlier. This indicates that any arbitrary run of this algorithm for this optimization problem will definitely converge to an acceptable solution satisfying all the threshold parameters and within less computation time compared to the other algorithms considered in this chapter. However the lowest mean value of the cost function, best cost value and the standard deviation of the cost values are obtained in case of conventional DE/rand/1 algorithm with the control parameters indicated earlier. DE/rand/1 also shows 100 % robustness but it has a slightly higher convergence rate (18 runs) compared to DEGL (10 runs).

The best convergence plots of the different algorithms are given below in Fig. 4.21.

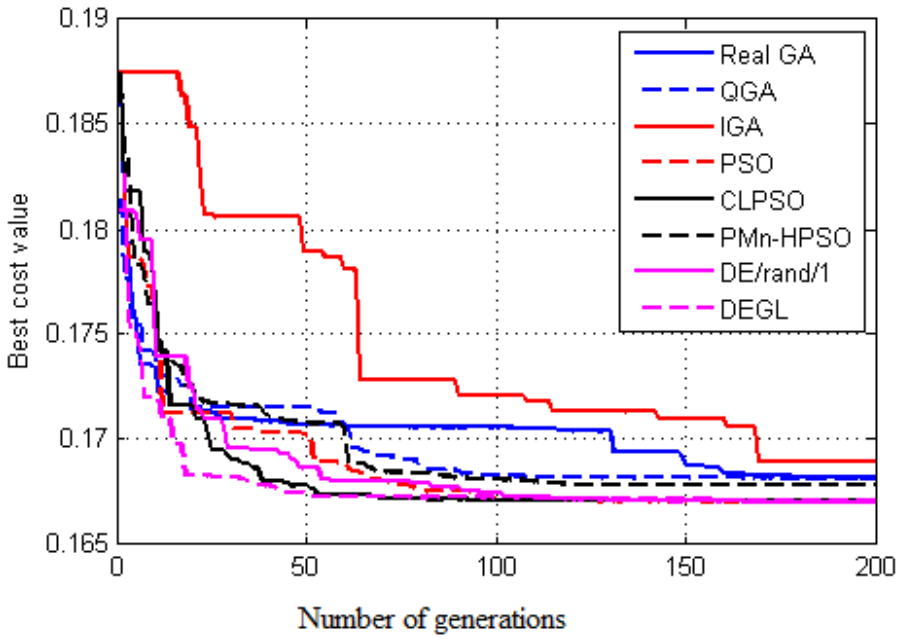

Fig. 4.21 Best convergence plots for the bio-inspired optimization algorithms in the optimization of unequally spaced linear antenna array.

The mean convergence plots are given in Fig. 4.22:

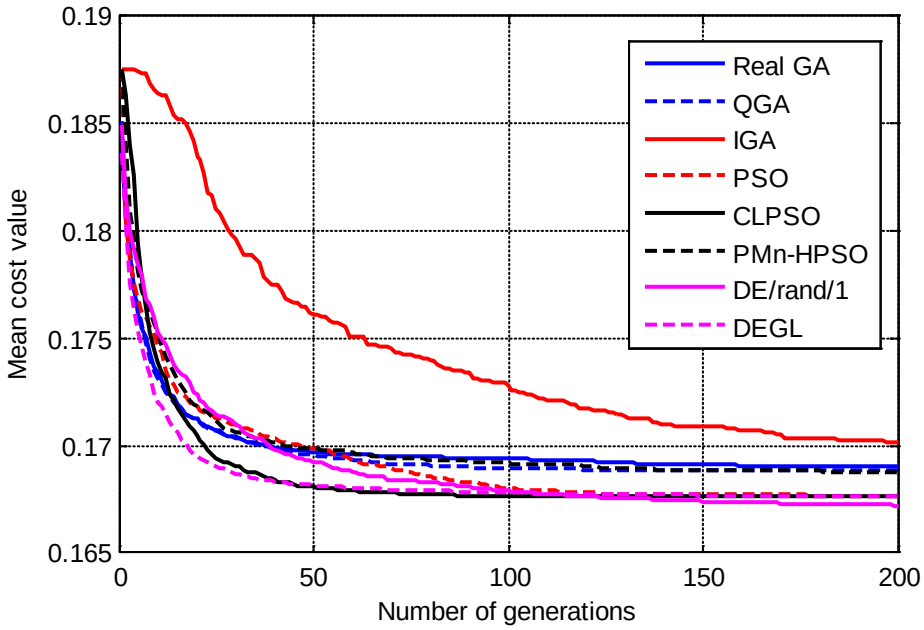

Fig. 4.22 Mean convergence plots for the bio-inspired optimization algorithms in the optimization of unequally spaced linear antenna array.

The performances of the unequally spaced linear antenna array obtained from the best run of each bio-inspired optimization algorithm are given in Table 4.12:

Table 4.12. Performances of the optimal arrays obtained from the best run of each bio-inspired optimization algorithm.

Optimization algorithms	BWFN (degrees)	Maximum SLL (dB)	Mean inter-element spacing
Real GA	11.45	-19.37	0.672 λ
QGA	11.45	-19.55	0.676 λ
IGA	12.44	-19.40	0.626 λ
PSO	11.95	-20.04	0.655 λ
CLPSO	11.95	-19.92	0.652 λ
PMn-HPSO	11.45	-19.54	0.674 λ

Optimization algorithms	BWFN (degrees)	Maximum SLL (dB)	Mean inter-element spacing
DE/rand/1	11.95	-20.07	0.655 λ
DEGL	11.95	-19.91	0.653 λ

Table 4.13. The parameters of the DEGL optimized array (inter-element spacing):

d_1	0.8203 λ	d_5	0.5238 λ
d_2	0.8469 λ	d_6	0.6272 λ
d_3	0.7743 λ	d_7	0.5159 λ
d_4	0.6110 λ	d_8	0.5012 λ

The normalized power pattern of the DEGL optimized array in shown in Fig 4.23:

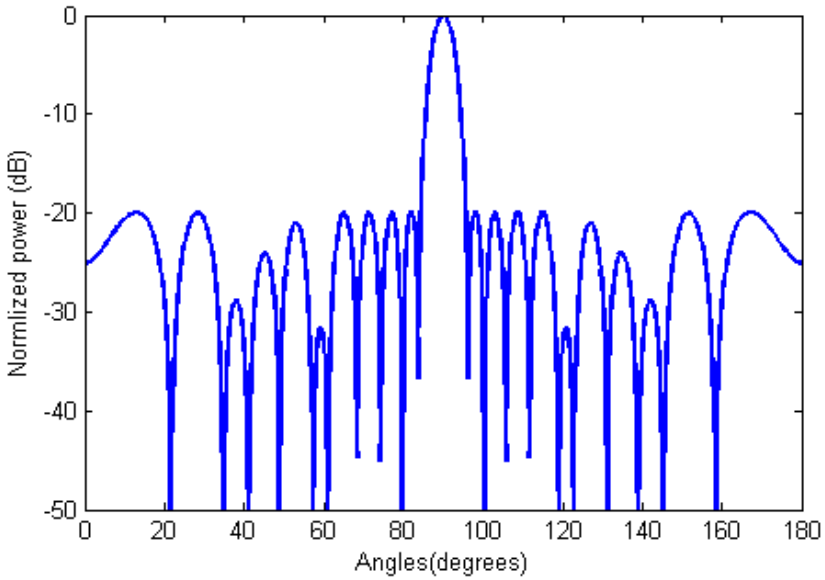

Fig.4.23 Normalized power pattern of the linear array of unequally spaced isotropic elements optimized from the best run of DEGL algorithm

The mean value of inter-element spacing of the DEGL optimized array is 0.653λ with BWFN of 11.95 degrees and maximum side lobe level of -19.91 dB.

4.8 Four –element Yagi-Uda Antenna Array

4.8.1 Theory

The previous optimization case study involved array of isotropic antennas. Here a practical array design case is considered where the impedance matching condition and mutual coupling effects between the antenna elements are considered. An optimal 4-element Yagi-Uda antenna array is designed with one reflector, one active and 2 director dipole antennas. The spacing between the active element and the first director element is assumed to be the same as that between the 2 director elements. The dimensions of the Yagi-Uda array are optimized to achieve low half power beam widths and low side lobe levels (in both E-plane and H-plane) and impedance matching at any particular design frequency. Optimization of Yagi –Uda antennas are reported in [86]-[89] but having cost functions with fixed weights. In [86]-[89] and in this chapter, the optimal antenna dimensions are specified in terms of wavelength corresponding to the design frequency. The Yagi-Uda antenna array is shown in the Fig. 4.24:

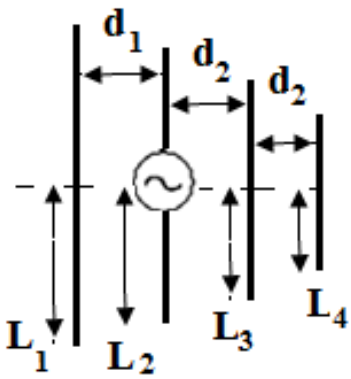

Fig. 4.24 Geometry of the 4-element Yagi-Uda antenna array

The objectives for optimization are described next. The first objective is the minimization of the half power beam widths of the major lobe in both E-plane and H-plane. Hence the corresponding cost is given as:

$$Cost_1 = \max(HPBW\ in\ E-plane, HPBW\ in\ H-plane) \quad (4.39)$$

The second objective is the minimization of the maximum side lobe levels in both E-plane and H-plane. The corresponding cost is given as:

$$Cost_2 = \max(SLL\ in\ E-plane, SLL\ in\ H-plane) \quad (4.40)$$

The third objective is the impedance matching at the center frequency. The corresponding cost is given as:

$$Cost_3 = |reflection\ coefficient\ at\ the\ design\ frequency| \quad (4.41)$$

The fourth objective is to achieve the main lobe along the axis of the array towards the director elements (desired direction).

$$Cost_4 = 1/\max(S_{EP}, S_{HP}) \quad (4.42)$$

Where E_p is the normalized power density in the E-plane along the desired direction and H_p is the normalized power density in the H-plane along the desired direction.

The overall cost function is formulated as:

$$Cost = w_1.Cost_1 + w_2.Cost_2 + w_3.Cost_3 + w_4.Cost_4 \quad (4.43)$$

The cost function evaluation is done by first analyzing the Yagi-Uda antenna structure using integral equation approach and then extracting the antenna performance parameters as mentioned above. All the weights are dynamically updated at each iteration of the optimization algorithm. Threshold values for half power beam width (maximum), maximum value of the side-lobe level and magnitude of reflection coefficient (maximum) at the center frequency are taken to be 90 degrees,-10 dB and 0.3162 (S_{11} of -10 dB) respectively.

4.8.2 Experimental Results

Table 4.14. Control parameter settings of the bio-inspired optimization algorithms for the optimization of 4-element Yagi-Uda antenna array

Optimization algorithms	Control Parameter Settings
Real coded genetic algorithm (Real GA)	Crossover probability=1 Mutation probability=0.1
Quantum genetic algorithm (QGA)	Crossover probability=1 Mutation probability=0.1
Improved genetic algorithm (IGA)	Crossover probability=1 Mutation Probability=0.2
Particle swarm optimization(PSO)	C_1=2.0 C_2=2.0 Damping boundary conditions are used. Linearly decreasing inertial weight used.
Improved Comprehensive learning particle swarm optimization (CLPSO)	Number of worst particles for mutation =5 Damping boundary conditions are used. Pc as in [122].
Position mutated hierarchical particle swarm optimization (PMn-HPSO)	Parameters same as in [128].
DE/rand/1	F=random number between 0 and 2 with uniform probability density function distribution. CR=0.96
Differential Evolution with global and local neighborhood search	Neighborhood radius=10% CR=0.70

The statistical performances of the bio-inspired optimization algorithms with respect to the Yagi-Uda antenna array optimization case study are given in Table 4.15:

Table 4.15.Statistical performances of the bio-inspired optimization algorithms in the optimization of the 4 element Yagi-Uda antenna array.

Optimization algorithms	Mean cost value	Best cost value	Worst cost value	Standard deviation	Robustness (%)	Convergence rate(iterations)
Real GA	1.4794	1.4725	1.5148	0.0081	32	27
QGA	1.4812	1.4726	1.4920	0.0053	20	20
IGA	1.5705	1.5412	1.6008	0.0204	0	NA
PSO	1.4764	1.4712	1.4855	0.0041	48	78
CLPSO	1.4769	1.4705	1.4890	0.0057	48	42
PMn-HPSO	1.4766	1.4738	1.4815	0.0024	28	24
DE/rand/1	1.4727	1.4708	1.4807	0.0022	76	66
DEGL	1.4721	1.4703	1.4750	0.0014	96	28

The mean cost values, best cost values and worst cost values are quite close for the optimization algorithms shown above. However significant differences are observed with respect to standard deviation , robustness and rate of convergence. Highest robustness is shown by differential evolution with global and local neighborhood search. The standard deviation of the cost values in DEGL is 0.0014. Convergence rate of DEGL is quite fast (only 28 generations on average). QGA has the fastest convergence rate. Taking these factors into account, DEGL can be considered the most suited algorithm for this particular optimization problem among all the bio-inspired optimization algorithms considered in this chapter. Algorithm IGA could not converge to any acceptable solution. Worst performance is shown by IGA as evident from the statistical performance table above. In addition, the computational cost of IGA is also higher compared to other algorithms because of its self supervised mutation strategy. The best convergence plots of the different optimization algorithms are given in Fig. 4.25 . The mean convergence plot is shown in Fig. 4.26.

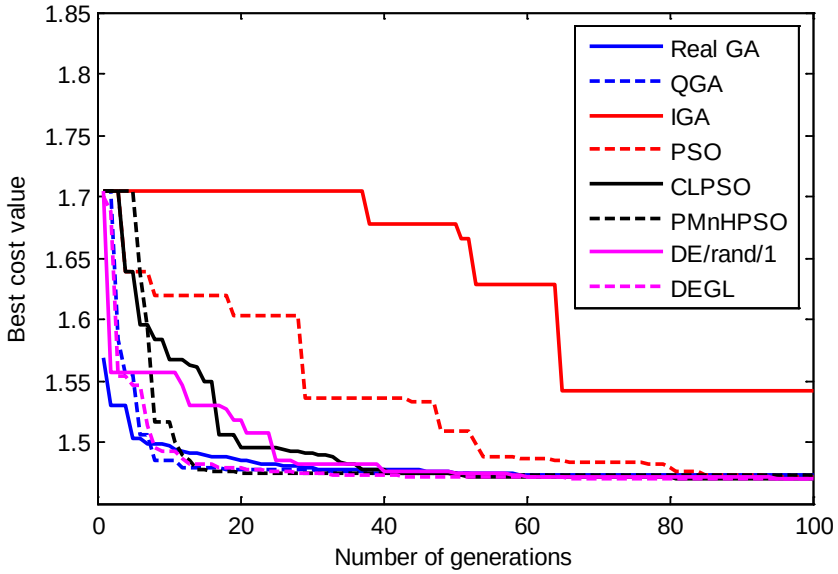

Fig. 4.25 Best convergence plots of the bio-inspired optimization algorithms in the optimization of Yagi-Uda antenna array

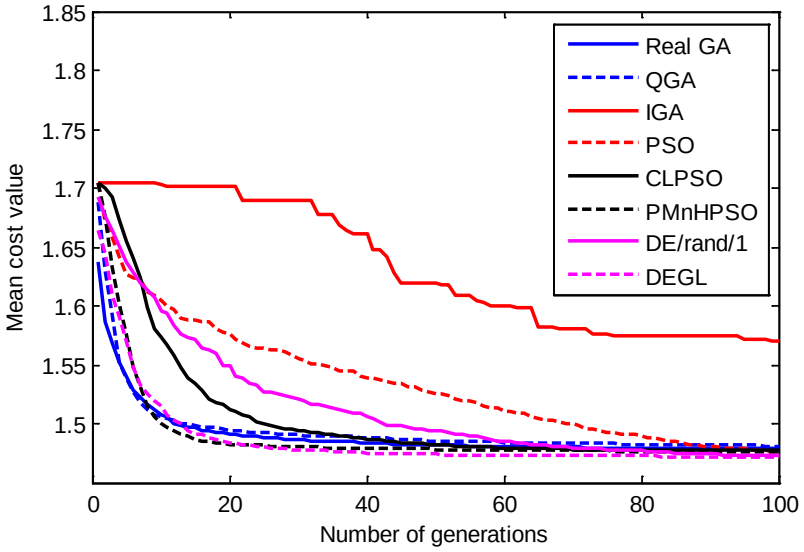

Fig. 4.26 Mean convergence plots of the bio-inspired optimization algorithms in the optimization of Yagi-Uda antenna array

The performance parameters of the Yagi-Uda (4-element) antenna array as obtained from the best run of each algorithm and satisfying all the threshold criteria are given in Table 4.16.

Table 4.16. Performances of the optimal Yagi-Uda antenna arrays obtained from the best run of each optimization algorithm.

Optimization algorithms	Half power beam width (degrees)(E-plane)	Half power beam width (degrees)(H-plane)	Maximum side-lobe level(dB) (E-plane)	Maximum side-lobe level(dB) (H-plane)	VSWR
Real GA	46.86	56.46	-10.20	-10.20	1.87
QGA	47.07	56.66	-10.35	-10.35	1.87
IGA	-	-	-	-	-
PSO	46.86	56.36	-10.43	-10.28	1.87
CLPSO	46.86	56.36	-10.41	-10.36	1.86
PMn-HPSO	47.07	56.76	-10.15	-10.15	1.85
DE/rand/1	46.86	56.36	-10.40	-10.40	1.87
DEGL	46.86	56.36	-10.34	-10.32	1.85

Table 4.17. Dimensions of the DEGL optimized Yagi-Uda antenna array:

Length of the Reflector Element	0.4638λ
Length of the Active element	0.4609 λ
Length of the Director element1	0.4360 λ
Length of the Director element2	0.4525 λ
Spacing between Reflector and Active element	0.3495 λ
Spacing between Active and Director Element	0.2756 λ

The radiation patterns of the optimized Yagi-Uda array in the E-plane and H-plane are given in Fig. 4.27:

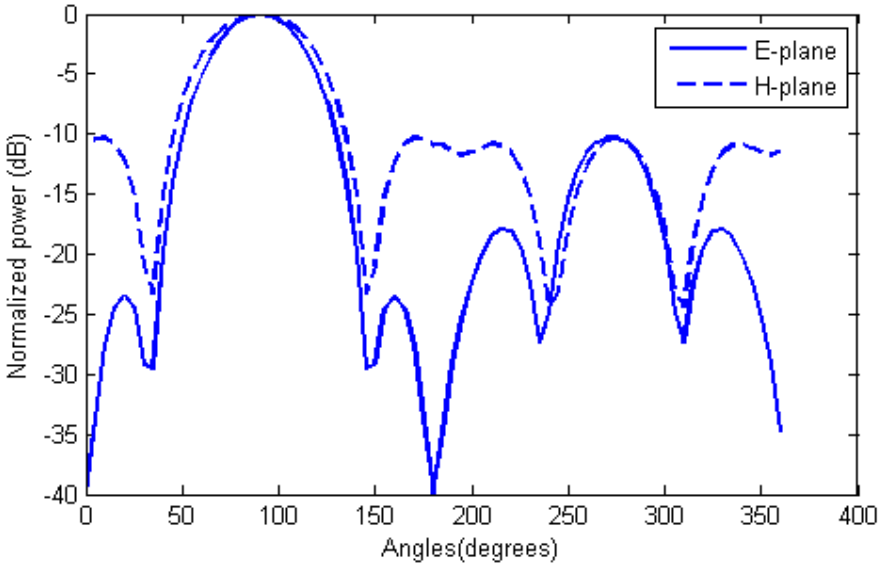

Fig. 4.27 Normalized power pattern of the DEGL optimized Yagi-Uda antenna array

4.9 Conclusion

Performance comparison between real coded genetic algorithm, particle swarm optimization and differential evolution algorithm (using random scale factor) has been done along with their advanced variants like quantum genetic algorithm, improved genetic algorithm with supervised mutation strategy, improved comprehensive learning PSO, position mutated hierarchical PSO and differential evolution with neighborhood search with respect to the design of circularly polarized microstrip antenna with different feed methods, design of unequally spaced linear array of isotropic elements and design of four element Yagi-Uda antenna array. Such an extensive algorithm comparison with respect to a particular antenna design problem was not reported previously. The control parameters of all algorithms are tuned nearly to their best performance by a meta-level position mutated hierarchical PSO and meta-DEGL algorithms, which is also a first attempt in comparing optimally tuned algorithms with respect to antenna design problem according to the knowledge of the authors. The value of the control parameters for different algorithms provided in this chapter may guide the readers to optimally use these algorithms for future designs. It is seen that due to the different traversal behavior of different algorithms in problem hyperspaces, their relative performances have varied significantly. DEGL is adjudged to be the statistically most superior algorithm in all the designs of RHCP microstrip antennas and

arrays studied in this chapter. PSO with appropriately tuned control parameters and boundary conditions have outrun its improved versions. A combination of quadratic crossover and time-decreasing mutation range combination for real coded GA has shown faster convergence than QGA and IGA. It has outperformed both QGA and IGA in the first two optimization problems although IGA emerged best in the cross-aperture fed CP antenna optimization. Real coded GA also outperformed conventional PSO in the optimization of transmission line-fed RHCP microstrip antenna. DE schemes, particularly DEGL considered in this chapter have emerged as superior over GA and PSO techniques for the CP microstrip antenna design with different antenna feeds. Also in case of the optimization of unequally spaced linear array of isotropic elements, although the statistical performances of the algorithms are very close, it is found that DEGL has slightly beaten others with its high convergence rate and 100% robustness. In case of the design and optimization of four element Yagi-Uda antenna arrays, it is found that DEGL has again claimed superiority over other algorithms as evident from the data available in section 8 of this chapter.

Very advanced DE schemes have come up claiming superiority over older ones. In the next chapter, these advanced versions of differential evolution algorithms will be explored in terms of their statistical performance based on the same numerical antenna and array design benchmark problems with slightly modified and improved cost functions.

Chapter 5

Performance Comparison of Differential Evolution Variants and Hybrid Algorithms in the Design of Microstrip Antennas and Arrays

5.1 Introduction

Different portable equipments like mobile phones, laptops are increasingly using microstrip antennas for their low weight, low fabrication cost and ease of integration facilities. Conventionally; the antenna can be designed using analytical models along with suitable optimizers and may be fine tuned later using electromagnetic simulation software. It is important for antenna designers to have an idea of the optimization scheme suited for the particular design problem at hand. Differential Evolution (DE) which works on stochastic vector based population approach was proposed in [129]. It is one of the favored optimization schemes among engineers today. As already mentioned in the previous chapter, it was proven superior with respect to the optimization of 34 widely used numerical benchmark problems and was regarded the fastest on a general basis over other existing evolutionary optimization algorithms in [130]. Research is continually carried on to improve the statistical performance of basic DE, resulting in certain variants of DE and other algorithms hybridized with pre-existing optimization schemes, each one claiming superiority over the old schemes. The performance of any optimization algorithm depends on the optimization problem at hand and requires proper tuning of control parameters involved in the algorithm. All the recent variants of DE explored in this chapter have not been compared together with respect to any particular antenna engineering design problem as a benchmark function earlier. In [132],[138], performances of some of the algorithms with single objective costs were compared but not all.

Antenna design often requires multiple objectives to be optimized at the same time e.g. axial ratio bandwidth and impedance matching about the centre frequency (in case of circularly polarized antennas) or maximum directivity with minimum side lobe level (in case of arrays). Since differential evolution has shown very promising statistical performance in antenna optimization and design benchmark problems in the previous chapter, attempts have been made

in this chapter to provide the antenna designers with an idea of which DE optimization scheme is to be used for different antenna and array optimization problems according to the benchmark problems or case studies reported in this chapter. Five case studies have been performed in this chapter and they are used as benchmark problems for performance comparison of different differential evolution algorithms and their variants. Nearly square rectangular microstrip antennas with conventional feeding methods like probe feed; transmission line feed and cross-aperture coupled feed are designed and optimized for right-handed circular polarization at 2.4 GHz as in the previous chapter. The objectives are slightly modified. The objectives are to maximize the gain at the center frequency and the axial ratio bandwidth, as also to provide maximum possible impedance matching within the axial ratio band. Impedance bandwidths for microstrip circularly polarized antennas are normally high compared to their 3 dB axial ratio bandwidths [19]. The cost functions for these antennas are evaluated using cavity-modeling and method of moments and approach. Numerical benchmark problem involving synthesis of linear arrays of unequally spaced isotropic antenna elements is also considered for evaluation of DE algorithms' performance and subsequent design as in the previous chapter. The optimization objectives are to achieve minimum beam width, minimum side-lobe level and as less length of the array as possible. No impedance matching criteria and mutual coupling between antenna elements are considered in this array design since only isotropic antenna elements are considered. The fifth case study is the design of a 4-element Yagi-Uda antenna array with similar design objectives as the unequally spaced linear array but it also takes into consideration impedance matching at the design frequency and mutual coupling between the dipole antennas. The half power beam widths and the maximum side lobe levels are optimized in both E-plane and H-plane for the Yagi-Uda antenna array. Simultaneous reduction in half power beam widths of the principal lobe of the antenna will lead to decrease in major beam area and subsequent increase in the directivity of the antenna. Since the wire antennas have very low loss, the maximum gain of this antenna can be considered to be approximately equal to that of its directivity. The cost function evaluation is done using integral equation approach. All the antenna optimization problems stated above are multi-objective in nature. All the objectives for any of the optimization problems are normally combined into a single objective using weighted sum approach. It may be difficult to estimate the values of the weights required in each case to achieve the desired antenna response. In most cases it is only sufficient to achieve the antenna

performance up to a threshold level. Hence all the objectives for all the optimization case studies considered in this paper are combined using dynamic and adaptive weights. If any objective is far from its threshold value, the corresponding weight is increased according to a defined rule and vice-versa.

All differential evolution optimization schemes may not be suitable for all the optimization case studies mentioned above where fuzzy-rule based cost functions with dynamic weights are used. Hence the statistical performance evaluation of differential evolution variants and hybrids are necessary with respect to antenna and array design problems in such type of situations. The statistical performance parameters used for comparing different variants of DE algorithms with respect to the antenna design benchmark problems considered in this chapter are the best cost value, worst cost value, mean cost value and standard deviation of cost values obtained from multiple runs of each algorithm. Two more statistical parameters studied are algorithm robustness and convergence rate. The robustness of an algorithm is the percentage of successful runs of the algorithm out of the total number of runs for a particular optimization problem. A particular run of the algorithm is successful if the algorithm returns optimal dimensions for an antenna for the design problem so that it satisfies at least all the threshold values of the antenna performance parameters. The convergence rate of an algorithm is the average number of iterations required by an algorithm before it returns optimal dimensions of an antenna satisfying at least all the threshold values of the antenna performance parameters. The convergence rate is calculated out of the successful runs of the algorithm.

The novelty of this chapter lies in using cost functions with dynamic weights for the optimization of circularly polarized antennas, linear isotropic array and Yagi-Uda antenna array. Further, all the optimization schemes using DE are compared together with respect to antenna design problems which are not reported earlier. In addition, the optimization algorithm control parameters are fine tuned for its best performance using meta-level differential evolution with neighborhood search.

The chapter is organized as follows. Section II provides a brief review of the algorithms with suitable references. Section III explains the tuning of different optimization schemes .Sections

IV, V, VI, VII and VIII analyze the solutions, performances of different DE variant and hybrid algorithms with respect to the design of circularly polarized microstrip antenna with probe feed, transmission line fed, cross aperture coupled feed, linear array with unequally spaced isotropic elements, and 4-element Yagi-Uda antenna array respectively. Section IX summarizes the results.

5.2. Differential Evolution Optimization Algorithms

5.2.1 Differential Evolution Algorithm with Random Scale Factor (DE/rand/1)

Differential Evolution (DE), [129] works by having a population of candidate vectors. These candidates explore the search-space by using simple mathematical formula to alter their positions by combining the positions of other candidates from the population. If the new position of the candidates provides some improvement, it is accepted and becomes part of the new population; otherwise the new position is discarded. The process is repeated until the goal is met or the maximum number of iterations specified by the programmer has been tried. A brief outline of the algorithm is given below:

1. An initial population of target or parent vectors is generated. Let the population size be P. Each vector contains 'n' number of genes. Each gene represents a particular antenna dimension or parameter. Each gene can have values between the limits specified by the programmer. The cost values of each vector in the initial population are evaluated before starting the optimization process. Each gene is represented as $X_G(i,j)$ where G represents the generation number, i represents the i^{th} parent vector and j denotes the j^{th} gene of the parent vector. The following steps (2-4) are repeated until the maximum numbers of generations are over or the termination criterion is met.

2. For the i^{th} vector, three other vectors are chosen, mutually exclusive in nature. An intermediate vector called the donor vector corresponding to X_G(i, 1…….n) is formed according to the following equation and denoted as V_G(i, 1…..n):

$$V_G(i,j) = X_G(n1,j) + F.(\left(X_G(n2,j) - X_G(n3,j)\right)) \quad (5.1)$$

where F is the scaling factor, its value being a random variable (with uniform distribution between 0 and 2).

3. The donor vector undergoes a binary crossover operation with the parent vector based on a crossover probability CR. This results in a corresponding trial vector T_G(i,1…….n). A random number (y) is generated based on uniform probability distribution for every gene of the vector. 'j_{rand}' is a random whole number between 1 and n.

$$T_G(i,j) = V_G(i,j)\ if\ y \leq CR\ or\ j = j_{rand}$$

$$T_G(i,j) = X_G(i,j) otherwise \quad (5.2)$$

4. The trial vector is evaluated for its cost. If the trial vector has a lower cost than the corresponding parent vector X_G(i,1……n), then the trial vector replaces the parent vector in the next generation.

5.2.2 Self Adaptive Differential Evolution Algorithm (SADE)

Self Adaptive scheme for DE (SADE) is designed to automatically adjust the values of scaling factor (F) and cross over probability (CR) over the generations to ensure faster convergence of the algorithm. Each candidate or parent vector in the population is extended by two parameters F_G and CR_G, which are used whenever the donor vector and trial vector corresponding to that candidate are generated. The values of F and CR are updated as in [139].This scheme has been recently used for microstrip antenna and filter design problems in [141]. A brief outline of the algorithm is given below:

1. An initial population of target or parent vectors is generated. Let the population size be P. Each vector contains 'n+2' number of genes. Each gene (from 1 to n) represents a particular antenna dimension or parameter. Each gene can have values between the limits specified by the programmer. Each vector has its own scaling factor F_G(i) and crossover probability CR_G(i) stored in X_G(i, n+1) and X_G(i, n+2) respectively. The values of F and CR for each vector is updated in each generation as described below. The cost values of each vector in the initial population are evaluated before starting the optimization process. Each gene is represented as X_G(i,j) where G represents the generation number, i represents the i^{th} parent vector and j denotes the j^{th} gene of

the parent vector. The following steps (2-4) are repeated until the maximum numbers of generations are over or the termination criterion is met.

2. For the i^{th} vector, three other vectors are chosen, different from 'i' and mutually exclusive. A donor vector corresponding to X_G(i, 1…….n) is formed according to the following equation and denoted as V_G(i, 1…..n):

$$V_G(i,j) = X_G(n1,j) + F_G(i).(\left(X_G(n2,j) - X_G(n3,j)\right)) \quad (5.3)$$

3. The donor vector undergoes a binary crossover operation with the parent vector based on a crossover probability CR. This results in a corresponding trial vector T_G(i,1…….n). A random number (y) is generated based on uniform probability distribution for every gene of the vector.

$$T_G(i,j) = V_G(i,j) if y \leq CR_G(i) or j = j_{rand}$$
$$T_G(i,j) = X_G(i,j) otherwise \quad (5.4)$$

4. The values of the scaling factor F and CR for each population vector are updated as given below (p_1 and p_2 are random numbers having values between 0 and 1):

$$F_{G+1}(i) = F_l + rand_{1[0,1]} x F_u \quad if rand_{2[0,1]} < p_1$$
$$F_{G+1}(i) = F_G(i) \ otherwise \quad (5.5a)$$

$$CR_{G+1}(i) = rand_{3[0,1]} \ if \ rand_{4[0,1]} < p_2$$

$$CR_{G+1}(i) = CR_G(i) otherwise \quad (5.5b)$$

F_l and F_u are lower and upper limits of F set to 0.1 and 0.9 respectively

5. The trial vector is evaluated for its cost. If the trial vector has a lower cost than the corresponding parent vector X_G(i,1……n), then the trial vector will replace the parent vector in the next generation.

5.2.3 Differential Evolution with Global and Local Neighborhood Search (DEGL)

Differential Evolution with Global and Local Neighborhood Search (DEGL) is proposed in [142]. Two terms namely global and local neighborhoods are introduced. Global neighborhood refers to the entire population during any generation of the algorithm. The candidates are assumed to be organized in a ring topology. For each candidate, a local neighborhood of size 'k' is defined. For each candidate vector, a local donor vector and a global donor vector are created from the two neighborhoods which are combined to yield the actual donor vector using a weight factor 'w' (determined by self adaptive algorithm [142]) which varies between 0 and 1.Once the actual donor vector is created, the rest of the DE process i.e. generation of trial vectors and choosing parents for the next generation are same as DE/rand/1. The value of the weight factor is restricted between 0.05 and 0.95. A brief outline of the algorithm is given below:

1. An initial population of target or parent vectors is generated. Let the population size be P. Each vector contains 'n' number of genes. Each gene represents a particular antenna dimension or parameter. Each gene can have values between the limits specified by the programmer. The cost values of each vector in the initial population are evaluated before starting the optimization process. Each gene is represented as $X_G(i,j)$ where G represents the generation number, i represents the i^{th} parent vector and j denotes the j^{th} gene of the parent vector.

2. A neighborhood of radius 'k' is assumed around all individual vectors. All the individuals in the population are assumed to be arranged in a ring topology according to their indices. The value of 'k' can range from 0 to (P-1)/2. Since the cost values of all the individual vectors are already evaluated, we identify the best vector in the neighborhood ($X_{local\_best}(i, 1…n)$)and globally best vector ($X_{global\_best}(i,1…n)$). The following steps (3-6) are repeated until the maximum numbers of generations are completed or the termination criterion is met.

3. For the i^{th} vector, the donor vector is formed as a combination of local donor vector and global donor vector. The local donor vector formation involves the best vector in the neighborhood of

the i^{th} vector and two other random vectors from the same neighborhood. Let these random vectors in the same neighborhood have indices 'p' and 'q'.

$$L_G(i,j) = X_G(i,j) + \alpha(X_G(Local_{best},j) - X_G(i,j) + \beta\big(X_G(p,j) - X_G(q,j)\big) \quad (5.6)$$

4. The global donor vector formation involves the global best vector and two other random vectors from the entire population. Let the random vectors have indices 'r' and 's'.

$$G_G(i,j) = X_G(i,j) + \alpha(X_G(Global_{best},j) - X_G(i,j) + \beta\big(X_G(r,j) - X_G(s,j)\big) \quad (5.7)$$

5. The net donor vector is formed as a combination of local donor vector and global donor vector

$$V_G(i,j) = w.L_G + (1-w).G_G \quad (5.8)$$

where α and β are random variables (with uniform distribution between 0 and 1).

The weight 'w' should maintain a balance between the contributions from Local donor vector and global donor vector. Each population vector has its own weighing factor $W_G(i)$.The value of the weighing factor is dynamically updated as given below:

$$w_G^{'}(i) = w_G(i) + F.\big(w_G(global_{best}) - w_G(i)\big) + F.(w_G\big(r1 - w_G(r2)\big) \quad (5.9)$$

6. The donor vector undergoes a binary crossover operation with the parent vector based on a crossover probability CR. This results in a corresponding trial vector $T_G(i,1…….n)$. A random number (y) is generated based on uniform probability distribution for every gene of the vector.

$$T_G(i,j) = V_G(i,j)\ if\ y \le CR or\ j = j_{rand}$$
$$T_G(i,j) = X_G(i,j) otherwise \quad (5.10)$$

7. The trial vector is evaluated for its cost. If the trial vector has a lower cost than the corresponding parent vector $X_G(i,1……n)$, then the trial vector replaces the parent vector in the next generation.

This algorithm is also referred as differential evolution with neighborhood based mutation operator.

5.2.4 Modified Differential Evolution with p-best Crossover Strategy (MDE-pBX)

Modified Differential Evolution with p-Best Crossover Strategy (MDE-pBX) as conceived in [152], alters the generation process of donor vectors and crossover strategy of DE/rand/1 to increase the diversity of the solutions and to make the algorithm more explorative in nature. For each candidate vector, an arbitrary group of 'q' vectors is created (chosen randomly from the total population excluding the present candidate vector) from which the donor vector is generated. The p-best crossover strategy uses binomial crossover between the donor vector and an arbitrarily chosen vector from among top p-candidate vectors of the population (sorted in ascending order of their cost values) to generate the trial vector. The parameter 'p' is linearly reduced with generations. A brief outline of the algorithm is given below:

1. An initial population of target or parent vectors is generated. Let the population size be P. Each vector contains 'n' number of genes. Each gene represents a particular antenna dimension or parameter. Each gene can have values between the limits specified by the programmer. The cost values of each vector in the initial population are evaluated before starting the optimization process. Each gene is represented as $X_G(i,j)$ where G represents the generation number, i represents the i^{th} parent vector and j denotes the j^{th} gene in the vector. The following steps (2-4) are repeated until the maximum numbers of generations are over or the termination criterion is met.

2. For the i^{th} vector, three other vectors are chosen, different from 'i' and mutually exclusive. Among the three, one includes the vector with the minimum cost function from among a group of arbitrarily chosen sub-group of vectors indexed as 'group_best'. Two other vectors contributing to donor vector generation are indexed as 'r_1' and 'r_2'.A donor vector corresponding to X_G(i, 1…….n) is formed according to the following equation and denoted as V_G(i, 1…..n):

$$V_G(i,j) = X_G(i,j) + F_i.\big((X_G(group_{best},j) - X_G(i,j) + X_G(r1,j) - X_G(r2,j)\big) \qquad (5.11)$$

where'F_i' is the scaling factor for the i^{th} individual vector in the population. 'F_i' is a random number with Cauchy distribution having a mean of F_m and standard deviation 0.1. The value of F_m is updated in every generation as given below:

$$F_m = w.F_m + (1 - w).mean_{pow}\,(F_{success}\,) \quad (5.12)$$

where '$mean_{pow}$' refers to power mean of values in the set $F_{success}$ containing all successful values of scaling factors. The weighing factor 'w' is a uniformly distributed random number between 0.8 and 1. The crossover probability for each individual is also generated and updated in a similar way as the scaling factor except a Gaussian distribution is used instead of Cauchy distribution and the weighing factor involved in the process is a uniformly distributed random number varying between 0.9 and 1.

3. The donor vector undergoes a binary crossover operation with the randomly selected vector from a group of p-best vectors in the population to generate the trial vector. The value of 'p' is changed in every generation according to the following formula.

$$p = ceil(\frac{P}{2}(1 - \frac{G-1}{G_{max}}) \quad (5.13)$$

4. The trial vector is evaluated for its cost. If the trial vector has a lower cost than the corresponding parent vector X_G(i,1……n), then the target vector replaces the parent vector in the next generation.

5.2.5 Harmonic Search Differential Evolution Algorithm (HSDE)

Harmonic Search Differential Evolution (HSDE) was recently proposed in [156]. The idea behind this novel DE optimization scheme is to enhance its explorative capability by merging conventional DE with harmonic search algorithm [157]. A brief outline of the algorithm is given next:

1. An initial population of target or parent vectors is generated. Let the population size be P. Each vector contains 'n' number of genes. Each gene represents a particular antenna dimension or parameter. Each gene can have values between the limits specified by the programmer. The cost values of each vector in the initial population are evaluated before starting the optimization process. Each gene is represented as X_G(i,j) where G represents the generation number, i

represents the i^{th} parent vector and j denotes the j^{th} array element excitation. The following steps (2-4) are repeated until the maximum numbers of generations is crossed or the termination criterion is met.

2. The control parameters scaling factor and crossover probabilities are updated in each generation as given below:

$$CR_G = CR_{Lower} + \left(CR_{Upper} - CR_{Lower}\right).\left(\frac{G}{G_{max}}\right) \quad (5.14a)$$

$$F_G = F_{max} \exp(c.G), c = \ln\left(\frac{F_{min}}{F_{max}}\right)/G_{max} \quad (5.14b)$$

3. For the i^{th} vector, three other vectors are chosen, different from 'i' and mutually exclusive. Among the three, one includes the vector with the minimum cost function. A donor vector corresponding to X_G(i, 1…….n) is formed according to the following equation and denoted as V_G(i, 1…..n):

$$V_G(i,j) = X_G(nbest,j) + F_G.\left(\left(X_G(n1,j) - X_G(n2,j)\right)\right) \quad (5.15)$$

where F is a random variable (with uniform distribution between 0 and 2).

4. The donor vector undergoes a binary crossover operation with the parent vector based on a crossover probability CR_G. This results in a corresponding pre-final trial vector T_G(i,1…….n). A random number (y) is generated based on uniform probability for every gene of the vector.

$$T_G(i,j) = V_G(i,j) if y \leq CR or j = j_{rand}$$
$$T_G(i,j) = X_G(i,j) otherwise \quad (5.16)$$

5. The final trial vector TT_G(i,1….n) is generated based on the pre-final trial vector and the harmonic constant in the following way:

$$TT_G(i,j) = Lower_{limit,i} + \left(Upper_{limit,j} - Lower_{limit,j}\right).rand_{1[0,1]} \; if \; rand_{2[0,1]} > HR$$
$$TT_G(i,j) = TT_G(i,j) otherwise \quad (5.17)$$

where HR is a harmonic constant.

6. The final trial vector is evaluated for its cost. If the trial vector has a lower cost than the corresponding parent vector $X_G(i,1……n)$, then the trial vector replaces the parent vector in the next generation.

5.2.6 Biogeography Based Differential Evolution Algorithm (BBODE)

The Biogeography based Optimization (BBO) algorithm was first proposed in [144]. The BBO was hybridized with the original DE (Hybridized Biogeography based Optimization with Differential Evolution (BBO-DE)) and applied to economic load dispatch problems in power systems in [145]. In BBO, each candidate vector in the population is considered equivalent to a certain geographic region or habitat where a certain species reside. If the fitness of the candidate vector is large or the cost is small, we consider it as a habitat more suitable for species survival. Hence more number of species resides in it. Due to large population in that habitat, emigration rate from the habitat is considered large and immigration rate equivalently small. The reverse notion follows for a less fit individual. In the BBO-DE population, each candidate has its specific immigration (λ) and emigration (μ) rate as an equivalent of its habitat representation. Using the concepts of BBO, the DE/rand/1 is modified in the generation of donor vector and the trial vector. The donor vector is assigned gene values depending on crossover probability and emigration rate based on a random number. The trial vector uses no crossover probability but incurs gene values from immigration rate based on another random number. A brief outline of the steps as given in [145] is provided below.

1. An initial population of target or parent vectors is generated. Different control parameters of the optimization algorithm like scaling factor, crossover probability, and maximum immigration rate and maximum emigration rate, lower bounds of lower and upper immigration and emigration probabilities per gene are initialized. Let the population size be P and let each vector contain ‘n’ number of genes. Each gene represents a particular antenna dimension or parameter. Each gene can have values between the limits specified by the programmer. The cost values of each vector in the initial population are evaluated before starting the optimization process. Each gene is represented as $X_G(i,j)$ where G represents the generation number, i represents the i^{th} parent vector and j denotes the j^{th} index of gene in the vector. The following steps (2-5) are repeated until the maximum numbers of generations or the termination criterion is met.

2. The cost function value for each individual vector in the population is determined next for decided values of immigration and emigration rates.

3. The hybrid migration operation according to [145] is performed probabilistically on selected individuals in the population. This operation results in a new offspring population set.

4. The cost function values of the new offspring population set are recomputed.

5. Selection operation is performed between the original population and new offspring population based on their cost function values before moving onto the next generation.

5.2.7 Improved Differential Evolution Algorithm (IDE)

Improved Differential Evolution (IDE) [149] provides the simplest modification to DE/rand/1. It improves upon donor vector generation strategy by replacing one arbitrary candidate by the sub-optimal candidate vector in the difference vector for donor generation. The sub-optimal candidate is the one having the second lowest cost function in the existing population. The sub-optimal candidate is updated not only at the end of each generation but also after the trial vector evaluation of each candidate. A brief outline of the algorithm is given below:

1. An initial population of target or parent vectors is generated. Let the population size be P and let each vector contain 'n' number of genes. Each gene represents a particular antenna dimension or parameter. Each gene can have values between the limits specified by the programmer. The cost values of each vector in the initial population are evaluated before starting the optimization process. Each gene is represented as $X_G(i,j)$ where G represents the generation number, i represents the i^{th} parent vector and j denotes the j^{th} gene of the vector. The following steps (2-4) are repeated until the maximum numbers of generations or the termination criterion is met.

2. For the i^{th} vector, three other vectors are chosen, two of them different from 'i' and mutually exclusive. The third one includes the sub –optimal vector ($X_{sub\_optimal,\ G}(i,1\ldots\ldots n)$). A sub-optimal vector is the one which is best among the entire population excluding the optimal vector. A donor vector corresponding to $X_G(\ i,\ 1\ldots\ldots\ldots n)$ is formed according to the following equation and denoted as $V_G(\ i,\ 1\ldots..n)$:

$$V_G(i,j) = X_G(n1,j) + F.(\left(X_G(sub-optimal,j) - X_G(n2,j)\right)) \quad (5.18)$$

3. The donor vector undergoes a binary crossover operation with the parent vector based on a crossover probability CR. This results in a corresponding trial vector T_G(i,1…….n). A random number (y) is generated based on uniform probability distribution for every gene of the vector.

$$T_G(i,j) = V_G(i,j) if y \leq CR or j = j_{rand}$$
$$T_G(i,j) = X_G(i,j) otherwise \quad (5.19)$$

4. The trial vector is evaluated for its cost. If the trial vector has a lower cost than the corresponding parent vector X_G(I,1……n), then the trial vector replaces the parent vector in the next generation.

5.2.8 Modified Differential Evolution Algorithm

Modified Differential Evolution (MDE) was proposed in [158]. It incorporates two basic modifications namely best of random mutation and randomized local search. A brief outline of the algorithm is given below:

1. An initial population of target or parent vectors is generated. Let the population size be P and let each vector contain 'n' number of genes. Each gene represents a particular antenna dimension or parameter. Each gene can have values between the limits specified by the programmer. The cost values of each vector in the initial population are evaluated before starting the optimization process. Each gene is represented as X_G(i,j) where G represents the generation number, i represents the i^{th} parent vector and j denotes the j^{th} gene of the parent vector. The following steps (2-4) are repeated until the maximum numbers of generations or the termination criterion is met.

2. For the i^{th} vector, three other vectors are chosen, two of them different from 'i' and mutually exclusive. The third vector is the one with the lowest cost function designated as X_G(nbest, 1…n). Among the three, one includes the vector with the minimum cost function. A donor vector corresponding to X_G(i, 1…….n) is formed according to the following equation and denoted as V_G(i, 1…..n):

$$V_G(i,j) = X_G(nbest,j) + F.(\left(X_G(n1,j) - X_G(n2,j)\right)) \quad (5.20)$$

where F is a random variable (with uniform distribution between 0 and 2).

3. The donor vector undergoes a binary crossover operation with the parent vector based on a crossover probability CR. This results in a corresponding trial vector T_G(i,1…….n). A random number (y) is generated based on uniform probability distribution for every gene of the vector.

$$T_G(i,j) = V_G(i,j)\ if\ y \leq CR\ or\ j = j_{rand}$$
$$T_G(i,j) = X_G(i,j) otherwise \quad (5.21)$$

4. The trial vector is evaluated for its cost. If the trial vector has a lower cost than the corresponding parent vector X_G(i,1……n), then the trial vector will replace the parent vector in the next generation.

5. The following vectors are determined: X_{G+1}(nbest,1….n), X_{G+1}(nworst,1…..n), cost_X_{G+1}(nbest,1……n) and cost_X_{G+1}(nworst,1……n). The steps 6-7 are repeated until 'LocalK' counter is less than ceil (β.P) or X_{G+1}(nworst,1….n) is not replaced by X*(best, 1…n).

6. Formation of the X*(best,1….n) vector by modifying its genes in the following way:

$$X^*(best,j) = X_{G+1}(best,j) + 0.1\left(X_{j,G}^{max} - X_{j,G}^{min}\right)Gauss(0,1) \quad (5.22)$$

7. If cost (X*(best,1….n))<cost_X_{G+1}(nworst,1….n),then X_{G+1}(nworst,1…n) is replaced by X*(best,1….n) or else the algorithm will go to step 6.

5.2.9 Adaptive Differential Evolution Algorithm (ADE)

Adaptive Differential Evolution with Optimization State Estimation (ADE) was proposed in [153]. It identifies each run of the algorithm as exploration state and exploitation state (by studying the population distribution) and accordingly adapts the scaling factor and crossover probability. A brief outline of the algorithm is given below:

1. In the start of each generation, the cost values of all the individual vectors are sorted in an ascending order (from the best to the worst). The ranking based on the cost value of individual *i* is denoted as 'f_i', where *i* = 1, 2… P and P is the population size.

2. The distance of each individual vector from the best vector in the present generation is computed next. Based on these distances, the individual vectors are again sorted in an ascending order and are given a corresponding rank denoted as'd_i'.

3. Once the two rankings explained in the above two steps are determined, an indicator of the current optimization state so as to determine whether the algorithm has reached the exploration state and exploitation state, called IOS is determined as shown below:

$$IOS = \sum_{i=1}^{P} |f_i - d_i| \tag{5.23}$$

4. The value of IOS is normalized between its maximum and minimum possible values as shown below:

$$IOS' = \frac{(IOS - IOS_{min})}{(IOS_{max} - IOS_{min})} \tag{5.24}$$

5. The optimization state is determined next. A random number between 0 and 1 is generated and it is compared with the value of IOS'.

Exploration state if rand(0,1)<=IOS'

Exploitation state if rand(0,1)>IOS'

6. The values of scaling factor F and crossover probability CR are accordingly updated depending on the state of the optimization algorithm during its runtime

for exploration state:

$$F_G = F_{G-1} + c_F.\Delta F$$
$$CR_G = CR_{G-1} - c_{CR}.\Delta CR \tag{5.25a}$$

for exploitation state:

$$F_G = F_{G-1} - c_F.\Delta F$$
$$CR_G = CR_{G-1} + c_{CR}.\Delta CR \tag{5.25b}$$

where

$$\Delta F, \Delta CR = \frac{(IOS - IOS_{min})}{(IOS_{max} - IOS_{min})} \; for\ exploration\ state \tag{5.25c}$$

$$\Delta F, \Delta CR = \frac{(IOS_{max} - IOS)}{(IOS_{max} - IOS_{min})} \; for\ exploitation\ state \tag{5.25d}$$

5.2.10 Differential Evolution with Individual Dependent Mechanism (DE-IDP-IDM)

Differential Evolution with an individual dependent mechanism (DE-IDP-IDM) was proposed in [159]. This is a recent and novel self adaptive strategy where the cost values of the individuals in the population are used for identifying them into groups of superior set and inferior set. Hence forth, depending on the classification of the individuals and differences of the cost values, the individuals are assigned their own control parameter values (Individual Dependent Parameter (IDP)) and mutation strategies (Individual Dependent Mutation (IDM)).Four mutation types with different search mechanisms are used. A brief outline of the algorithm is given below:

1. An initial population of target or parent vectors is generated. Let the population size be P. Each vector contains 'n' number of genes. Each gene represents a particular antenna dimension or parameter. Each gene can have values between the limits specified by the programmer. The cost values of each vector in the initial population are evaluated before starting the optimization process. Each gene is represented as $X_G(i,j)$ where G represents the generation number, i represents the i^{th}parent vector and j denotes the j^{th}gene of the parent vector. The following steps (2-4) are repeated until the maximum numbers of generations or the termination criterion is met.

2. The individual vectors of the current population are arranged and indexed in ascending order of their cost (objective function) values, and are classified into two sets: the superior (*S*) and the inferior (*I*) using the proportion model [159].

3. For the i^{th} vector, four other vectors are chosen, different from 'i' and mutually exclusive (with indices 'o','r1','r2' and 'r3', however 'o'='i' when the current generation number G is less than G_T). A donor vector corresponding to X_G(i, 1…….n) is formed according to the following equation and denoted as V_G(i, 1…..n):

$$V_G(i,j) = \\ X_G(o,j) + F_o.\Big(\big(X_G(r1,j) - X_G(o,j)\big)\Big) + F_o.\big(X_G(r2,j) - d_G(r3,j)\big) \quad if\ 'o' \in superior\ set \tag{5.26}$$

$$V_G(i,j) =$$
$$X_G(o,j) + F_o.\Big(\big(X_G(better,j) - X_G(o,j)\big)\Big) + F_o.\big(X_G(r2,j) - d_G(r3,j)\big) \; if \;\; 'o' \in$$
$$inferior\ set \tag{5.27}$$

where the scaling factor is a variable as discussed in [159]. The above operation is carried out using mutation strategies and under conditions described in [159]. This step is repeated for all individual vectors in the population.

4. The donor vector undergoes a binary crossover operation with the parent vector based on a crossover probability CR. This results in a corresponding trial vector T_G(i,1…….n). A random number (y) is generated based on uniform probability distribution for every gene of the vector. The value of CR is obtained by rank based IDP strategy as random number with normal distribution having mean of i/NP and standard deviation 0.1.

$$T_G(i,j) = V_G(i,j) if\ y \le CR or\ j = j_{rand}$$
$$T_G(i,j) = X_G(i,j) otherwise \tag{5.28}$$

5. The trial vector is evaluated for its cost. If the trial vector has a lower cost than the corresponding parent vector X_G(i,1……n), then the trial vector replaces the parent vector in the next generation.

5.3 Tuning of Optimization Algorithms

The population size is represented by P for all algorithms and the dimensions to be optimized are D. Normally it is suggested that P should be 10D for differential evolution algorithms [129]. This makes the population size very large and convergence slow. For time economy, we have taken P~6D [131] while evaluating the performances of all algorithms for design problems considered in this chapter except for the transmission line fed and cross aperture coupled antenna where P=3D. Each algorithm is controlled by certain control parameters mostly, the scaling factor 'F' and cross over probability 'CR'. The optimal values of control parameters depend on the population size, dimensions and the nature of optimization problem. It is very difficult to find out the value of CR for optimal performance.

Tuning of optimization algorithm using meta-level genetic algorithm was attempted in [79].We

have used a meta-DEGL algorithm to find out the optimal value of CR in every case(except the optimization of 4 element Yagi-Uda antenna, transmission line fed and cross aperture coupled antenna) as an improvisation except for those algorithms which are self adaptive in nature. The DEGL algorithm is chosen for meta-optimization since it has shown very fast convergence for different numerical benchmark functions earlier [142]. The meta-DEGL algorithm uses F as a random variable, CR as 0.7 and a neighborhood radius of 20%. The meta–DEGL attempts to minimize the mean and standard deviation of 20 runs of the required algorithm with different values of control parameters. Statistical data from the values of control parameters near the optimal control parameter solution provided by the meta-optimizer are also computed to ensure and finalize the control parameter values of the algorithm which are best suited for the optimization problem.

The cost function evaluation for the transmission line fed, cross aperture coupled antenna and 4 element Yagi-Uda antenna are very time consuming. Meta-optimization of the control parameters for the different optimization algorithms considered in this chapter would have required extremely high computation time. Hence, the control parameters best suited for the optimization algorithms for these problem are determined by repeated trial and error procedure with values in close range around the ones mentioned in [129],[139],[141],[142],[144],[145],[149],[152],[153],[156],[157],[158],[159].

5.4 Probe Fed Microstrip Antenna for Circular Polarization

5.4.1 Theory

One of the simplest ways of exciting a microstrip antenna is to use probe feeding technique [3]. Only five parameters are available for optimization in this case, the length (a) and width of the patch (b), co-ordinates of probe feed (x_o,y_o) and the height of the substrate (h). The substrate used has a dielectric constant of 4.3. The geometry of the antenna is shown in Fig. 5.1.

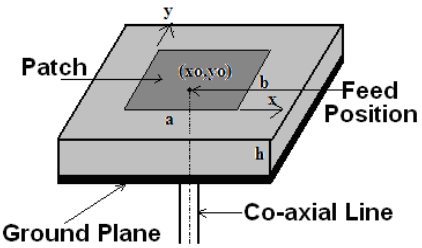

Fig. 5.1 Probe fed circularly polarized microstrip antenna

The present optimization problem is of multi objective nature where several criteria for a right handed circularly polarized antenna are to be satisfied. The frequency range is chosen from 2.38-2.42 GHz. The lower and upper limit of the substrate height within which the optimization algorithm searches for the optimized height is 0.5mm and 3mm respectively. The first objective requires that the antenna should have maximized axial ratio bandwidth (<3 dB) about a center frequency and hence the corresponding cost is defined as:

$$Cost_1 = 1/(ARB + \varepsilon) \tag{5.29}$$

where ARB is the 3 dB axial ratio bandwidth between 2.38-2.42 GHz. 'ε' is a very small number to avoid infinite value of $Cost_1$ when the axial ratio bandwidth is zero.

The second objective is maximum impedance matching over the entire axial ratio band and the corresponding cost is defined as:

$$Cost_2 = \sum_{i=1}^{N} |\tau_i| / N \tag{5.30}$$

where τ_i represents the reflection coefficient at the i^{th} frequency point. The final objective is the maximization of realizable antenna gain in the bore sight direction at the center frequency of 2.4 GHz. The corresponding cost is given as:

$$Cost_3 = \frac{1}{Gain} \tag{5.31}$$

All the individual costs described above are combined into a single cost by assigning dynamically varying weights to each of them.

$$Cost = w_1.Cost_1 + w_2.Cost_2 + w_3.Cost_3 \quad (5.32)$$

Equal distribution of weights causes the optimization algorithm to randomly prefer one or some of the objectives and neglect others. Biased weight distribution does not always guarantee that all the objectives will satisfy at least to a threshold level. A dynamic weight distribution is used here which will cause the corresponding weights for each objective to dynamically vary in each generation according to certain rules. The weights are assigned initial values randomly between 0 and 1 to start the algorithm. Whenever any one of the objectives goes above a threshold value, the dynamic weight allocated to it is simultaneously augmented to temporarily provide more preference to it. The threshold values (for this optimization problem) for axial ratio bandwidth (minimum), mean S_{11} in the axial ratio band (maximum) and gain at the center frequency (minimum) are 15 MHz, -15 dB and 4dBi respectively.

5.4.2 Experimental Results

The optimization of the probe fed patch antenna is carried out with the objectives discussed above. The substrate used has dielectric constant of 4.3. We assumed that substrate height is allowed to vary from 0.5mm to 3 mm. The dimensions of the antenna are optimized using the mentioned 10 DE schemes in section II. The algorithms are run for 25 independent trials and their statistical performance measures are estimated and indicated in Table 5.2. All the algorithms use the same initial population. The initial population contained some candidates whose corresponding antenna geometry will provide non zero axial ratio bandwidth. However, it does not provide any matching or acceptable gain within the axial ratio bandwidth. This is required for the algorithm to ultimately converge to acceptable solution. The best algorithm adjudged from the statistical performance table will be further used to design and simulate the antenna with available substrate of same dielectric constant and thickness of 0.76mm for testing and validation.

Table 5.1. Control parameter settings of the DE algorithms for the optimization of probe fed RHCP microstrip antenna

DE algorithms	Control Parameter Settings
Adaptive differential evolution	Self adaptive
Biogeography based optimization with differential evolution	F=random number between 0 and 1 with uniform probability density function distribution CR=0.95
DE/rand/1	F=random number between 0 and 2 with uniform probability density function distribution. CR=0.98
Differential evolution with individual dependent mechanism	Self adaptive
Differential Evolution with global and local neighborhood search	Neighborhood radius=20% CR=0.65
Harmonic search differential evolution	CR (minimum)=0.20 CR(maximum)=0.95 F(minimum)=0.10 F(minimum)=0.65
Improved differential evolution	F=random number between 0 and 1 with uniform probability density function distribution CR=0.95

Modified differential evolution	F=random number between 0 and 2 with uniform probability density function distribution CR=0.94 Beta=0.40
DE algorithms	Control Parameter Settings
Modified differential evolution with p-best crossover strategy	Adaptive
Self adaptive differential evolution	Self adaptive

The statistical performances of the algorithms are given in Table 5.2.

Table 5.2. Statistical performances of the DE algorithms in the optimization of probe fed RHCP microstrip antenna.

DE algorithm	Mean cost value	Best cost value	Worst cost value	Standard deviation	Robustness (%)	Convergence rate(generations)
ADE	0.2997	0.2444	0.6799	0.1018	68	83
BBODE	0.3081	0.2440	0.4882	0.0772	56	46
DE/rand/1	0.2444	0.2433	0.2454	7.96e-04	100	31
DE-IDP-IDM	0.2535	0.2439	0.4169	0.0342	96	22
DEGL	0.2447	0.2435	0.2469	0.0011	100	21
HSDE	0.3436	0.2458	0.5590	0.1023	56	96
IDE	0.2449	0.2431	0.2500	0.0015	100	26
MDE	0.2440	0.2431	0.2451	6.98e-4	100	24
MDEPBX	0.3731	0.2528	0.5599	0.0985	28	32
SADE	0.2550	0.2455	0.3222	0.0157	96	62

The applicability of DE/rand/1, DEGL, DE-IDP-IDM, MDE and IDE is very much pronounced in this optimization problem according to the statistical data in the table above. Best performance

is shown by MDE which showed 100% robustness with minimum mean cost value, lowest worst cost value and minimum standard deviation. Convergence rate also confirms that MDE shows very fast convergence. This implies any arbitrary run of the MDE algorithm for this optimization problem will provide desirable results and within lesser number of iterations compared to the most of the other variants of DE algorithms considered in this chapter. Performance of IDE is very close to that of MDE and it shows the fastest convergence. IDE loses out to MDE in terms of mean cost value, worst cost value and standard deviation. DE/rand/1 loses out to IDE in terms of convergence rate. Among the self adaptive algorithms, best performance is shown by DE-IDP-IDM which has shown 100% robustness and fastest convergence rate. ADE, HSDE and MDEPBX algorithms have shown comparatively low robustness. The best cost convergence graphs of all the optimization algorithms are depicted in Fig.5.2 and Fig. 5.3.

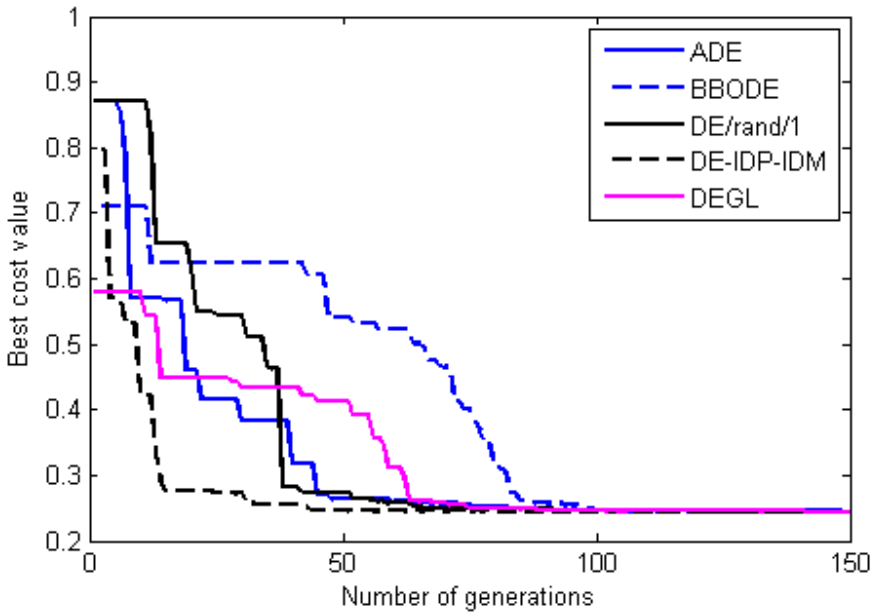

Fig. 5.2 Best convergence plots for ADE, BBODE, DE/rand/1, DE-IDP-IDM and DEGL in the optimization of RHCP probe fed microstrip antenna

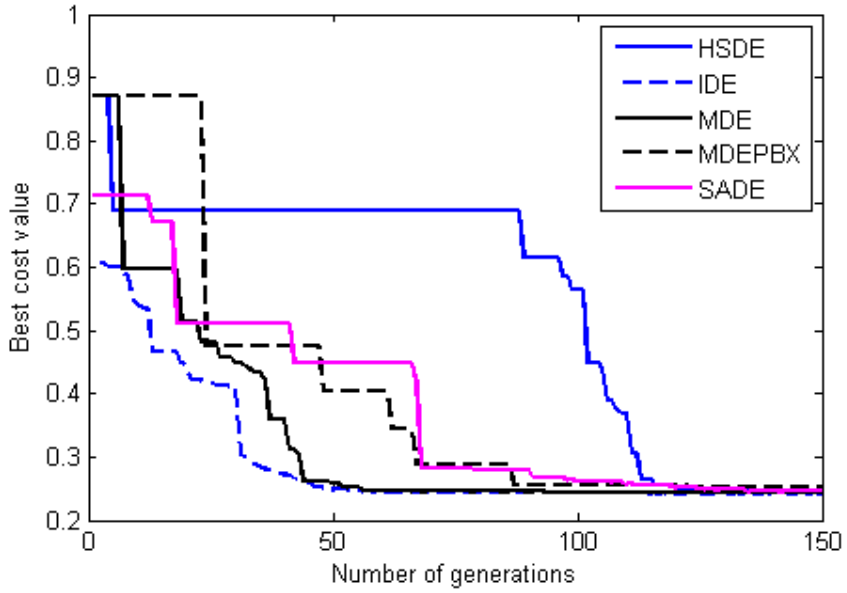

Fig. 5.3 Best convergence plots for HSDE, IDE, MDE, MDEPBX and SADE in the optimization of RHCP probe fed microstrip antenna

The mean cost convergence curves are shown below in Fig. 5.4 and Fig. 5.5:

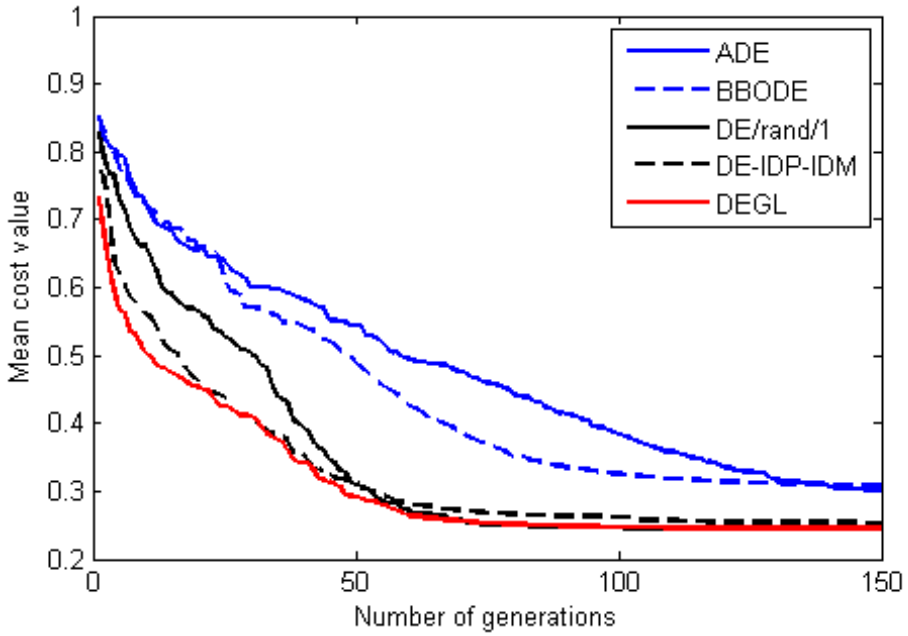

Fig 5.4 Mean convergence plots for ADE, BBODE, DE/rand/1, DE-IDP-IDM and DEGL in the optimization of RHCP probe fed microstrip antenna

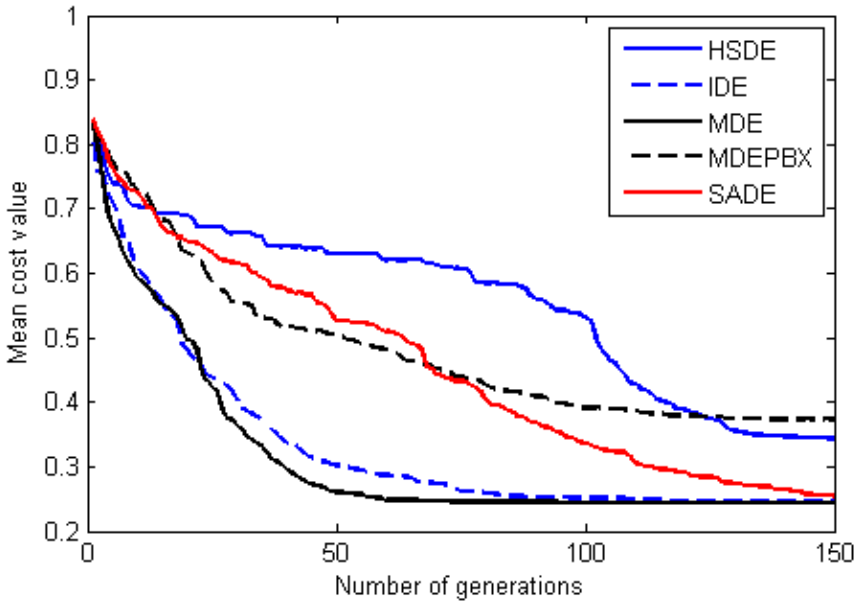

Fig 5.5 Mean convergence plots for HSDE, IDE, MDE, MDEPBX and SADE in the optimization of RHCP probe fed microstrip antenna

The antenna performances obtained from the best run of reach algorithm are given in Table 5.3.

Table 5.3. Performances of the optimized probe fed RHCP microstrip antennas obtained from the best run of each algorithm.

DE algorithm	Axial ratio bandwidth (MHz)	Impedance matching within the axial ratio band(mean S_{11} in dB)	Gain (dBi) at the center frequency
ADE	18.08	-17.84	4.64
BBODE	18.24	-17.85	4.64
DE/rand/1	18.24	-17.83	4.68
DE-IDP-IDM	18.24	-17.86	4.65
DEGL	18.24	-17.80	4.67
HSDE	18.08	-17.86	4.62
IDE	18.24	-17.86	4.69
MDE	18.24	-17.86	4.69
MDEPBX	17.28	-17.66	4.64
SADE	18.08	-17.68	4.65

MDE is adjudged to be the most suitable optimization algorithm for this case. From Table 5.3, the antenna obtained from the best run of MDE algorithm showed an axial ratio bandwidth of 18.24 MHz, mean S_{11} of -17.86 dB in the axial ratio band and a gain of 4.69 dBi at the design frequency of 2.4 GHz. The antenna has dimensions of a=27.34 mm, b=28.04 mm, h= 2.49 mm and probe location of (10.625mm, 11.21 mm) from lower left vertex of the patch. MDE is also used for designing and fabricating a RHCP microstrip antenna with the same substrate but having a fixed height of 0.76 mm and loss tangent of 0.003. It has dimensions of a=29.80 mm, b=30.12 mm with probe locations (10.59 mm, 10.88 mm). The comparisons between the simulated and measured results are shown in Fig.4. The measured axial ratio bandwidth is 9.00 MHz, mean S_{11} of -13.2 dB in the axial ratio band and a gain of 3.52 dBi at the center frequency.

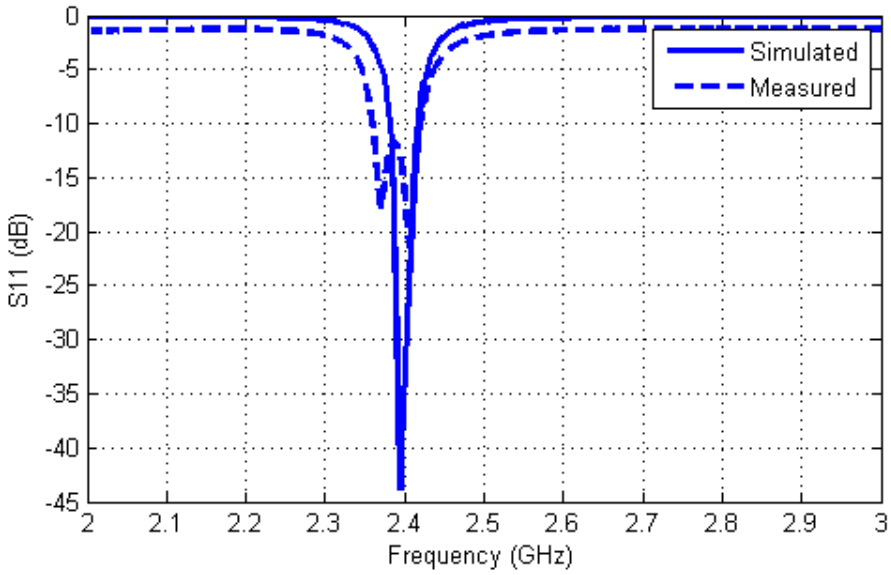

Fig 5.6 Simulated and measured S_{11} versus frequency for the probe fed RHCP microstrip antenna with substrate height of 0.76 mm

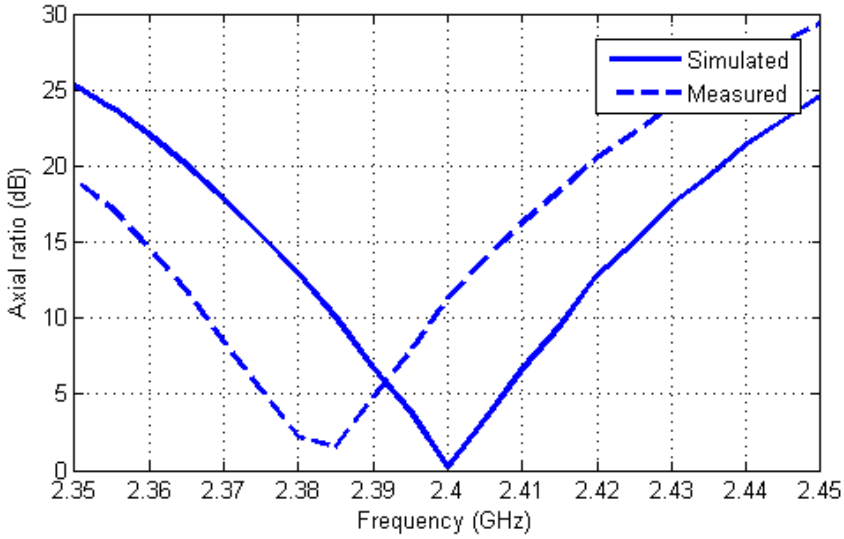

Fig 5.7 Simulated and measured axial ratio versus frequency for the probe fed RHCP microstrip antenna with substrate height of 0.76 mm

The fabricated prototype of the probe fed circularly polarized microstrip antenna obtained from the MDE algorithm is shown in Fig. 5.8.

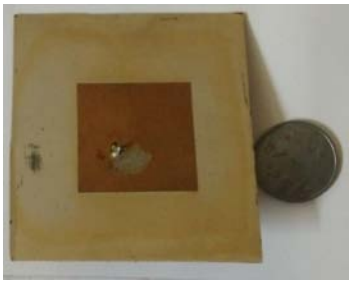

Fig. 5.8 Fabricated prototype of the probe fed circularly polarized microstrip antenna obtained from the MDE algorithm

5.5Transmission Line Fed Microstrip Antenna for Circular Polarization

5.5.1 Theory

One way of exciting a nearly square microstrip antenna for right handed circularly polarized operation is to use a dual transmission line feed to equally excite TM_{10} and TM_{01} mode of operation with a phase difference of 90 degrees between them. An example of such network is available in [3]. The discontinuity effects in the transmission line network must be considered. Use of couplers and power dividers in designing such transmission line networks for RHCP antenna feed is also available in [3]. Here a similar transmission line feeding network is used as shown in the figure below. The substrate used has a dielectric constant of 4.3. The geometry of the antenna is shown in Fig 5.9.

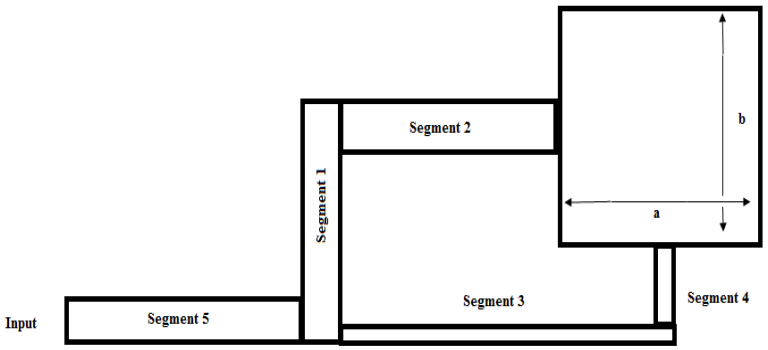

Fig 5.9 Transmission line fed circularly polarized microstrip antenna

The antenna structure shown in the figure above is analyzed using multiport network modeling approach [3] so that the microstrip line discontinuity effects can be taken in to account. The feed line network has five straight microstrip line segments numbered from one to five as shown in the figure above. Each segment has its own length and width to be optimized for the objectives described below. For example segment 1 has length L_1 and width W_1 and so on. The dimensions of the nearly square patch antenna are ‘a’ x’b’.

The dimensions L_1 and L_2 are related to the other dimensions by the following equations:

$$L_1 = L_3 - L_2 - \frac{W_4}{2} \tag{5.33}$$

$$L_2 = W_3 + L_4 + \frac{W_1}{2} + \frac{b}{2} \tag{5.34}$$

As already mentioned, the structure is analyzed using the multiport network modeling method. Different ports are defined at the microstrip interconnections and junctions in the figure above. The Z-matrix needs to be computed for the multiport network model. The matrix value for any two ports (for example 'i' and 'j') associated with the same microstrip segment can be calculated as [3]:

$$Z_{ij}^{s} = \frac{1}{W_i W_j} \iint_{PW_i PW_j} G^{S}(s, s_o) ds ds_o \tag{5.35}$$

Z_{ij} represents the (i, j) element of the impedance matrix. W_i and PW_i represent the effective width and physical width of the i^{th} port. Similarly W_j and PW_j represent the effective width and physical width of the j^{th} port. The effective widths are calculated after taking into account the fringing field extensions along the edges of the microstrip structure. It is assumed that the microstrip planar structure is placed on the x-y plane above a substrate of dielectric constant ε and height 'h'. The substrate layout is assumed to be infinite along x and y axis and is placed on an infinite ground plane. $G^s(s,s_o)$ represent the Green's function which has the following form [3]:

$$G_s(x, y|x_o, y_o) = \frac{j\omega\mu h}{ab} \sum_{m=-\infty}^{+\infty} \sum_{n=-\infty}^{+\infty} \frac{\psi_{mn}^{s}(x,y)\psi_{mn}^{s*}(x_o,y_o)}{k_{mn}^2 - k^2} \tag{5.36}$$

Where ψ^s_{mn} (x,y) represent the Eigen function of the (m,n) mode of the microstrip segment under consideration and k_{mn} is the corresponding Eigen-value. For a rectangular microstrip segment the Eigen function is given by [3]:

$$G(x,y|x_o,y_o) = \frac{j\omega\mu h}{a'b'} \sum_{m=-\infty}^{+\infty} \sum_{n=-\infty}^{+\infty} \frac{\sigma_m \sigma_n}{k_x^2 + k_y^2 - k^2} \cos(k_x x)\, cos(k_x x_o) \cos(k_y y) \cos(k_y y_o) \quad (5.37)$$

where the parameter σ_m=1 if m=0 otherwise σ_m=1. This also holds true for σ_n.

Also,

$$k_x = \frac{m\pi}{a'} \quad (5.38a)$$

$$k_y = \frac{n\pi}{b'} \quad (5.38b)$$

$$k^2 = \omega^2 \mu_o \varepsilon_o \varepsilon_{eff} \quad (5.38c)$$

a' and b' are the dimensions (along x-axis and y-axis) of the microstrip segment under consideration.

The present optimization problem is of multi objective nature where several criteria for a right handed circularly polarized antenna are to be satisfied. The frequency range is chosen from 2.38-2.42 GHz. The lower and upper limit of the substrate height within which the optimization algorithm searches for the optimized height is 0.5mm and 2.5mm respectively.

The computation of optimization objectives is done by applying the multiport network modeling and analysis techniques to the dual transmission line fed microstrip antenna. Since, multiport network analysis is time consuming; low population size of 33 candidate vectors corresponding to 11 antenna dimensions is used. It is observed that the cost function needs to be altered slightly to enable the optimizations algorithms converge to the optimization goals. The design objectives and corresponding cost functions are the same as used in case of probe fed RHCP microstrip antenna. The first objective requires that the antenna should have maximized axial ratio bandwidth (<3 dB) about a center frequency and hence the corresponding cost is defined as:

$$Cost_1 = 1/(3\ dB\ Axial\ ratio\ bandwidth\ (GHz)\ within\ 2.38 - 2.42\ GHz + \varepsilon) \quad (5.39)$$

The second objective is improving the axial ratio at the center frequency:

$$Cost_2 = Axial\ ratio\ at\ the\ center\ frequency \quad (5.40)$$

The third objective is maximum impedance matching over the entire axial ratio band and the corresponding cost is defined as:

$$Cost_3 = \sum_{i=1}^{N} |\tau_i| / N \quad (5.41)$$

where τ_i represents the reflection coefficient at the i^{th} frequency point.

The fourth objective is improving the impedance matching at the center frequency:

$$Cost_4 = |\tau| at\ the\ center\ frequency \quad (5.42)$$

The final objective is the maximization of realizable antenna gain in the bore sight direction at the center frequency of 2.4 GHz. The corresponding cost is given as:

$$Cost_5 = \frac{1}{Gain} \quad (5.43)$$

All the individual costs described above are combined into a single cost by assigning dynamically varying weights to each of them.

$$Cost = w_1.Cost_1 + w_2.Cost_2 + w_3.Cost_3 + w_4.Cost_4 + w_5.Cost_5 \quad (5.44)$$

The weight adjustments are done in the same manner as in the case of probe fed RHCP microstrip antenna. The threshold values (for this optimization problem) for axial ratio bandwidth (minimum), axial ratio at the center frequency (minimum) mean S_{11} in the axial ratio band (maximum), S_{11} at the center frequency, and gain at the center frequency (minimum) are 6 MHz, 1.1,-15 dB, -15 dB and 3.5dBi respectively.

5.5.2 Experimental Results

The optimization of the transmission line fed RHCP patch antenna is carried out with the objectives discussed above. The substrate used has dielectric constant of 4.3 and loss tangent 0.003. We assumed that substrate height is allowed to vary from 0.5mm to 2.5 mm. The dimensions of the antenna are optimized using the mentioned 10 DE schemes in section 2. The

algorithms are run for 20 independent trials and their statistical performance measures are estimated and indicated in Table 5.5. The initial conditions for the algorithms in this optimization problem are similar to those of the previous one. The best algorithm adjudged from the statistical performance table will be further used to design and simulate the antenna with available substrate of same dielectric constant and thickness of 0.76mm for testing and validation.
The control parameter settings of the DE algorithms are given in the Table 5.4 below:

Table 5.4. Control parameter settings of the DE algorithms for the optimization of transmission line fed RHCP microstrip antenna

DE algorithms	Control Parameter Settings
Adaptive differential evolution	Self adaptive
Biogeography based optimization with differential evolution	F=random number between 0 and 1 with uniform probability density function distribution CR=0.90
DE/rand/1	F=random number between 0 and 2 with uniform probability density function distribution. CR=0.98
Differential evolution with individual dependent mechanism	Self adaptive
Differential Evolution with global and local neighborhood search	Neighborhood radius=18% CR=0.80
Harmonic search differential evolution	CR (minimum)=0.20 CR(maximum)=0.95 F(minimum)=0.10 F(minimum)=0.65

Improved differential evolution	F=random number between 0 and 1 with uniform probability density function distribution CR=0.90
Modified differential evolution	F=random number between 0 and 2 with uniform probability density function distribution CR=0.95 Beta=0.40
Modified differential evolution with p-best crossover strategy	Adaptive
Self adaptive differential evolution	Self adaptive

The statistical performances of the algorithms are given in Table 5.5.

Table 5.5. Statistical performances of the DE algorithms in the optimization of transmission line fed RHCP microstrip antenna.

DE algorithm	Mean cost value	Best cost value	Worst cost value	Standard deviation	Robustness (%)	Convergence rate (generations)
ADE	51.98	1.696	110.10	31.00	15	98
BBODE	4.431	1.425	37.560	9.276	85	97
DE/rand/1	2.326	1.392	4.9034	1.257	75	91
DE-IDP-IDM	1.906	1.387	3.8023	0.859	85	63
DEGL	25.93	1.419	116.05	39.41	65	65
HSDE	15.90	1.588	48.745	17.13	55	136
IDE	2.117	1.392	8.8512	1.948	85	49
MDE	1.753	1.406	4.8002	0.850	95	69
MDEPBX	56.50	1.697	176.05	51.61	0	NA
SADE	23.08	1.569	70.206	25.80	45	108

The applicability of BBODE, DE/rand/1, DE-IDP-IDM, MDE and IDE is very much pronounced in this optimization problem according to the statistical data in the table above. Best robustness is shown by MDE algorithm. The convergence rate of MDE is moderate. MDE algorithm also showed minimum values for mean cost value and standard deviation from the mean cost value. Among the other algorithms, second best performance is shown by DE-IDP-IDM algorithm. It showed minimum best cost value, second best values for mean cost value and standard deviation. It also has high robustness. MDE-pBX has however failed to show any convergence. Hence this algorithm is not considered appropriate for this particular optimization. Depending on the statistical data in the table above, MDE algorithm is considered to be the best algorithm for this design problem. The best convergence cost convergence graphs of all the optimization algorithms are depicted in Fig. 5.10 and Fig. 5.11 respectively.

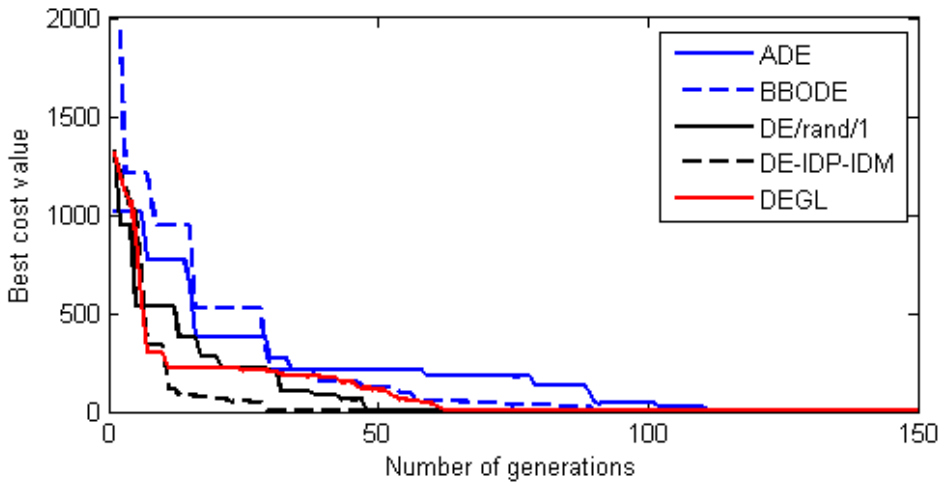

Fig 5.10 Best convergence plots for ADE, BBODE, DE/rand/1, DE-IDP-IDM and DEGL algorithms in the optimization of transmission line fed RHCP microstrip antenna.

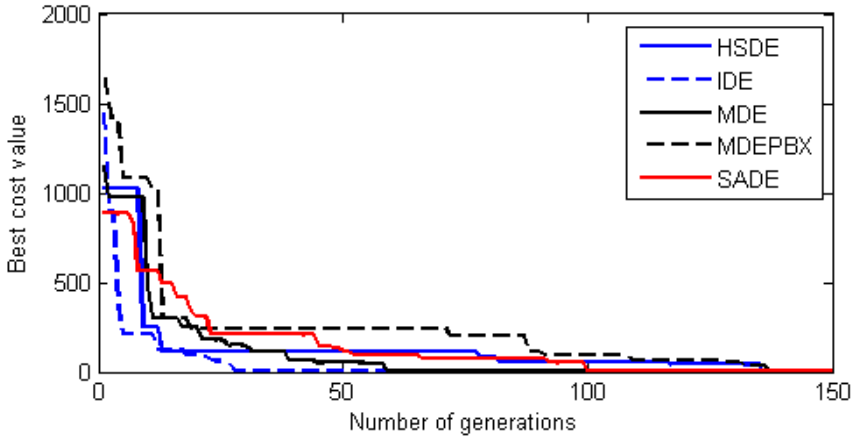

Fig 5.11 Best convergence plots for HSDE, IDE, MDE, MDE-pBX and SADE algorithms in the optimization of transmission line fed RHCP microstrip antenna.

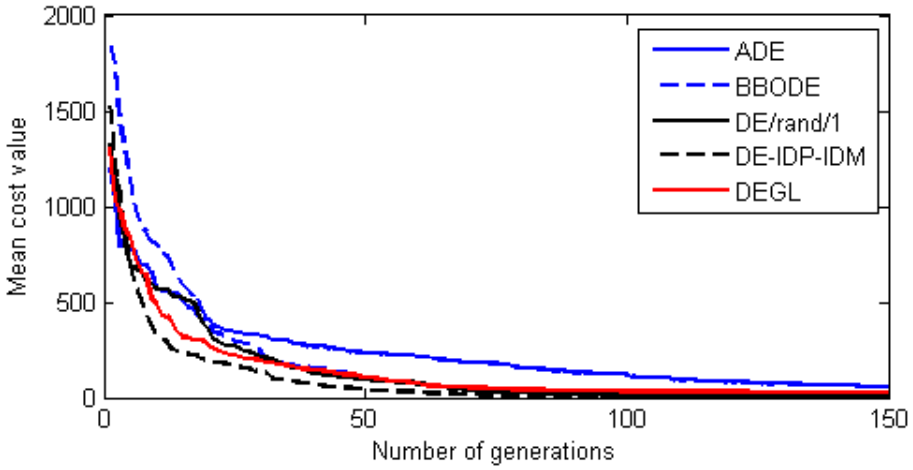

Fig 5.12 Mean convergence plots for ADE, BBODE, DE/rand/1, DE-IDP-DM and DEGL algorithms in the optimization of transmission line fed RHCP microstrip antenna.

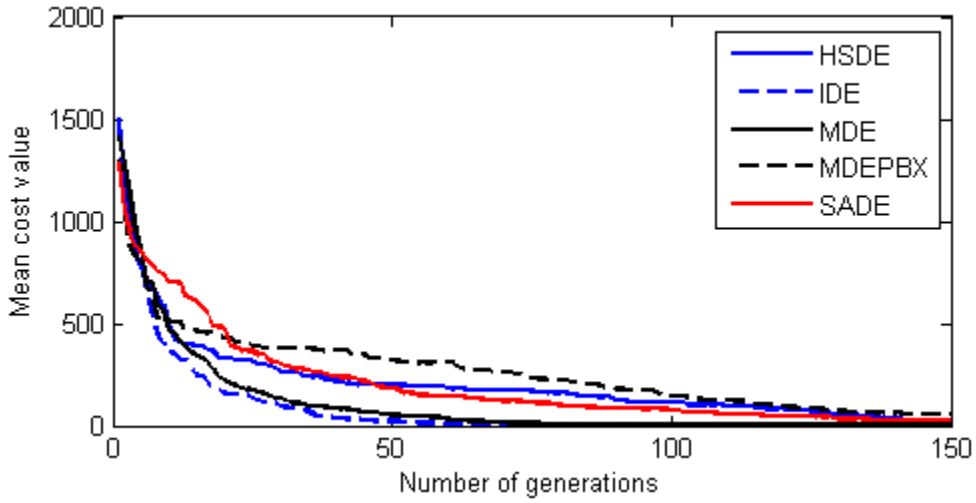

Fig 5.13 Mean convergence plots for HSDE, IDE, MDE, MDE-pBX and SADE algorithms in the optimization of transmission line fed RHCP microstrip antenna.

The antenna performances obtained from the best run of reach algorithm are given in Table 5.6.

Table 5.6. Performances of the optimized transmission line fed RHCP microstrip antennas obtained from the best run of each algorithm.

DE algorithm	Axial ratio bandwidth (MHz)	Axial ratio at the center frequency	Impedance matching within the axial ratio band(mean S_{11} in dB)	S_{11} (dB) at the center frequency	Gain (dBi)at the center frequency
ADE	17.20	1.057	-24.950	-27.768	4.1398
BBODE	19.60	1.001	-24.628	-26.620	5.0004
DE/rand/1	19.60	1.000	-32.154	-32.874	5.0586
DE-IDP-IDM	19.60	1.000	-35.372	-44.894	5.0682
DEGL	18.80	1.002	-33.602	-41.813	4.9687
HSDE	17.60	1.040	-22.042	-22.637	4.9385
IDE	19.60	1.000	-35.079	-47.867	5.0174

MDE	19.20	1.002	-31.367	-39.096	5.0378
MDEPBX	-		-		-
SADE	18.00	1.0451	-23.97	-26.46	4.8098

MDE is adjudged to be the most suitable optimization algorithm for this case. From the table above, the antenna obtained from the best run of MDE algorithm showed an axial ratio bandwidth of 19.20 MHz, mean S_{11} of -31.367 dB in the axial ratio band and a gain of 5.0378dBi at the design frequency of 2.4 GHz. The patch antenna has dimensions of a=28.35 mm, b=31.08 mm, and h= 1.78 mm. The feed line network has dimensions (L_1,W_1)=(7.62 mm, 4.92 mm), (L_2, W_2)=(44.31 mm,9.27 mm), (L_3, W_3)=(28.53 mm, 4.32 mm), (L_4, W_4)=(20.20 mm,9.92 mm) and (L_5, W_5)=(31.45 mm, 4.83 mm). MDE is also used for designing and fabricating a RHCP microstrip antenna with the available substrate having the same dielectric constant but having a fixed height of 0.76 mm and avoiding proximity between parallel edges. It has patch antenna dimensions having a=29.55 mm and b=29.88 mm. The transmission line feed network has dimensions (L_1,W_1)=(58.26 mm, 1.60 mm), (L_2, W_2)=(30.69 mm,2.85 mm), (L_3, W_3)=(45.78 mm, 1.094 mm), (L_4, W_4)=(40.79 mm, 0.52 mm) and (L_5, W_5)=(18.165 mm, 5 mm). The comparisons between the simulated and measured results are shown in Fig. 5.14 and Fig. 5.15 respectively. The measured axial ratio bandwidth is 3.6 MHz, mean S_{11} of -14.01 dB in the axial ratio band and a gain of 2.01dBi at the center frequency.

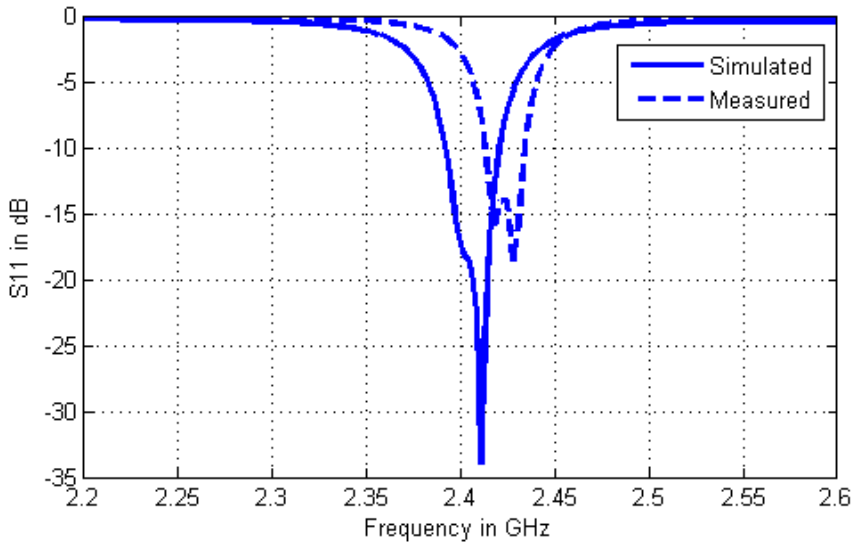

Fig 5.14 Simulated and measured S_{11} versus frequency for the transmission line fed RHCP microstrip antenna with substrate height of 0.76 mm

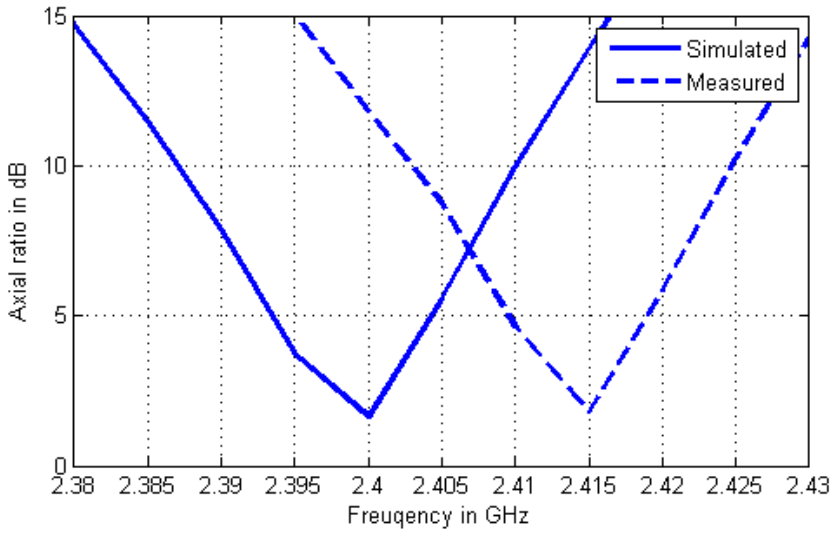

Fig 5.15 Simulated and measured axial ratio versus frequency for the transmission line fed RHCP microstrip antenna with substrate height of 0.76 mm

The fabricated prototype of the transmission line fed circularly polarized microstrip antenna obtained from the MDE algorithm is shown below:

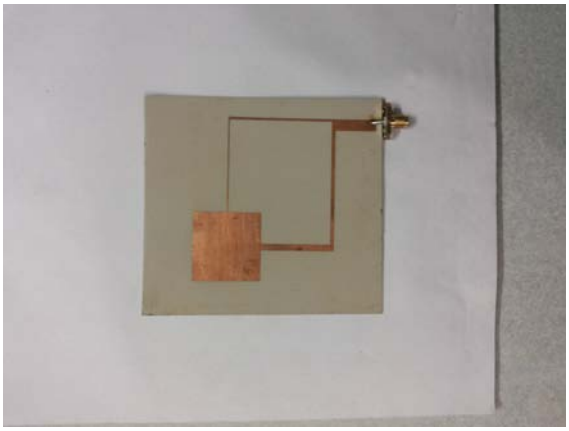

Fig. 5.16 Fabricated prototype of the transmission line fed circularly polarized microstrip antenna obtained from the MDE algorithm

5.6 Cross Aperture Coupled Microstrip Antenna for Circular Polarization

5.6.1 Theory

An aperture coupled patch antenna provides a wide range of parameters described below for optimization in terms of impedance bandwidth, axial ratio in case of circular polarization and gain. One inherent advantage of using the aperture feeding technique is the separate optimization for the patch structure and the feed line which often helps in maintaining impedance matching over a wide range of frequencies.

Different analytical methods are used for estimating the aperture coupled antenna parameters in the past [23],[37]. The cost or objective values in our case are derived using the MoM technique. The top and side views of the antenna are shown below in Fig 5.17. The substrate parameters remain the same as before.

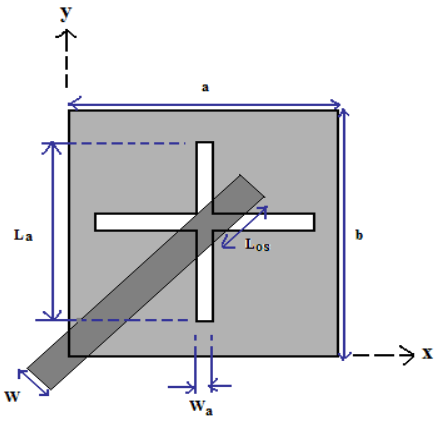

(a) Top view

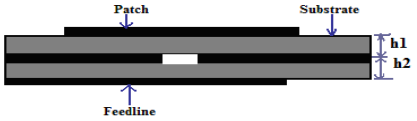

(b)Side view

Fig 5.17 Cross aperture coupled RHCP microstrip antenna

5.6.2 Experimental Results

The optimization of the cross slotted patch antenna is carried out with the similar objectives explained in probe fed rectangular RHCP microstrip antenna. The threshold values used are 12 MHz for axial ratio bandwidth (minimum), -15 dB for mean S_{11} in the axial ratio band (maximum) and 3.5 dBi for the gain (minimum) in the bore sight direction.

The initial conditions for the algorithms in this optimization problem are almost similar to those of the previous one. However in this case the population size is chosen to be thrice the number of variables involved and to ensure convergence to a desired solution (even if the small initial population does not have a candidate with non zero axial ratio bandwidth), the cost function is slightly altered. The cost function in this case has a fourth component as given below:

$$Cost_4 = w_4.AR(fc) \tag{5.45}$$

Table 5.7. Control parameter settings of the DE algorithms for the optimization of aperture coupled RHCP microstrip antenna

DE algorithms	Control Parameter Settings
Adaptive differential evolution	Self adaptive
Biogeography based optimization with differential evolution	F=random number between 0 and 1 with uniform probability density function distribution CR=0.80
DE/rand/1	F=random number between 0 and 2 with uniform probability density function distribution. CR=0.98
Differential evolution with individual dependent mechanism	Self adaptive
Differential Evolution with global and local neighborhood search	Neighborhood radius~20% CR=0.72
Harmonic search differential evolution	CR (minimum)=0.20 CR(maximum)=0.95 F(minimum)=0.10 F(minimum)=0.65
Improved differential evolution	F=random number between 0 and 1 with uniform probability density function distribution CR=0.80
Modified differential evolution	F=random number between 0 and 2 with uniform probability density function distribution CR=0.95 Beta=0.40

Modified differential evolution with p-best crossover strategy	Adaptive
Self adaptive differential evolution	Self adaptive

The statistical performances of the algorithms are given in Table 5.8.

Table 5.8. Statistical performances of the DE algorithms for the optimization of cross aperture coupled RHCP microstrip antenna.

DE algorithm	Mean cost value	Best cost value	Worst cost value	Standard deviation	Robustness (%)	Convergence rate (Generations)
ADE	2.9065	0.7938	12.127	3.0200	64	73
BBODE	6.9675	0.7780	12.119	5.5961	44	48
DE/rand/1	2.6988	0.7869	11.909	4.0789	84	75
DE-IDP-IDM	0.7879	0.7836	0.7979	0.0052	100	43
DEGL	0.7896	0.7812	0.7934	0.0040	100	46
HSDE	0.8127	0.8001	0.8206	0.0071	100	109
IDE	1.1868	0.7769	4.0834	0.9474	92	87
MDE	0.7850	0.7810	0.7934	0.0045	100	30
MDEPBX	9.1185	2.3816	12.45	4.4259	12	125
SADE	1.6907	0.7999	9.1596	2.2857	92	85

The applicability of DE-IDP-IDM, DEGL, HSDE and MDE is more pronounced in this case. All these algorithms have shown 100% robustness. Among these three algorithms, MDE has shown minimum values of mean cost value and fastest convergence rate of only 30 runs. The performance of DEGL and DE-IDP-IDM is very close to that of MDE and both of them have almost the same convergence rate. However their convergence rate is comparatively slower compared to that of MDE. Hence MDE is adjudged to be the best algorithm for this optimization problem.

The best cost convergence plots are shown in Fig 5.18 and Fig. 5.19below:

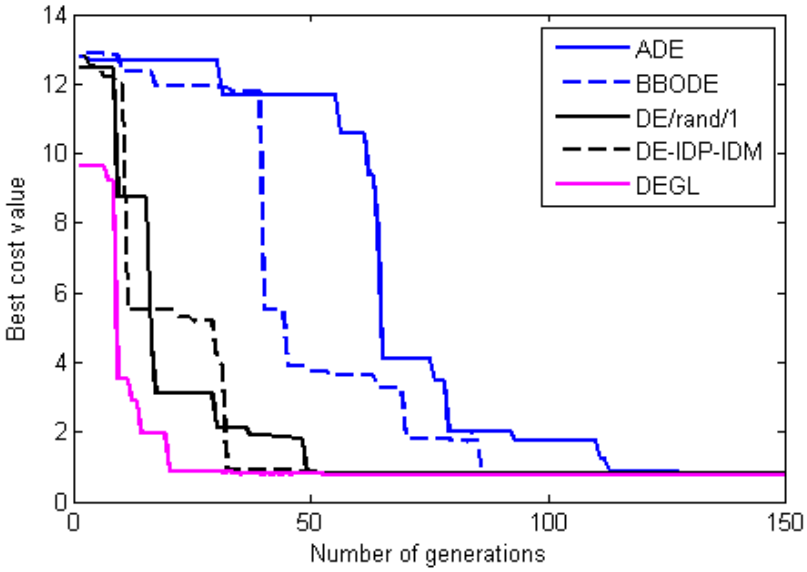

Fig 5.18 Best convergence plots for ADE, BBODE, DE/rand/1, DE-IDP-IDM and DEGL in the optimization of RHCP cross aperture coupled microstrip antenna

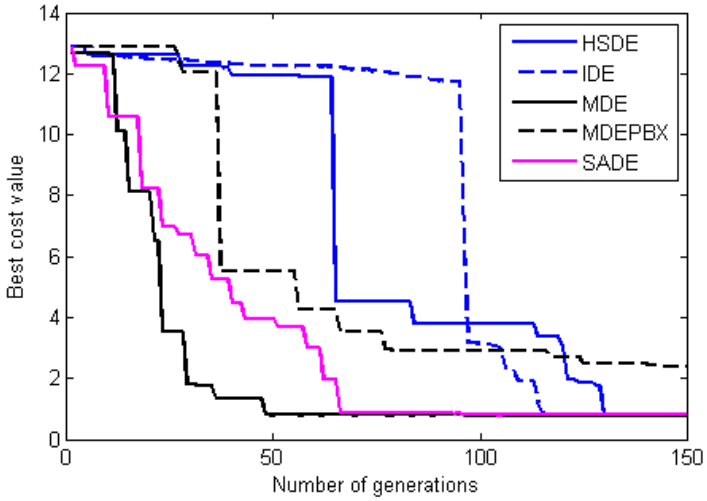

Fig. 5.19 Best convergence plots for HSDE, IDE, MDE, MDEPBX and SADE in the optimization of RHCP cross aperture coupled microstrip antenna

The mean cost convergence plots are shown below in Fig 5.20 and Fig. 5.21 respectively:

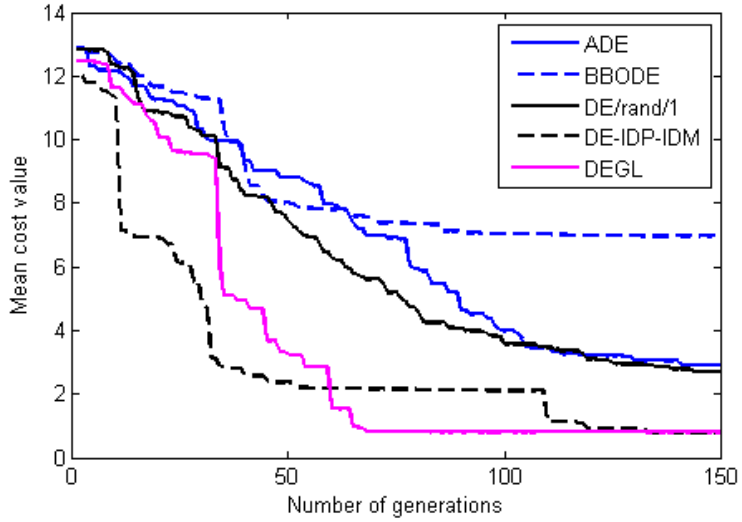

Fig 5.20 Mean convergence plots for ADE, BBODE, DE/rand/1, DE-IDP-IDM and DEGL in the optimization of RHCP cross aperture coupled microstrip antenna

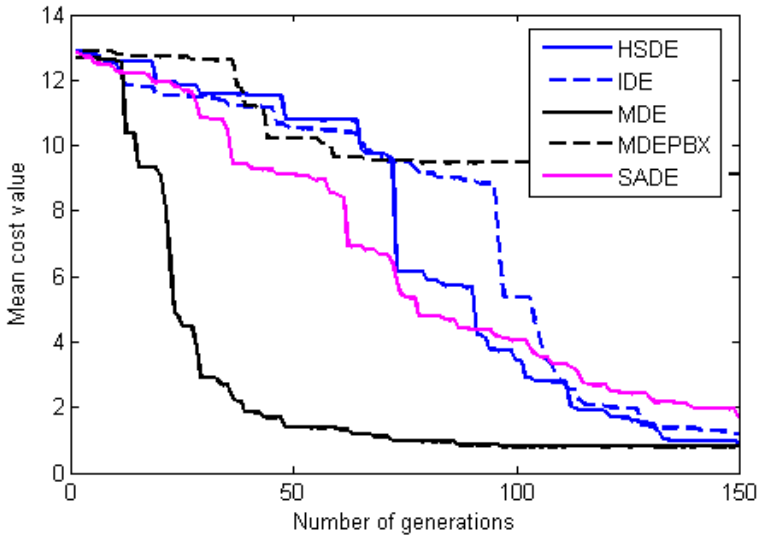

Fig 5.21 Mean convergence plots for HSDE, IDE, MDE, MDEPBX and SADE in the optimization of RHCP cross aperture coupled microstrip antenna

The performances of the optimally designed antennas obtained from the best run of each algorithm are given in Table 5.9.

Table 5.9.The optimal cross aperture coupled RHCP microstrip antenna performances obtained from the best run of each algorithm:

DE algorithm	Axial ratio bandwidth (MHz)	Impedance matching within the axial ratio band(mean S_{11} in dB)	Gain (dBi) at the center frequency
ADE	13.60	-22.06	4.82
BBODE	14.80	-32.55	4.80
DE/rand/1	14.80	-30.60	4.84
DE-IDP-IDM	14.80	-35.96	4.83
DEGL	14.40	-34.53	4.84
HSDE	14.40	-28.05	4.83
IDE	14.80	-28.50	4.83
MDE	14.40	-33.39	4.82
MDEPBX	12.40	-16.30	4.53
SADE	14.40	-29.37	4.78

MDE is adjudged to be the best algorithm in this case. The antenna dimensions obtained from the MDE algorithm provides an axial ratio bandwidth of 14.40 MHz, mean S_{11} of –33.39 dB in the axial ratio band, and gain of 4.82 dBi at the design frequency of 2.4 GHz in the bore sight direction. The antenna has dimensions a=27.98 mm, b=28.59 mm, h=1.79 mm, L_a=11.50 mm, W_a=0.50 mm, W=1.38 mm and L_{os}=12.12 mm. The same algorithm is used to design and fabricate the cross aperture coupled RHCP microstrip antenna on the same substrate with the fixed substrate height of 0.76 mm. The dimensions of the optimized antenna are a=27.81 mm, b=28.14 mm, L_a=9.5 mm, W_a=1.00 mm, W=1.01 mm, L_{os}=13.68 mm. The comparisons between simulated and measured results are shown in Fig. 7. The measured axial ratio bandwidth is 8.2 MHz, mean S_{11} of -14.88 dB and gain of 3.06 dBi. The differences observed between the simulated and measured results may be due to fabrication tolerances and numerical approximations involved in the analysis and cost function evaluations.

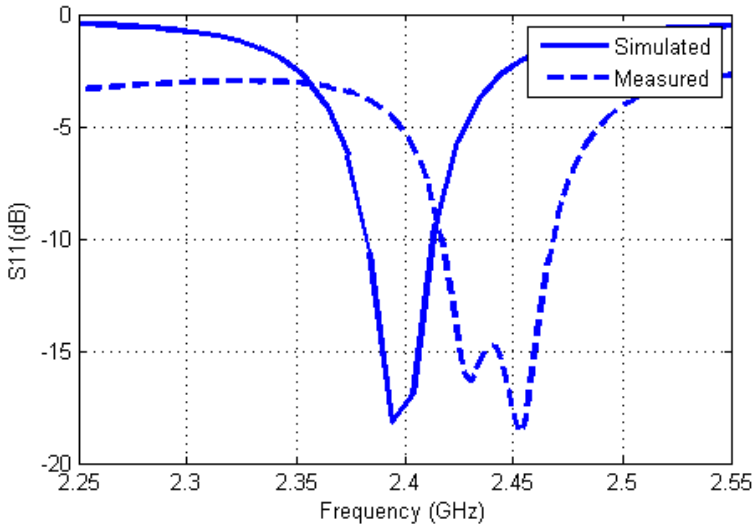

Fig 5.22 Simulated and measured S_{11} versus frequency for the aperture coupled microstrip antenna with substrate height of 0.76 mm

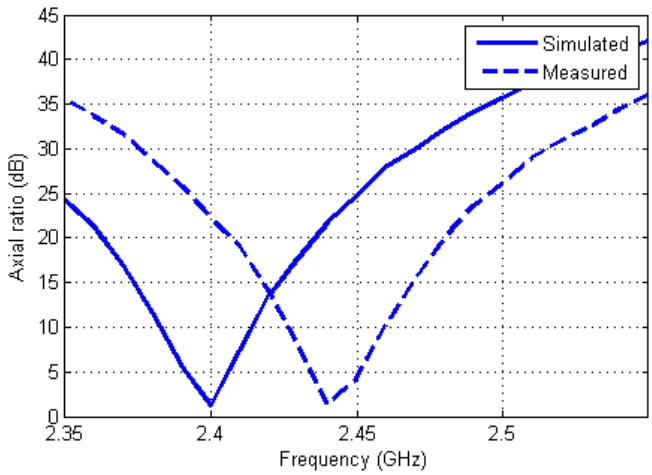

Fig 5.23 Simulated and measured axial ratio versus frequency for the aperture coupled microstrip antenna with substrate height of 0.76 mm

The fabricated prototype of the cross aperture coupled circularly polarized microstrip antenna obtained from the MDE algorithm is shown below in Fig. 5.24.

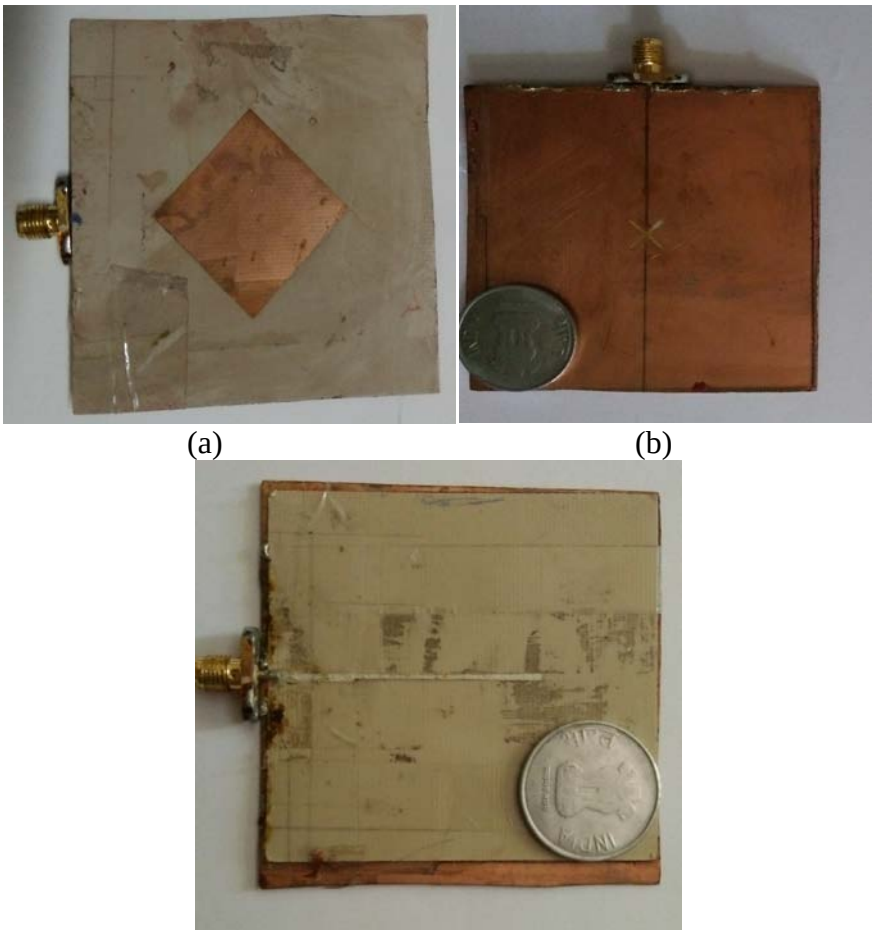

(a) (b)

(c)

Fig. 5.24 Fabricated prototype of the cross aperture coupled circularly polarized microstrip antenna obtained from the MDE algorithm (a) top view (b) slots on the ground plane (c) bottom view

5.7 Linear Array of Unequally Spaced Isotropic Antenna Elements

5.7.1 Theory

A linear array of unequally spaced linear antenna elements is shown in the Fig. 5.25. The array has unequal inter-element spacing between the adjacent elements. 16 isotropic antenna elements are used in this optimization case study. The arrangement of the array is assumed to be symmetric about the center of the array. Hence only 8 variables or 8 inter-element spacing are to be optimized. The lower and upper boundaries of inter-element spacing are assumed to be 0.5λ and 1λ respectively to avoid mutual coupling and grating lobe effects:

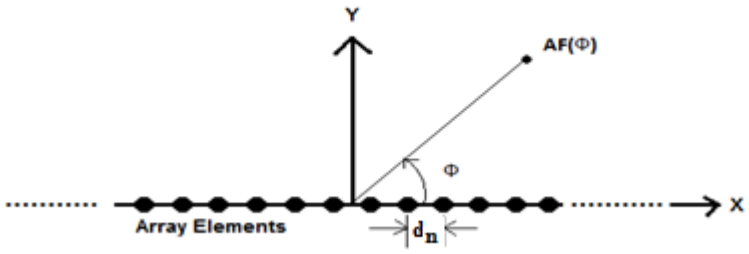

Fig 5.25 Geometry of unequally spaced linear array of isotropic elements

If all the antenna elements are assumed to be isotropic, then the array factor (AF) of the antenna can be written as:

$$AF = \sum_{n=-N}^{n=+N} A_n e^{[jk\,(dd_n)cos\,(\phi)+n\alpha\,]} \quad (5.46)$$

A_n is the excitation amplitude of the n^{th} antenna element (N=8 in (6.1)), k is the wave number, dd_n is the distance of the n^{th} antenna element from the center of the array,α is the progressive phase shift between elements (here α =0) and φ is the scan angle. Normalized power pattern P (φ) can be expressed in terms of array factor as given below:

$$P(\Phi) = 20\ log_{10}(AF(\Phi)/AF(\Phi)max) \quad (5.47)$$

The design objectives are to minimize the beam width between first nulls, maximum value of side-lobe level in the elevation plane of the array and reduce the overall size of the array (by minimizing the mean value of inter-element spacing in the array). However the mutual coupling between antenna elements and impedance matching of the overall array arrangement are not considered. The corresponding costs according to the design objectives mentioned are given below:

$Cost_1$=*BWFN (Beam-width between first nulls)* (5.48)

$Cost_2$=*max(SLL)* (5.49)

$Cost_3 = mean(inter\text{-}element\ spacing) = (1/N)\sum_{i=1}^{i=N} d_i$ (5.50)

The overall cost function can be written as:

$Cost = w_1.Cost_1 + w_2.Cost_2 + w_3.Cost_3$ (5.51)

The threshold values of beam width between first nulls (maximum) , maximum side-lobe level and mean of first 8 inter-element spacing (maximum) are 15 degrees,-18 dB and 0.70λ respectively.

5.7.2 Experimental Results

Table 5.10. Control parameter settings of the DE algorithms for the optimization of unequally spaced linear antenna array

DE algorithms	Control Parameter Settings
Adaptive differential evolution	Self adaptive
Biogeography based optimization with differential evolution	F=random number between 0 and 1 with uniform probability density function distribution CR=0.96
DE/rand/1	F=random number between 0 and 2 with uniform probability density function distribution. CR=0.99
Differential evolution with individual dependent mechanism	Self adaptive
Differential Evolution with global and local neighborhood search	Neighborhood radius=20% CR=0.6
Harmonic search differential evolution	CR (minimum)=0.20 CR(maximum)=0.95 F(minimum)=0.10 F(minimum)=0.65

DE algorithms	Control Parameter Settings
Improved differential evolution	F=random number between 0 and 1 with uniform probability density function distribution CR=0.97
Modified differential evolution	F=random number between 0 and 2 with uniform probability density function distribution CR=0.98 Beta=0.40
Modified differential evolution with p-best crossover strategy	Adaptive
Self adaptive differential evolution	Self adaptive

The statistical performances of the different DE algorithms are given below in Table 5.11.

Table 5.11. Statistical performances of the DE algorithms in the optimization of linear array of unequally spaced isotropic antenna elements.

DE algorithm	Mean cost value	Best cost value	Worst cost value	Standard deviation	Robustness (%)	Convergence rate(generations)
ADE	0.1676	0.1671	0.1680	2.43e-4	100	17
BBODE	0.1679	0.1671	0.1706	7.35e-4	100	17
DE/rand/1	0.1672	0.1670	0.1675	1.56e-4	100	18
DE-IDP-IDM	0.1679	0.1673	0.1684	3.03e-4	100	05
DEGL	0.1676	0.1671	0.1682	2.53e-4	100	10
HSDE	0.1673	0.1671	0.1675	1.06e-4	100	18
IDE	0.1675	0.1670	0.1692	5.17e-4	100	09
MDE	0.1672	0.1670	0.1676	1.96e-4	100	11
MDEPBX	0.1687	0.1679	0.1696	4.27e-4	100	17
SADE	0.1676	0.1672	0.1680	2.18e-4	100	15

All the DE algorithms can be applied for this optimization problem. All the algorithms show 100% robustness. The mean cost values, best cost values and worst cost values are very close. Under these conditions, the judging criteria are the standard deviation and convergence rate. Very low standard deviations are shown by all algorithms except DEGL. Among these algorithms, DE-IDP-IDM has the fastest convergence rate and is adjudged to be the best algorithm for this design problem. The best convergence plots of the different algorithms are given below in Fig. 5.26 and Fig. 5.27 respectively:

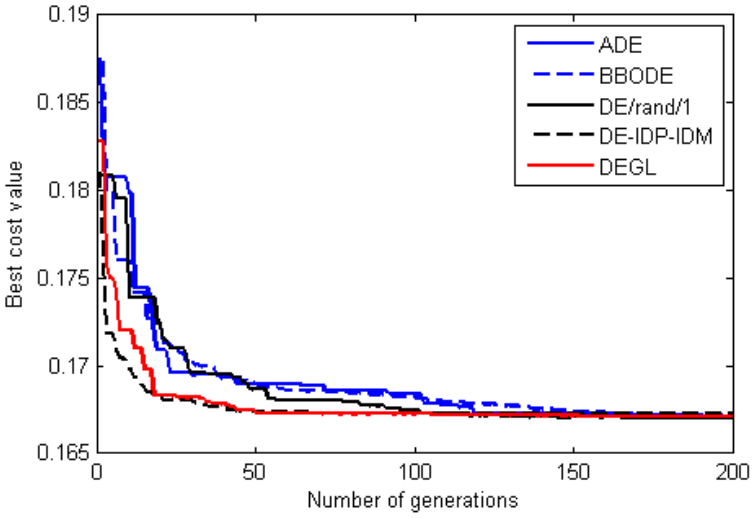

Fig 5.26 Best convergence plots for ADE, BBODE, DE/rand/1, DE-IDP-IDM and DEGL in the optimization of unequally spaced linear antenna array.

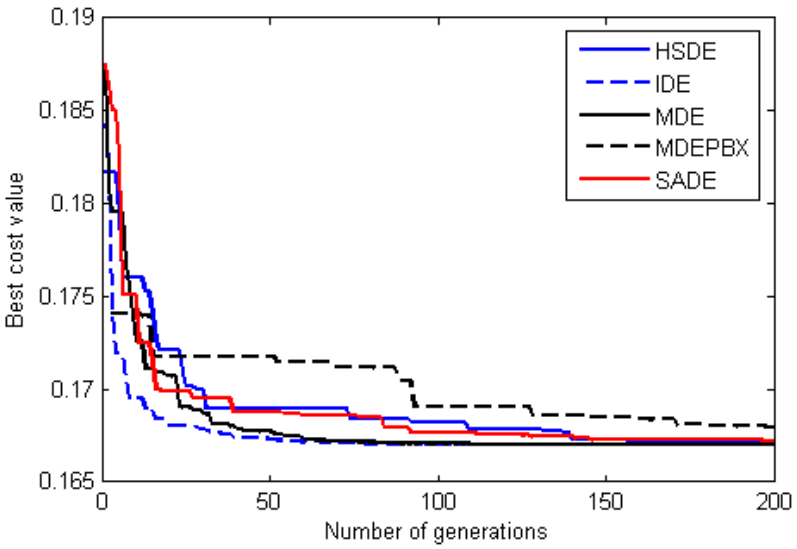

Fig 5.27 Best convergence plots for HSDE, IDE, MDE, MDEPBX and SADE in the optimization of unequally spaced linear antenna array.

The mean convergence plots are given in Fig. 5.29 and Fig. 5.30 respectively:

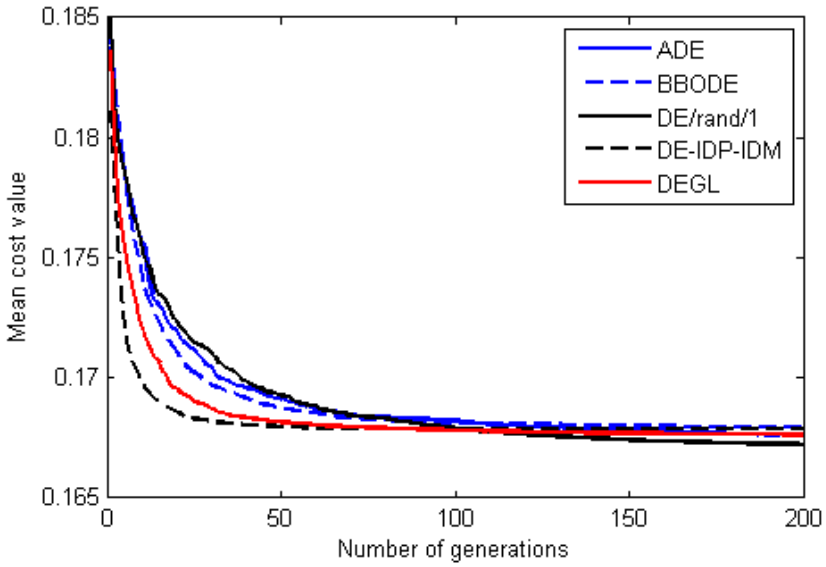

Fig 5.28 Mean convergence plots for ADE, BBODE, DE/rand/1, DE-IDP-IDM and DEGL in the optimization of unequally spaced linear antenna array.

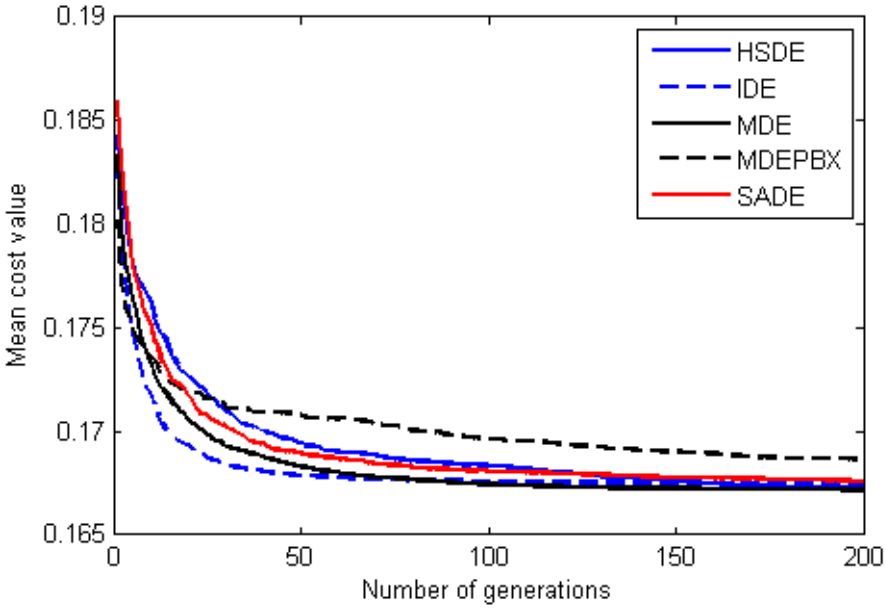

Fig 5.29 Mean convergence plots for HSDE, IDE, MDE, MDEPBX and SADE in the optimization of unequally spaced linear antenna array.

The performances of the unequally spaced linear antenna array obtained from the best run of each algorithm are given in Table 5.12:

Table 5.12. Performances of the optimal arrays obtained from the best run of each algorithm.

DE algorithm	BWFN (degrees)	Maximum SLL (dB)	Mean inter-element spacing
ADE	11.95	-20.05	0.656 λ
BBODE	11.95	-20.01	0.655 λ
DE/rand/1	11.95	-20.07	0.656 λ
DE-IDP-IDM	11.95	-19.83	0.652 λ
DEGL	11.95	-19.91	0.653 λ
HSDE	11.95	-19.94	0.653 λ
IDE	11.95	-20.08	0.656 λ
MDE	11.95	-20.07	0.655 λ
MDEPBX	12.44	-19.27	0.643λ
SADE	11.95	-19.98	0.655 λ

Table 5.13.The parameters of the DE-IDP-IDM optimized array (inter-element spacing)

d_1	0.8295λ	d_5	0.5263λ
d_2	0.8241λ	d_6	0.6085λ
d_3	0.7816λ	d_7	0.5247λ
d_4	0.6177λ	d_8	0.5056λ

The normalized power pattern of the DE-IDP-IDM optimized array in shown in Fig.5.30:

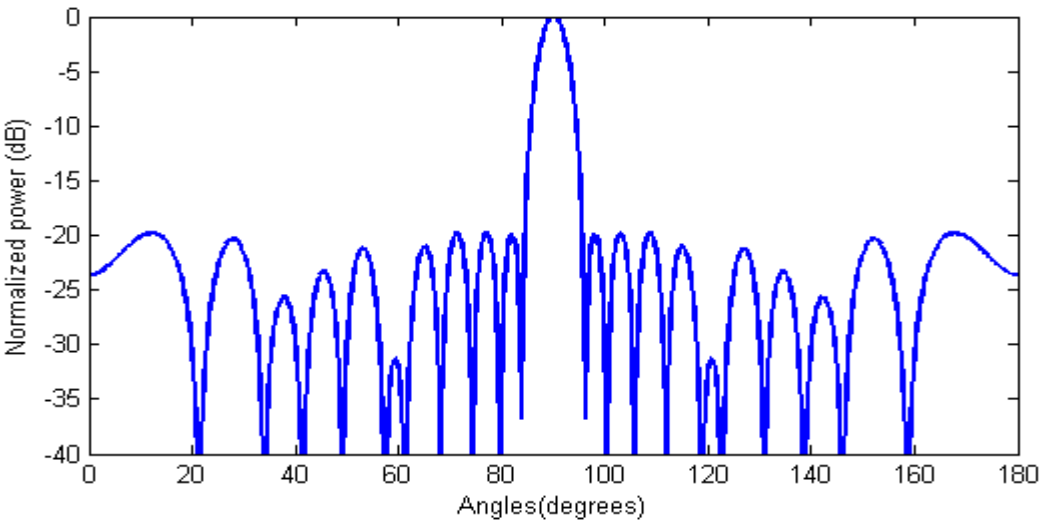

Fig 5.30 Normalized power pattern of the linear array of unequally spaced isotropic elements optimized from the best run of DE-IDP-IDM algorithm

The mean value of inter-element spacing of the DE-IDP-IDM optimized array is 0.652λ with BWFN of 11.95 degrees and maximum side lobe level of -19.83dB.

5.8 Four –element Yagi-Uda Antenna Array

5.8.1 Theory

The previous optimization case study involved array of isotropic antennas. Here a practical array design case is considered where the impedance matching condition and mutual coupling effects between the antenna elements are considered. An optimal 4-element Yagi-Uda antenna array is designed with one reflector, one active and 2 director dipole antennas. The spacing between the active element and the first director element is assumed to be the same as that between the 2 director elements. The dimensions of the Yagi-Uda array are optimized to achieve low half power beam widths and low side lobe levels (in both E-plane and H-plane) and impedance matching at any particular design frequency. Optimization of Yagi –Uda antennas are reported in [86],[87],[89] but having cost functions with fixed weights. In [86].[87],[89] and in this chapter, the optimal antenna dimensions are specified in terms of wavelength corresponding to the design frequency. The Yagi-Uda antenna array is shown in the Fig. 5.31:

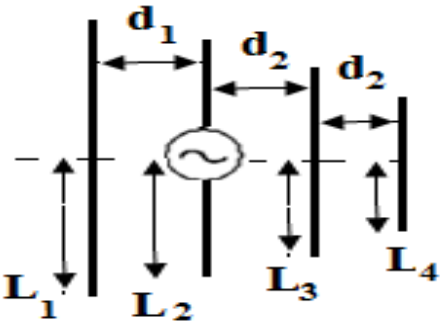

Fig 5.31 Geometry of the 4-element Yagi-Uda antenna array

The objectives for optimization are described next. The first objective is the minimization of the half power beam widths of the major lobe in both E-plane and H-plane. Hence the corresponding cost is given as:

$Cost_1 = \max(HPBW\ in\ E-plane, HPBW\ in\ H-plane)$ (5.52)

The second objective is the minimization of the maximum side lobe levels in both E-plane and H-plane. The corresponding cost is given as:

$Cost_2 = \max(SLL\ in\ E-plane, SLL\ in\ H-plane)$ (5.53)

The third objective is the impedance matching at the center frequency. The corresponding cost is given as:

$Cost_3 = |reflection\ coefficient\ at\ the\ design\ frequency|$ (5.54)

The fourth objective is to achieve the main lobe along the axis of the array towards the director elements (desired direction).

$Cost_4 = 1/\max(S_{EP}, S_{HP})$ (5.55)

Where SE_p is the normalized power density in the E-plane along the desired direction and SH_p is the normalized power density in the H-plane along the desired direction.
The overall cost function is formulated as:

$$Cost = w_1.Cost_1 + w_2.Cost_2 + w_3.Cost_3 + w_4.Cost_4 \quad (5.56)$$

The cost function evaluation is done by first analyzing the Yagi-Uda antenna structure using integral equation approach and then extracting the antenna performance parameters as mentioned above. All the weights are dynamically updated at each iteration of the optimization algorithm. Threshold values for half power beam width (maximum), maximum value of the side-lobe level and magnitude of reflection coefficient (maximum) at the center frequency are taken to be 90 degrees,-10 dB and 0.3162 (S_{11} of -10 dB) respectively.

5.8.2 Experimental Results

Table 5.14. Control parameter settings for the optimization algorithms in the design of Yagi-Uda antenna arrays

DE algorithms	Control Parameter Settings
Adaptive differential evolution	Self adaptive
Biogeography based optimization with differential evolution	F=random number between 0 and 1 with uniform probability density function distribution CR=0.91
DE/rand/1	F=random number between 0 and 2 with uniform probability density function distribution. CR=0.96
Differential evolution with individual dependent mechanism	Self adaptive

DE algorithms	Control Parameter Settings
Differential Evolution with global and local neighborhood search	Neighborhood radius=10% CR=0.70
Harmonic search differential evolution	CR (minimum)=0.20 CR(maximum)=0.95 F(minimum)=0.10 F(minimum)=0.65
Improved differential evolution	F=random number between 0 and 1 with uniform probability density function distribution CR=0.92
Modified differential evolution	F=random number between 0 and 2 with uniform probability density function distribution CR=0.95 Beta=0.40
Modified differential evolution with p-best crossover strategy	Adaptive
Self adaptive differential evolution	Self adaptive

The statistical performances of the optimization algorithms with respect to the Yagi-Uda antenna array optimization case study are given in Table 5.15:

Table 5.15.Statistical performances of the DE algorithms in the optimization of the 4 element Yagi-Uda antenna array.

DE algorithm	Mean cost value	Best cost value	Worst cost value	Standard deviation	Robustness (%)	Convergence rate(generations)
ADE	1.4748	1.4721	1.4829	0.0026	32	58
BBODE	1.4758	1.4705	1.4907	0.0052	40	51
DE/rand/1	1.4727	1.4708	1.4807	0.0022	76	66
DE-IDP-IDM	1.4728	1.4709	1.4747	0.0013	80	31
DEGL	1.4721	1.4703	1.4750	0.0014	96	28
HSDE	1.4735	1.4729	1.4762	0.0016	52	69
IDE	1.4706	1.4703	1.4712	2.88e-4	92	20
MDE	1.4707	1.4704	1.4719	4.33e-4	100	46
MDEPBX	1.4767	1.4733	1.4816	0.0031	16	70
SADE	1.5142	1.4902	1.5461	0.0151	0	NA

The mean cost values, best cost values and worst cost values are quite close for the DE algorithms listed in the table above. However significant differences are observed with respect to standard deviation , robustness and rate of convergence. Highest robustness is shown by MDE. The standard deviation is second best to that of IDE. Convergence rate of MDE is moderate. Very fastest convergence is shown by IDE and DEGL. However their robustness is lower compared to MDE. Hence MDE is adjudged to be the best algorithm for this optimization problem. Among the self adaptive algorithms, SADE could not converge to any acceptable solution (satisfying all the threshold values for antenna performance) within the stipulated number of generations. However DE-IDP-IDM showed 80% robustness.The convergence plots of the different optimization algorithms are given in Fig. 5.32 , Fig. 5.33, Fig. 5.34 and Fig. 5.35 respectively.

The best cost convergence plots are shown in Fig. 5.32 and Fig. 5.33 below:

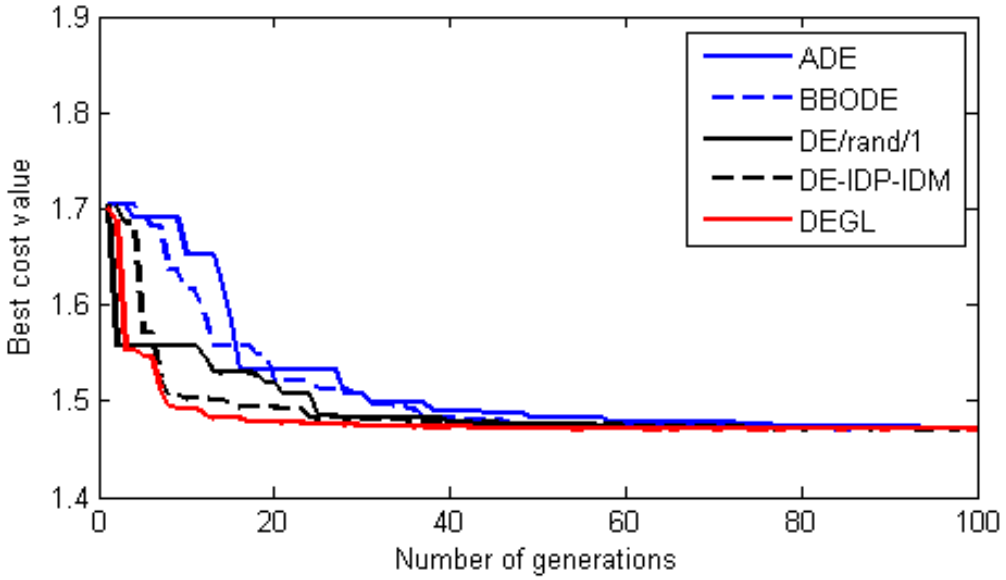

Fig 5.32 Best convergence plots for ADE, BBODE, DE/rand/1, DE-IDP-IDM and DEGL in the optimization of Yagi-Uda antenna array

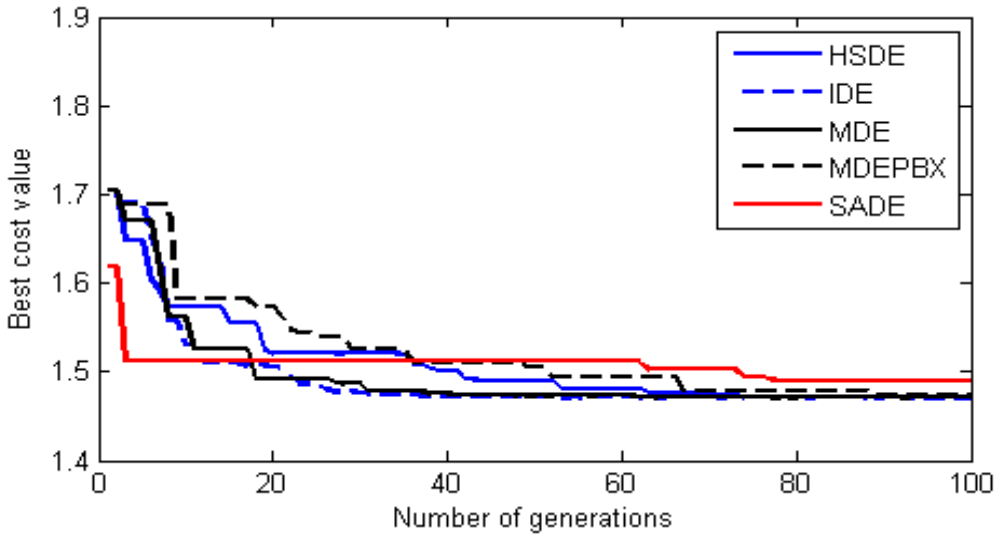

Fig. 5.33 Best convergence plots for HSDE, IDE, MDE, MDEPBX and SADE in the optimization of Yagi-Uda antenna array

The mean cost convergence plots are shown below in Fig. 5.34 and Fig. 5.35 respectively:

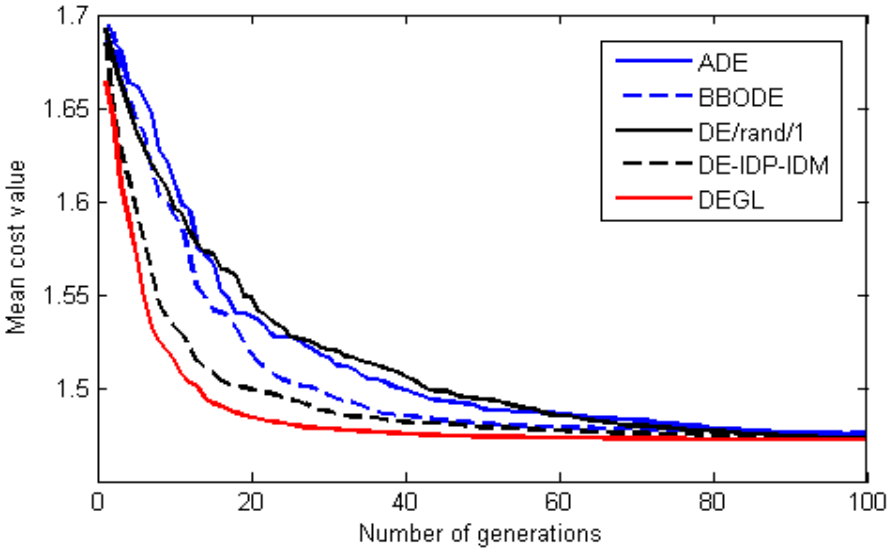

Fig 5.34 Mean convergence plots for ADE, BBODE, DE/rand/1, DE-IDP-IDM and DEGL in the optimization of Yagi-Uda antenna array

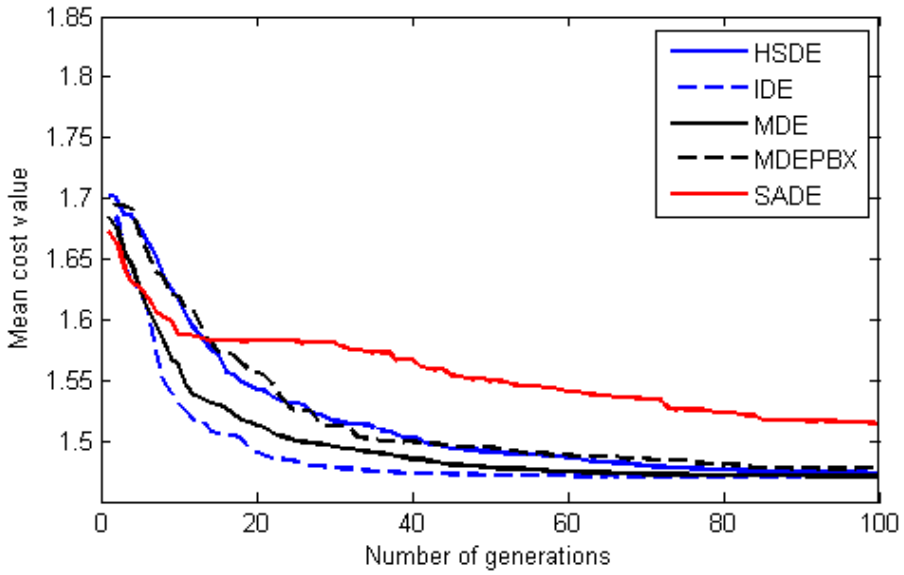

Fig. 5.35 Mean convergence plots for HSDE, IDE, MDE, MDEPBX and SADE in the optimization of Yagi-Uda antenna array

The performance parameters of the Yagi-Uda (4-element) antenna array as obtained from the best run of each algorithm and satisfying all the threshold criteria are given in Table 5.16.

Table 5.16. Performances of the optimal Yagi-Uda antenna arrays obtained from the best run of each algorithm.

DE algorithm	Half power beam width (degrees)(E-plane)	Half power beam width (degrees)(H-plane)	Maximum side-lobe level(dB) (E-plane)	Maximum side-lobe level(dB) (H-plane)	VSWR
ADE	46.86	56.36	-10.32	-10.21	1.88
BBODE	46.96	56.66	-11.29	-10.80	1.87
DE/rand/1	46.86	56.36	-10.40	-10.40	1.87
DE-IDP-IDM	46.86	56.36	-10.39	-10.39	1.88
DEGL	46.86	56.36	-10.34	-10.32	1.85
HSDE	46.86	56.36	-10.34	-10.32	1.85
IDE	46.86	56.36	-10.27	-10.34	1.84
MDE	46.86	56.36	-10.45	-10.44	1.87
MDEPBX	47.27	57.07	-10.58	-10.48	1.85
SADE	-	-	-	-	-

Table 5.17.Dimensions of the MDE optimized Yagi-Uda antenna array:

Length of the Reflector Element ($2L_1$)	0.4631λ
Length of the Active element($2L_2$)	0.4610 λ
Length of the Director element1($2L_3$)	0.4360 λ
Length of the Director element2($2L_4$)	0.4528λ
Spacing between Reflector and Active element (S_1)	0.3483 λ
Spacing between Active and Director Element(S_2)	0.2747 λ

The radiation patterns of the optimized Yagi-Uda array in the E-plane and H-plane are given in Fig. 5.36.:

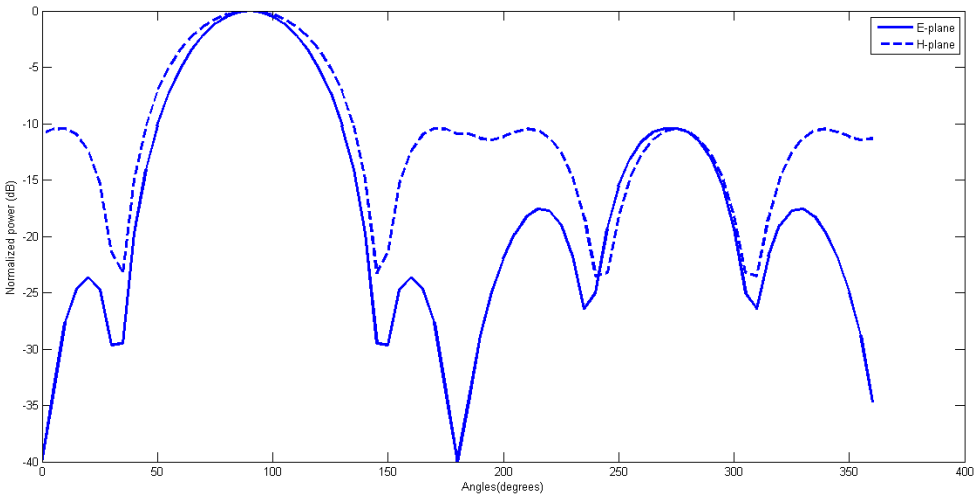

Fig. 5.36 Normalized power pattern of the Yagi-Uda antenna array

5.9 Conclusion

The applicability of 10 differential evolution algorithms including both self-adaptive and non self-adative schemes with respect to antenna and array optimization are investigated in this chapter. Five optimization case studies are investigated. Optimization of probe fed,transmission line fed and cross aperture coupled circularly polarized microstrip antenna are done using the DE algorithms. Array optimization is done for an unequally spaced linear isotropic array with 16 elements and Yagi-Uda antenna array with 4 elements. All the optimization problems are multi-objective in nature where all the objectives are combined together in cost functions using dynamic weights. The performance statistics of the DE algorithms are evaluated onbasis of these cost functions to investigate their applicability for the benchmark optimization problems. Performance of all DE algorithms varied for the benchmark optimization problems. For the probe fed circularly polarized microstrip antenna, MDE is adjudged to be the best suited DE optimization problem. In case of transmission line fed and cross aperture coupled fed circularly polarized microstrip antenna, MDE is again are found to be the most suited optimization algorithms respectively. For the unequally spaced isotropic linear array and 4-element Yagi-Uda

antenna array, DE-IDP-IDM and MDE are found to be the most applicable DE algorithms respectively. The data and study results on the applicability of the different optimization algorithms for antenna and array optimization problems will help the future researchers to choose the optimization algorithm aptly for their design problem.

The study on the appplicability of these algorithms to different antenna and array numerical benchmark problems is used in chapter 7 to choose appropriate DE algorithm for design and optimization of multi-frequency microstrip antennas for WLAN and vehicular communications.

Chapter 6

Design of Thinned Antenna Arrays using Self Adaptive Real-Boolean Differential Evolution Algorithm

6.1 Introduction

Differential Evolution (DE) was first introduced in [129]. It has shown comparatively better performance over conventional evolutionary optimization algorithms in [130]. Since then, DE has been applied to various engineering problems including antenna array synthesis and optimization. Optimal design of thinned antenna arrays has been an interesting topic in recent past [77],[81],[82],[115],[146],[147]. Thinned arrays work on turned-on (active) and turned-off (inactive) antenna elements concept resulting in better array performance, reduced size and cost. Optimization of thinned arrays using DE can be categorized in two ways; one involving the use of Boolean Differential Evolution (BDE) algorithms [77],[81],[115],[147] and the other using non-Boolean Differential Evolution (non-BDE) algorithms [82],[146]. It has been proved that BDE algorithm performs better compared to non-BDE algorithms in terms of convergence rate and optimal parameters obtained while optimizing the performances of 6x6 and 10x10 thinned planar array configurations[82],[146]. BDE is also used to design multi-band antennas [155]. Some work using Real-Boolean Differential Evolution (RBDE) in the optimization of unequally spaced linear antenna arrays (with maximum number of active elements set at 20 and population size of 40) was also reported in [154].

Differential evolution requires large population size for better exploration of the problem search space and as a result it requires large number of generations and computation time to reach the global optimum [129]. Reducing the population size cuts down the number of generations and computation time required for convergence but increases the chance of getting trapped into local extrema. It is desirable for real time optimization problems to choose an algorithm which provides better exploration as well as increased convergence speed. The performance of the differential evolution algorithm for a particular optimization problem also depends on the choice of control parameters (population size, scaling factor and crossover probability) and the donor

vector generation strategy [161]. The performance of the optimization algorithm is optimum for optimal choice of these control parameters. One has to perform multiple runs of the same algorithm with different choice of control parameters on trial and error basis for finding the appropriate combination of control parameters for a particular optimization problem. Meta – optimization of differential evolution for tuning of control parameters for a particular optimization problem is also possible but the procedure is extremely time- consuming. Further, the choice of control parameters may also change at different stages of optimization during a single run of the algorithm. Several researches have been carried out where the control parameters are made self adaptive i.e. the optimization algorithm is capable of deciding its own values of its control parameters at different stages of the optimization procedures [138],[139],[140],[141],[148],[160],[161]. However all these self adaptive strategies are applied to real valued differential evolution algorithms with appropriate donor vector generation procedure and normally use a large population size. No research is carried out till date to apply self-adaptive control parameter techniques to real-Boolean differential evolution algorithm. An attempt has been made in this chapter to identify suitable self adaptive strategies for real-Boolean DE algorithms and apply them successfully for design of thinned linear and planar antenna arrays. It should be noted that the population size used here is low compared to [138],[139],[140],[161] and it is ensured that the statistical performance of the new algorithm is comparatively better compared to the original Boolean differential evolution algorithms or real-Boolean differential evolution algorithms. The algorithm exhibits faster convergence to the global optimum and has a statistically better performance over the existing BDE and RBDE algorithms. This novel Self Adaptive Real-Boolean Differential Evolution (SA-RBDE) algorithm employs composite trial vector generation strategy (CoDE) as in [161], self adaptive scheme for control parameters proposed in [139],[140], population dynamics for maintaining population diversity and a population manager as proposed in [161]. The novelty of the chapter lies in choice of appropriate strategies and using them together for the array optimization.

The Self-Adaptive Real-Boolean Differential Evolution (SA-RBDE) algorithm is applied for the optimization of thinned linear and planar antenna arrays. Two different types of cost functions are formulated. In the cost function of the first type, the objective is to maintain similar beam width as the fully filled array but with reduced side lobes. In the second case, the cost function has same objectives as the first one but it is also aimed at optimizing the array size and number

of active elements in the array. Additionally, the new algorithm is used to optimize a thinned linear array with unequal inter-element spacing with the same objectives. This optimization was earlier attempted in [154] but with real-Boolean differential evolution algorithm. The statistical performance of the proposed SA-RBDE algorithm is compared with those of the conventional BDE and RBDE. In both cases SA-RBDE performs statistically better compared to BDE and RBDE algorithms. Further, performance comparison of self adaptive real-Boolean Differential algorithm with conventional Boolean and real-Boolean differential evolution algorithms using thinned array as numerical benchmark problem has not been reported earlier.

An overview of the existing BDE algorithm and the RBDE algorithm along with their control parameter settings are discussed in sections II and III. The self-adaptive real-Boolean differential evolution algorithm (SA-RBDE) is described in section IV. Section IV also explains the choice of control parameter adaptation strategy, trial vector generation strategy and population diversity scheme for the optimization algorithm. Section V describes the real-binary self adaptive differential evolution algorithm. Section VI discusses the formulation of the cost functions of two types explained above. Optimization of thinned linear and planar antenna arrays are described in sections VII and VIII respectively. Optimization of the unequally spaced thinned linear array is discussed in section IX. Section X concludes the chapter.

6.2 Original Boolean Differential Evolution Algorithm

The original Boolean differential evolution algorithm is proposed in [147]. The different steps in the algorithm are outlined below:

1. Generate an initial population of target or parent vectors. Let the population size be P. Each vector contains ‘n’ number of genes. Each gene represents an array element excitation and each vector represents a particular combination of array element excitations. Therefore n is same as the number of antenna elements in an array. Each gene can have values either 0 or 1. If the array element is not active, then the corresponding gene takes a value ‘0’ and vice versa. The cost values of each vector in the initial population are evaluated before starting the optimization process. Each gene is represented as $X_G(i,j)$ where G represents the generation number, i represents the i^{th} vector and j denotes the j^{th} array element excitation. The following steps (2-4)

are repeated until the maximum numbers of generations are over or the termination criterion is met.

2. For the i^{th} vector, three other vectors are chosen, different from 'i' and mutually exclusive. Among the three, one includes the vector with the minimum cost function. A donor vector corresponding to X_G(i, 1…….n) is formed according to the following equation and denoted as V_G(i, 1…..n):

$$V_G(i,j) = X_G(nbest,j) + F.(xor\left(X_G(n1,j), X_G(n2,j)\right)) \quad (6.1)$$

where '+' represents the Boolean OR operation, '.' represents the Boolean AND operation and F is a random Boolean variable.

3. The donor vector undergoes a binary crossover operation with the parent vector based on a crossover probability CR. This results in a corresponding trial vector T_G(i,1…….n). A random number (y) is generated based on uniform probability distribution for every gene of the vector. 'j_{rand}' is a random whole number between 1 and n.

$$T_G(i,j) = V_G(i,j)\ if\ y \leq CR or\ j = j_{rand}$$
$$T_G(i,j) = X_G(i,j)\ otherwise \quad (6.2)$$

4. The trial vector is evaluated for its cost. If the trial vector has a lower cost than the corresponding parent vector X_G(i,1……n), then the trial vector replaces the parent vector in the next generation.

The BDE algorithm is very simple to implement and it uses only one control parameter, 'CR'. It is shown that the optimal value for CR is 0.2 [147]. The BDE algorithm also uses DE/best/1 strategy for donor vector generation as mentioned above. Different donor vector generation strategies have been tried for numerical experimentation and it is confirmed that the DE/best/1 is indeed the optimal choice for the thinned array design problem.

6.3 Original Real-Boolean Differential Evolution Algorithm (RBDE)

The first work on Real-Boolean Differential Evolution (RBDE) algorithm is reported in [154]. All the vectors involved in the algorithm (donor vectors and trial vectors) contained Boolean genes as well as real valued genes. The Boolean genes in the donor vector are obtained using equation (6.1) whereas the real genes are obtained according to [129]. During trial vector generation, the Boolean genes are evolved using a crossover probability of 0.2 whereas the real valued genes are evolved using a crossover probability of 0.8. The donor vector generation strategy used is DE/best/1. It is noted that the donor vector generation strategy and the crossover probability for Boolean genes are same in case of BDE and RBDE.

6.4 Self-Adaptive Real-Boolean Differential Evolution Algorithm (SA-RBDE)

The proposed Self-Adaptive Real-Boolean Differential Evolution (SA-RBDE) algorithm uses a composite donor vector generation strategy and is a modified version of the original real-Boolean differential evolution [154]. This algorithm employs strategies like dynamic update of the population vector, self adjustment of crossover probability CR [139],[140], and a population manager [161] for identification and removal of redundant and non-performing vectors. All the strategies are discussed below:

6.4.1 Self Adjustable Crossover Probability

The value of the crossover probability (CR) in original BDE and RBDE algorithms is kept fixed at 0.2 for all generations. Two values of crossover probability CR_{real} and $CR_{Boolean}$are used in the RBDE algorithm in [154]. The values of CR_{real} and $CR_{Boolean}$ are kept fixed at 0.8 and 0.2 respectively. However the best suited value of crossover probability for both real valued and Boolean valued genes may change depending on the optimization problem and from generation to generation for the same problem. Different self adaptive strategies in [138]-[140],[161] which are applied to real valued antenna designs are investigated and large numbers of numerical experiments are performed. Standard control parameter adaptation strategy is reported in [138] but it is applicable for both ‘F’ and ‘CR’ together and requires a much larger population size. Since the population size is kept low in this chapter, this strategy is not explored. In the proposed new algorithm, two CR values are associated with each population vector during initialization. Let us call the CR values as CR_real and CR_Boolean. CR_real and CR_Boolean represent the

crossover rates for real valued genes and Boolean valued genes for the population vectors. The values of the CR_real are chosen randomly between 0.5 and 1 whereas the values of CR_Boolean are chosen randomly between 0.1 and 0.5. The boundary values for choosing CR_real and CR_Boolean are fixed for different optimization problems on thinned antenna arrays as shown in subsequent sections. For generation G, a set called $CR_{SUCCESS\_REAL}$ is maintained for all successful crossover probabilities of real valued genes in that generation. Another set called $CR_{SUCCESS\_BOOLEAN}$ is maintained for all successful crossover probabilities of Boolean valued genes in that generation. The expected values of CR_real and CR_Boolean for the next generation may be calculated as shown below:

$$mean\_CR\_real_{G+1} = c.mean\_CR\_real_G + (1-c).mean\,(CR_{success\_real}) \quad (6.3a)$$

$$mean\_CR\_Boolean_{G+1} = c.mean\_CR\_Boolean_G + (1-c).mean\,(CR_{success\_Boolean}) \quad (6.3b)$$

where'c' is a user defined value. This value is chosen as 0.5 in the numerical experiments reported in this chapter. In generation (G+1), all vectors are given their individual crossover probabilities for real and Boolean valued genes separately as random numbers based on a Gaussian distribution with their updated means in equation (6.3) having standard deviation 0.1[140]. If the updated mean values of the crossover rates exceed the boundaries mentioned, then the crossover rates for real valued genes and Boolean valued genes are randomly reset within their respective boundaries.

The crossover rate update strategy can also be done using the scheme in [139] but it is observed that the statistical performance of [139] with Boolean genes is not satisfactory. In contrast, the self adaptive scheme in [140] performs statistically better .The donor vector generation strategy reported in [140] is however replaced by composite donor vector generation strategy [161]. In all literature till date, self adaptive control parameter strategies are used for DE algorithms using real coded genes. This chapter makes a novel attempt of using them with Boolean genes as well real coded genes and reporting the best choice of strategies for thinned array design problem.

6.4.2 Composite Donor Vector Generation Strategy

It is also necessary to use appropriate donor vector generation strategy along with self adaptive control parameters for optimal performance of the differential evolution algorithm. It is confirmed through different numerical experiments that composite donor vector generation strategy [161] is best suited for the optimization problems discussed in this chapter. Application of composite donor vector generation strategy of Composite Differential Evolution (CoDE) algorithm to antenna design problems and that too with Boolean optimization variables is another novel and successful attempt made in this chapter.

Two donor vectors are formed at each generation for each population vector as shown below by equations (6.4) and (6.5):

$$V_{G1}(i,j) = X_G(nbest,j) + F.\left(xor\left(X_G(n1,j), X_G(n2,j)\right)\right) \quad for\ boolean\ genes \tag{6.4a}$$

$$V_{G1}(i,j) = X_G(nbest,j) + F'.\left(\left(X_G(n1,j) - X_G(n2,j)\right)\right) \quad for\ real\ valued\ genes \tag{6.4b}$$

$$V_{G2}(i,j) = X_G(n3,j) + F.\left(xor\left(X_G(n1,j), X_G(n2,j)\right)\right) \quad for\ boolean\ genes \tag{6.5a}$$

$$V_{G2}(i,j) = X_G(n3,j) + F'.\left(\left(X_G(n1,j) - X_G(n2,j)\right)\right) \quad for\ real\ valued\ genes \tag{6.5b}$$

'F in equations (6.4a) and (6.5a) is a random Boolean variable whereas 'F'' in equations (6.4b) and (6.5b) is a random number (between 0 and 1) based on uniform distribution. The vector with the lowest cost is referred by the index 'nbest' in the current population. The other indices 'n1', 'n2' and 'n3' refer to three other mutually exclusive population vectors in the current generation. The two sets of donor vectors are formed based on DE/best/1 as used in [154] and DE/rand /1 as used in [129]. The choices of the donor vector generation strategies are made to favor both exploration of search space and quick convergence. DE/rand/1 enhances the exploration capability of the proposed algorithm whereas DE/best/1 favors quick convergence of the algorithm.

It is observed that using only DE/rand/1 for thinned array design delays the convergence to the global optimum whereas using only DE/best/1 increases the probability of getting trapped into local optima. Several other donor vector generation strategies exist [161] but extensive numerical

experimentation on different combinations of these strategies suggested DE/rand/1 and DE/best/1 to be the optimal combination for the thinned array designs. Use of composite donor vector generation strategy using both real and Boolean genes has not been attempted before on any engineering design problem according to the literature survey conducted in this regard and this is one of the novelties presented in this chapter.

Once the two donor vectors are generated, two trial vectors are also formed based on the crossover probabilities described in the earlier section. The cost values of the two trial vectors are evaluated and the better one is passed over to the next generation.

The application of CoDE[161] also means that the number of cost function evaluations doubles for every generation in this chapter compared to the original BDE or RBDE. This means more computation time for the new algorithm. This is compensated by using the dynamic population strategy described in the next section.

6.4.3 Population Dynamics

The starting population size for the new algorithm is assumed to be P. In the original BDE [147] and RBDE [154] the population size is kept fixed throughout the entire optimization. However in the new algorithm, the population size is made variable. At every generation, the best population vector is identified and the Hamming distance of the other population vectors from the best one is calculated. If the distance of any vector or the difference of the cost value is below a predefined minute value ε , then it is assumed that the concerned population vector is going to converge with the best available vector and it is discarded from the current population. This reduces the total population size, resulting in faster computation speed. The value of ε is to be judiciously chosen. A very small value may delay the search process whereas large values may discard potentially good vectors. In our numerical experiments, the value of ε is kept at 10^{-4}. The population size can fall to extremely low value which may again affect the search process. To circumvent this problem, random vectors are appended to the existing population so that the population size goes up to its initial value. This population size increase is performed only if the current population falls below a threshold value which is taken to be 6 in this chapter.

6.4.4 Population Manager

A population manager is also incorporated within the algorithm which becomes active after NP generations and removes redundant and non performing population vectors. The non performing vectors are those which have not changed their gene structure over a specified number of generations (in our case 20).

6.5 Self Adaptive Real-Binary Differential Evolution Algorithm (SA-RBiDE)

The self adaptive real-binary differential evolution algorithm is similar to the self adaptive real-Boolean differential evolution algorithm except for the allotment of values to different genes in the chromosomes. In case of self adaptive real-Boolean differential evolution algorithm, the turned-on (active) and turned off(inactive) status of the antenna elements are indicated by '1' and '0' respectively in the corresponding gene values of the chromosomes. However for self adaptive real-binary differential evolution algorithm, all the gene positions contain real values. For gene positions indicating the status of the antenna elements, the values lie between 0 and 1. While evaluating the cost function, an antenna element is considered active if its status value in the gene position is more than or equal to 0.5. The same antenna element will be considered inactive if the gene value is less than 0.5.

6.6 Formulation of the Cost Functions

The optimizations of thinned linear and planar isotropic antenna arrays are done twice each using two different types of cost functions. In the cost function of the first type, the objective is to reduce the maximum side lobe level of the array while keeping the first null beam width as close as possible to that of the fully filled array. For the thinned linear array, the radiation pattern is obtained in only one plane and hence only the maximum side lobe level in that plane is reduced as given in (6.6). In the planar isotropic antenna array, two radiation patterns are considered (for $\phi=0^o$ and $\phi=90^o$planes). The first cost function for the thinned planar isotropic array is given in (6.7).

$$Cost\ Function1_{Thinned\ Linear\ Array} = \max(SLL_1) \tag{6.6}$$

$$Cost\ Function1_{Thinned\ Planar\ Array} = \max\left(SLL_{1(\varphi=0)}, SLL_{1(\varphi=90)}\right) \tag{6.7}$$

The cost functions given above do not take into consideration the number of turned-on (active) elements and the total size of the array. However these factors are crucial for cost-effective and compact thinned array antennas. Hence a second cost function is formulated as given in (6.8) and (6.9) to additionally optimize the number of turned-on (active) elements and the size of the array.

$$Cost\ Function2_{Thinned\ Linear\ Array} = C_1.\max\ (SLL_1) + C_2.(Number\ of\ active\ elements/Total\ element\ s) + C_3.(mean\ inter - element\ spacing) \quad (6.8)$$

$$Cost\ Function2_{Thinned\ Planar\ Array} = C_1.\max\ (SLL_{1(\phi=0),}SLL_{1(\varphi=90)}) + C_2.(Number\ of\ active\ elements/Total\ elements) + C_3.max(mean\ inter - element\ spacing\ along\ x, mean\ inter - element\ spacing\ along\ y) \quad (6.9)$$

The inter element spacing is varied between 0.5λ and 1λ to avoid mutual coupling between antenna elements and grating lobes. While achieving the objectives described in the cost function of the second type, it has been ensured that the first null beam width is as close as possible to that of the fully filled array with the same inter-element spacing as that of the optimal thinned array.

For each type of cost function corresponding to each array type, two varieties of optimization are performed; one in which the weights used in the evaluation of cost function are kept fixed and the other where the weights are made dynamic and adaptive. For the second variety of optimization, threshold values for each optimization objective are defined. Whenever the objective value is far from the threshold value, the corresponding weight is temporarily increased and vice versa.

6.7 Optimization of Thinned Linear Antenna Array

6.7.1 Theory

Thinning of an array can be carried out on a linear layout or on a planar layout. A linear antenna array structure is shown below in Fig. 6.1:

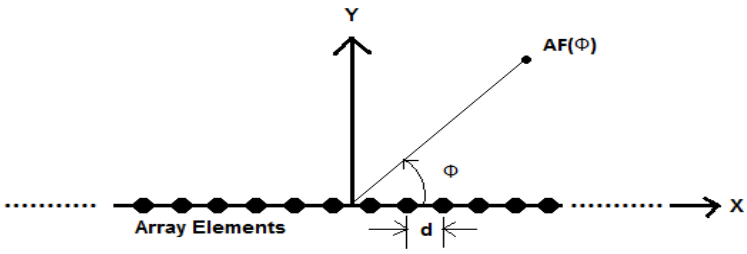

Fig.6.1 Geometry of N element linear array

Array factor of the antenna can be written as [77].

$$AF = \sum_{-N}^{+N} Ane^{[jk\,dd_n \cos(\Phi)+n\alpha]} \tag{6.10}$$

A_n is the excitation amplitude of the antenna element (1 or 0). If the value is '1', it means that the corresponding antenna element is active whereas if the value is '0', then the antenna element is inactive, k is the wave number, d is the inter-element spacing, dd_n is the distance of the n^{th} array element from the center, α is the progressive phase shift between elements (here α =0) and φ is the scan angle. Normalized power pattern P (φ) can be expressed in terms of array factor as given below:

$$P(\Phi) = 20\,log_{10}(AF(\Phi)/AF(\Phi)max) \tag{6.11}$$

6.7.2 Optimization of Thinned Boolean Linear Array with Cost Function 1 and Constant Weights

Optimization of the thinned Boolean linear array with cost function 1 described earlier is done using real-Boolean differential evolution algorithm, self -adaptive real-Boolean differential evolution algorithms and self-adaptive real-binary differential evolution algorithm. The array is assumed to have 50 elements. The inter-element spacing is assumed to be constant between successive antenna elements. However the value of the inter-element spacing can lie between 0.5λ to 1λ to avoid mutual coupling effects and grating lobes. This inter-element spacing value is also to be optimized. Hence the number of optimization variables is 51 with 50 Boolean variables and one real coded variable. The statistical performance of the different optimization algorithms are given below in Table6.1. Each of the algorithms is run for 25 independent runs starting from the same population.

Table 6.1.Statistical performance of the optimization algorithms for thinned linear array with constant inter-element spacing, cost function 1 and static weights.

Optimization Algorithms	Mean value	Best cost value	Worst cost value	Standard deviation of the cost values
Real-Boolean DE	0.1022	0.0950	0.1072	0.0031
Self Adaptive Real-Boolean DE	0.1013	0.0943	0.1064	0.0029
Self Adaptive Real-Binary DE	0.1041	0.0993	0.1124	0.0029

The best convergence graphs for the optimization algorithms are given below in Fig. 6.2.

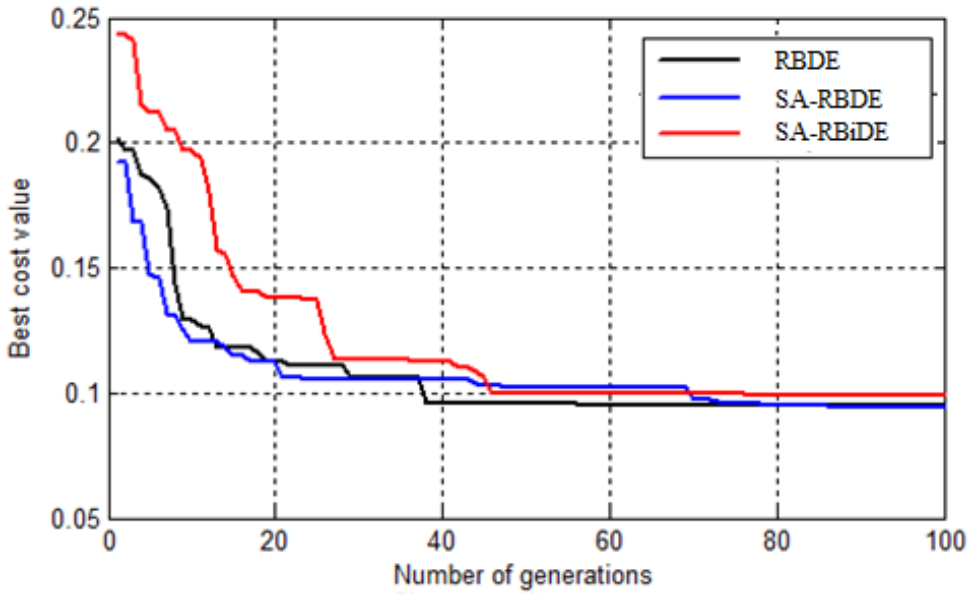

Fig. 6.2 Best convergence plots of the optimization algorithms for thinned linear array with constant inter-element spacing, cost function 1 and static weights.

The mean convergence graphs for the optimization algorithms are given below in Fig.6.3.

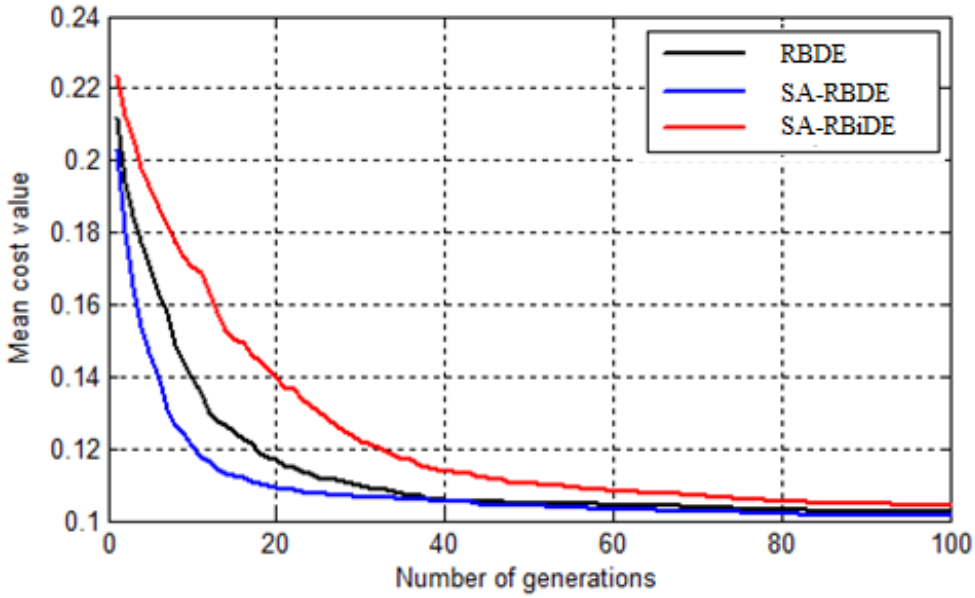

Fig.6.3Mean convergence plots of the optimization algorithms for thinned linear array with constant inter-element spacing, cost function 1 and static weights.

The performances of the optimal thinned arrays obtained from the best run of each algorithm are given in Table 6.2.

Table6.2 Performance of the optimal thinned linear arrays with constant inter-element spacing obtained from the optimization algorithms using cost function 1 and static weights.

Optimization Algorithms	Maximum side lobe level (dB)	Beam width between 1^{st} nulls (in degrees)	Number of active elements in the array
Real-Boolean DE	-20.4472	5.04^{o}	41
Self Adaptive Real-Boolean DE	-20.5078	2.88^{o}	42
Self Adaptive Real-Binary DE	-20.0637	5.04^{o}	41

The parameters of the optimal arrays are given in Table6.3.

Table6.3. Parameters of the optimal thinned linear arrays with constant inter-element spacing obtained from the optimization algorithms using cost function 1 and static weights.

Optimization Algorithms	Sequence of turned-on (active) elements	Inter-element spacing
Real-Boolean DE	1011010111111111111111111111111111110 11001000111	0.5784λ
Self Adaptive Real-Boolean DE	1111010101111111111111111111111111111 01101100011	0.8851λ
Self Adaptive Real-Binary DE	1111001111111111111111111111111111110 11000100101	0.5553λ

The statistical performance parameters of the optimization algorithms are almost same in terms of mean cost value, best cost value, worst cost value and standard deviation of cost values. However the performance of the real-Boolean SADE algorithm is slightly better compared to the other algorithms. In terms of convergence rate, the real-Boolean SADE algorithm shows the fastest convergence compared to the other algorithms as evident from the mean convergence plots in Fig 6.3. The real-Boolean SADE algorithm used an average population size of approximately 38 vectors or chromosomes across all its runs. The same population size is used for the real-Boolean DE algorithm. The optimal array obtained from the best run of real-Boolean SADE algorithm has an inter-element spacing of 0.8851λ and 84% turned-on (active) elements. The normalized array factor plot of the optimal array obtained from self-adaptive real-Boolean DE algorithm is given in Fig.6.4.

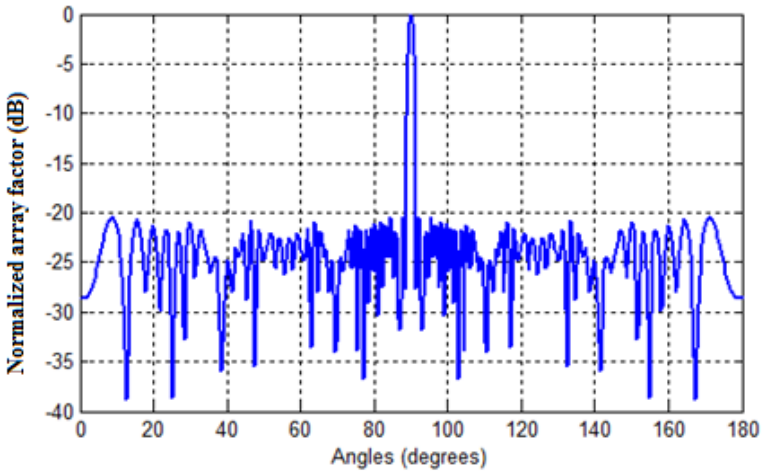

Fig .6.4 Normalized array factor of the optimal thinned linear array (with constant inter-element spacing) obtained using self-adaptive Boolean DE algorithm using cost function 1 and static weights

6.7.3Optimization of Thinned Boolean Linear Array with Cost function 2 and Constant Weights

Optimization of the thinned Boolean linear array with cost function 2 described earlier is done using real-Boolean differential evolution algorithm, self-adaptive real-Boolean differential evolution algorithm and self-adaptive real-binary differential evolution algorithm. The array parameters and constraints are assumed to be same as in the previous section. The number of optimization variables is 51 with 50 Boolean variables and one real coded variable. The statistical performance of the different optimization algorithms are given below in Table6.4. Each of the algorithms is run for 25 independent runs starting from the same population.

Table 6.4.Statistical performance of the optimization algorithms for thinned linear array with constant inter-element spacing, cost function 2 and static weights.

Optimization Algorithms	Mean value	Best cost value	Worst cost value	Standard deviation of the cost values
Real-Boolean DE	5.7952	5.5723	6.0732	0.1200
Self Adaptive Real-Boolean DE	5.7588	5.4756	5.9858	0.1138

Optimization Algorithms	Mean value	Best cost value	Worst cost value	Standard deviation of the cost values
Self AdaptiveReal-Binary DE	5.9571	5.6457	6.4994	0.1844

The best convergence graphs for the optimization algorithms are given below in Fig.6.5

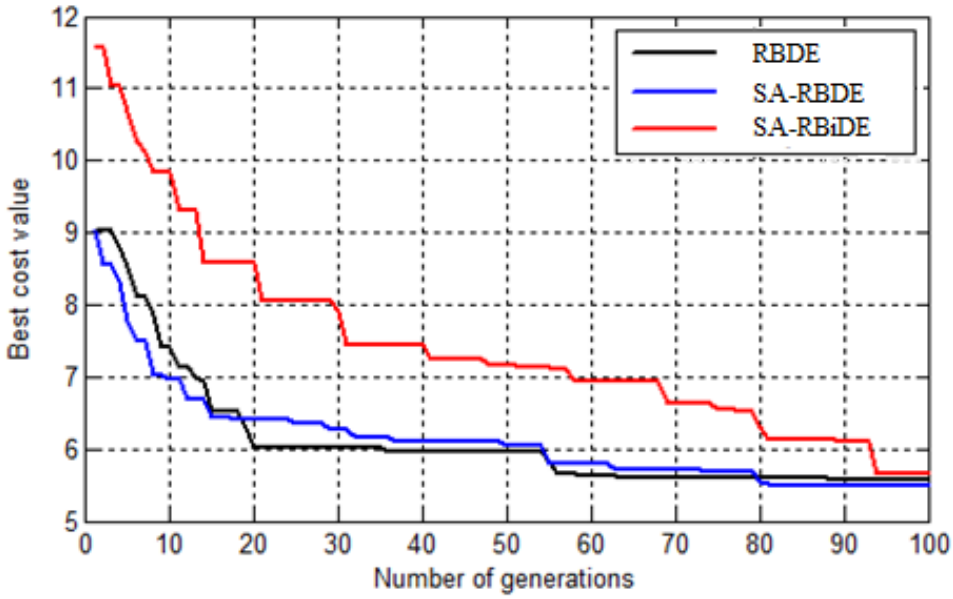

Fig.6.5Best convergenceplots of the optimization algorithms for thinned linear array with constant inter-element spacing, cost function 2 and static weights.

The mean convergence graphs for the optimization algorithms are given below in Fig.6.6.

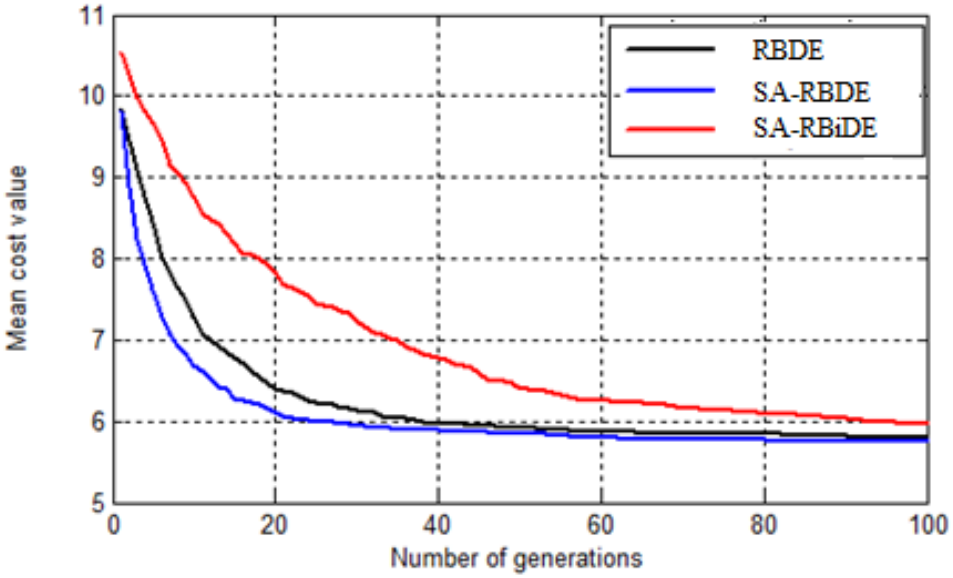

Fig.6.6Mean convergence plots of the optimization algorithms for thinned linear array with constant inter-element spacing, cost function 2 and static weights.

The performances of the optimal thinned arrays obtained from the best run of each algorithm are given in Table6.5.

Table6.5. Performance of the optimal thinned linear arrays with constant inter-element spacing obtained from the optimization algorithms using cost function 2 and static weights.

Optimization Algorithms	Maximum side lobe level (dB)	Beam width between 1st nulls(in degrees)	Number of active elements in the array
Real-Boolean DE	-20.1406	4.32^{o}	41
Self AdaptiveReal-Boolean DE	-20.4404	2.88^{o}	42
Self AdaptiveReal-Binary DE	-20.0482	2.88^{o}	41

The parameters of the optimal arrays are given in Table6.6.

Table6.6. Parameters of the optimal thinned linear arrays with constant inter-element spacing obtained from the optimization algorithms using cost function 2 and static weights.

Optimization Algorithms	Sequence of turned-on (active) elements	Inter-element spacing
Real-Boolean DE	1100111110111111111111111111111111111110100001101	0.6086λ
Self Adaptive Real-Boolean DE	1111001010101111111111111111111111111111110110011	0.8614λ
Self Adaptive Real-Binary DE	1011101101111111111111111111111111111010110110001	0.8759λ

The statistical performance parameters of the optimization algorithms are almost same in terms of mean cost value, best cost value, worst cost value and standard deviation of cost values. However the performance of the real-Boolean SADE algorithm is slightly better compared to the other algorithms. In terms of convergence rate, the real-Boolean SADE algorithm shows the fastest convergence compared to the other algorithms as evident from the mean convergence plots in Fig6.5. The real-Boolean SADE algorithm used an average population size of approximately 38 vectors or chromosomes across all its runs. The same population size is used for the real-Boolean DE algorithm. The optimal array obtained from the best run of the real-Boolean SADE algorithm has an inter-element spacing of 0.8614λ and 84% turned-on (active) elements. The normalized array factor plot of the optimal array obtained from self-adaptive real-Boolean DE algorithm is given in Fig.6.7.

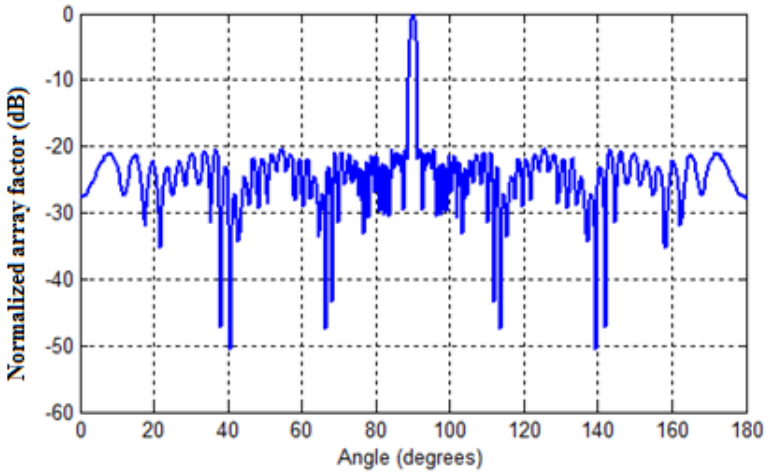

Fig .6.7 Normalized array factor of the optimal thinned linear array (with constant inter-element spacing) obtained using self-adaptive Boolean DE algorithm using cost function 2 and static weights

6.7.4Optimization of Thinned Boolean Linear Array with Cost Function 1 and Dynamic Weight

Optimization of the thinned Boolean linear array with cost function 1 and dynamic weight described earlier is done using real-Boolean differential evolution algorithm, self adaptive real-Boolean differential evolution algorithm and self-adaptive real-binary differential evolution algorithm. The array parameters and constraints are assumed to be same as in the previous section. The number of optimization variables is 51 with 50 Boolean variables and one real coded variable. The statistical performance of the different optimization algorithms are given below in Table6.7. Each of the algorithms is run for 25 independent runs starting from the same population. The cost function used a dynamic weight with the side lobe level. The threshold value for the side lobe level (maximum) is -20 dB.

Table6.7. Statistical performance of the optimization algorithms for thinned linear array with constant inter-element spacing, cost function 1 and dynamic weight.

Optimization Algorithms	Mean value	Best cost value	Worst cost value	Standard deviation of the cost values	Robustness (%)	Convergence rate (generations)
Real-Boolean DE	21.4154	0.9830	40.7138	20.0287	48	54
Self Adaptive Real-Boolean DE	21.4034	0.9813	40.5014	20.0153	48	50
Self Adaptive Real-Binary DE	32.6537	0.9936	40.9704	16.1563	20	74

The best convergence graphs for the optimization algorithms are given below in Fig.6.8.

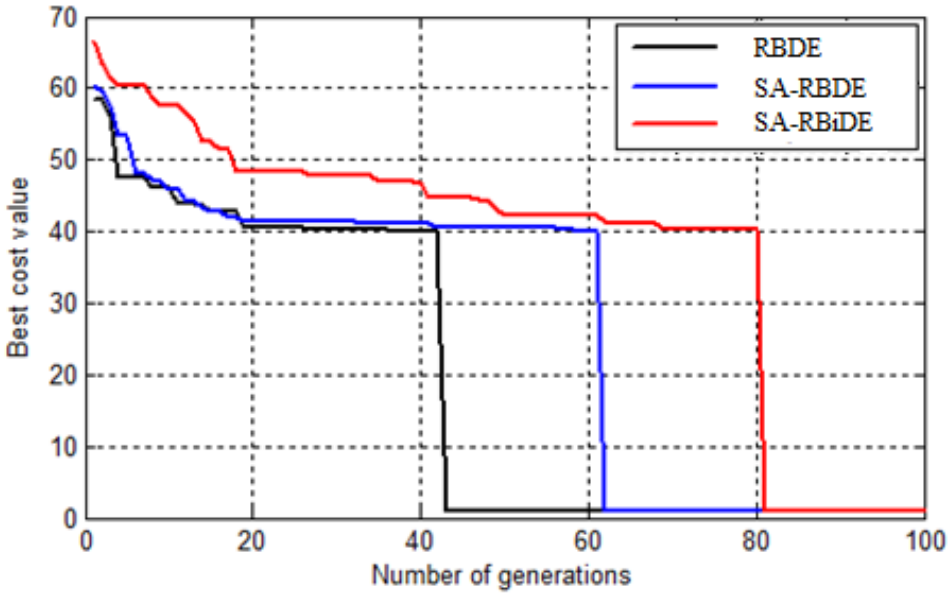

Fig.6.8 Best convergence plots of the optimization algorithms for thinned linear array with constant inter-element spacing, cost function 1 and dynamic weight.

The mean convergence graphs for the optimization algorithms are given below in Fig.6.9.

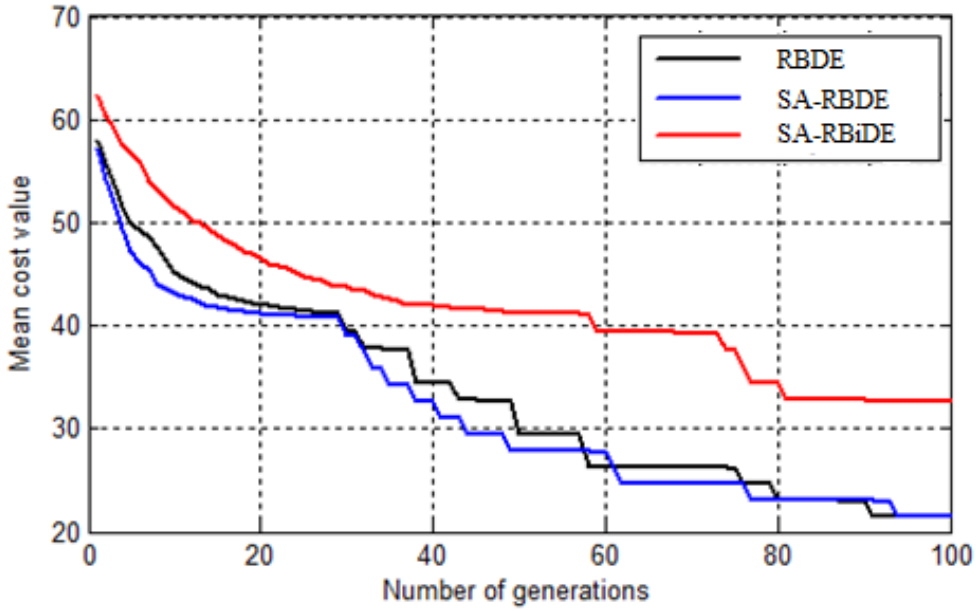

Fig.6.9Mean convergence plots of the optimization algorithms for thinned linear array with constant inter-element spacing, cost function 1 and dynamic weight.

The performances of the optimal thinned arrays obtained from the best run of each algorithm are given in Table6.8.

Table6.8. Performance of the optimal thinned linear arrays with constant inter-element spacing obtained from the optimization algorithms using cost function 1 and dynamic weight.

Optimization Algorithms	Maximum side lobe level (dB)	Beam width between 1st nulls(in degrees)	Number of active elements in the array
Real-Boolean DE	-20.3463	2.88^{o}	41
Self Adaptive Real-Boolean DE	-20.3819	3.60^{o}	41
Self Adaptive Real-Binary DE	-20.1280	2.88^{o}	39

The parameters of the optimal arrays are given in Table6.9.

Table6.9. Parameters of the optimal thinned linear arrays with constant inter-element spacing obtained from the optimization algorithms using cost function 1 and dynamic weight.

Optimization Algorithms	Sequence of turned-on (active) elements	Inter-element spacing
Real-Boolean DE	1010110111111111111111111111111111110 0001110011	0.8889λ
Self Adaptive Real-Boolean DE	1010110111111111111111111111111111110 0001110011	0.8025λ
Self Adaptive Real-Binary DE	1010110111111111111111111111111111111 00001110011	0.9630λ

The statistical performance parameters of the real-Boolean SADE and real-Boolean DE optimization algorithms are almost same in terms of mean cost value, best cost value, worst cost value and standard deviation of cost values. The optimal linear array obtained from the best run of the real-Boolean SADE algorithm has an inter-element spacing of 0.8025λ having 82% turned-on (active) elements. The real-Boolean SADE algorithm used an average population size of approximately 38 vectors or chromosomes across all its runs. The same population size is used for the real-Boolean DE algorithm. The normalized array factor plot of the optimal array obtained from Self-Adaptive real-Boolean DE algorithm is given in Fig.6.10.

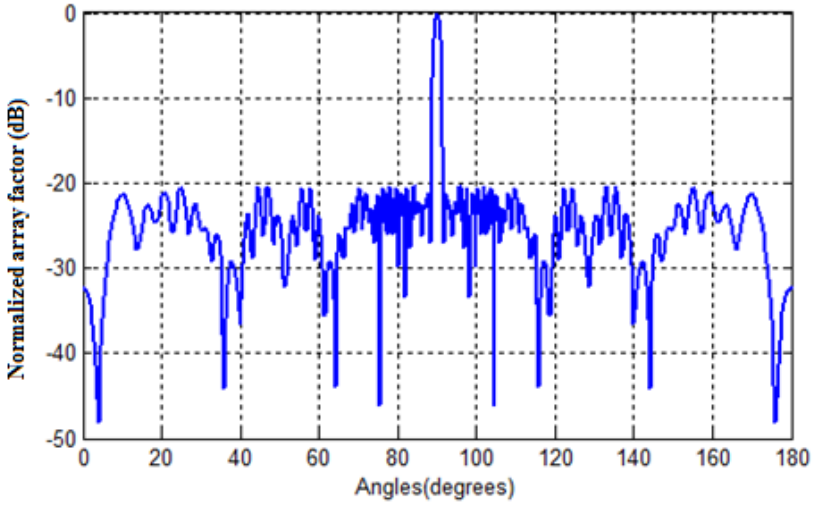

Fig .6.10 Normalized array factor of the optimal thinned linear array (with constant inter-element spacing) obtained using self-adaptive Boolean DE algorithm using cost function 1 and dynamic weight.

6.7.5 Optimization of Thinned Boolean Linear Array with Cost Function 2 and Dynamic Weights

Optimization of the thinned Boolean linear array with cost function 2 and dynamic weights described earlier is done using real-Boolean differential evolution algorithm, self -adaptive real-Boolean differential evolution algorithm and self-adaptive real-binary differential evolution algorithm. The array parameters and constraints are assumed to be same as in the previous section. The number of optimization variables is 51 with 50 Boolean variables and one real coded variable. The statistical performance of the different optimization algorithms are given below in Table6.10. Each of the algorithms is run for 25 independent runs starting from the same population. The cost function used a dynamic weight with the side lobe level, number of elements of the array and inter-element spacing. The threshold value for the side lobe level (maximum), number of turned-on(active) elements in the array (maximum) and inter-element spacing (maximum) are -18 dB, 45 and 0.7λ respectively.

Table6.10. Statistical performance of the optimization algorithms for thinned linear array with constant inter-element spacing, cost function 2 and dynamic weights.

Optimization Algorithms	Mean value	Best cost value	Worst cost value	Standard deviation of the cost values	Robustness (%)	Convergence rate (Generations)
Real-Boolean DE	3.4891	3.3923	4.0446	0.2049	100	16
Self Adaptive Real-Boolean DE	3.4145	3.3936	3.4361	0.0113	100	11
Self Adaptive Real-Binary DE	3.4319	3.3985	3.4521	0.0142	100	36

The best convergence graphs for the optimization algorithms are given below in Fig.6.11.

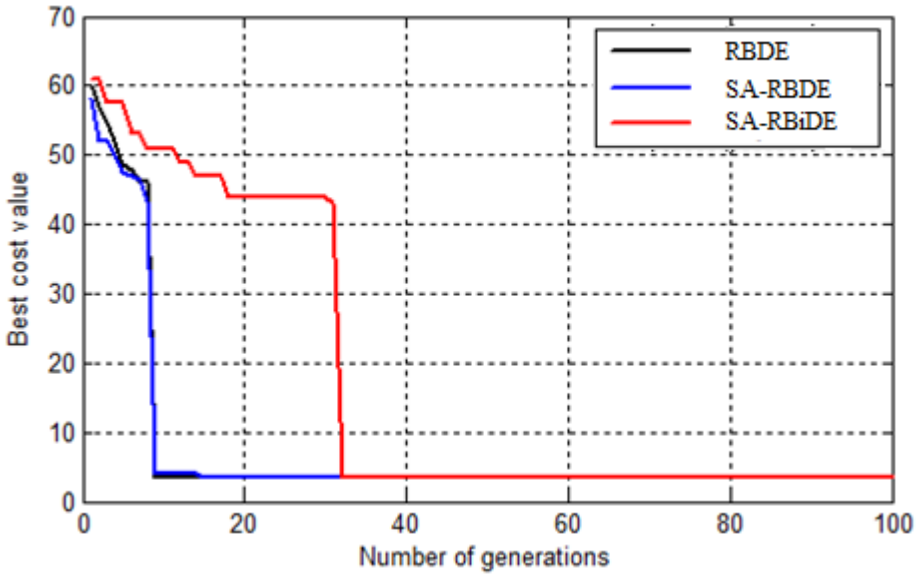

Fig.6.11Best convergence plots of the optimization algorithms for thinned linear array with constant inter-element spacing, cost function 2 and dynamic weights.

The mean convergence graphs for the optimization algorithms are given below in Fig.6.12.

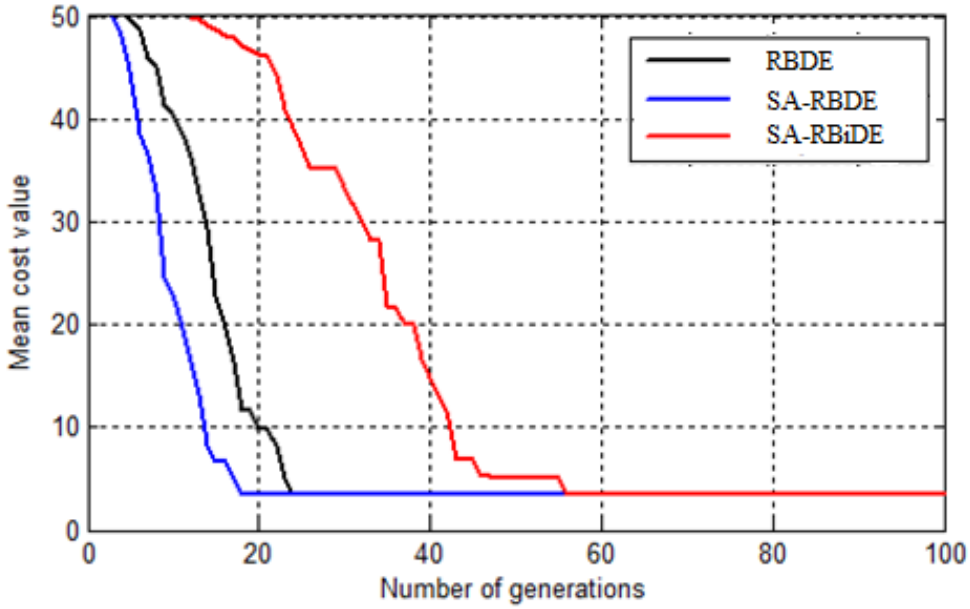

Fig.6.12 Mean convergence plots of the optimization algorithms for thinned linear array with constant inter-element spacing, cost function 2 and dynamic weights.

The performances of the optimal thinned arrays obtained from the best run of each algorithm are given in Table6.11.

Table6.11. Performance of the optimal thinned linear arrays with constant inter-element spacing obtained from the optimization algorithms using cost function 2 and dynamic weights.

Optimization Algorithms	Maximum side lobe level (dB)	Beam width between 1st nulls (in degrees)	Number of active elements in the array
Real-Boolean DE	-19.8856	4.32^{o}	41
Self Adaptive Real-Boolean DE	-18.9597	4.32^{o}	41
Self Adaptive Real-Binary DE	-19.3353	4.32^{o}	40

The parameters of the optimal arrays are given in Table6.12.

Table6.12. Parameters of the optimal thinned linear arrays with constant inter-element spacing obtained from the optimization algorithms using cost function 2 and dynamic weights.

Optimization Algorithms	Sequence of turned-on (active) elements	Inter-element spacing
Real-Boolean DE	1101111000111111111111111111111111111110 1110101001	0.5900 λ
Self AdaptiveReal-Boolean DE	1110101010111101111111111111111111011110 1111011011	0.5592 λ
Self AdaptiveReal-Binary DE	1111101011101111111111111111111111011110 1011001100	0.5914 λ

The statistical performance parameters of the optimization algorithms are almost same in terms of mean cost value, best cost value, worst cost value and standard deviation of cost values. However the performance of the real-Boolean SADE algorithm is slightly better compared to the other algorithms. In terms of convergence rate, the real-Boolean SADE algorithm shows the fastest convergence compared to the other algorithms as evident from the mean convergence plots in Fig6.12. The optimal linear array obtained from the best run of the real-Boolean SADE algorithm has an inter-element spacing of 0.5592λ and 82% turned-on (active). The real-Boolean SADE algorithm used an average population size of approximately 34 vectors or chromosomes across all its runs. The same population size is used for the real-Boolean DE algorithm. The normalized array factor plot of the optimal array obtained from self-adaptive real-Boolean DE algorithm is given in Fig.6.13.

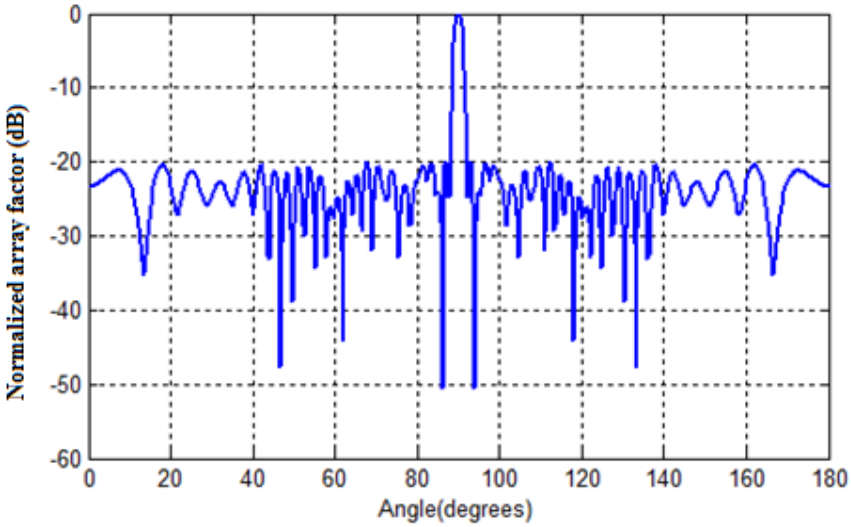

Fig .6.13 Normalized array factor of the optimal thinned linear array (with constant inter-element spacing) obtained using self-adaptive Boolean DE algorithm using cost function 2 and dynamic weights.

6.8 Optimization of Thinned Planar Antenna Array

6.8.1 Theory

Antenna array elements can be arranged in a square or rectangular matrix arrangement. The layout of a planar array is shown below in Fig. 6.14:

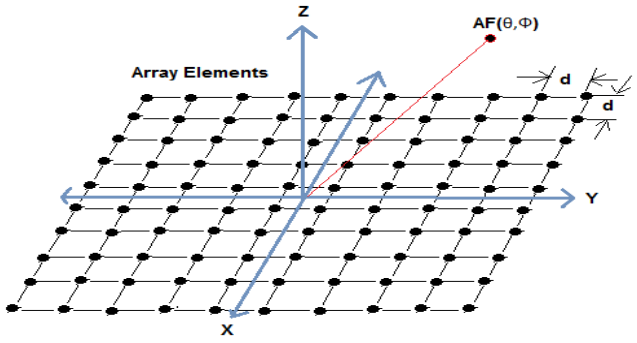

Fig. 6.14 Geometry of a N x N element asymmetric planar array

The First-Null Beam-Width (FNBW) in the case of the thinned array should be as close as possible to that of the fully populated array. The inter element spacing along both X and Y axes

are optimized to keep the planar antenna array area as small as possible. The array factor of a planar array can be written as [77]:

$$AF(\theta, \Phi) = \sum_{-N}^{+N} \sum_{-N}^{+N} A(x_n, y_n) \exp[jk \sin\theta \ (x_n cos\Phi + \ y_n \sin\Phi)] \quad (6.12)$$

6.8.2Optimization of Thinned Boolean Planar Array with Cost Function 1 and Constant Weight

Optimization of the thinned Boolean planar array with cost function 1 and constant weight described earlier is done using real-Boolean differential evolution algorithm, self-adaptive real-Boolean differential evolution algorithm and self-adaptive real-binary differential evolution algorithm. The array is assumed to have antenna elements arranged in 10x 10 matrices on the x-y plane. The inter-element spacing along the x-direction and y-direction are assumed to be constant between successive antenna elements. However the value of the inter-element spacing can lie between 0.5λ to 1λ to avoid mutual coupling effects and grating lobes. The inter-element spacing values are also to be optimized. The number of optimization variables is 102 with 100 Boolean variables and 2 real coded variables. The statistical performance of the different optimization algorithms are given below in Table6.13. Each of the algorithms is run for 25 independent runs starting from the same population.

Table6.13. Statistical performance of the optimization algorithms for thinned planar array with constant inter-element spacing, cost function 1 and static weights.

Optimization Algorithms	Mean value	Best cost value	Worst cost value	Standard deviation of the cost values
Real-Boolean DE	0.1285	0.1245	0.1360	0.0033
Self Adaptive Real-Boolean DE	0.1284	0.1212	0.1337	0.0029
Self Adaptive Real-Binary DE	0.1528	0.1413	0.1718	0.0081

The best convergence graphs for the optimization algorithms are given below in Fig.6.15.

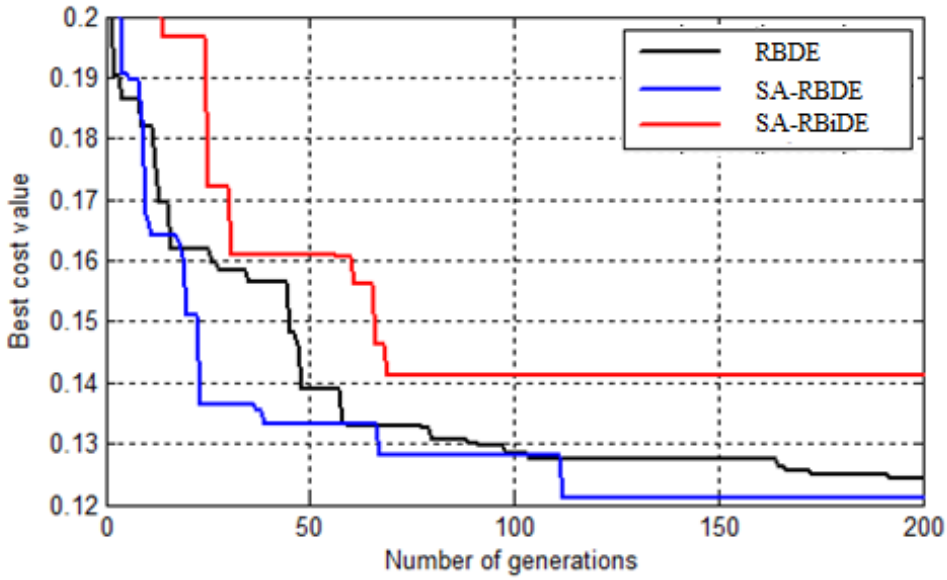

Fig.6.15Best convergenceplots of the optimization algorithms for thinned planar array with constant inter-element spacing, cost function 1 and static weights.

The mean convergence graphs for the optimization algorithms are given below in Fig.6.16.

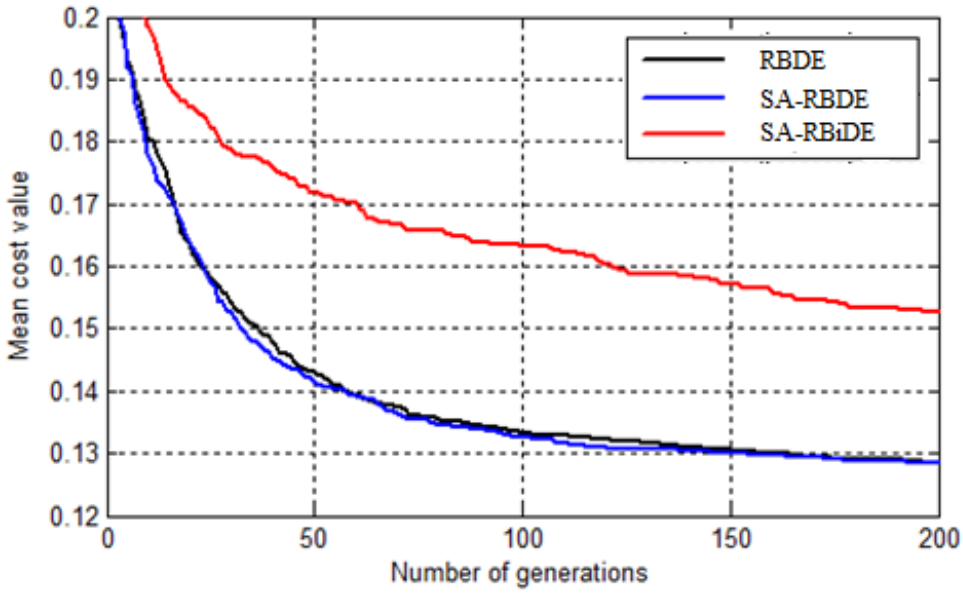

Fig.6.16 Mean convergence plots of the optimization algorithms for thinned planar array with constant inter-element spacing, cost function 1 and static weights.

The performances of the optimal thinned arrays obtained from the best run of each algorithm are given in Table6.14.

Table6.14. Performance of the optimal thinned planar arrays with constant inter-element spacing obtained from the optimization algorithms using cost function 1 and static weights.

Optimization Algorithms	Maximum side lobe level (dB) for phi=0 degrees	Maximum side lobe level (dB) for phi=90 degrees	Beam width between 1st nulls (in degrees) for phi=0 degrees	Beam width between 1st nulls (in degrees) for phi=90 degrees
Real-Boolean DE	-19.0493	-18.1000	14.4^{o}	14.4^{o}
Self Adaptive Real-Boolean DE	-19.0621	-18.3330	14.4^{o}	14.4^{o}
Self Adaptive Real-Binary DE	-17.2505	-16.9963	14.4^{o}	14.4^{o}

The parameters of the optimal arrays are given in Table6.15.

Table6.15. Parameters of the optimal thinned linear arrays with constant inter-element spacing obtained from the optimization algorithms using cost function 1 and static weights.

Optimization Algorithms	Inter-element spacing along x-direction	Inter-element spacing along y-direction	Number of active elements in the array
Real-Boolean DE	0.8933λ	0.8471λ	77
Self Adaptive Real-Boolean DE	0.8929λ	0.8538λ	78
Self Adaptive Real-Binary DE	0.7752λ	0.7504λ	78

The arrangement of the thinned planar obtained from the best run of real-Boolean DE algorithm is given in Fig.6.17.

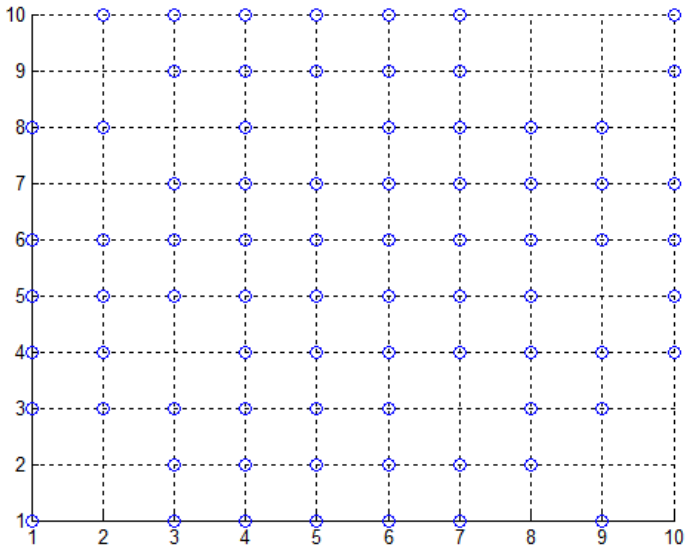

Fig.6.17 Arrangement of the thinned Boolean planar array obtained from the best run of real-Boolean DE algorithm using cost function 1 with static weights

The arrangement of the thinned planar obtained from the best run of real-Boolean SADE algorithm is given in Fig.6.18.

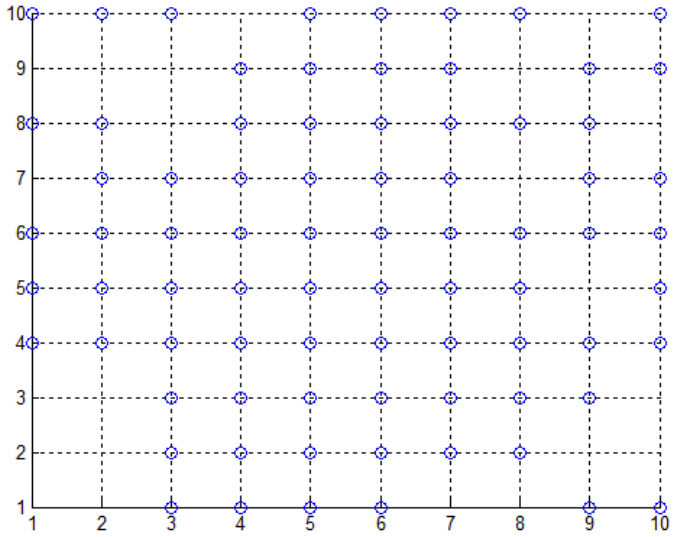

Fig.6.18 Arrangement of the thinned Boolean planar array obtained from the best run of real-Boolean SADE algorithm using cost function 1 with static weights

The arrangement of the thinned planar obtained from the best run of real-binary SADE algorithm is given in Fig.6.19.

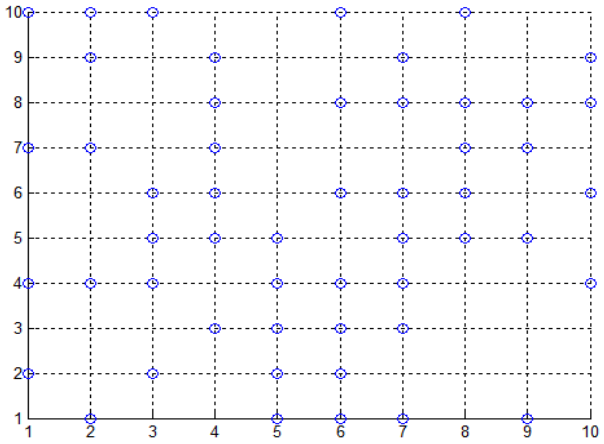

Fig.6.19 Arrangement of the thinned Boolean planar array obtained from the best run of real-Binary SADE algorithm using cost function 1 with static weights

The cost function is designed to achieve a pattern with FNBW in both phi=0 degree and phi=90 degree as close as possible to that of a fully filled planar array with same inter-element spacing as that of the thinned array. The statistical performance parameters of the optimization algorithms are almost same in terms of mean cost value, best cost value, worst cost value and standard deviation of cost values. However the performance of the real-Boolean SADE algorithm is slightly better compared to the other algorithms. In terms of convergence rate, the real-Boolean SADE algorithm shows the fastest convergence compared to the other algorithms as evident from the mean convergence plots in Fig.6.16. The real-Boolean SADE algorithm used an average population size of approximately 39 vectors or chromosomes across all its runs. The optimal planar array obtained from the best run of the real-Boolean SADE algorithm has an inter-element spacing of 0.8929λ and 0.8538λ in the X and Y-directions with 78% filling of turned-on (active) elements. The normalized array factor plots of the optimal array obtained from self-adaptive real-Boolean DE algorithm is given in Fig.6.20.

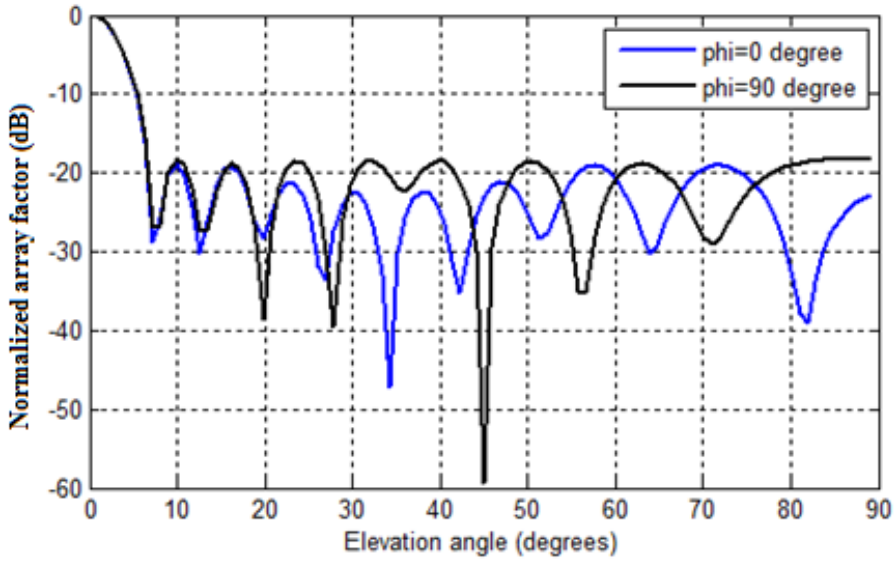

Fig .6.20 Normalized array factors of the optimal thinned planar array (with constant inter-element spacing) obtained using self-adaptive Boolean DE algorithm using cost function 1 and static weights

6.8.3Optimization of Thinned Boolean Planar Array with Cost Function 2 and Constant Weights

Optimization of the thinned Boolean planar array with cost function 2 and constant weights described earlier is done using real-Boolean differential evolution algorithm, self-adaptive real-Boolean differential evolution algorithm and self-adaptive real-binary differential evolution algorithm. The array parameters remain same as in the previous section. Hence the number of optimization variables is 102 with 100 Boolean variables and 2 real coded variables. The statistical performance of the different optimization algorithms are given below in Table6.16. Each of the algorithms is run for 25 independent runs starting from the same population.

Table6.16. Statistical performance of the optimization algorithms for thinned planar array with constant inter-element spacing, cost function 2 and static weights.

Optimization Algorithms	Mean value	Best cost value	Worst cost value	Standard deviation of the cost values
Real-Boolean DE	6.5309	6.3814	6.7660	0.1175
Self AdaptiveReal-Boolean DE	6.5251	6.2799	6.6966	0.0965
Self AdaptiveReal-Binary DE	7.0287	6.7323	7.2914	0.1624

The best convergence graphs for the optimization algorithms are given below in Fig.6.21.

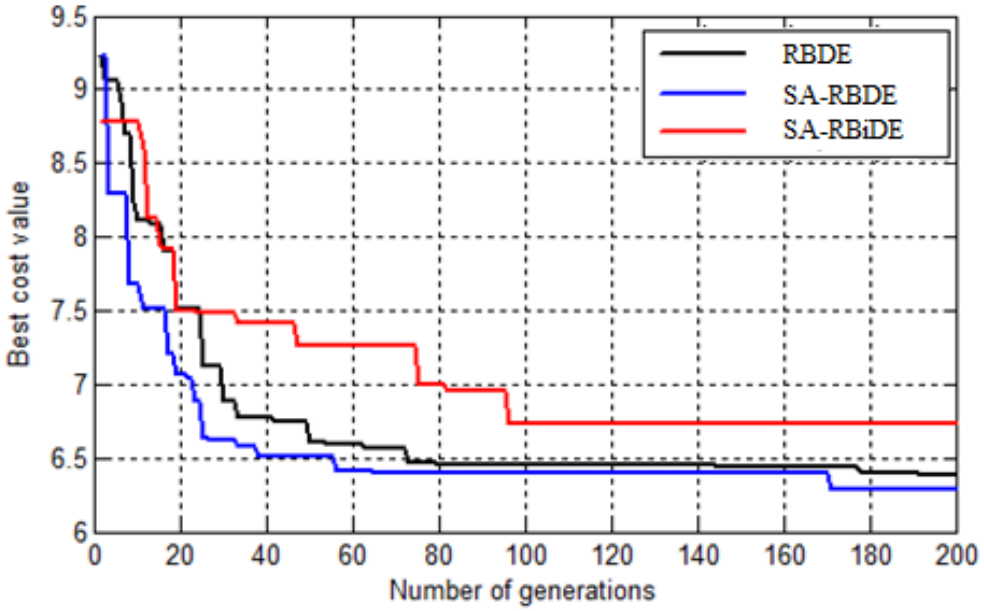

Fig.6.21 Best convergence plots of the optimization algorithms for thinned planar array with constant inter-element spacing, cost function 2 and static weights.

The mean convergence graphs for the optimization algorithms are given below in Fig.6.22.

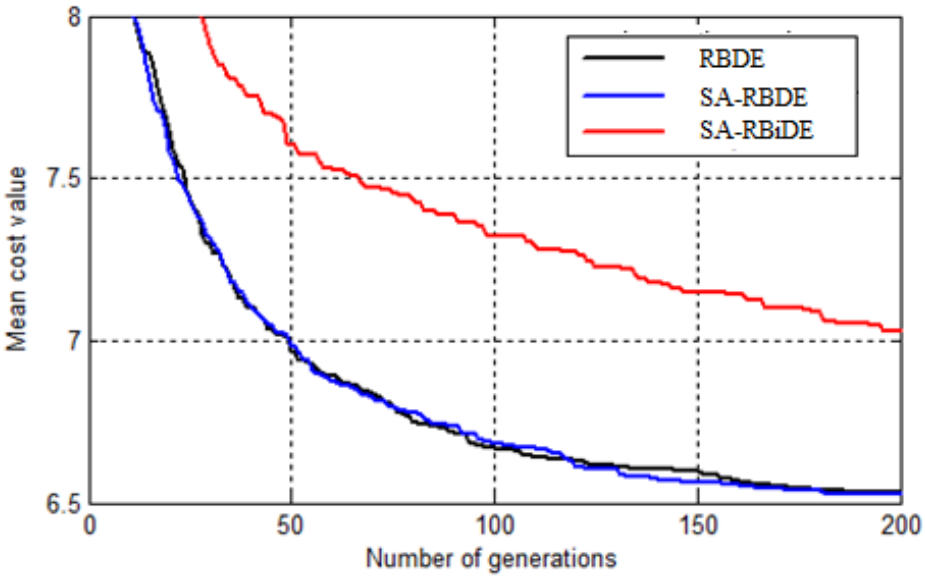

Fig.6.22 Mean convergence plots of the optimization algorithms for thinned planar array with constant inter-element spacing, cost function 2 and static weights.

The performances of the optimal thinned arrays obtained from the best run of each algorithm are given in Table6.17.

Table6.17. Performance of the optimal thinned planar arrays with constant inter-element spacing obtained from the optimization algorithms using cost function 2 and static weights.

Optimization Algorithms	Maximum side lobe level (dB) for phi=0 degrees	Maximum side lobe level (dB) for phi=90 degrees	Beam width between 1st nulls (in degrees)for phi=0 degrees	Beam width between 1st nulls (in degrees)for phi=90 degrees
Real-Boolean DE	-18.0910	-17.9925	16.2^{o}	16.2^{o}
Self Adaptive Real-Boolean DE	-18.7986	-18.0666	16.2^{o}	16.2^{o}

Optimization Algorithms	Maximum side lobe level (dB) for phi=0 degrees	Maximum side lobe level (dB) for phi=90 degrees	Beam width between 1st nulls (in degrees)for phi=0 degrees	Beam width between 1st nulls (in degrees)for phi=90 degrees
Self Adaptive Real-Binary DE	-16.5847	-16.5587	19.8^{o}	19.8^{o}

The parameters of the optimal arrays are given in Table6.18.

Table6.18. Parameters of the optimal thinned linear arrays with constant inter-element spacing obtained from the optimization algorithms using cost function 2 and static weights.

Optimization Algorithms	Inter-element spacing along x-direction	Inter-element spacing along y-direction	Number of active elements in the array
Real-Boolean DE	0.7684λ	0.7529λ	82
Self Adaptive Real-Boolean DE	0.8192λ	0.7535λ	71
Self Adaptive Real-Binary DE	0.6375λ	0.6101λ	54

The arrangement of the thinned planar obtained from the best run of real-Boolean DE algorithm is given in Fig.6.23.

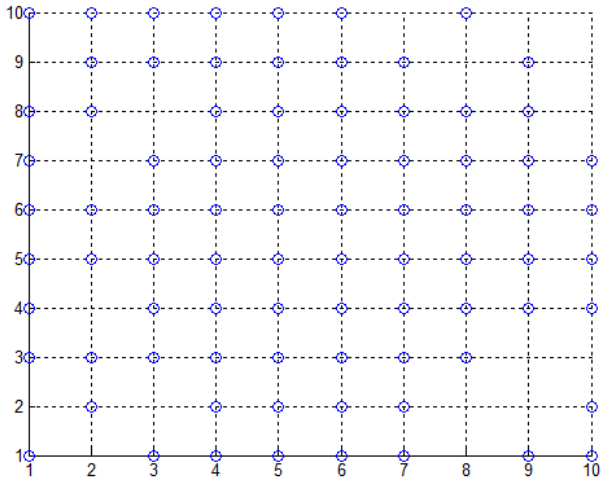

Fig.6.23 Arrangement of the thinned Boolean planar array obtained from the best run of real-Boolean DE algorithm using cost function 2 with static weights

The arrangement of the thinned planar obtained from the best run of real-Boolean SADE algorithm is given in Fig.6.24.

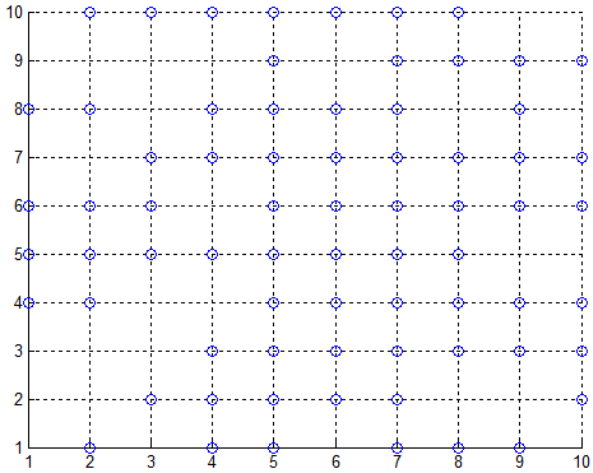

Fig.6.24 Arrangement of the thinned Boolean planar array obtained from the best run of real-Boolean SADE algorithm using cost function 2 with static weights

The arrangement of the thinned planar obtained from the best run of real-binary SADE algorithm is given in Fig.6.25.

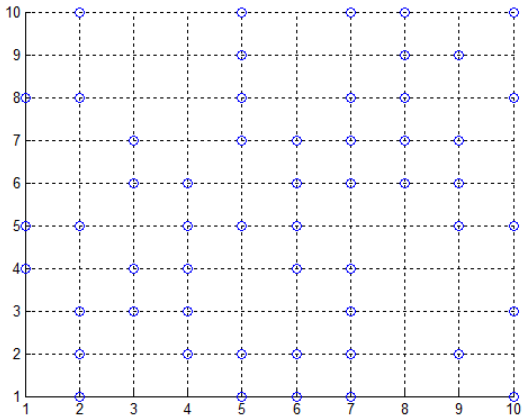

Fig.6.25 Arrangement of the thinned Boolean planar array obtained from the best run of real-binary SADE algorithm using cost function 2 with static weights

The statistical performance parameters of the optimization algorithms are almost same in terms of mean cost value, best cost value, worst cost value and standard deviation of cost values. However the performance of the real-Boolean SADE algorithm is slightly better compared to the other algorithms. In terms of convergence rate, the real-Boolean SADE algorithm shows the fastest convergence compared to the other algorithms as evident from the mean convergence plots in Fig.6.22. The real-Boolean SADE algorithm used an average population size of approximately 39 vectors or chromosomes across all its runs. The optimal planar array obtained from the best run of the real-Boolean SADE algorithm has an inter-element spacing of 0.8192λ and 0.7535λ in the X and Y-directions with 71% turned-on (active) elements. The normalized array factor patterns of the optimal array obtained from self-adaptive real-Boolean DE algorithm is given in Fig.6.26.

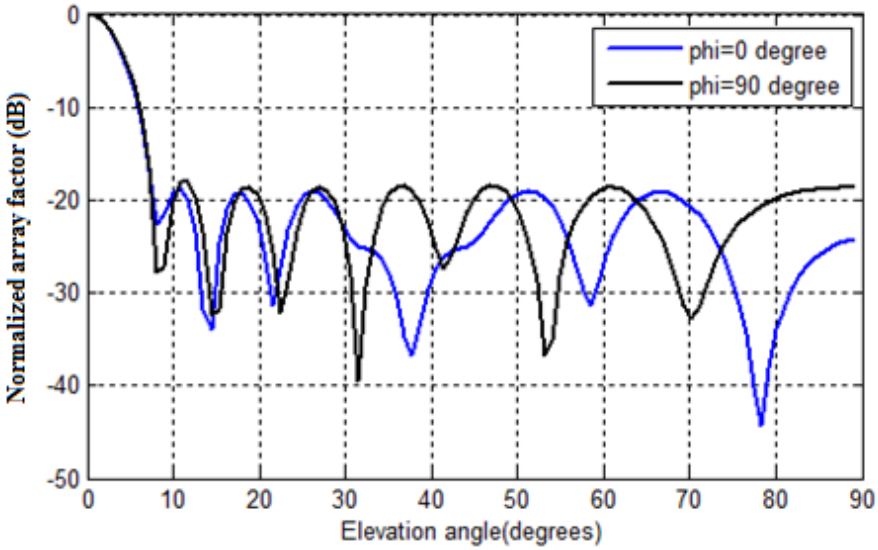

Fig .6.26 Normalized array factors of the optimal thinned planar array (with constant inter-element spacing) obtained using self-adaptive real-Boolean DE algorithm using cost function 2 and static weights

6.8.4Optimization of Thinned Boolean Planar Array with Cost Function 1 and Dynamic Weight

Optimization of the thinned Boolean planar array with cost function 1 and dynamic weight described earlier is done using real-Boolean differential evolution algorithm, self-adaptive real-Boolean differential evolution algorithm and self-adaptive real-binary differential evolution algorithm. The array parameters and constraints are assumed to be same as in the previous section. The number of optimization variables is 102 with 100 Boolean variables and two real coded variables. The statistical performance of the different optimization algorithms are given below in Table 6.19. Each of the algorithms is run for 25 independent runs starting from the same population. The maximum of the side lobe levels in the normalized power plots in the phi=0 degree and phi=90 degree planes is considered. The weight associated with the concerned side lobe level is a dynamic one. The threshold value of maximum side lobe level considering both phi=0 degree and phi=90 degree planes is -20 dB (maximum).

Table6.19. Statistical performance of the optimization algorithms for thinned planar array with constant inter-element spacing, cost function 1 and dynamic weights.

Optimization Algorithms	Mean value	Best cost value	Worst cost value	Standard deviation of the cost values	Robustness (%)	Convergence rate (generations)
Real-Boolean DE	6.5037	2.7585	42.362	10.809	100	61
Self Adaptive Real-Boolean DE	2.9844	2.7519	4.5817	0.5930	100	47
Self Adaptive Real-Binary DE	4.7867	4.5120	6.3923	0.5918	100	64

The best convergence graphs for the optimization algorithms are given below in Fig.6.27.

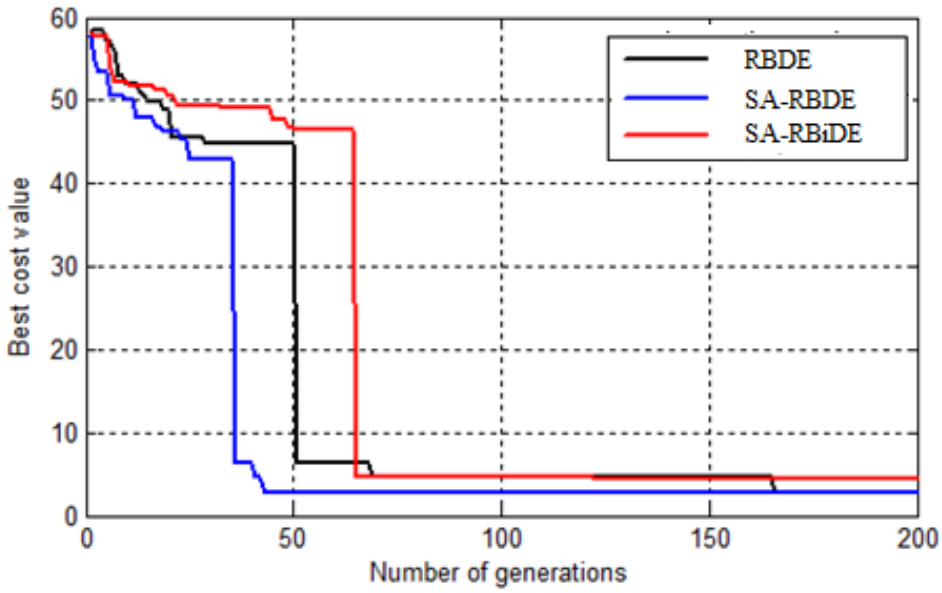

Fig.6.27Best convergence plots of the optimization algorithms for thinned planar array with constant inter-element spacing, cost function 1 and dynamic weights.

The mean convergence graphs for the optimization algorithms are given below in Fig.6.28.

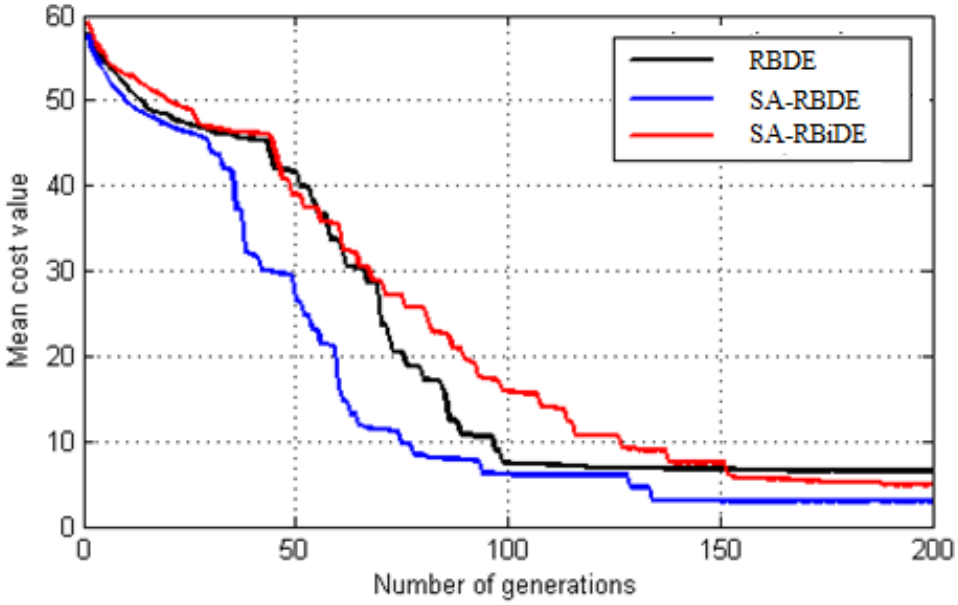

Fig.6.28Mean convergence plots of the optimization algorithms for thinned planar array with constant inter-element spacing, cost function 1 and dynamic weight.

The performances of the optimal thinned arrays obtained from the best run of each algorithm are given in Table6.20.

Table6.20. Performance of the optimal thinned planar arrays with constant inter-element spacing obtained from the optimization algorithms using cost function 1 and dynamic weight.

Optimization Algorithms	Maximum side lobe level (dB) for phi=0 degrees	Maximum side lobe level (dB) for phi=90 degrees	Beam width between 1st nulls(in degrees) for phi=0 degrees	Beam width between 1st nulls(in degrees) for phi=90 degrees
Real-Boolean DE	-21.1762	-20.8661	16.2^{o}	18.0^{o}
Self Adaptive Real-Boolean DE	-21.1822	-21.0099	16.2^{o}	18.0^{o}

Optimization Algorithms	Maximum side lobe level (dB) for phi=0 degrees	Maximum side lobe level (dB) for phi=90 degrees	Beam width between 1st nulls(in degrees) for phi=0 degrees	Beam width between 1st nulls(in degrees) for phi=90 degrees
Self Adaptive Real-Binary DE	-21.9306	-22.5228	18.0^{o}	21.6^{o}

The parameters of the optimal arrays are given in Table 6.21.

Table 6.21. Parameters of the optimal thinned linear arrays with constant inter-element spacing obtained from the optimization algorithms using cost function 1 and dynamic weight.

Optimization Algorithms	Inter-element spacing along x-direction	Inter-element spacing along y-direction	Number of active elements in the array
Real-Boolean DE	0.8705λ	0.7486 λ	72
Self Adaptive Real-Boolean DE	0.8641 λ	0.7527 λ	75
Self Adaptive Real-Binary DE	0.8518 λ	0.6624 λ	59

The arrangement of the thinned planar obtained from the best run of real-Boolean DE algorithm is given in Fig.6.29.

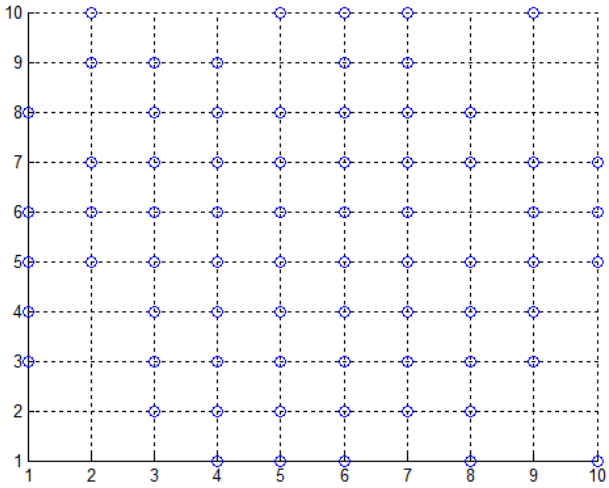

Fig.6.29 Arrangement of the thinned Boolean planar array obtained from the best run of real-Boolean DE algorithm using cost function 1 with dynamic weight

The arrangement of the thinned planar obtained from the best run of real-Boolean SADE algorithm is given in Fig.6.30.

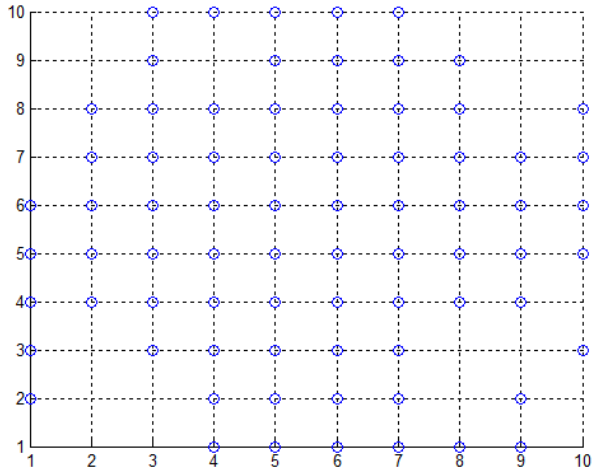

Fig.6.30 Arrangement of the thinned Boolean planar array obtained from the best run of real-Boolean SADE algorithm using cost function 1 with dynamic weight.

The arrangement of the thinned planar obtained from the best run of real-binary SADE algorithm is given in Fig.6.31.

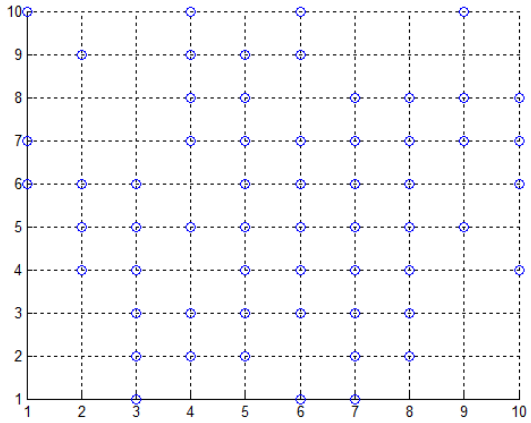

Fig.6.31 Arrangement of the thinned Boolean planar array obtained from the best run of real-binary SADE algorithm using cost function 1 with dynamic weight.

The statistical performance parameters of the optimization algorithms are given in terms of mean cost value, best cost value, worst cost value, standard deviation of cost values, and robustness and convergence rate in Table 6.22. Although all the algorithms show 100% robustness, the real-Boolean SADE algorithm shows a much faster convergence rate compared to the other two algorithms in this optimization problem as evident from Table6.22 and Fig.6.27 and Fig. 6.28. However the performance of the real-Boolean SADE algorithm is slightly better compared to the other algorithms. The real-Boolean SADE algorithm has a very low mean cost value and low standard deviation compared to the other algorithms. The best cost value of real-Boolean DE algorithm is very close to that of real-Boolean SADE algorithm. The real-Boolean SADE algorithm used an average population size of approximately 35 vectors or chromosomes across all its runs. The optimal planar array obtained from the best run of the real-Boolean SADE algorithm has an inter-element spacing of 0.8641λ and 0.7527λ in the X and Y-directions with 75% turned-on (active) elements. The normalized array factor plots of the optimal array obtained from self-adaptive real-Boolean DE algorithm is given in Fig.6.32.

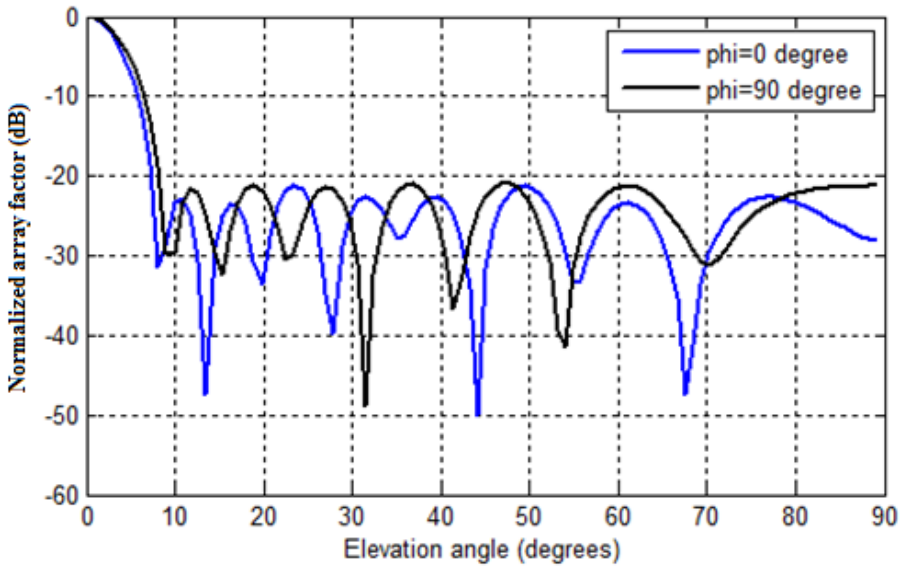

Fig .6.32 Normalized array factors of the optimal thinned planar array (with constant inter-element spacing) obtained using self-adaptive real-Boolean DE algorithm using cost function 1 and dynamic weights.

6.8.5Optimization of Thinned Boolean Planar Array with Cost Function 2 and Dynamic Weights

Optimization of the thinned Boolean planar array with cost function 2 described earlier is done using real-Boolean differential evolution algorithm, self adaptive real-Boolean differential evolution algorithm and self-adaptive real-binary differential evolution algorithm. The array parameters and constraints are assumed to be same as in the previous section. The inter-element spacing values are also to be optimized. The number of optimization variables is 102 with 100 Boolean variables and two real coded variables. The statistical performance of the different optimization algorithms are given below in Table6.22. Each of the algorithms is run for 25 independent runs starting from the same population. The maximum value of the side lobe levels in the normalized power plots in the phi=0 degree and phi=90 degree planes is considered. The weight associated with the concerned side lobe level is a dynamic one. The threshold value of maximum side lobe level considering both phi=0 degree and phi=90 degree planes, number of turned-on (active) in the array and maximum inter-element spacing along x and y direction are -20 dB (maximum), 75(maximum) and 0.7λ (maximum) respectively.

Table6.22. Statistical performance of the optimization algorithms for thinned planar array with constant inter-element spacing, cost function 2 and dynamic weights.

Optimization Algorithms	Mean value	Best cost value	Worst cost value	Standard deviation of the cost values	Robustness (%)	Convergence rate (Generations)
Real-Boolean DE	10.156	4.7191	47.853	11.315	92	62
Self Adaptive Real-Boolean DE	6.5781	6.3262	8.2592	0.4991	100	55
Self Adaptive Real-Binary DE	8.0954	6.1229	11.5268	1.4336	100	63

The best convergence graphs for the optimization algorithms are given below in Fig.6.33.

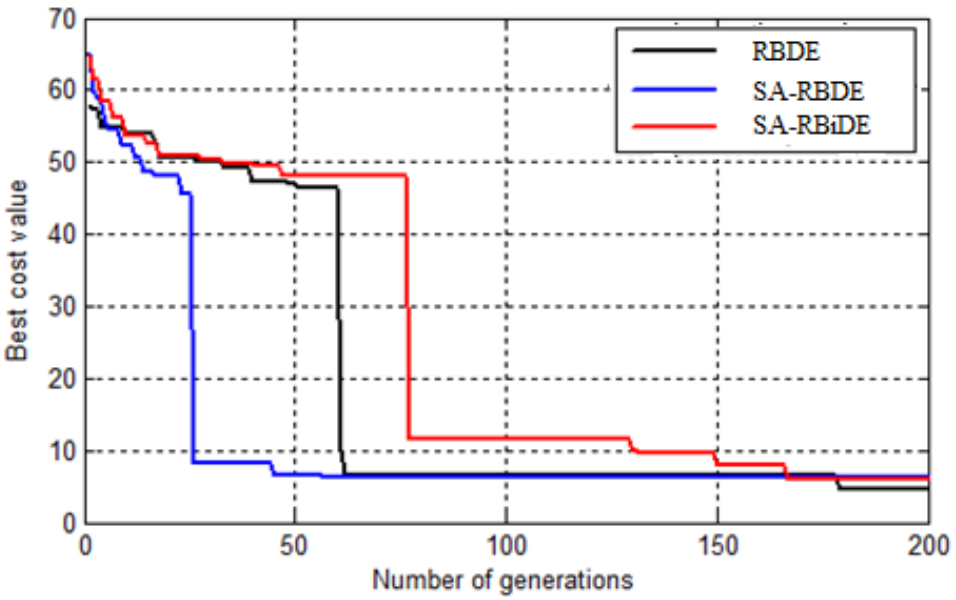

Fig.6.33Best convergence plots of the optimization algorithms for thinned planar array with constant inter-element spacing, cost function 2 and dynamic weights.

The mean convergence graphs for the optimization algorithms are given below in Fig.6.34.

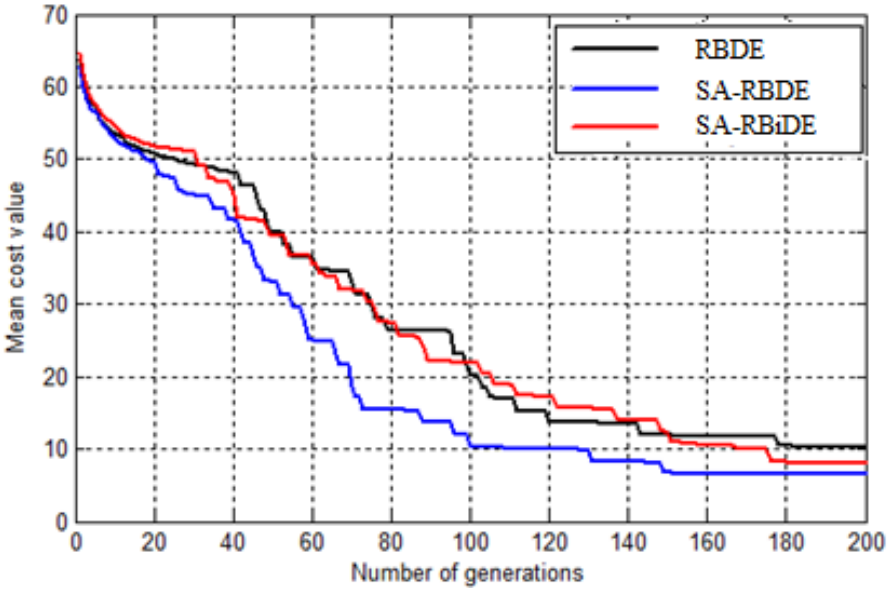

Fig.6.34Mean convergence plots of the optimization algorithms for thinned planar array with constant inter-element spacing, cost function 2 and dynamic weight.

The performances of the optimal thinned arrays obtained from the best run of each algorithm are given in Table6.23.

Table6.23. Performance of the optimal thinned planar arrays with constant inter-element spacing obtained from the optimization algorithms using cost function 2 and dynamic weights.

Optimization Algorithms	Maximum side lobe level (dB) for phi=0 degree	Maximum side lobe level (dB) for phi=90 degrees	Beam width between 1st nulls (phi=0 degree) (in degree)	Beam width between 1st nulls (phi=90 degree) (in degree)
Real-Boolean DE	-20.2682	-20.0210	19.8^{o}	21.6^{o}
Self Adaptive Real-Boolean DE	-20.5333	-20.5232	21.6^{o}	25.2^{o}
Self Adaptive Real-Binary DE	-20.0802	-20.0478	23.4^{o}	27.0^{o}

The parameters of the optimal arrays are given in Table6.24.

Table6.24. Parameters of the optimal thinned linear arrays with constant inter-element spacing obtained from the optimization algorithms using cost function 2 and dynamic weights.

Optimization Algorithms	Inter-element spacing along x-direction	Inter-element spacing along y-direction	Number of active elements in the array
Real-Boolean DE	0.6811λ	0.6094λ	71
Self Adaptive Real-Boolean DE	0.6475λ	0.5549λ	62
Self Adaptive Real-Binary DE	0.6010λ	0.5098λ	50

The arrangement of the thinned planar obtained from the best run of real-Boolean DE algorithm is given in Fig.6.35.

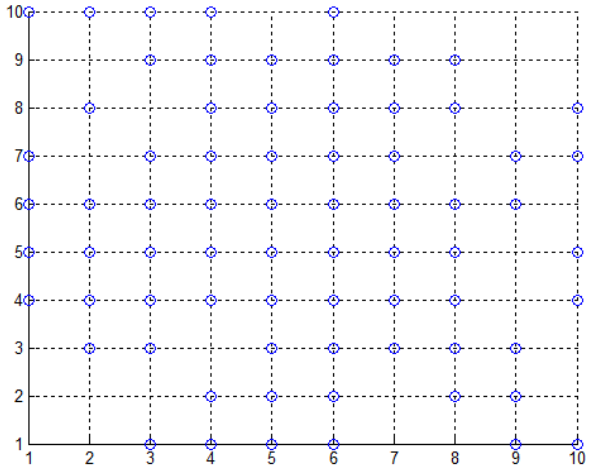

Fig.6.35 Arrangement of the thinned Boolean planar array obtained from the best run of real-Boolean DE algorithm using cost function 2 with dynamic weights

The arrangement of the thinned planar obtained from the best run of real-Boolean SADE algorithm is given in Fig.6.36.

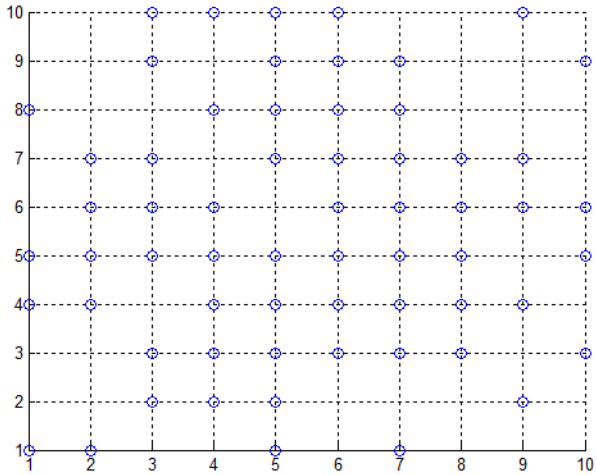

Fig.6.36 Arrangement of the thinned Boolean planar array obtained from the best run of real-Boolean SADE algorithm using cost function 2 with dynamic weights.

The arrangement of the thinned planar obtained from the best run of real-binary SADE algorithm is given in Fig.6.37.

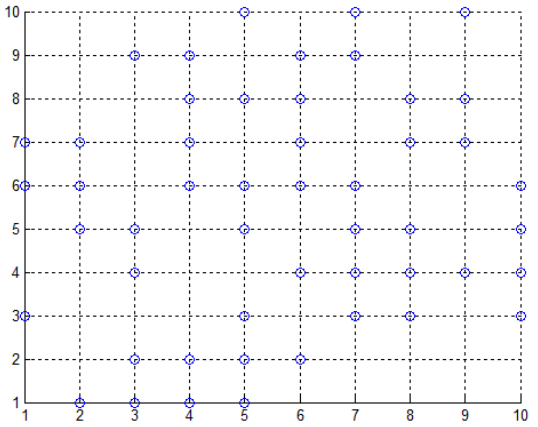

Fig.6.37 Arrangement of the thinned Boolean planar array obtained from the best run of real-binary SADE algorithm using cost function 2 with dynamic weights.

The statistical performance parameters of the optimization algorithms are given in Table6.24. Although the minimum best cost value is obtained in case of real-Boolean DE, it does not show 100% robustness and has a comparatively high mean cost value, worst cost value and standard deviation than the other two algorithms in this design problem. The lowest mean cost value, worst cost value and lowest standard deviation of cost values are exhibited by the real-Boolean SADE algorithm. The real-Boolean SADE algorithm is adjudged to be the best algorithm for this design problem with 100% robustness and fastest convergence rate. The real-binary SADE algorithm is adjudged to be the second best algorithm for this design problem. The real-Boolean SADE algorithm used an average population size of approximately 39 vectors or chromosomes across all its runs. The optimal planar array obtained from the best run of the real-Boolean SADE algorithm has an inter-element spacing of 0.6475λ and 0.5549λ in the X and Y-directions with 62% filling by turned-on (active) elements. In terms of convergence rate, the real-Boolean SADE algorithm shows the fastest convergence compared to the other algorithms as evident from the mean convergence plots in Fig.6.34. The normalized array factor plots of the optimal array obtained from self-adaptive real-Boolean DE algorithm is given in Fig.6.38.

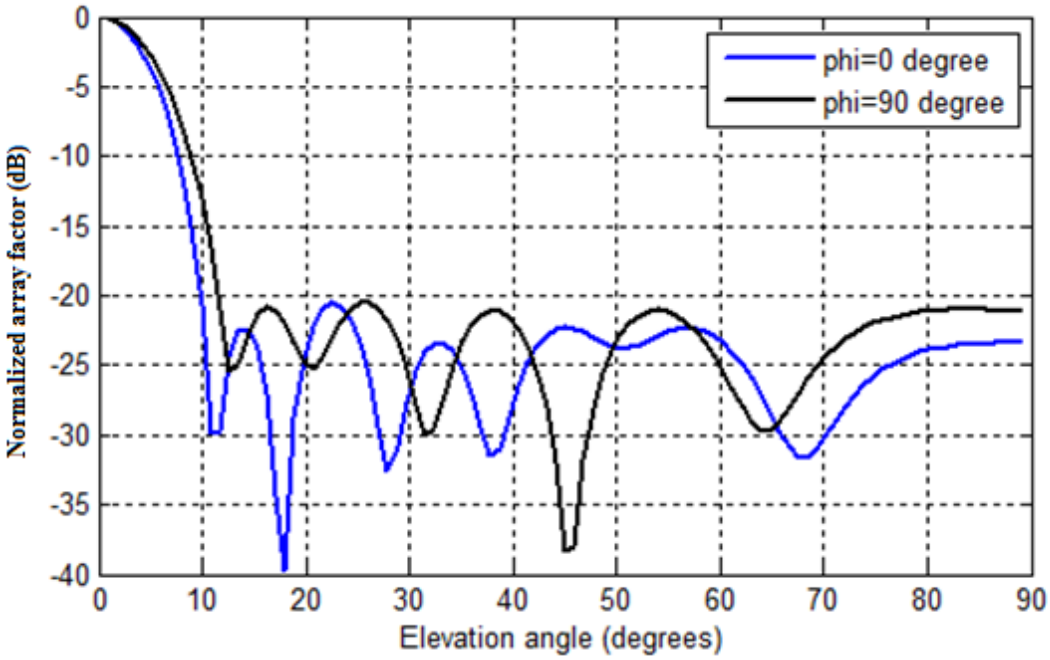

Fig .6.38 Normalized array factors of the optimal thinned planar array (with constant inter-element spacing) obtained using self-adaptive real-Boolean DE algorithm using cost function 2 and dynamic weights.

6.9 Optimization of Unequally Spaced Thinned Linear Array

6.9.1 Theory

The layout of the thinned linear unequally spaced antenna array is shown below in Fig. 6.39.

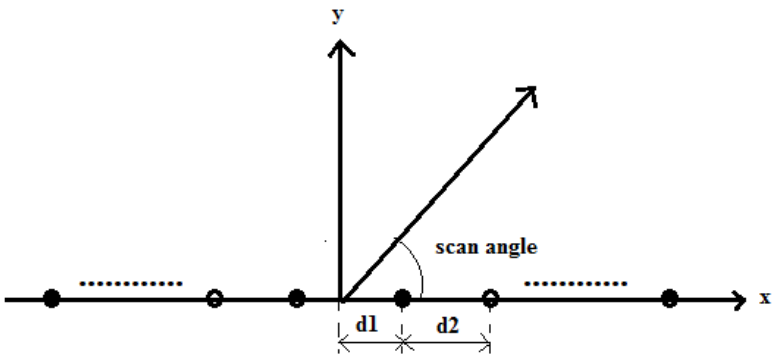

Fig. 6.39 Thinned linear array with non uniform inter-element spacing

In this case the states of the antenna array elements (ON /OFF) are to be optimized using Boolean genes and the locations of the antenna elements along the x-axis are to be optimized using real coded genes. The array uses 50 elements with symmetry along the center line ($a_n=a_{-n}$, where a_n refers to the excitation of the n^{th} element starting from the origin). Hence the optimized states of only 25 elements and their locations are required in this case.

The array factor of the antenna can be written as [77].

$$AF = \sum_{-N}^{+N} Ane^{[jkRn\ \cos(\Phi)]} \tag{6.13}$$

where

$$R_n = \sum_{i=1}^{n} di \tag{6.14}$$

The optimization of the unequally spaced thinned linear array is done using the real-Boolean optimization algorithms using the following cost function:

$$CostFunction_{ThinnedLinearnon\ -uniformArray} = C_1.\max\ (SLL_1) + C_2.(Numberofon - elements/Totalelements) \tag{6.15}$$

Each of the optimization algorithms are run for 25 generations each and their statistical performances are recorded. All the algorithms use the same initial population to start the optimization process. All the optimization algorithms are run for a predefined maximum generations as indicated later. It is also ensured that the average number of cost function evaluations for each generation should be same for all algorithms for ensuring fair comparison. The SA-RBDE algorithm uses dynamic population size and hence the number of cost function evaluations varies from generation to generation. The average number of function evaluations per generation from 25 independent runs of the algorithm is taken in to consideration under the circumstances.

6.9.2Optimization of Thinned Boolean Linear Array with Unequal Inter-element Spacing using Cost Function 2 and Constant Weights

Optimization of the thinned Boolean linear array with unequal inter-element spacing using cost function 2 (having constant weights) is done using real-Boolean differential evolution algorithm,

self-adaptive real-Boolean differential evolution algorithm and self-adaptive real-binary differential evolution Algorithm. The array is assumed to have 50 elements and is symmetric about its center. The inter-element spacing is assumed to be different between successive antenna elements. However the value of the inter-element spacing can lie between 0.5λ to 1λ to avoid mutual coupling effects and grating lobes. The inter-element spacing values are also optimized along with the positions of the on and off elements in the array. The number of optimization variables is 50 with 25 Boolean variables and 25 real coded variables. The statistical performance of the different optimization algorithms are given below in Table6.25. Each of the algorithms is run for 25 independent runs starting from the same population.

Table6.25. Statistical performance of the optimization algorithms for thinned linear array with unequal inter-element spacing using cost function 2 and static weights.

Optimization Algorithms	Mean value	Best cost value	Worst cost value	Standard deviation of the cost values
Real-Boolean DE	4.8462	4.1596	6.2124	0.4404
Self Adaptive Real-Boolean DE	4.4606	4.0500	4.9427	0.2389
Self Adaptive Real-Binary DE	5.2536	4.5656	6.0089	0.3713

The best convergence graphs for the optimization algorithms are given below in Fig.6.40.

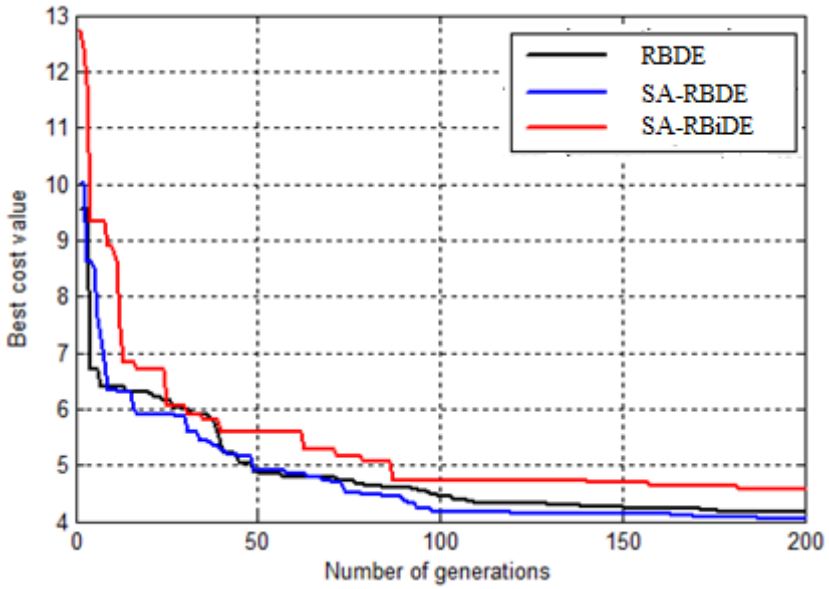

Fig.6.40 Best convergence plots of the optimization algorithms for thinned linear array with unequal inter-element spacing using cost function 2 and static weights.

The mean convergence graphs for the optimization algorithms are given below in Fig.6.41.

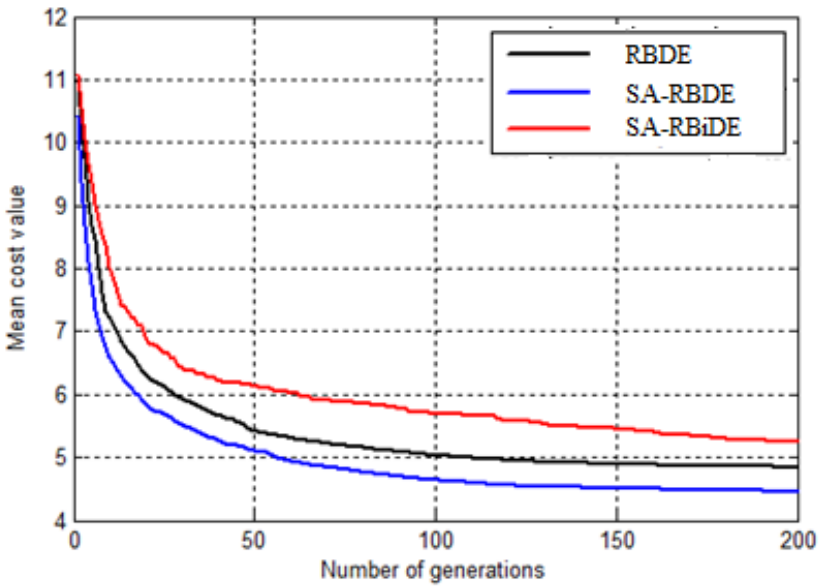

Fig.6.41 Mean convergence plots of the optimization algorithms for thinned linear array with unequal inter-element spacing using cost function 2 and static weights.

The performances of the optimal thinned arrays obtained from the best run of each algorithm are given in Table6.26.

Table6.26. Performance of the optimal thinned linear arrays with unequal inter-element spacing obtained from the optimization algorithms using cost function 2 and static weights.

Optimization Algorithms	Maximum side lobe level (dB)	Beam width between 1^{st} nulls(in degrees)	Number of active elements in the array
Real-Boolean DE	-22.21	4.32^{o}	40
Self Adaptive Real-Boolean DE	-22.58	4.32^{o}	46
Self Adaptive Real-Binary DE	-31.36	4.32^{o}	46

The parameters of the optimal arrays are given in Table6.27.

Table6.27. Parameters of the optimal thinned linear arrays with unequal inter-element spacing obtained from the optimization algorithms using cost function 2 and static weights.

Optimization Algorithms	Sequence of turned-on (active) elements	Mean inter-element spacing
Real-Boolean DE	0010001111111111111111111111111111111111111111000100	0.7483λ
Self Adaptive Real-Boolean DE	1110110111111111111111111111111111111111111110110111	0.6485λ
Self Adaptive Real-Binary DE	1101011111111111111111111111111111111111111111101011	0.7159λ

The arrangement of the optimal array obtained from the best run of the real-Boolean DE algorithm is shown in Fig.6.42.

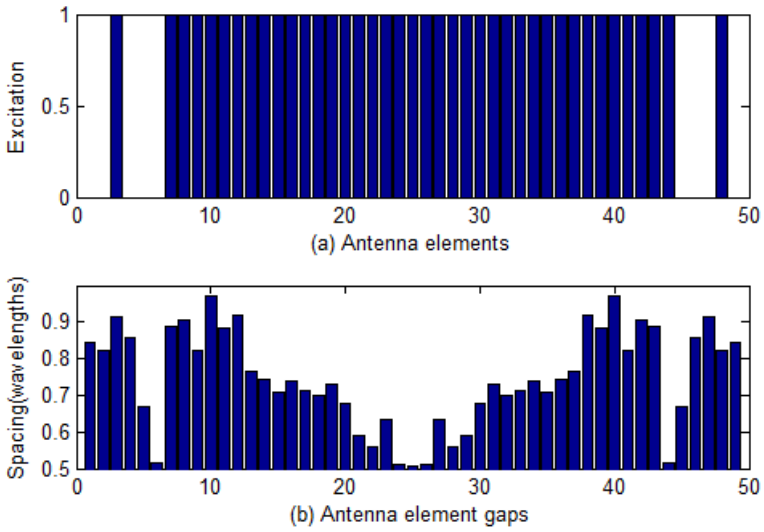

Fig.6.42 Arrangement of the optimal thinned linear array with unequal inter-element spacing obtained from the best run of the real-Boolean DE algorithm.

The arrangement of the optimal array obtained from the best run of the real-Boolean SADE algorithm is shown in Fig.6.43.

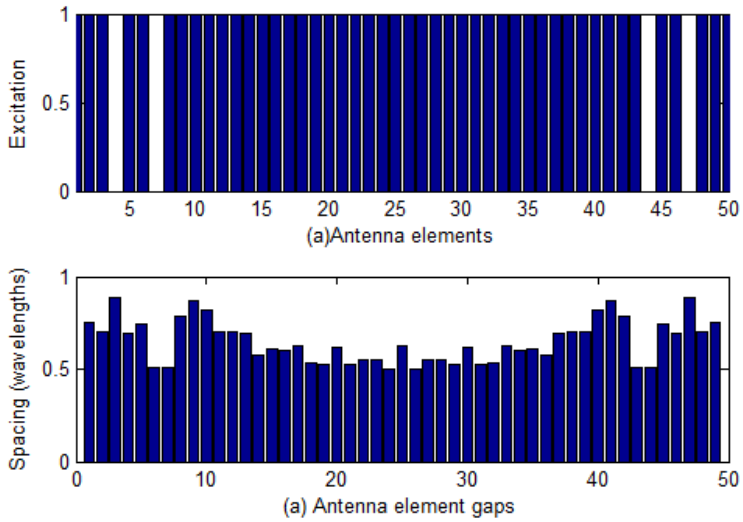

Fig.6.43 Arrangement of the optimal thinned linear array with unequal inter-element spacing obtained from the best run of the real-Boolean SADE algorithm.

The arrangement of the optimal array obtained from the best run of the real-binary SADE algorithm is shown in Fig.6.44.

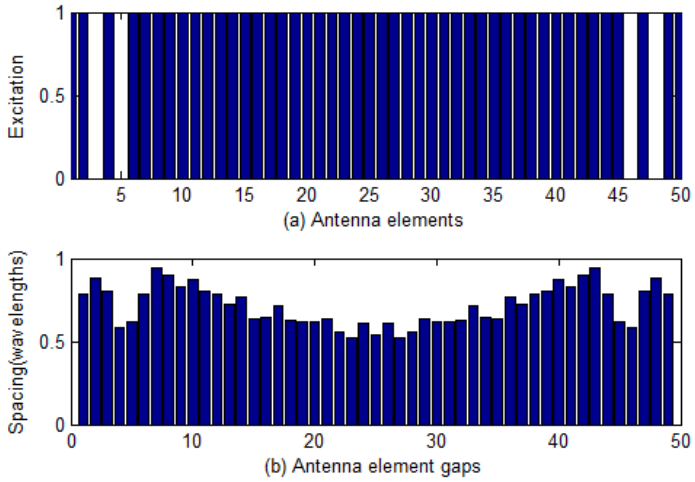

Fig.6.44 Arrangement of the optimal thinned linear array with unequal inter-element spacing obtained from the best run of the real-binary SADE algorithm.

The statistical performance parameters of the optimization algorithms are almost same. However the real-Boolean SADE algorithm exhibited minimum worst cost value and correspondingly minimum standard deviation among all the algorithms used in this chapter for this optimization problem. The performance of the real-Boolean SADE algorithm is slightly better compared to the other algorithms in terms of best cost value and mean cost value. In terms of convergence rate, the real-Boolean SADE algorithm shows the fastest convergence compared to the other algorithms as evident from the mean convergence plots in Fig.6.41. The real-Boolean SADE algorithm used an average of approximately 35 vectors or chromosomes in its population across all its runs. The same population size is used for the real-Boolean DE algorithm as well. The normalized array factor plot of the optimal array obtained from self-adaptive real-Boolean DE algorithm is given in Fig.6.45.

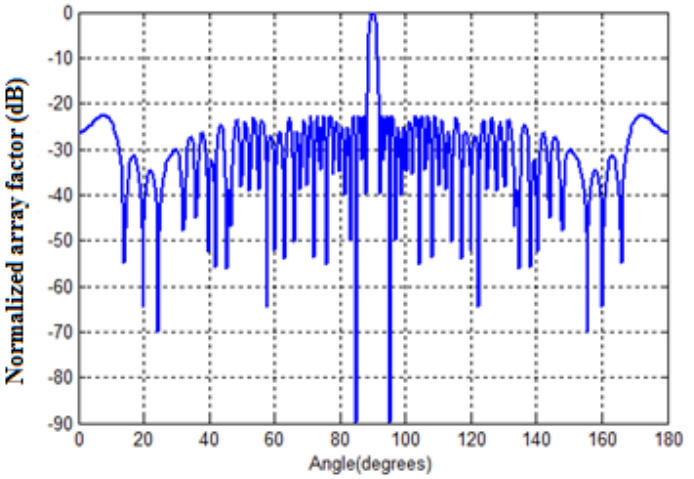

Fig. 6.45 Normalized array factors of the optimal thinned linear array (with unequal inter-element spacing) obtained using self-adaptive Boolean DE algorithm using cost function 2 and static weights

6.9.3 Optimization of Thinned Boolean Linear Array with Unequal Inter-element Spacing using Cost Function 2 and Dynamic Weights

Optimization of the thinned Boolean linear array with unequal inter-element spacing using cost function 2 (having dynamic weights) is done using real-Boolean differential evolution algorithm, self-adaptive real-Boolean differential evolution algorithm and self-adaptive real-binary differential evolution algorithm. The array parameters and constraints are assumed to be same as in the previous section. The number of optimization variables is 50 with 25 Boolean variables and 25 real coded variables. The threshold values for maximum side lobe level, mean inter-element spacing and number of turned-on (active) elements in the array are -20 dB (maximum), 0.7λ (maximum) and 40 (maximum) respectively. The statistical performance of the different optimization algorithms are given below in Table6.28. Each of the algorithms is run for 25 independent runs using the same initial population.

Table6.28. Statistical performance of the optimization algorithms for thinned linear array with unequal inter-element spacing using cost function 2 and dynamic weights.

Optimization Algorithms	Mean value	Best cost value	Worst cost value	Standard deviation of the cost values	Robustness (%)	Convergence rate (Generations)
Real-Boolean DE	18.940	2.6866	45.809	20.149	60	101
Self Adaptive Real-Boolean DE	7.5653	2.6743	42.688	13.073	88	78
Self Adaptive Real-Binary DE	21.071	2.7624	46.159	20.934	56	231

The best convergence graphs for the optimization algorithms are given below in Fig.6.46.

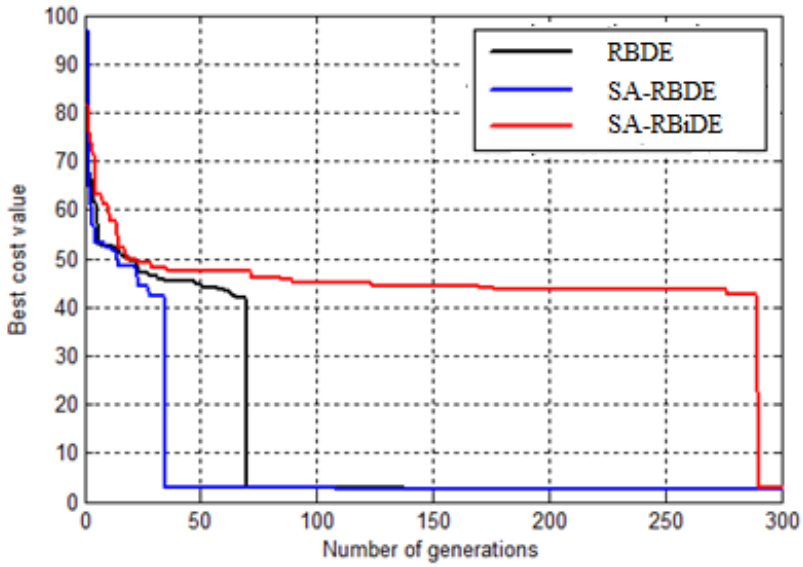

Fig.6.46 Best convergence plots of the optimization algorithms for thinned linear array with unequal inter-element spacing using cost function 2 and dynamic weights.

The mean convergence graphs for the optimization algorithms are given below in Fig.6.47.

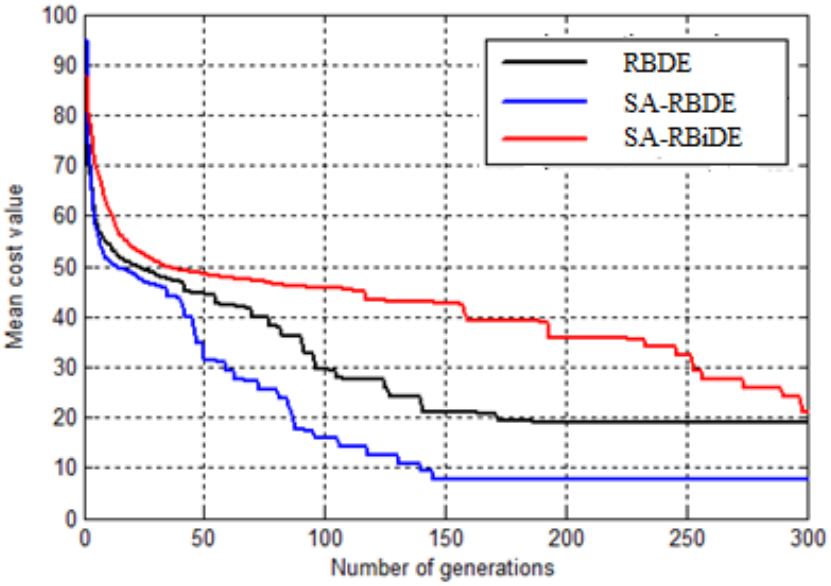

Fig.6.47Mean convergence plots of the optimization algorithms for thinned linear array with unequal inter-element spacing using cost function 2 and dynamic weights.

The performances of the optimal thinned arrays obtained from the best run of each algorithm are given in Table6.29.

Table6.29. Performance of the optimal thinned linear arrays with unequal inter-element spacing obtained from the optimization algorithms using cost function 2 and dynamic weights.

Optimization Algorithms	Maximum side lobe level (dB)	Beam width between 1st nulls(in degrees)	Number of active elements in the array
Real-Boolean DE	-22.2434	5.76^{o}	36
Self Adaptive Real-Boolean DE	-20.9532	6.48^{o}	34
Self Adaptive Real-Binary DE	-20.4498	5.76^{o}	32

The parameters of the optimal arrays are given in Table6.30

Table6.30 Parameters of the optimal thinned linear arrays with unequal inter-element spacing obtained from the optimization algorithms using cost function 2 and dynamic weights.

Optimization Algorithms	Sequence of turned-on (active) elements	Mean inter-element spacing
Real-Boolean DE	0000001110111111111111111111111111111111 0111000000	0.5950λ
Self Adaptive Real-Boolean DE	0000100001111111111111111111111111111111 1000010000	0.5738λ
Self Adaptive Real-Binary DE	0000000011011111111111111111111111111110 1100000000	0.6629λ

The arrangement of the optimal array obtained from the best run of the real-Boolean DE algorithm is shown in Fig.6.48.

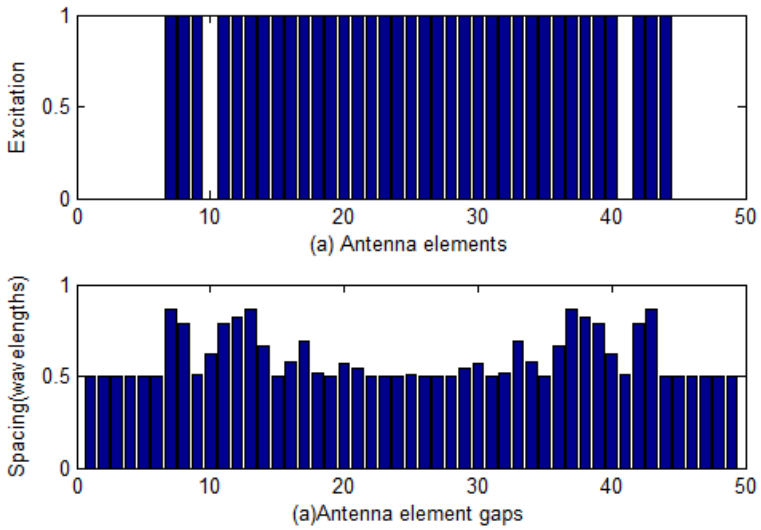

Fig.6.48 Arrangement of the optimal thinned linear array with unequal inter-element spacing obtained from the best run of the real-Boolean DE algorithm using cost function 2 and dynamic weights.

The arrangement of the optimal array obtained from the best run of the real-Boolean SADE algorithm is shown in Fig.6.49.

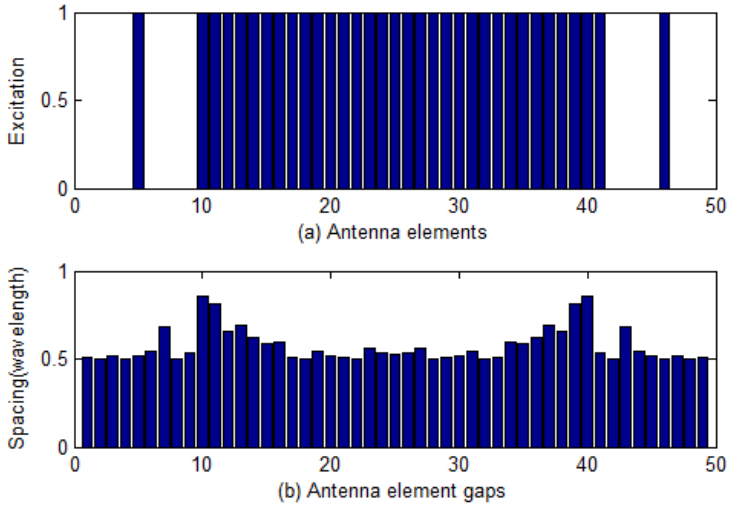

Fig.6.49 Arrangement of the optimal thinned linear array with unequal inter-element spacing obtained from the best run of the real-Boolean SADE algorithm using cost function 2 and dynamic weights.

The arrangement of the optimal array obtained from the best run of the Binary SADE algorithm is shown in Fig.6.50.

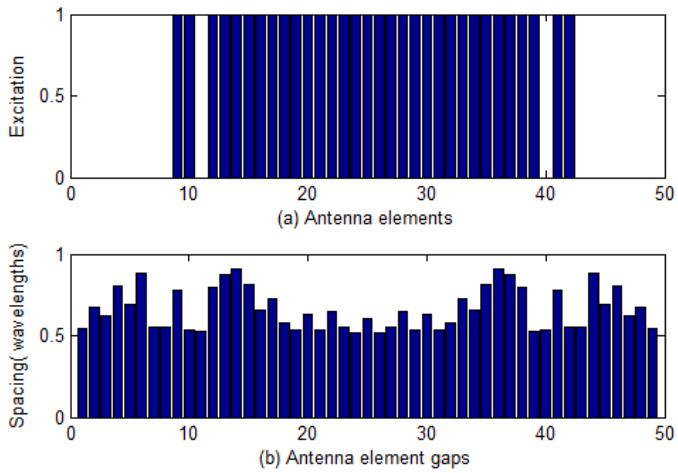

Fig.6.50 Arrangement of the optimal thinned linear array with unequal inter-element spacing obtained from the best run of the real-binary SADE algorithm using cost function 2 and

The statistical performance parameters of the optimization algorithms indicate that the performance of the real-Boolean SADE algorithm is better compared to the other two algorithms studied here. The cost function is designed to achieve a pattern with FNBW as close as possible to that of a fully filled array (after satisfying the given threshold values) with same inter-element spacing as that of the fully filled array. The real-Boolean SADE algorithm used an average population size of approximately 35 vectors or chromosomes across all its runs. The same population size is used for the real-Boolean DE algorithm. The real-Boolean DE algorithm is also superior in performance compared to the real-binary SADE algorithm. The real-Boolean SADE algorithm exhibits the lowest mean cost value, lowest standard deviation, highest robustness and fastest convergence rate compared to the other two algorithms for this optimization problem. However the worst cost values and best cost values are very close for the optimization algorithms. Although the best cost values are nearly same for the optimization algorithms, the array performances vary for each of the algorithms. The array parameters and array performances obtained from the best run of each algorithm are given Table6.30. The array obtained from the best run of the real-Boolean SADE algorithm has 68% filling of turned-on (active) and minimum mean inter-element spacing of 0.5738λ. In terms of convergence rate, the real-Boolean SADE algorithm shows the fastest convergence compared to the other algorithms as evident from the mean convergence plots in Fig.6.47. The normalized array factor plot of the optimal array obtained from self-adaptive real-Boolean DE algorithm is given in Fig.6.51.

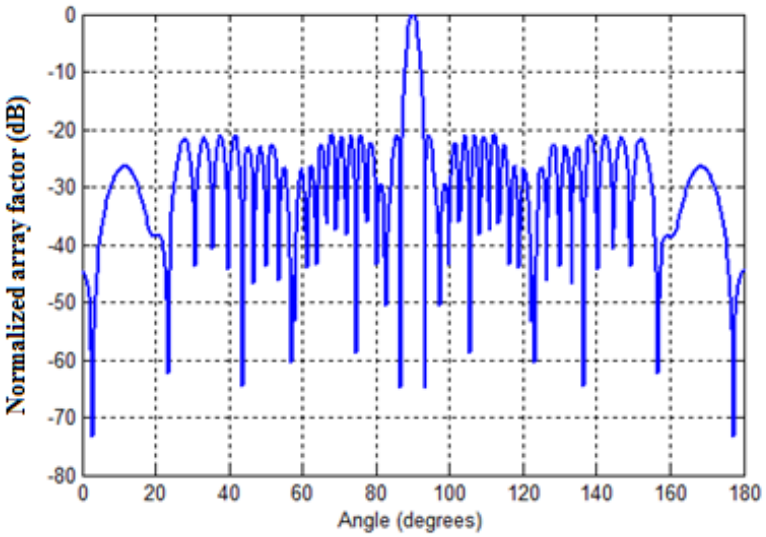

Fig .6.51 Normalized array factor of the optimal thinned linear array (with unequal inter-element spacing) obtained using self-adaptive real-Boolean DE algorithm using cost function 2 and dynamic weights

6.10 Conclusion

Self-Adaptive Real-Boolean Differential Evolution algorithm is proposed in this chapter for the optimization of thinned linear and thinned planar antenna arrays. The statistical performance of the algorithms is compared with those of real-Boolean differential evolution algorithm and the self-adaptive real-binary differential evolution optimization algorithm. The proposed algorithm has shown comparatively better or nearly same statistical performance compared to the other algorithms discussed in this chapter. The proposed algorithm requires no guess or tuning of the control parameters. The novelty of the proposed algorithm lie in the suitable choice and combinations of self adaptive control parameter adaptation strategies, donor vector generation strategies and population dynamics involved in them. Although the composite donor vector generation strategies and population dynamics are common to all the proposed algorithms, the control parameter adaptation strategies are different. The proposed algorithm provides adequate exploration and exploitation of the search indicated by their statistical performances in this chapter. Work is carried out in applying these algorithms to other real-Boolean valued antenna design problems as explained in the next chapter.

Chapter 7

Design and Optimization of Microstrip Antennas for WLAN and Vehicular Communications using Differential Evolution Algorithms

7.1 Introduction

Microstrip antennas are being widely used for Wireless Local Area Network (WLAN) and Vehicular communications nowadays. This is because of the robust and planar structure of the antenna and its ability to get easily integrated with MIC and MMIC modules. Microstrip antennas are also suitable candidates for transmitting and receiving circularly polarized waves. Circularly polarized microstrip antennas [3] are favored in many communication modules nowadays because of their ability to receive electromagnetic signal with any orientation of the electric field vector and giving rise to improved user experience. Another aspect in the designing of microstrip antennas is compactness. Antennas often need to be miniaturized to fit in to the available space in the communication module without changing its frequency band of operation and major deterioration of its performance. Various compactness techniques for microstrip antennas have been reported [43],[45],[46],[49] in the recent past. One more feature of microstrip antenna which is often explored is its ability to have multi-band or multi-frequency characteristics. Various designs of microstrip antennas having such characteristics and suitable radiation properties for specific applications have also been reported [57]-[61]. The three characteristics namely circular polarization, compactness and multi-frequency operation when implemented in a single microstrip antenna will further increase its applications in commercial and daily life. However it is extremely difficult to implement all these three characteristics in a single microstrip antenna design. Most often, designs are implemented by combining any two of these three characteristics i.e. design of compact circularly polarized microstrip antennas [47],[50]-[54] and multi-band or multi-frequency circularly polarized microstrip antennas [62],[64],[65],[70].

In this chapter, investigations and optimizations have been carried out on design of compact linearly polarized microstrip antennas and dual-frequency circularly polarized microstrip antenna for applications in WLAN and vehicular communications. Applicability of various versions and variants of real and Boolean coded differential evolution algorithms have been tested with

various circularly polarized microstrip antennas and arrays in the previous chapters. Experience of using these algorithms in terms of their suitability, control parameter values, robustness and convergence speed has been applied in choosing the suitable DE algorithm for different real life antenna design problems in this chapter. The antenna design and optimization are mostly performed by coupling the DE optimization code (implemented in MATLAB) with the Method of Moment (MoM) based electromagnetic simulation software IE3D. Since the optimizations and evaluation of cost function is a time consuming process, DE algorithm needs to be the one which can give a good compromise between working with low population size, high robustness and fast convergence. The choice of DE algorithm changes depending on the type of antenna design and cost function formulated for optimizing it. The use of bio-inspired optimization algorithms for real-time optimization of antenna structure by coupling it with commercial electromagnetic simulation software were reported earlier in [84],[85],[90],[91],[92],[93],[97],[109],[119],[141],[154],[155]. Once the antenna designs are optimized, those are fabricated and measurements of its impedance and pattern properties are carried out.

The organization of this chapter is as follows. Section I provides the introduction to the chapter. Section II describes the design and optimization of a linearly polarized compact short circuited microstrip antenna using DE/rand/1 algorithm to operate in the GPS L1 band . This antenna is fabricated on a lossy substrate and measurement of its impedance properties has been carried out. Section III describes the design of a dual-frequency microstrip antenna for applications in vehicular communication i.e. in the GPS L1 band (at 1.575 GHz) and for Direct Short Range Communication (DSRC) between vehicles (at 5.88 GHz). The antenna design exhibits right handed circular polarization at the lower frequency and linear polarization at the higher frequency. Section IV describes the design of a modified version of the antenna in section III and for the same applications. The modified version exhibits circular polarization at both the lower (RHCP) and higher frequencies (LHCP). This antenna is fabricated on a low loss substrate and measurements of its impedance and radiation characteristics have been carried out. Both the antennas in section III and section IV are optimized using differential evolution with neighborhood based mutation operator. Section V describes the design of a dual frequency circularly polarized probe fed microstrip antenna with slots to operate at 2.45 GHz and 3.65 GHz. This antenna is also fabricated and measurements of its characteristics carried out. This

antenna is optimized by the modified differential evolution algorithm. Section VI describes the design of a dual-frequency circularly polarized grounded slot antenna based on automated pixel geometry to operate at 2.45 GHz and 5.15 GHz. The self-adaptive real-Boolean differential evolution algorithm proposed in the previous chapter is used for the automated design. This antenna is also fabricated and measurements of its characteristics carried out. Section VII describes the design of a triple-band linearly polarized grounded slot antenna based on automated pixel geometry to operate at 2.46 GHz, 3.65 GHz and 5.85 GHz. It is optimized using improved real-Boolean differential evolution algorithm. Section VIII concludes the chapter.

7.2 Design and Optimization of Short Circuited Microstrip Antenna

Miniaturization of microstrip antennas has been a challenging task to adapt the size to fit it into smaller, space limited modules used for different wireless communication systems. Various techniques for miniaturization are proposed in recent literatures among which shorting pin is a favorable option [19],[20],[26],[28] due to its ability to miniaturize the antenna to nearly 50% of its original size with possibility of good impedance matching at the resonant frequency[28]. Miniaturized dual frequency microstrip antennas can be designed with reduced gain using short circuited microstrip antennas [19],[20],[26]. The main difficulty in designing a short circuited microstrip antenna is to find out the proper position of coaxial feed and position of shorted pin on the radiating patch. In this paper, the position of coaxial feed and position of shorted pin in a rectangular patch antenna is optimized using differential evolution algorithm with random scale factor. The antenna is designed to resonate in GPS L1 band.

7.2.1 Antenna Configuration and Optimization

The co-axially fed microstrip antenna investigated with shorting pin is shown in Fig. 7.1. Substrate with dielectric permittivity of 4.36, and thickness of 60 mils is used. Length and width of the patch are designated by L and W. x_p represents the distance of the probe feed from the left radiating edge whereas x_s denotes the distance of the shorting pin from the same radiating edge.

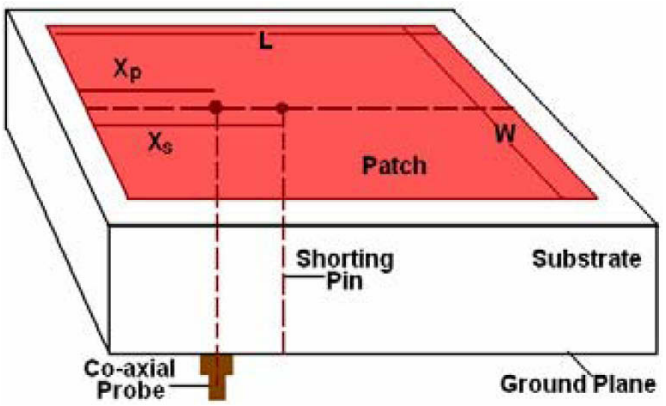

Fig 7.1 Probe fed microstrip antenna with shorting pin

The proposed antenna can be treated as a two port network with the probe feed at the input port and the output port being shorted. The driving point input impedance is given by [2]:

$$Z_{in} = Z_{11} - {Z^2}_{12}/Z_{22} \tag{7.1}$$

where, Z_{11}, Z_{12} and Z_{22} represent Z-parameters of the two port network. These Z parameter values for TM_{mn} mode can be calculated by using cavity model analysis [2] of the antenna.

$$Z_{11} = {V_1}/{I_1}\,(I_2 = 0) = j\omega\mu_o I_o \sum_{m=0}^{M}\sum_{n=0}^{N} \frac{{\psi_{mn}}^2(x_p,y_p)sinc\left(\frac{m\pi D_x}{2L}\right)sinc\left(\frac{n\pi D_y}{2W}\right)}{k^2-{k_{mn}}^2} \tag{7.2}$$

$$Z_{22} = {V_2}/{I_2}\,(I_1 = 0) = j\omega\mu_o I_o \sum_{m=0}^{M}\sum_{n=0}^{N} \frac{{\psi_{mn}}^2(x_s,y_s)sinc\left(\frac{m\pi D_x}{2L}\right)sinc\left(\frac{n\pi D_y}{2W}\right)}{k^2-{k_{mn}}^2} \tag{7.3}$$

$$Z_{12} = {V_1}/{I_2}\,(I_1 = 0) = j\omega\mu_o I_o \sum_{m=0}^{M}\sum_{n=0}^{N} \frac{\psi_{mn}\,(x_p,y_p)\psi_{mn}\,(x_s,y_s)sinc\left(\frac{m\pi D_x}{2L}\right)sinc\left(\frac{n\pi D_y}{2W}\right)}{k^2-{k_{mn}}^2} \tag{7.4}$$

where,

$${k_{mn}}^2 = \left(\frac{m\pi}{L}\right)^2 + \left(\frac{n\pi}{W}\right)^2 \tag{7.5a}$$

$$\psi_{mn}(x,y) = \sqrt{\frac{\epsilon_m \epsilon_n}{LW}}\ \cos\left(\frac{m\pi x}{L}\right)\cos\left(\frac{n\pi y}{W}\right) \tag{7.5b}$$

$\in_p = 1\ for\ p = 0\ and\ \in_p = 2\ otherwise$

where, p=m or n, depending on mode of excitation. I_o is the feeding current, (x_p,y_p) represent position of probe feed, (x_s,y_s) represent position of shorting pin and 'k' is the wave number. 'D_x' and 'D_y' represent the dimensions of probe feed when the cross sectional area of the inner conductor is approximated to be a rectangle. For simplicity, cross sectional area of the shorting pin is taken to be same as that of the probe feed. In measurement, commercially available probe connectors and the shorting pins are used whose cross sections are circular. Although, the cross sections of the shorting pin and the inner conductor are chosen to be square shaped for mathematical simplicity in theoretical explanations and MATLAB simulations, their areas of cross section are maintained same as that used in the fabricated antenna. When the conductor is very thin, the inductive effect produced by square and circular cross sections of same area of the pins, are almost same. Once, Z_{in} is calculated, S_{11} can be found as:

$$S_{11} = 20log_{10}|\tau| \tag{7.6a}$$

where,

$$\tau = \frac{Z_{in} - Z_o}{Z_{in} + Z_o} \tag{7.6b}$$

The cost function for optimization is given as:

$$Cost = |\tau_{Design\_frequency}| \tag{7.7}$$

The antenna is optimized using the DE/rand/1 algorithm using a crossover probability of 0.95. The differential evolution is run for 40 iterations with a population size of 40 after which the optimized values of the dimensional parameters i.e. L, W, x_p and x_s are obtained.

The differential evolution algorithm is run for 50 independent trials. Each time it is run for 40 generations. The best result out of those 50 independent trials is shown in Fig. 7.2 as the best cost curve. The best cost variation graphs from each of the trials (from 1-50) are averaged and is presented in Fig. 7.2 as the mean cost variation graph. This is done because stochastic optimization algorithm does not ensure the best optimized result in a single run.

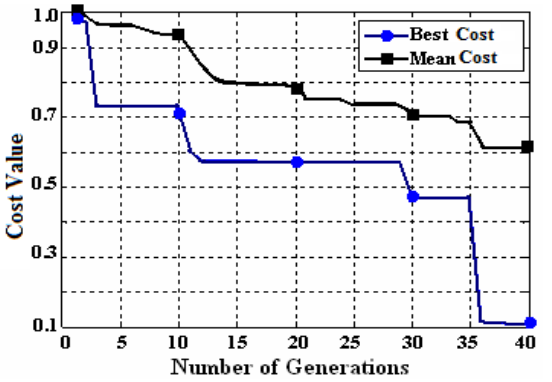

Fig.7.2 Variation of best and mean cost with number of generations for the optimized short circuited microstrip antenna

The optimal values of the antenna dimensions are given below in Table 7.1.

Table 7.1.Optimal values of dimensions for the short circuited microstrip antenna (all dimensions in mm)

L	18.40
W	17.86
X_p	12.87
X_s	11.65

7.2.2 Results and Observations

The antenna is fabricated on glass epoxy substrate with dielectric permittivity of 4.36 and thickness of 60 mils. Dimensions of the antenna are given above along with feed position and the position of shorting pin. The diameter of the shorting pin is 0.3 mm. Measurement is done using vector network analyzer. In Fig. 7.3, measured return loss of the antenna is compared with the result obtained using DE. The variation of maximum directivity near the resonant frequency is shown in Fig. 7.4. From cavity model analysis, electric and magnetic fields, inside the cavity, are computed and from these fields far field components E_θ and E_φ are calculated. Then from E_θ and E_φ, directivity is computed [2]. Directivity at resonant frequency is 2.93 dB. The radiation

pattern of the short circuited microstrip antenna is shown in Fig. 7.5. Due to short circuit by a pin, the radiation patterns of short circuited patch antennas become distorted [44],[48].

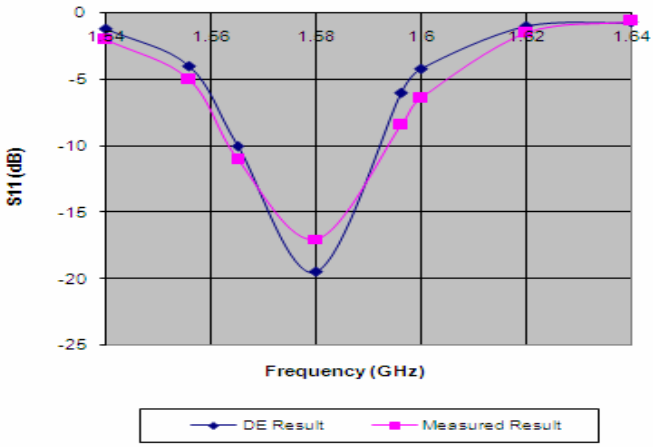

Fig. 7.3 Variation of S_{11} with frequency for the optimized short circuited microstrip antenna

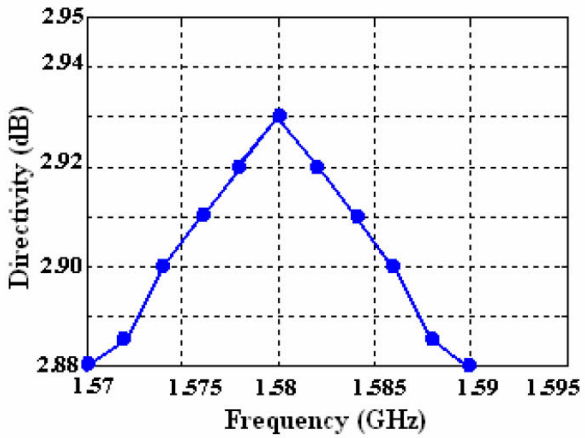

Fig. 7.4 Variation of directivity with frequency for the optimized short circuited microstrip antenna

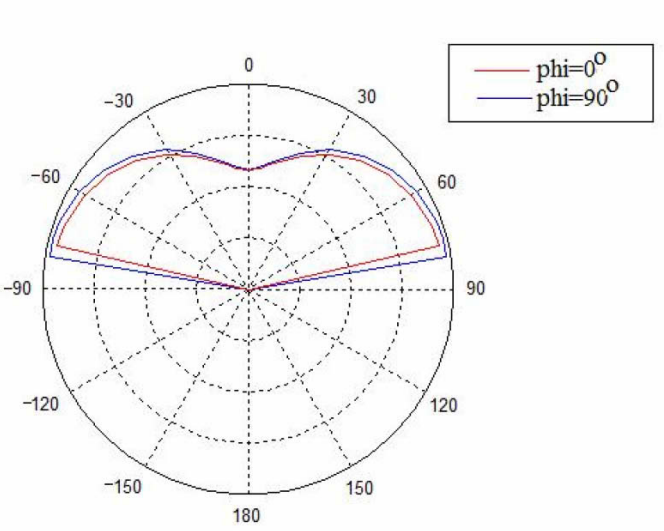

Fig. 7.5 Normalized radiation pattern of the of the optimized short circuited microstrip antenna

The optimized values of different parameters are obtained after 37 runs. In a short circuited microstrip antenna, due to reduction in overall size of the antenna, the directivity reduces. The fabricated prototype of the antenna is shown in the Fig. 7.6 below:

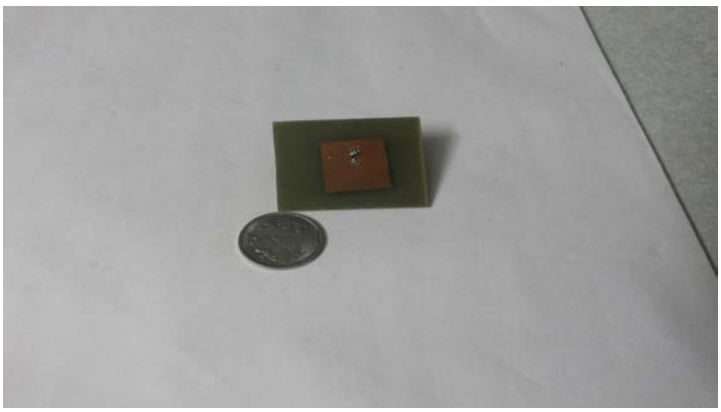

Fig. 7.6 Fabricated prototype of optimized short circuited microstrip antenna

7.3 Dual Frequency Microstrip Antenna for Vehicular Applications

A dual frequency probe fed microstrip antenna is designed for vehicular applications using corner parasitic loading. The dual frequency microstrip antenna is meant to operate at L1 band frequency of 1.575 GHz for Global Positioning System (GPS) applications and 5.88 GHz for Dedicated Short Range Communication (DSRC). This antenna is also suitable for applications with respect to Intelligent Transportation Systems (ITS). The antenna radiates right handed circularly polarized waves at 1.575 GHz in the broad side direction. It radiates linearly polarized waves at 5.88 GHz. The antenna dimensions are optimized using Differential Evolution with Global and Local Neighborhood Search algorithm. The optimization objectives include impedance matching at the dual frequencies, maximization of gain in the broadside direction for both frequencies and minimization of axial ratio for RHCP at the GPS frequency.

7.3.1 Antenna Configuration and Optimization

The geometry of the antenna (with the top and side views) is given below in Fig. 7.7. The antenna uses a very low loss substrate with dielectric constant of 4.4, and thickness 0.8 mm. The main patch should resonate at 1.575 GHz. TM_{10} and TM_{01} modes are equally excited at this frequency with a phase difference of 90 degrees to generate circularly polarized waves. The phase difference is created using the corner truncations and parasitic patch loadings. The parasitic patch loads used for loading the main patch at 1.575 GHz in turn should resonate at 5.88 GHz.

.

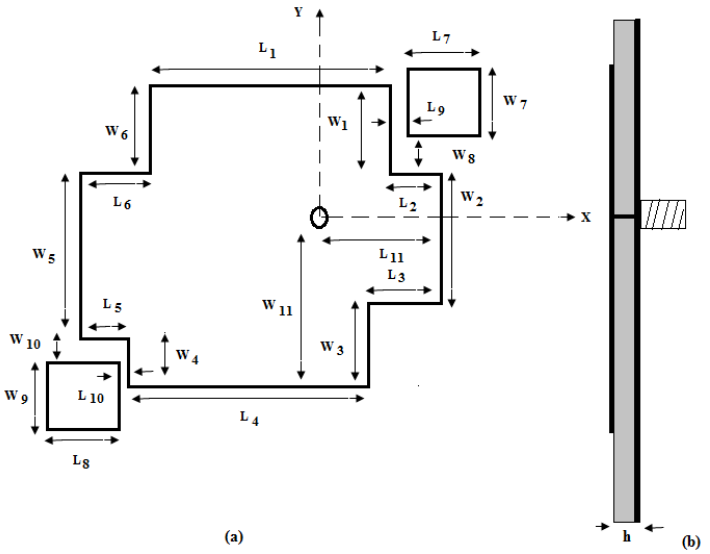

Fig. 7.7 Dual frequency microstrip antenna for vehicular communications (a) Top view (b) Side view

The optimization objectives of the antenna to be designed are given below. Frequencies f_1 and f_2 refer to 1.575 and 5.88 GHz respectively:

$$Objective_1 = \max\ (reflection\ coefficient\ at\ f_1\ GHz, reflection\ coefficient\ at f_2\ GHz) \tag{7.8a}$$

$$Objective_2 = Axial\ ratio\ at\ f_1\ GHz \tag{7.8b}$$

$$Objective_3 = 1/\min\ (\ gain\ at\ f_1 GHz, gain\ at f_2\ GHz) \tag{7.8c}$$

Objectives 1 and 3 are aimed at minimizing reflection coefficients and maximizing gain in the broadside directions at the dual frequencies respectively. Objective 2 is aimed at minimizing axial ratio in the broadside direction at f_1 GHz.

Cost function for the optimization of the antenna structure is formulated as shown below:

$$Cost = w_1.Objective_1 + w_2.Objective_2 + w_3.Objective_3 \tag{7.9}$$

The antenna is optimized using Differential Evolution with Global and Local neighborhood search algorithm which is coupled with the Method of Moments based simulation software for

cost function evaluation of the antenna structure. There are 8 variables to be optimized and a population size of 50 is used. The crossover probability is kept at 0.7.

The plot showing the variation of best cost value with number of generations for the algorithm is shown below:

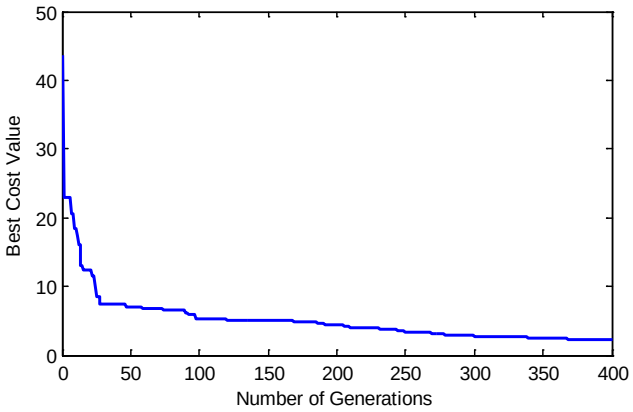

Fig. 7.8 Variation of best cost value with number of generations for the dual frequency microstrip antenna for vehicular communications

The optimal dimensions of the antenna are given in Table 7.2

Table 7.2 Optimal dimensions of the dual frequency microstrip antenna for vehicular communications (all dimensions in mm)

L_1	36.800	L_7	11.925	W_1	13.700	W_7	11.925
L_2	4.5250	L_8	11.925	W_2	26.425	W_8	0.4800
L_3	7.7500	L_9	0.4800	W_3	7.7500	W_9	11.925
L_4	36.800	L_{10}	0.4800	W_4	13.700	W_{10}	0.4800
L_5	4.5250	L_{11}	11.300	W_5	26.425	W_{11}	23.900
L_6	7.7500			W_6	7.7500		

7.3.2 Results and Observations

The S_{11} versus frequency plots at the dual frequencies are shown below in Fig. 7.9:

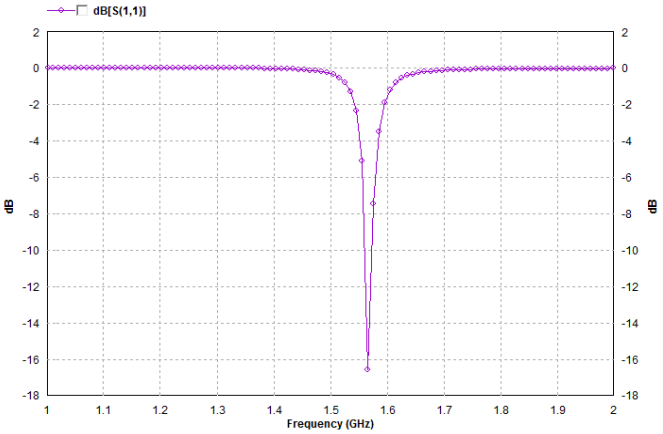

Fig 7.9(a) S_{11} versus frequency plot showing impedance matching in GPS L1 band for the dual frequency microstrip antenna for vehicular communications

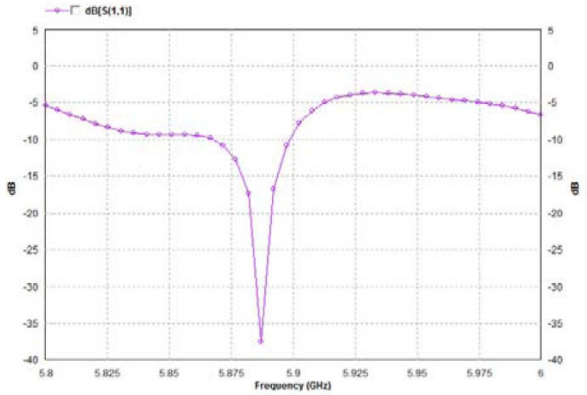

Fig 7.9(b) S_{11} versus frequency plot showing impedance matching in DSRC band for the dual frequency microstrip antenna for vehicular communications

The following impedance bandwidths are observed in the two bands:

Impedance bandwidth in GPS L1 band=20 MHz

Impedance bandwidth in DSRC band=30 MHz

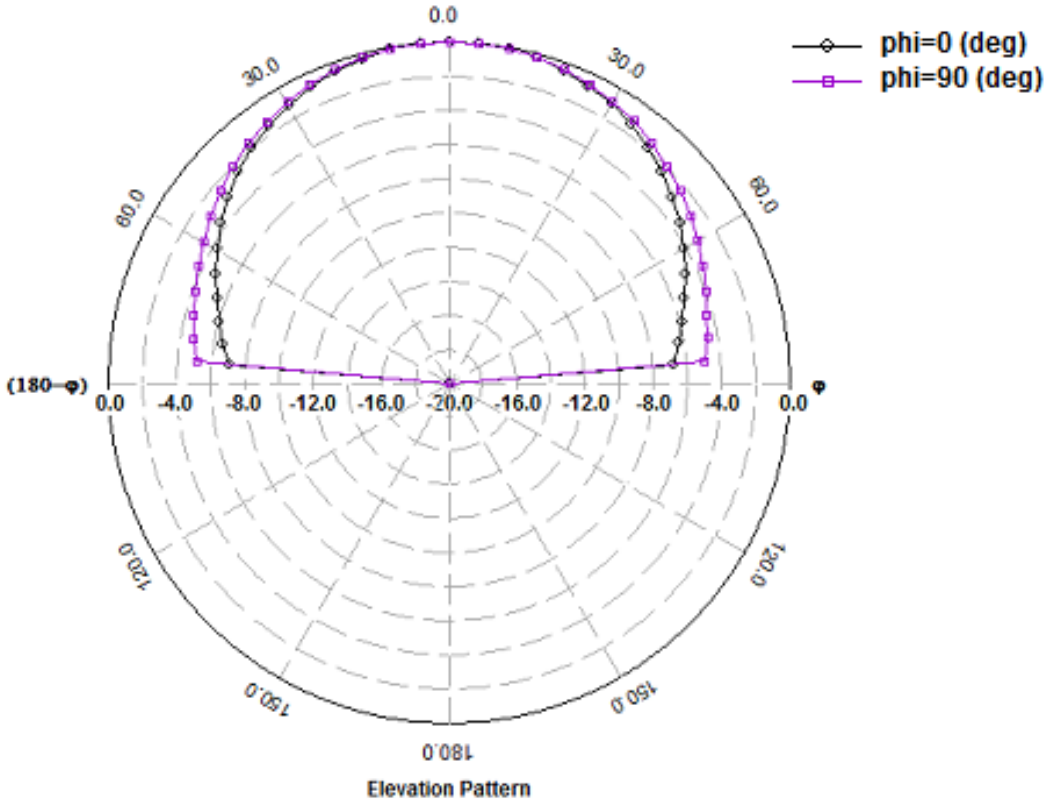

Fig 7.10(a) Normalized power pattern of the dual frequency microstrip antenna for vehicular applications at 1.575 GHz

The parasitic patch loadings resonate at 5.88 GHz. Since there are two parasitic patch loads, it forms a three element array. Since probe feed position is located asymmetrically with respect to the patch loadings at the DSRC frequency, the two parasitic patches have some finite phase difference in their excitations. This phase difference results in a slight tilt of the main beam as seen in Fig.7.10(b).

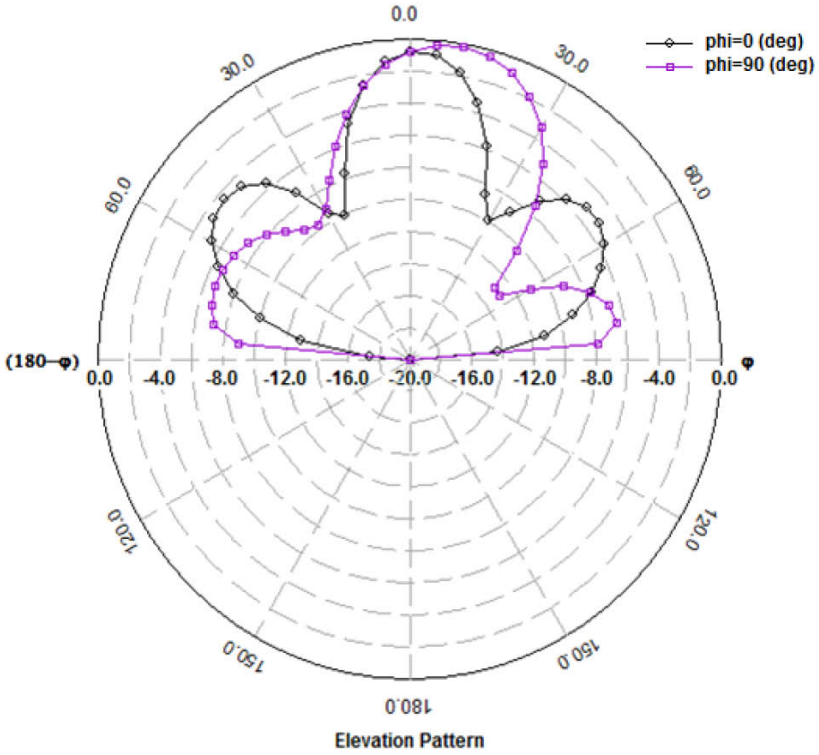

Fig 7.10(b) Normalized power pattern of the dual frequency microstrip antenna for vehicular applications at 5.88 GHz

The gain versus frequency variation in the broad side direction is shown below:

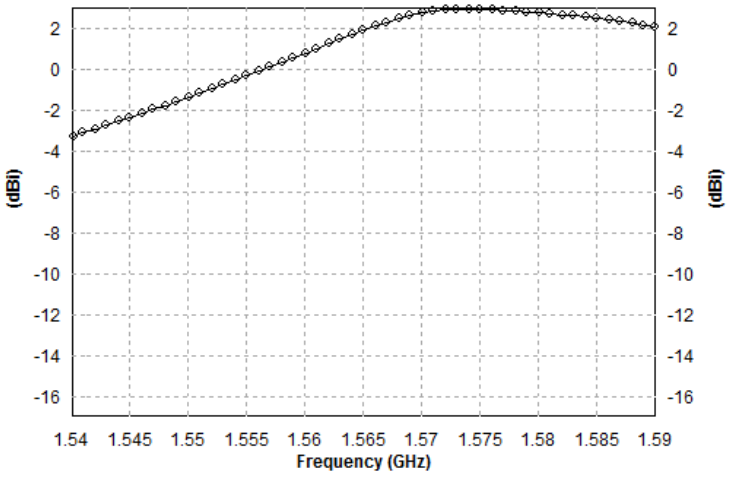

Fig 7.11(a) Variation of gain with frequency in the broadside direction of the dual frequency microstrip antenna for vehicular applications in the GPS L1 band

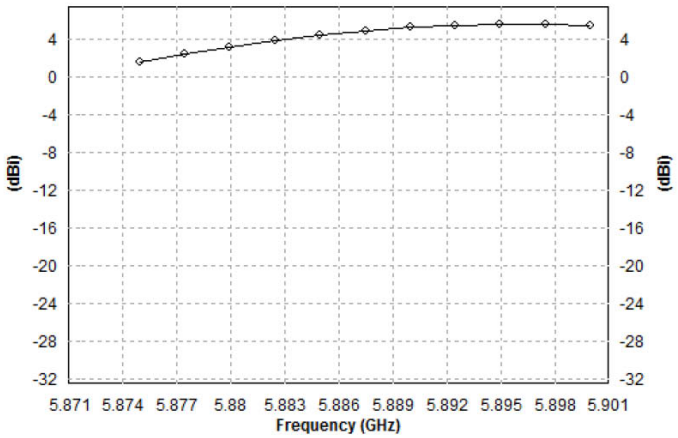

Fig 7.11(b) Variation of gain with frequency in the broadside direction of the dual frequency microstrip antenna for vehicular applications in the DSRC band

Simulated broadside gain at 1.575 GHz=3.00 dBi

Simulated broad side gain at 5.88 GHz= 4.75 dBi

The axial ratio versus frequency variation at the GPS L1 band is given below:

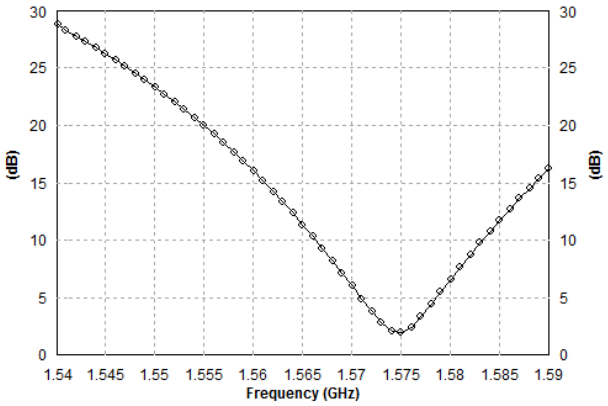

Fig. 7.12 Variation of axial ratio with frequency in the broadside direction of the dual frequency microstrip antenna for vehicular applications in the GPS L1 band

Axial ratio bandwidth in the GPS L1 band=4 MHz.

7.4 Dual Frequency Circularly Polarized Microstrip Antenna for Vehicular Applications

Dual band and dual frequency circularly polarized antennas normally use multiple dielectric layers or complicated feeding structure to achieve impedance matching and circular polarization at the dual frequencies. Very few single layer microstrip antenna configurations are reported [62],[64],[65],[70] which employ probe feed to achieve circular polarization and impedance matching at both frequencies. A simple single layer microstrip antenna configuration with probe feed is proposed in this section with high frequency ratio. The antenna is expected to be used for vehicular communication particularly for the GPS L1 band and Direct Short Range Communication (DSRC) between vehicles.

7.4.1 Antenna Configuration and Optimization

The single layer dual frequency circularly polarized microstrip antenna configuration for applications in vehicular communication is shown in Fig. 7.13 below (a low loss substrate is taken into consideration with relative permittivity 4.3 and thickness 30 mils):

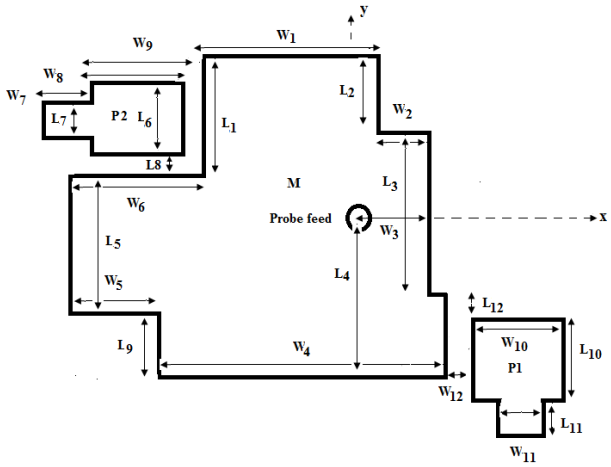

Fig 7.13 Top view of the dual frequency circularly polarized gap coupled microstrip antenna.

The antenna configuration employs a main patch 'M' to resonate at the lower frequency. The corner truncations and the parasitic patch loadings result in two orthogonal modes TM_{10} and TM_{01} at the lower frequency nearly in phase quadrature. The antenna dimensions and the position of probe feed are found to be extremely critical in achieving right handed circular polarization at the lower frequency. The parasitic patches 'P1' and 'P2'gap coupled to the main patch near the corner truncations resonate at the higher frequency in phase quadrature. The patch 'P1' gets excited by the TM_{10} mode while the patch 'P2' gets excited by the TM_{01} mode. The optimization objectives need to be redefined as given below:

$$Objective_1 = \max\ (\ reflection\ coefficient\ at\ f_1\ GHz, reflection\ coefficient\ at f_2\ GHz) \tag{7.10a}$$

$$Objective_2 = \max\ (\ axial\ ratio\ at\ f_1\ GHz, axial\ ratio\ at\ f_2\ GHz) \tag{7.10b}$$

$$Objective_3 = 1/\min\ (gain\ at\ f_1 GHz, gain\ at f_2\ GHz) \tag{7.10c}$$

Objectives 1 and 3 are aimed at minimizing reflection coefficients and maximizing gain in the broadside directions at the dual frequencies respectively. Objective 2 is aimed at minimizing axial ratio in the broadside direction for both f_1 and f_2 GHz.

Cost function for the optimization of the antenna structure is formulated as shown below:

$$Cost = w_1.Objective_1 + w_2.Objective_2 + w_3.Objective_3 \quad (7.11)$$

Evaluation of the cost function for the antenna configuration is done using method of moment technique. Optimization is done using the differential evolution algorithm with neighborhood based mutation operator [142]. The reason for choosing this algorithm is its fast convergence rate since evaluation of cost function for a particular antenna structure is a time consuming process. There are 19 variables to be optimized and a population size of 100 is used. The crossover probability is kept at 0.8 and neighborhood radius of 20[142].

The plot showing the variation of best cost value with number of generations of the algorithm is shown below in Fig. 7.14:

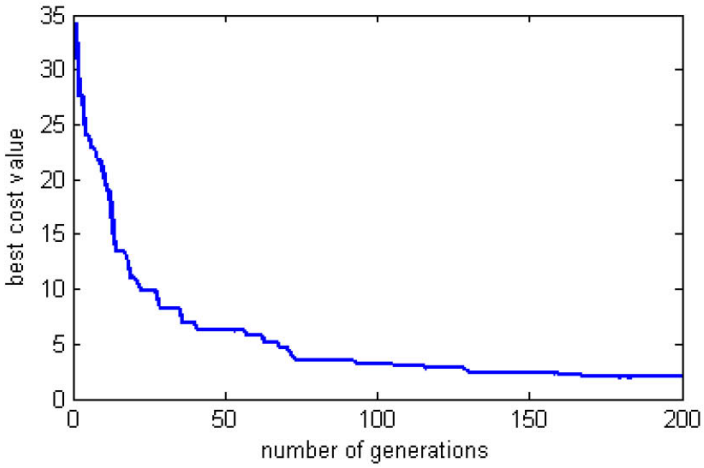

Fig. 7.14 Variation of best cost value with number of generations for the dual frequency circularly polarized microstrip antenna for vehicular communications

The dimensions of the antenna optimized by the differential evolution algorithm with neighborhood based mutation operator after 200 generations are given in Table 7.3.

Table 7.3. Dimensions of the optimal dual frequency circularly polarized gap coupled microstrip antenna (all dimensions in mm).

L_1	13.964	L_7	6.3590	W_1	24.41	W_7	3.035
L_2	11.426	L_8	0.4850	W_2	8.564	W_8	9.920
L_3	26.325	L_9	8.6460	W_3	9.743	W_9	10.57
L_4	23.150	L_{10}	9.9180	W_4	38.19	W_{10}	9.919
L_5	26.470	L_{11}	2.5470	W_5	11.41	W_{11}	8.217
L_6	9.9190	L_{12}	0.5720	W_6	14.36	W_{12}	0.595

7.4.2 Results and Observations

The antenna is fabricated on the low loss substrate of dielectric constant 4.3 and thickness 0.76 mm. Measurements of both impedance and pattern properties of the antenna are carried out using vector network analyzer. The impedance measurements show slight shift of the operating frequencies to 1.619 GHz and 5.98 GHz. Impedance bandwidths of 12 MHz and 30 MHz are obtained at 1.619 GHz and 5.985 GHz respectively. The variation of S_{11} with frequency is given below in Fig. 7.15.

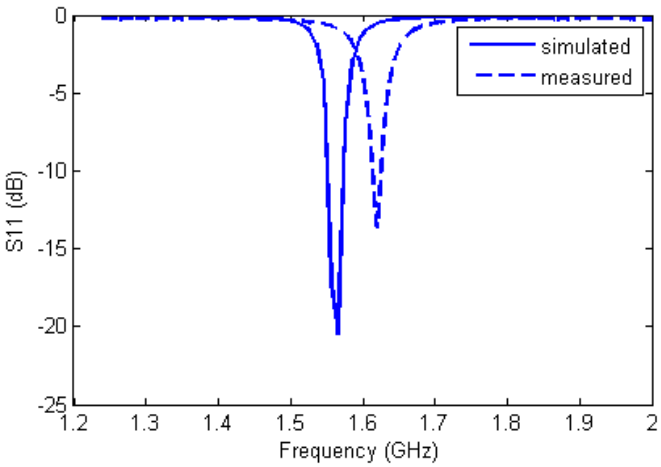

Fig 7.15(a) S_{11} versus frequency plot showing impedance matching in GPS L1 band for the dual frequency circularly polarized microstrip antenna for vehicular

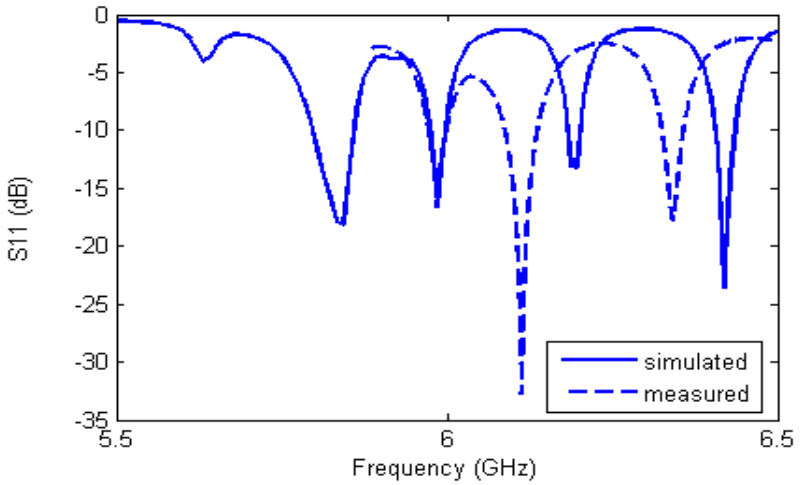

Fig 7.15(b) S_{11} versus frequency plot showing impedance matching in DSRC band for the dual frequency circularly polarized microstrip antenna for vehicular communications

The antenna exhibited CP bandwidths of 3.6 MHz and 24 MHz at 1.619 GHz and 5.985 GHz respectively. The variation of axial ratio with frequency is given below in Fig. 7.16.

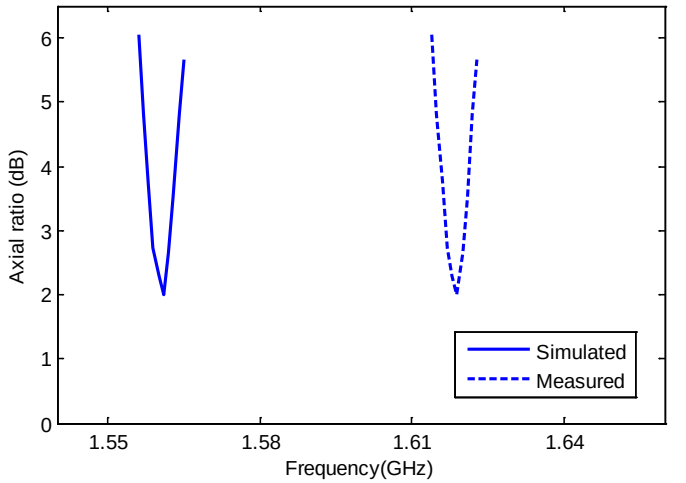

Fig. 7.16(a) Variation of axial ratio with frequency in the broadside direction of the dual frequency circularly polarized microstrip antenna for vehicular applications in the GPS L1 band

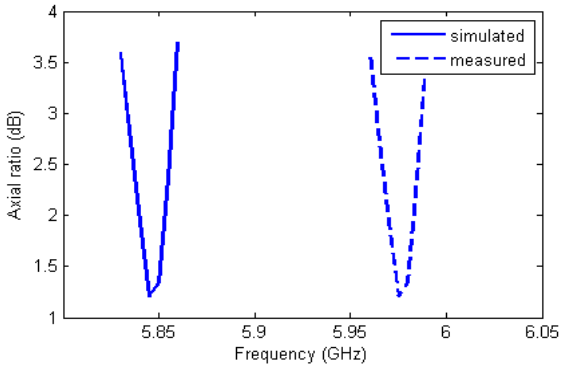

Fig. 7.16(b) Variation of axial ratio with frequency in the broadside direction of the dual frequency circularly polarized microstrip antenna for vehicular applications in the DSRC band

The measured gain at 1.619 GHz is 1.93 dBi. The measured gain at 5.985 GHz is 3.98 dBi. The variations of gain with frequencies at the dual frequencies are shown below in Fig. 7.17.

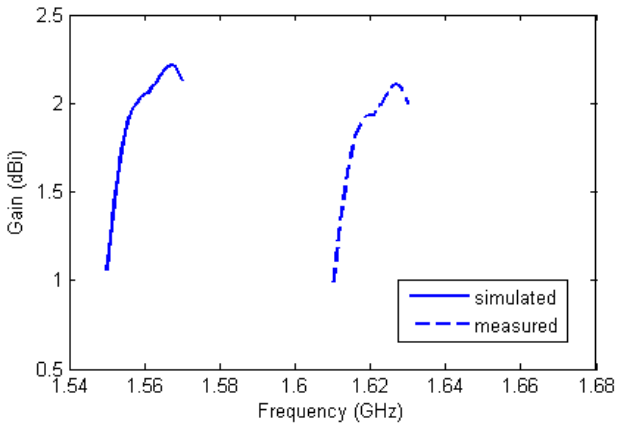

Fig. 7.17(a) Variation of gain with frequency in the broadside direction of the dual frequency circularly polarized microstrip antenna for vehicular applications in the GPS L1 band

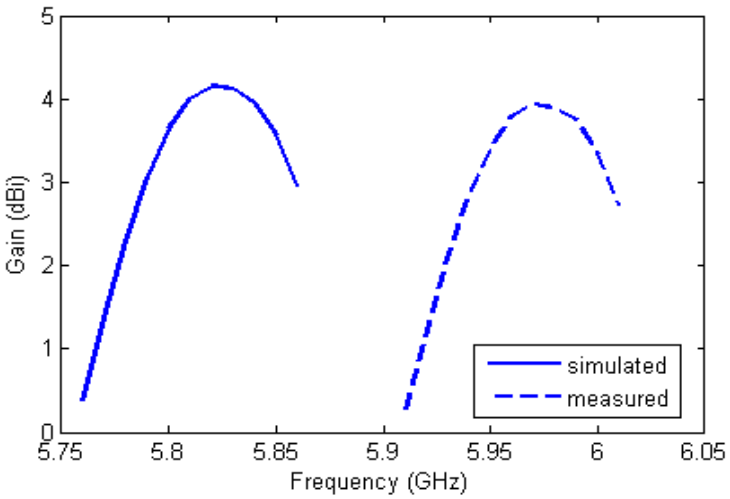

Fig. 7.17(b) Variation of gain with frequency in the broadside direction of the dual frequency circularly polarized microstrip antenna for vehicular applications in the DSRC band

The normalized power plots at the dual frequencies in orthogonal planes are given below in Fig. 7.18.

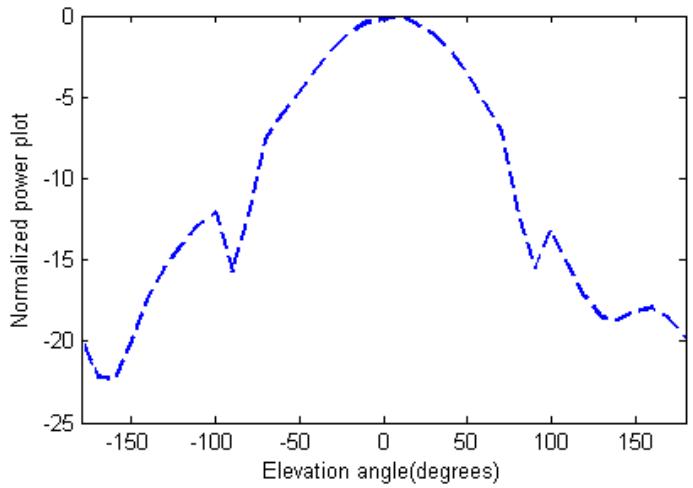

Fig. 7.18(a) Normalized power plot of the dual frequency circularly polarized microstrip antenna for vehicular communications at 1.619 GHz (x-z plane)

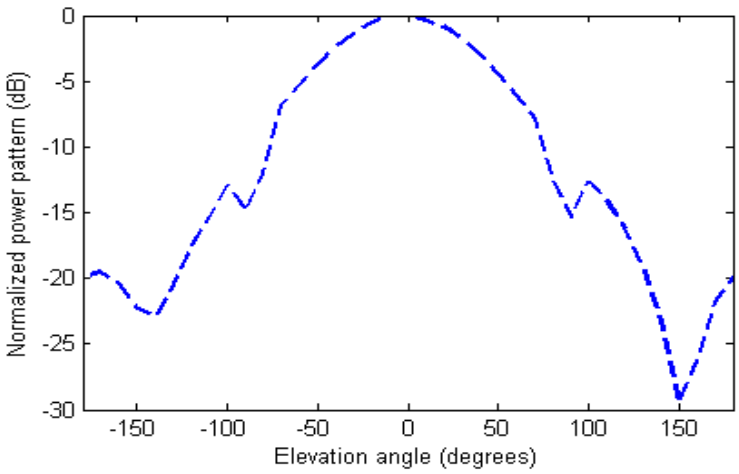

Fig. 7.18(b) Normalized power plot of the dual frequency circularly polarized microstrip antenna for vehicular communications at 1.619 GHz (y-z plane)

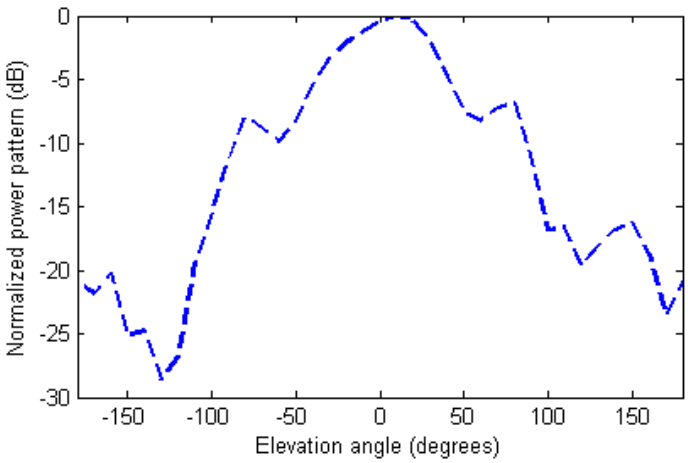

Fig. 7.18(c) Normalized power plot of the dual frequency circularly polarized microstrip antenna for vehicular communications at 5.985 GHz (x-z plane)

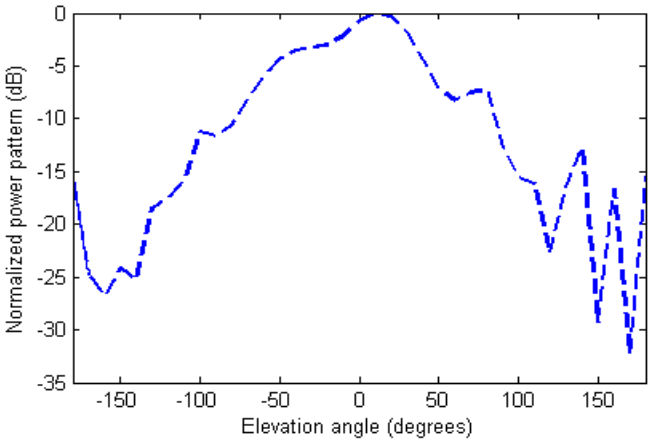

Fig. 7.18(d) Normalized power plot of the dual frequency circularly polarized microstrip antenna for vehicular communications at 5.985 GHz (y-z plane)

The fabricated prototype of the antenna is shown below:

Fig. 7.19 Fabricated prototype of the optimized dual frequency circularly polarized microstrip antenna for vehicular applications

7.5 Dual Frequency Circularly Polarized Microstrip Antenna for WLAN

A dual frequency probe fed circularly polarized microstrip antenna is designed for WLAN applications using slots of appropriate dimensions and located on specific locations on the patch. The dual frequency microstrip antenna is intended to operate at 2.45 GHz and 3.65 GHz respectively. This antenna will also be suitable for applications with respect to WLAN

communications. The designed antenna radiates right handed elliptically polarized wave at 2.45 GHz in the broad side direction. It also radiates right handed circularly polarized waves in the broadside directions at 3.65 GHz. The antenna dimensions are optimized using modified differential evolution algorithm [158]. The optimization objectives include impedance matching at the dual frequencies, maximization of gain in the broadside direction for both frequencies and minimization of axial ratio at the dual frequencies.

7.5.1 Antenna Configuration and Optimization

The single layer dual frequency microstrip antenna configuration for applications in WLAN communication is shown in Fig. 7.20 below (a low loss substrate is taken into consideration with relative permittivity 4.3 and thickness 30 mils):

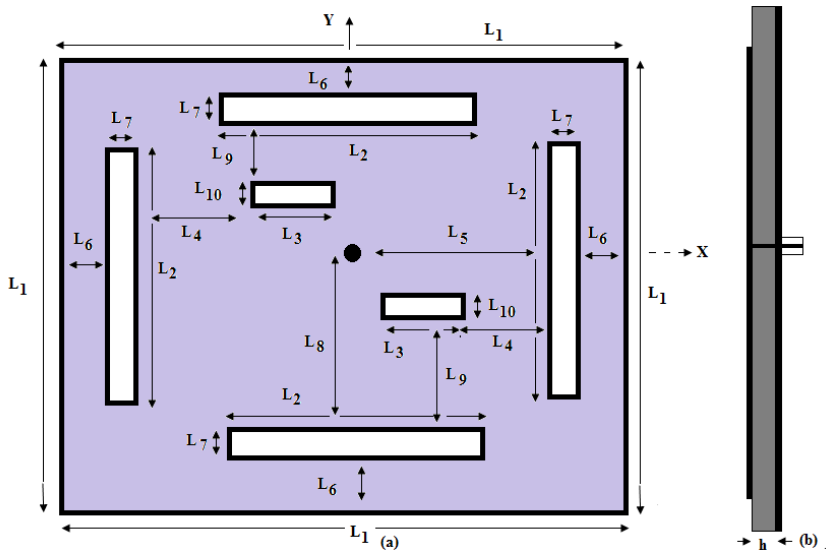

Fig. 7.20 Geometry of the dual frequency circularly polarized microstrip antenna for WLAN (a) top view (b) side view

The antenna is composed of a square microstrip patch with six slots and a probe feed for excitation. There are four symmetric slots along the edges of the patch. These four slots give rise to dual frequency resonance of the patch for TM_{10}, TM_{01}, TM_{30} and TM_{03} with almost identical radiation patterns above the infinite ground plane [65]. Since a square patch is used, the resonant frequencies are supposed to be same TM_{10} and TM_{01} modes as well as for TM_{30} and TM_{03}

modes. This will give rise to dual polarized behavior at the resonant frequencies corresponding to TM_{10} and TM_{30} modes. However to convert the radiation characteristics to dual frequency circularly polarized one, resonant frequencies of TM_{10} and TM_{01} modes need to be slightly different so that they are in phase quadrature at the lower operating frequency (f_1). Similarly, to achieve circular polarization in the broadside direction at the higher operating frequency (f_2), TM_{30} and TM_{03} modes should be in phase quadrature. This is achieved by incorporating two extra slots in the patch geometry as evident in the figure above. These extra slots change the path of orthogonal mode currents at the operating frequencies to provide the required phase difference. The dimensions and positions of the slot and the probe feed need to be optimized to achieve the desired antenna impedance and radiation characteristics at the dual frequencies.

The optimization objectives are given below:

$$Objective_1 = \max\ (reflection\ coefficient\ at\ f_1\ GHz, reflection\ coefficient\ at f_2\ GHz) \tag{7.12a}$$

$$Objective_2 = \max(axial\ ratio\ at\ f_1\ GHz, axial\ ratio\ at\ f_2\ GHz) \tag{7.12b}$$

$$Objective_3 = 1/\min\ (\ gain\ at\ f_1 GHz, gain\ at f_2\ GHz) \tag{7.12c}$$

Objectives 1 and 3 are aimed at minimizing reflection coefficients and maximizing gain in the broadside directions at the dual frequencies respectively. Objective 2 is aimed at minimizing axial ratio in the broadside direction for both f_1 and f_2 GHz.

Cost function for the optimization of the antenna structure is formulated as shown below:

$$Cost = w_1.Objective_1 + w_2.Objective_2 + w_3.Objective_3 \tag{7.13}$$

The evaluation of the cost function for the antenna configuration is done using method of moment technique. The optimization is done using the modified differential evolution algorithm [142]. The reason for choosing this algorithm is its fast convergence rate and high robustness since evaluation of cost function for a particular antenna structure is a time consuming process. The modified differential evolution algorithm is coupled with the Method of Moments based simulation software IE3D for cost function evaluation of the antenna structure. There are 10

variables to be optimized and a population size of 50 is used. The crossover probability is kept at 0.95 and beta value of 0.4[158].

The plot showing the variation of best cost value with number of generations of the algorithm is shown below in Fig. 7.21:

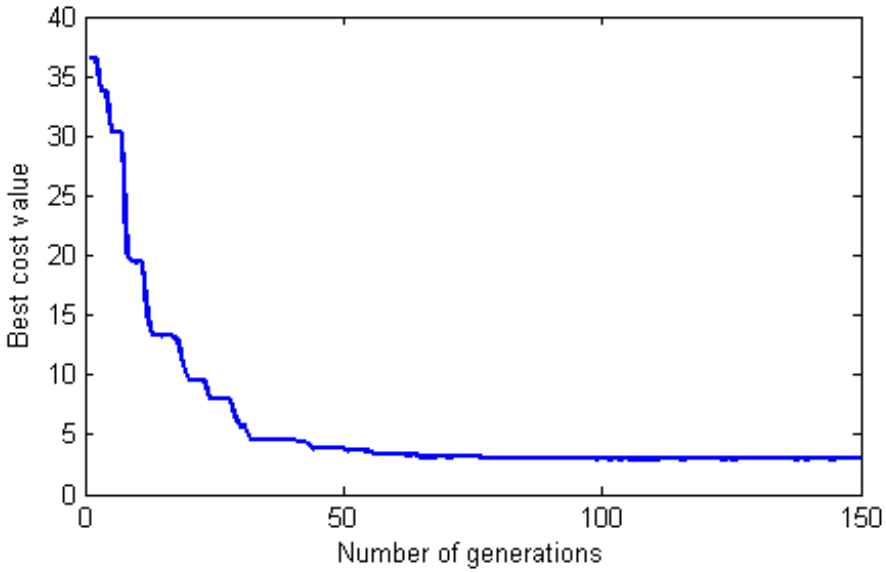

Fig. 7.21 Variation of best cost value with generations in the optimization of the dual frequency circularly polarized microstrip antenna for WLAN communication

The dimensions of the antenna optimized by the modified differential evolution algorithm after 150 generations are given in Table 7.4.

Table 7.4. Dimensions of the optimal dual frequency circularly polarized microstrip antenna for WLAN communications (all dimensions in mm).

L_1	28.22	L_6	0.33
L_2	23.24	L_7	0.78
L_3	5.90	L_8	7.25
L_4	2.91	L_9	3.29
L_5	14.83	L_{10}	0.84

7.5.2 Results and Observations

Measurements of both impedance and pattern properties of the antenna are carried out using vector network analyzer. The variations of S_{11} with frequency at the dual frequencies are shown below in Fig. 7.22:

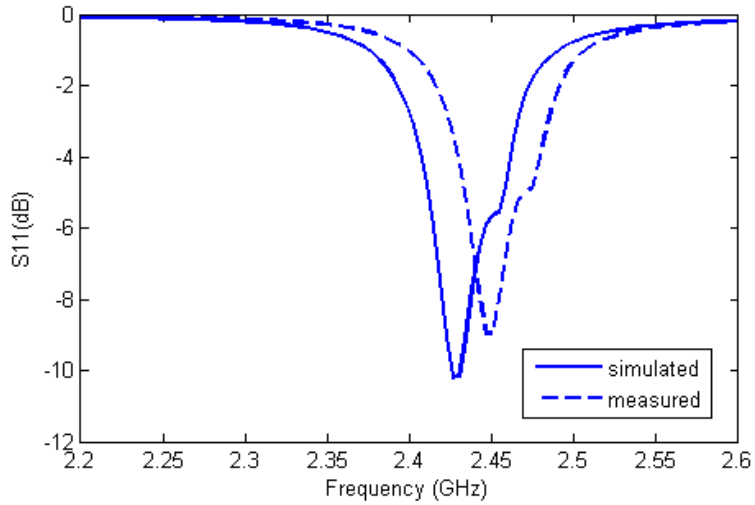

Fig. 7.22 (a) Variation of S_{11} with frequency in the lower frequency band of the dual frequency circularly polarized microstrip antenna for WLAN communication

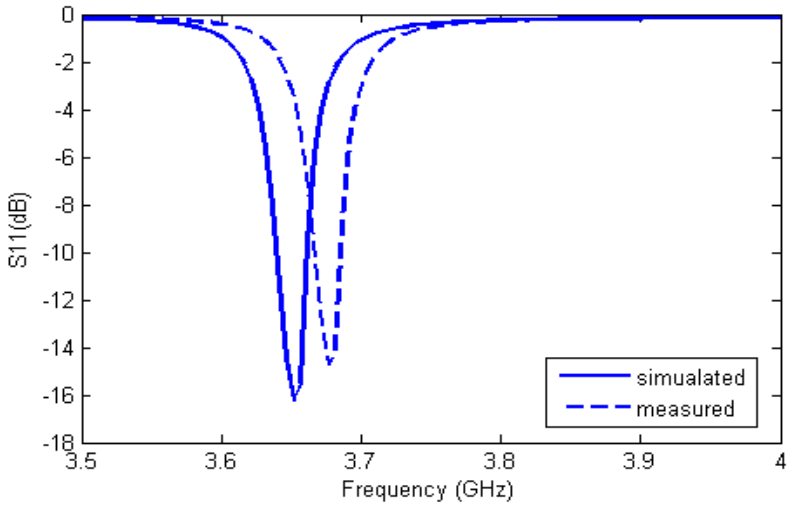

Fig. 7.22 (b) Variation of S_{11} with frequency in the upper frequency band of the dual frequency circularly polarized microstrip antenna for WLAN communication

Impedance matching is moderately achieved at the first operating frequency and the impedance bandwidth is extremely small. Impedance matching at the second operating frequency is quite good with good agreement between the simulated and measured results. A slight shift in operating frequencies is observed from the measured data. This is attributed to the limitations in fabrication technologies available. The first operating frequency is 2.45 GHz whereas the second operating frequency is 3.675 GHz. Impedance bandwidth at the second operating frequency is 23.5 MHz. The variation of axial ratio with frequency is given below:

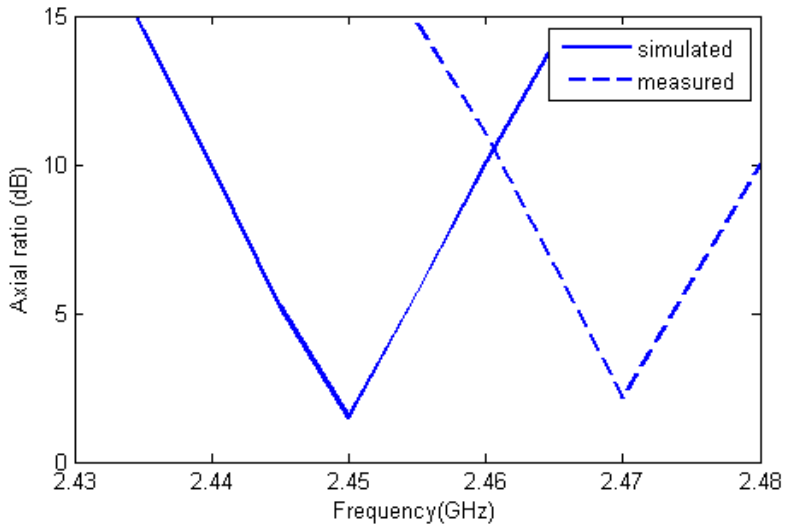

Fig. 7.23 (a) Variation of axial ratio with frequency in the lower frequency band of the dual frequency circularly polarized microstrip antenna for WLAN communication

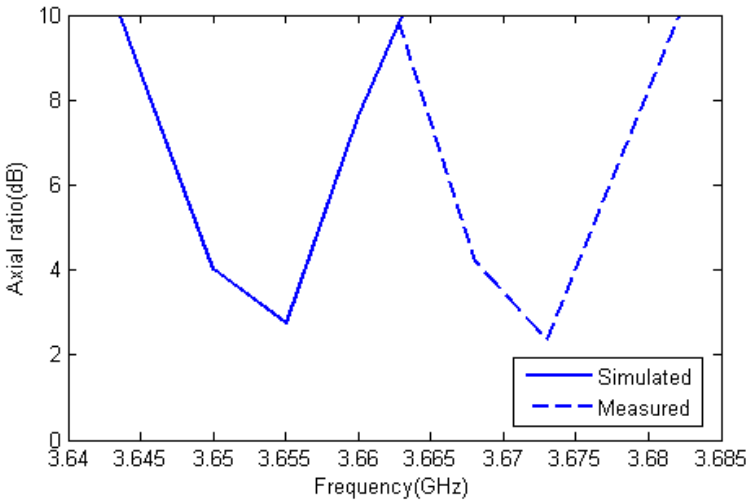

Fig. 7.23 (b) Variation of axial ratio with frequency in the upper frequency band of the dual frequency circularly polarized microstrip antenna for WLAN communication

The 3 dB axial ratio bandwidths are 3.8 MHz and 1.3 MHZ at the lower and higher operating frequencies respectively. The variations of gain with frequency are shown in the figure below:

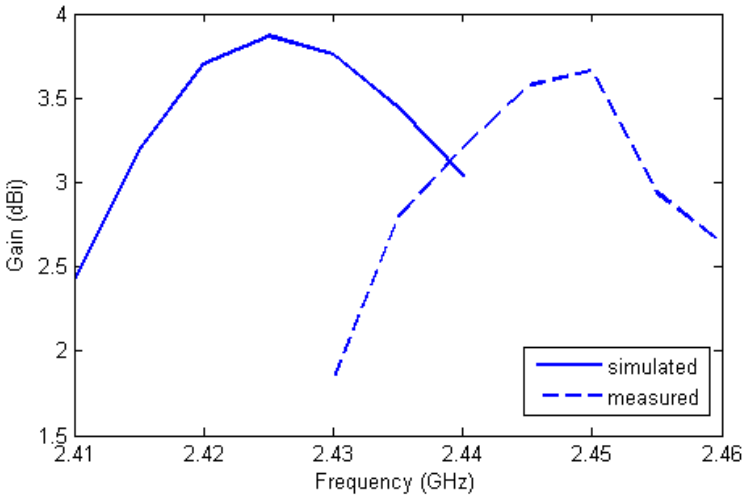

Fig. 7.24 (a) Variation of gain with frequency in the lower frequency band of the dual frequency circularly polarized microstrip antenna for WLAN communication

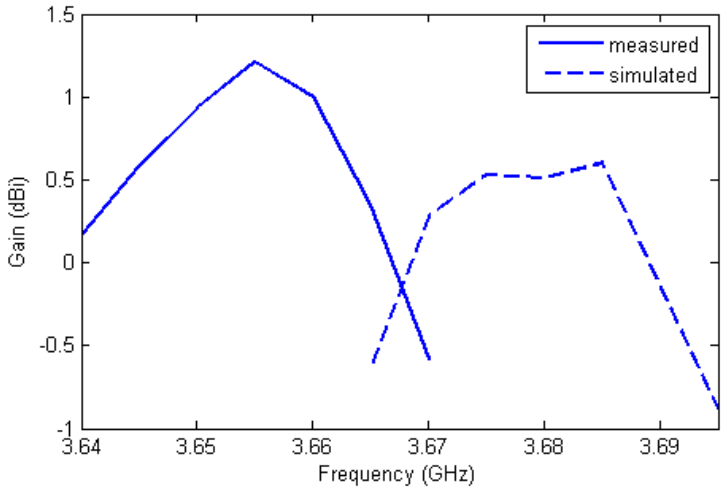

Fig. 7.24 (b) Variation of gain with frequency in the upper frequency band of the dual frequency circularly polarized microstrip antenna for WLAN communication

Antenna gains in the lower and higher operating frequencies are 3.66 dBi and 0.53 dBi respectively. The normalized power patterns at 2.45 GHz and 3.675 GHz are shown below:

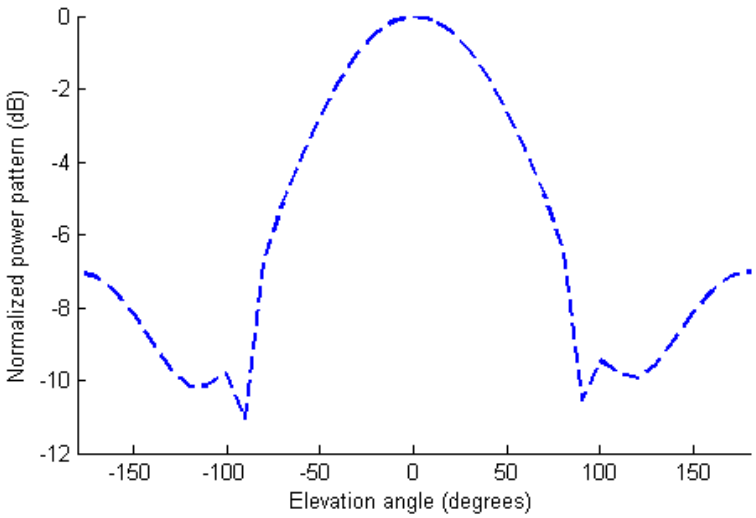

Fig. 7.25 (a) Normalized power pattern at 2.45 GHz(x-z plane) of the dual frequency circularly polarized microstrip antenna for WLAN communication

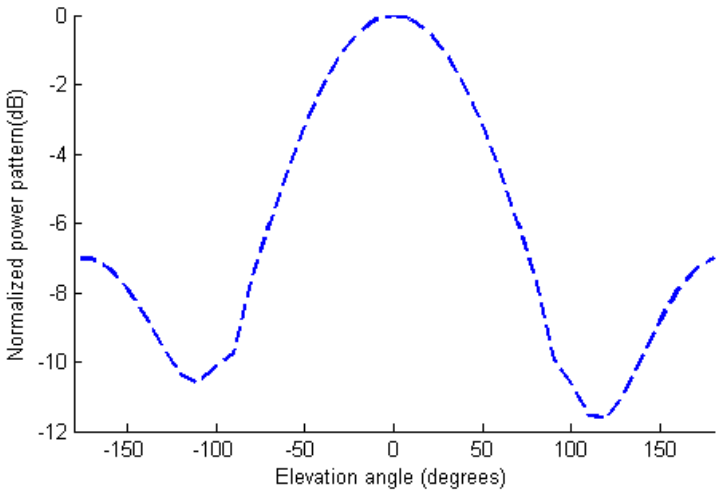

Fig. 7.25 (b) Normalized power pattern at 2.45 GHz(y-z plane) of the dual frequency circularly polarized microstrip antenna for WLAN communication

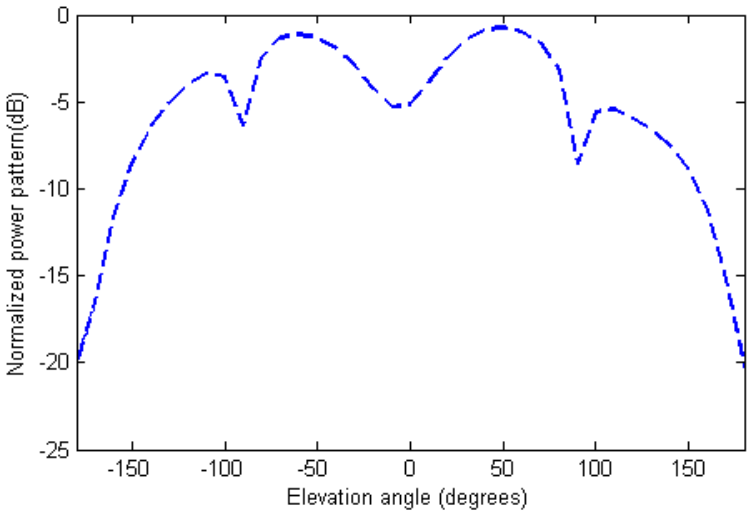

Fig. 7.25 (c) Normalized power pattern at 3.675 GHz(x-z plane) of the dual frequency circularly polarized microstrip antenna for WLAN communication

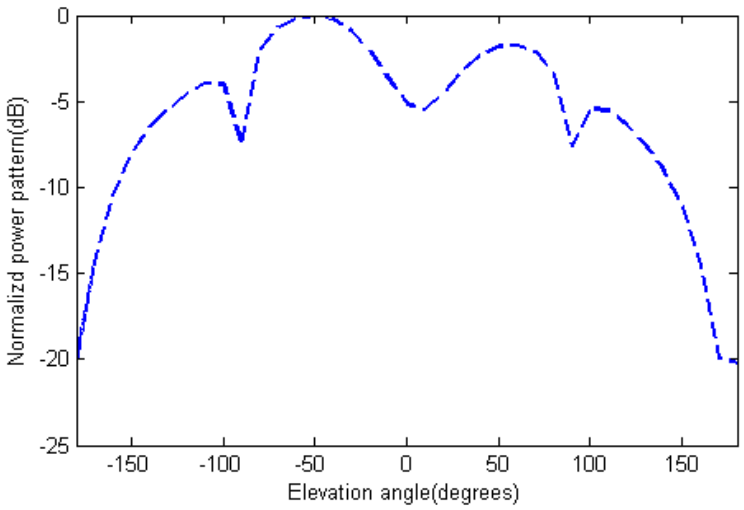

Fig. 7.25 (d) Normalized power pattern at 3.675 GHz(y-z plane) of the dual frequency circularly polarized microstrip antenna for WLAN communication

The fabricated prototype of the antenna is shown below:

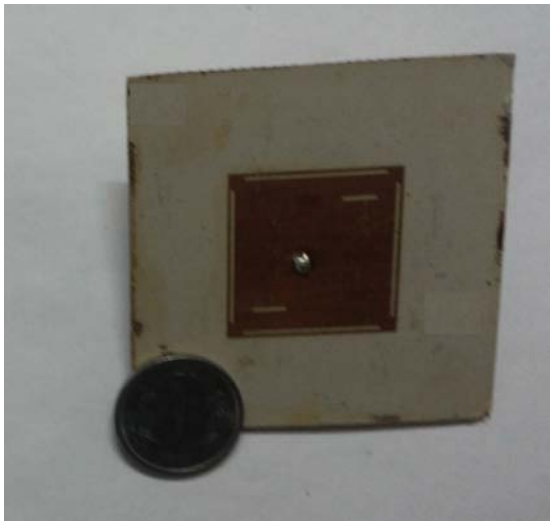

Fig. 7.26 Fabricated prototype of the dual frequency circularly polarized microstrip antenna for WLAN

7.6 Dual Frequency Circularly Polarized Grounded Slot Antenna for WLAN

Design of a dual frequency transmission line fed grounded slot antenna for WLAN applications is proposed in this section. The dual frequency antenna is intended to operate at 2.45 GHz and 5.15 GHz respectively. The designed antenna radiates left handed circularly polarized waves in the broad side direction at 2.45 GHz (represented as f_1) and 5.15 GHz (represented as f_2) respectively. The antenna design is generated by an automated procedure where the self-adaptive real-Boolean differential evolution algorithm is coupled with Method of Moments (MoM) based Electromagnetic Simulation (EM) software IE3D. The optimization objectives include impedance matching at the dual frequencies, maximization of gain in the broadside direction for both frequencies and minimization of axial ratio at the dual frequencies.

7.6.1 Antenna Configuration and Optimization

The geometry of the dual frequency transmission line fed grounded slot antenna is generated by an automated procedure by coupling the self-adaptive real-Boolean differential evolution algorithm with the MoM based EM software IE3D. The transmission line feed network is composed of three impedance transformers cascaded with each other on one side of the substrate. The other side of the substrate constitutes the region for the grounded slots. The substrate area for placing the grounded slots is divided into10x 10 non-uniform cells with each cell having its own dimensions as shown below:

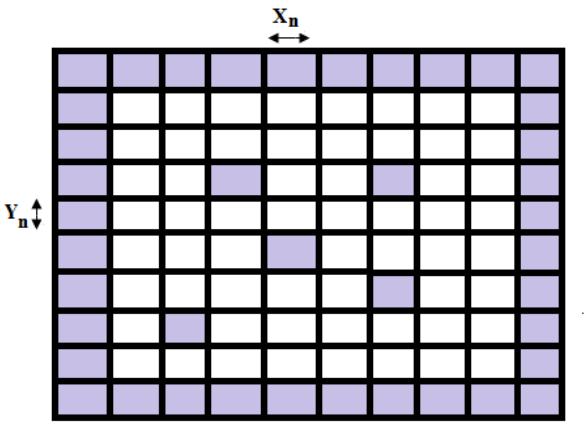

Fig. 7.27 Layout of the slots on the ground plane. ‘n’ ranges from 1 to 10. Un-shaded regions or cells indicate grounded slots in that location.

A cell may be a metallic layer or substrate. Accordingly each cell is allotted a cell value. If the cell value is '1', it represents a metallic layer. If the cell value is '0', it represents a grounded slot in that location. There are 100 such cells representing 100 Boolean variables to be optimized. Apart from that there are 20 values representing the dimensions of each cell as represented in the figure above (x1 to x10 and y1 to y10) to be optimized. In total there are 128 real-Boolean variables to be optimized.

The optimization objectives are given below:

$$Objective_1 = \max\ (\ reflection\ coefficient\ at\ f_1\ GHz, reflection\ coefficient\ at f_2\ GHz) \tag{7.14a}$$

$$Objective_2 = \max\ (\ axial\ ratio\ at\ f_1\ GHz, axial\ ratio\ at\ f_2\ GHz) \tag{7.14b}$$

$$Objective_3 = 1/\min\ (gain\ at\ f_1 GHz, gain\ at f_2\ GHz) \tag{7.14c}$$

Objectives 1 and 3 are aimed at minimizing reflection coefficients and maximizing gain in the broadside directions at the dual frequencies respectively. Objective 2 is aimed at minimizing axial ratio in the broadside direction for both f_1 and f_2 GHz.

Cost function for the optimization of the antenna structure is formulated as shown below:

$$Cost = w_1.Objective_1 + w_2.Objective_2 + w_3.Objective_3 \tag{7.15}$$

The plot showing the variation of best cost value with number of generations of the algorithm is shown below:

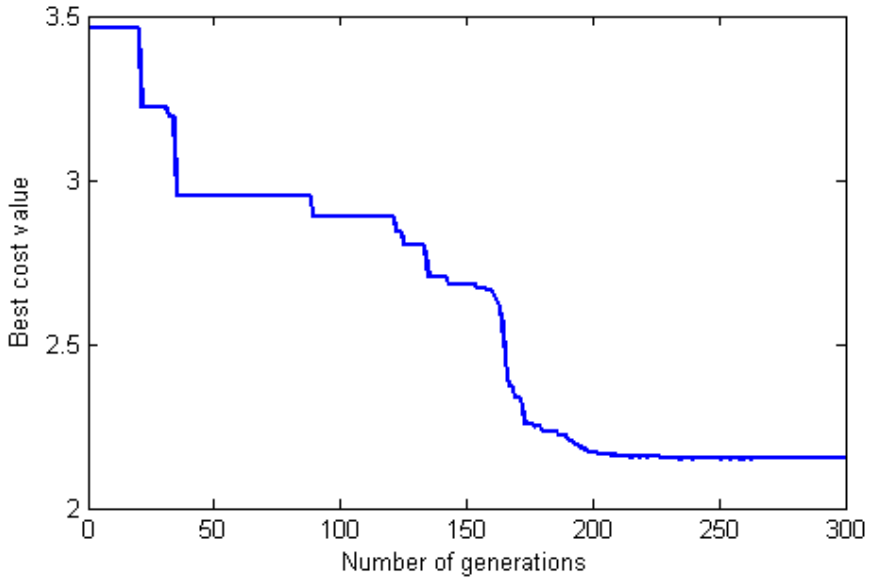

Fig. 7.28 Variation of the best cost value with generations for the dual frequency circularly polarized grounded slot antenna for WLAN

The optimized geometry is shown in the figure below:

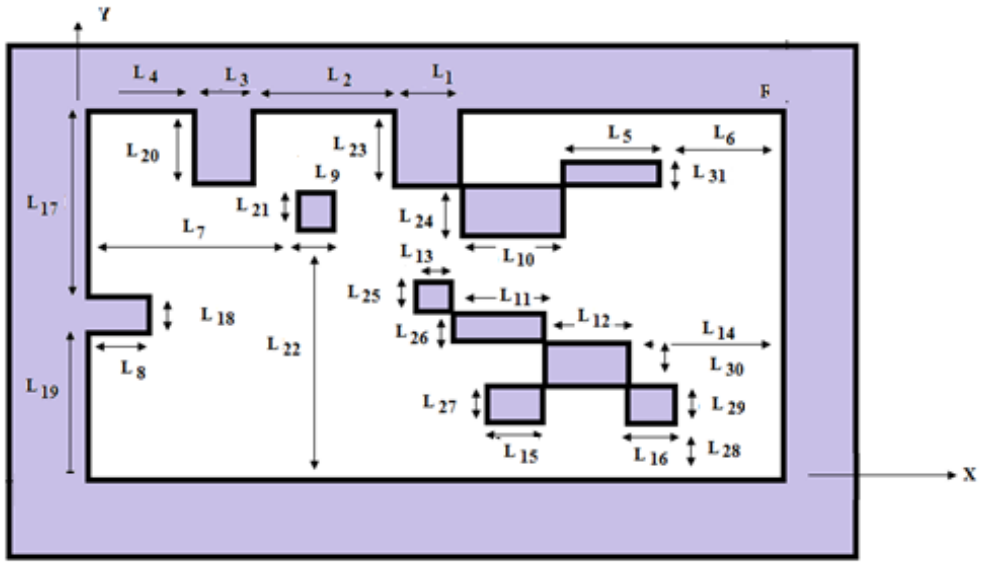

Fig. 7.29(a). Top view of the dual frequency circularly polarized grounded slot antenna for WLAN

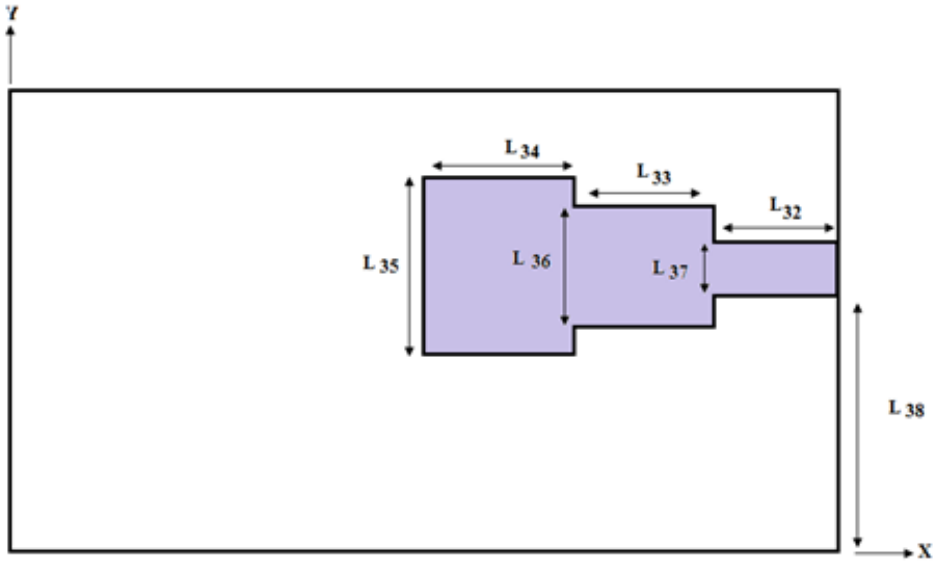

Fig. 7.29(b). Bottom view of the dual frequency circularly polarized grounded slot antenna for WLAN

The optimal dimensions of the antenna are given in Table 7.5.

Table 7.5. Dimensions of the optimal dual frequency circularly polarized grounded slot antenna for WLAN communications (all dimensions in mm).

L_1	3.39	L_{20}	2.77
L_2	8.6	L_{21}	0.81
L_3	5.17	L_{22}	23.62
L_4	5.22	L_{23}	3.58
L_5	5.20	L_{24}	3.00
L_6	11.12	L_{25}	4.25
L_7	14.91	L_{26}	2.68
L_8	5.22	L_{27}	4.34
L_9	1.26	L_{28}	3.56
L_{10}	4.59	L_{29}	4.34
L_{11}	7.98	L_{30}	4.77
L_{12}	5.20	L_{31}	0.82
L_{13}	4.08	L_{32}	1.00

L_{14}	11.12	L_{33}	5.78
L_{15}	4.59	L_{34}	10.95
L_{16}	5.51	L_{35}	7.64
L_{17}	11.85	L_{36}	3.22
L_{18}	2.68	L_{37}	2.66
L_{19}	12.67	L_{38}	27.7

7.6.2 Results and Observations

The antenna is fabricated on a substrate of permittivity 2.5 and thickness 30 mils. Measurements of both impedance and pattern properties of the antenna are carried out. The variations of S_{11} with frequency at the dual frequencies are shown below:

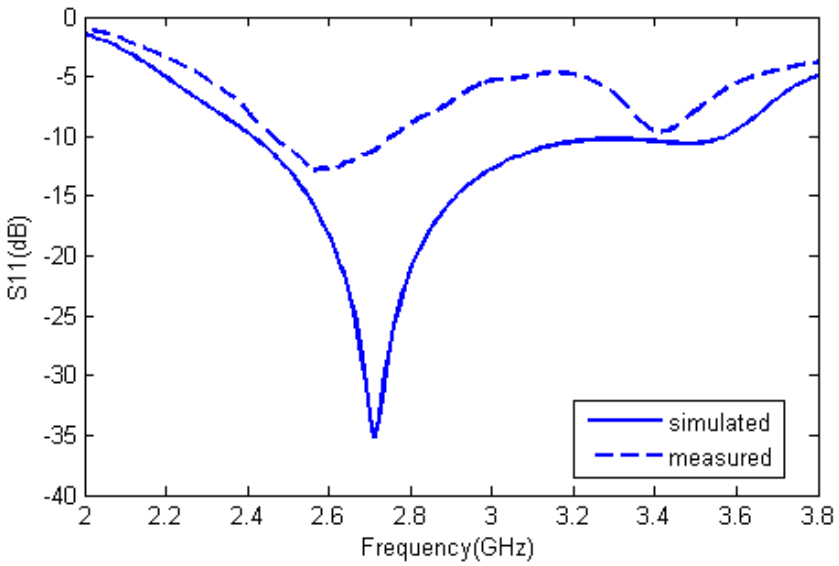

Fig. 7.30 (a) Variation of S_{11} with frequency in the lower frequency band of the dual frequency circularly polarized grounded slot antenna

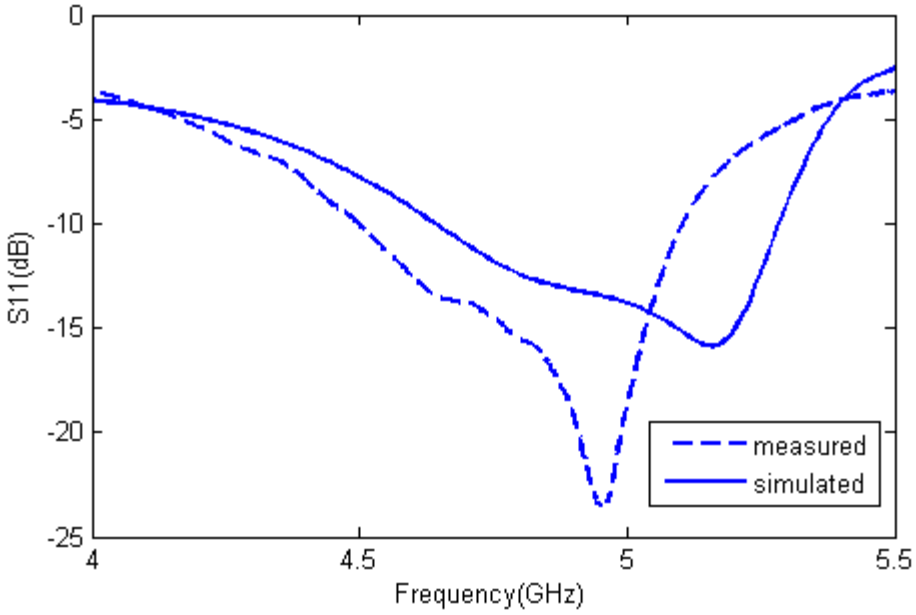

Fig. 7.30 (b) Variation of S_{11} with frequency in the upper frequency band of the dual frequency circularly polarized grounded slot antenna

Impedance matching is achieved at the first and second operating frequencies with good agreement between the simulated and measured results. A slight shift in operating frequencies is observed from the measured data. This is attributed to the limitations in fabrication technologies available. The first operating frequency is at 2.5 GHz whereas the second operating frequency is at 4.9 GHz after measurements. Impedance bandwidths are 293 MHz and 606 MHz at the first and second operating frequencies respectively. The variation of axial ratio with frequency is given below:

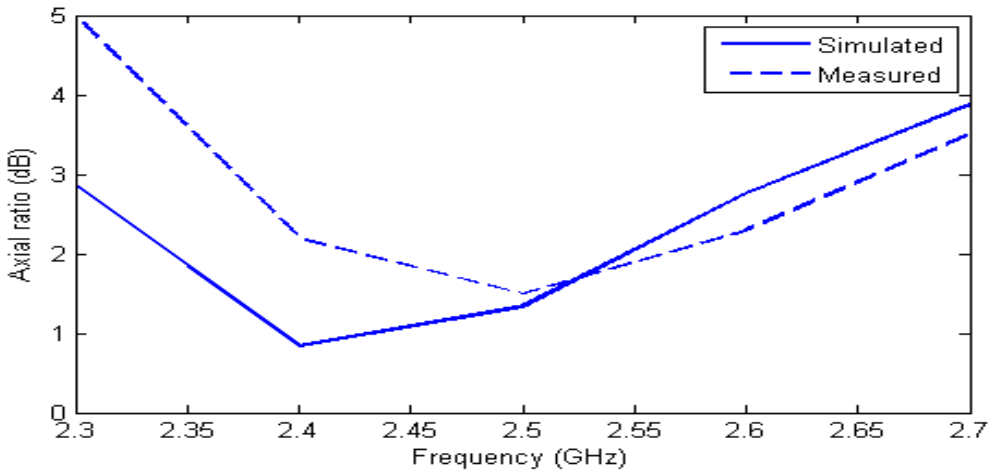

Fig. 7.31 (a) Variation of axial ratio with frequency in the lower frequency band of the dual frequency circularly polarized grounded slot antenna

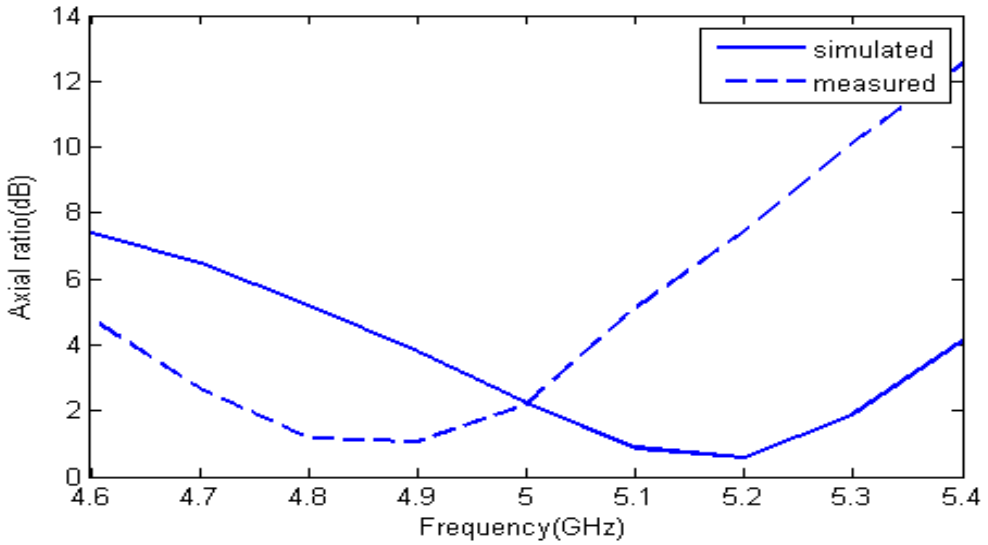

Fig. 7.31 (b) Variation of axial ratio with frequency in the upper frequency band of the dual frequency circularly polarized grounded slot antenna

The 3 dB axial ratio bandwidths are 230 MHz and 340MHz at the lower and higher operating frequencies respectively. The variations of gain with frequency are shown in the figure below:

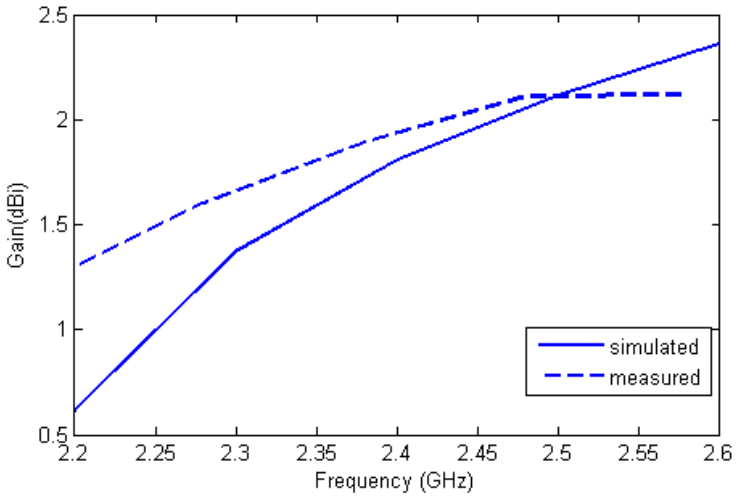

Fig. 7.32 (a) Variation of gain with frequency in the lower frequency band of the dual frequency circularly polarized grounded slot antenna

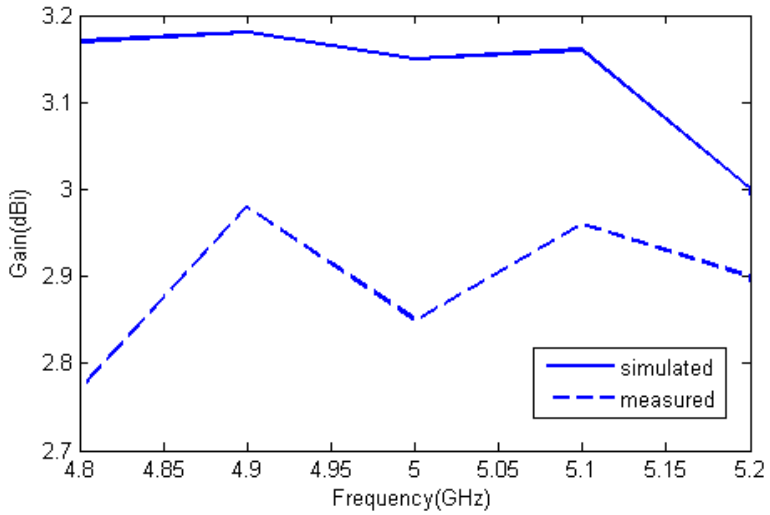

Fig. 7.32 (b) Variation of gain with frequency in the upper frequency band of the dual frequency circularly polarized grounded slot antenna

Antenna gains in the lower and higher operating frequencies are 2.05 dBi and 2.93 dBi respectively. The normalized power patterns at 2.5 GHz and 4.9 GHz are shown below:

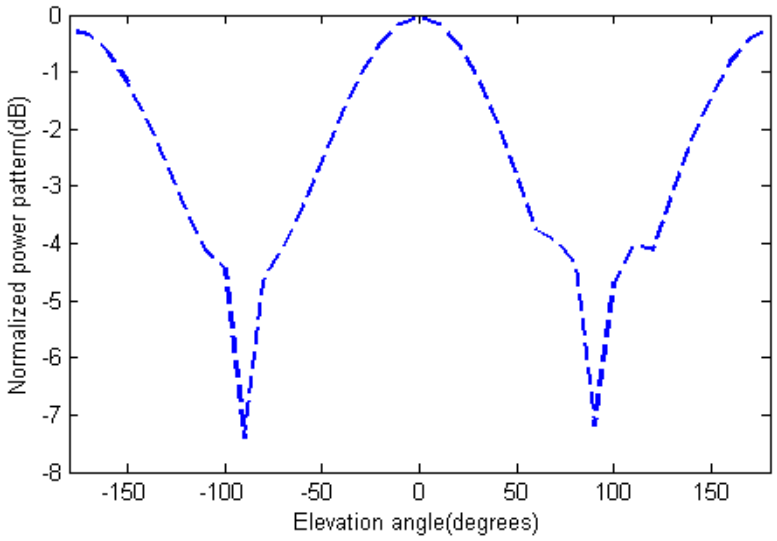

Fig. 7.33 (a) Normalized power pattern at lower operating frequency for the dual frequency circularly polarized grounded slot antenna (x-z plane)

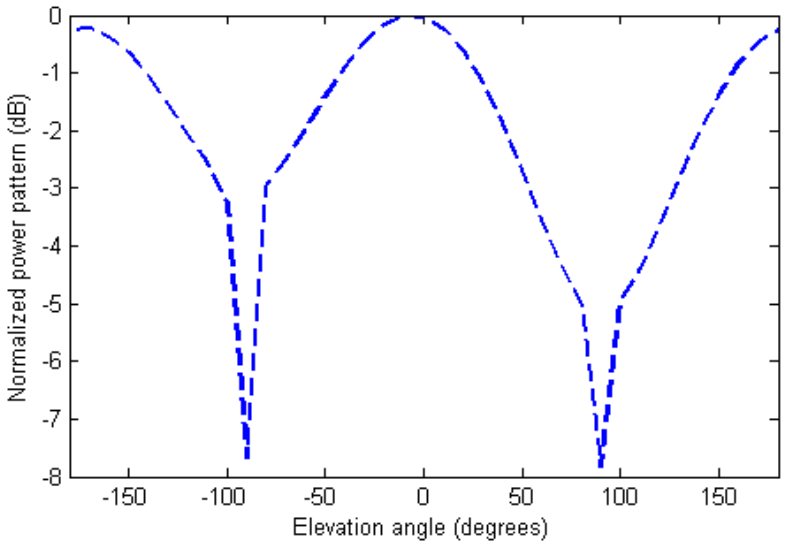

Fig. 7.33(b) Normalized power pattern at lower operating frequency of the dual frequency circularly polarized grounded slot antenna (y-z plane)

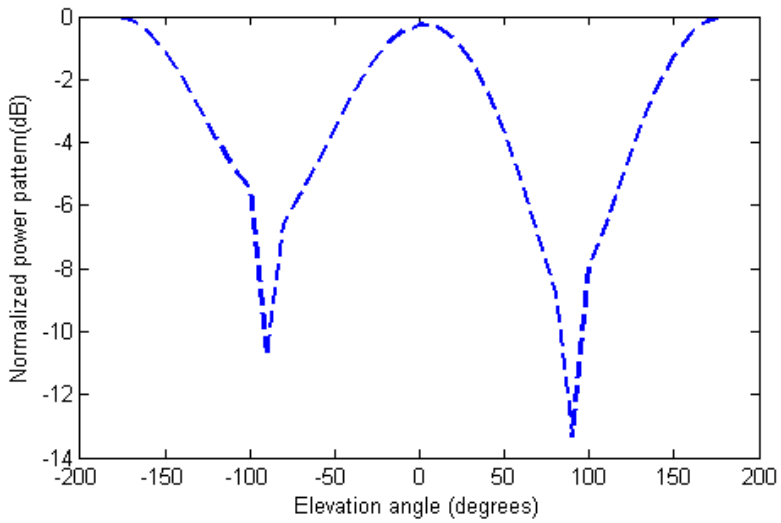

Fig. 7.33 (c) Normalized power pattern at higher operating frequency for the dual frequency circularly polarized grounded slot antenna (x-z plane)

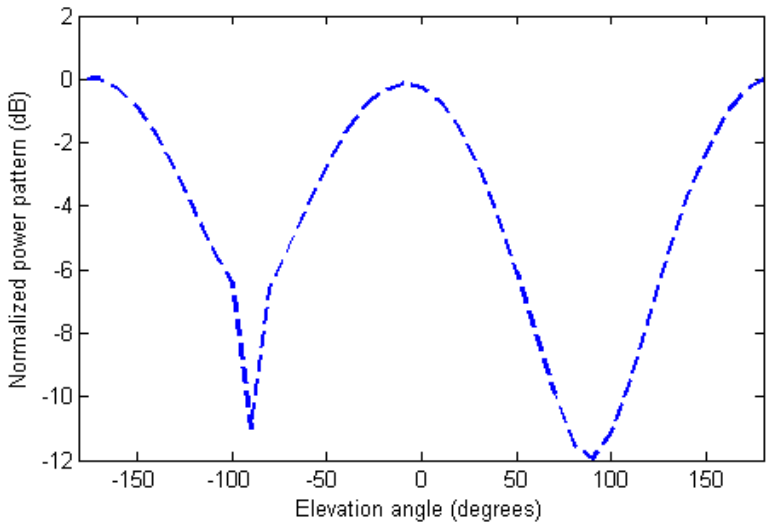

Fig. 7.33 (d) Normalized power pattern at higher operating frequency for the dual frequency circularly polarized grounded slot antenna (y-z plane)

The fabricated prototype of the antenna is shown below:

Fig. 7.34(a) Fabricated prototype of the dual frequency circularly polarized grounded slot antenna for WLAN

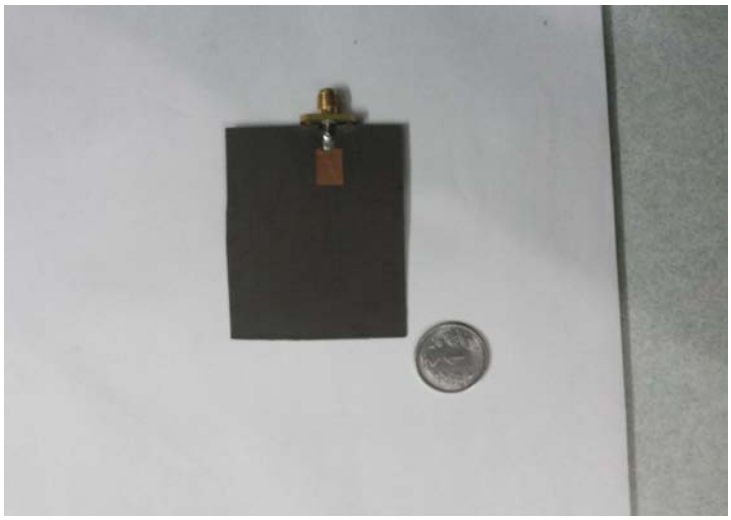

Fig. 7.34(b). Fabricated prototype of the dual frequency circularly polarized grounded slot antenna for WLAN

7.7 Triple-Band Grounded Slot Antenna for WLAN and Vehicular Applications

Design of a triple-band transmission line fed grounded slot antenna for WLAN and vehicular applications is proposed in this section. The dual antenna is intended to operate at 2.46 GHz, 3.65 GHz and 5.85 GHz respectively. The designed antenna radiates linearly polarized waves in the broadside direction at the triple frequencies. The antenna design is generated by an

automated procedure where an improved real-Boolean differential evolution algorithm is coupled with Method of Moments (MoM) based Electromagnetic Simulation (EM) software IE3D. The improved real-Boolean differential evolution algorithm is a modification of conventional real-Boolean differential evolution algorithm [147] where the donor vector generation is done using the sub-optimal vector as in [149]. The optimization objectives include impedance matching at the triple frequencies and maximization of gain in the broadside direction for all those frequencies.

7.7.1 Antenna Configuration and Optimization

The geometry of the triple-band transmission line fed grounded slot antenna is generated by an automated procedure by coupling the improved real-Boolean differential evolution algorithm with the MoM based EM software IE3D. The transmission line feed network is composed of three impedance transformers cascaded with each other on one side of the substrate. The other side of the substrate represents the area for the grounded slots. The substrate area for placing the grounded slots is divided in to 6x6 non-uniform cells with each cell having its own dimensions.

The optimization objectives are given below:

$Objective_1 =$
$\max\ (reflection\ coefficient\ at\ f_1\ GHz, reflection\ coefficient\ at f_2\ GHz, reflection\ coefficient\ at f_3\ GHz)$

(7.16a)

$$Objective_2 = 1/\min\ (gain\ at\ f_1 GHz, gain\ at f_2\ GHz, gain\ at f_3\ GHz) \quad (7.16b)$$

Objectives 1 and 2 are aimed at minimizing reflection coefficients and maximizing gain in the broadside directions at the triple frequencies respectively. Cost function for the optimization of the antenna structure is formulated as shown below:

$$Cost = w_1.Objective_1 + w_2.Objective_2 \quad (7.17)$$

The plot showing the variation of best cost value with number of generations of the algorithm is shown below:

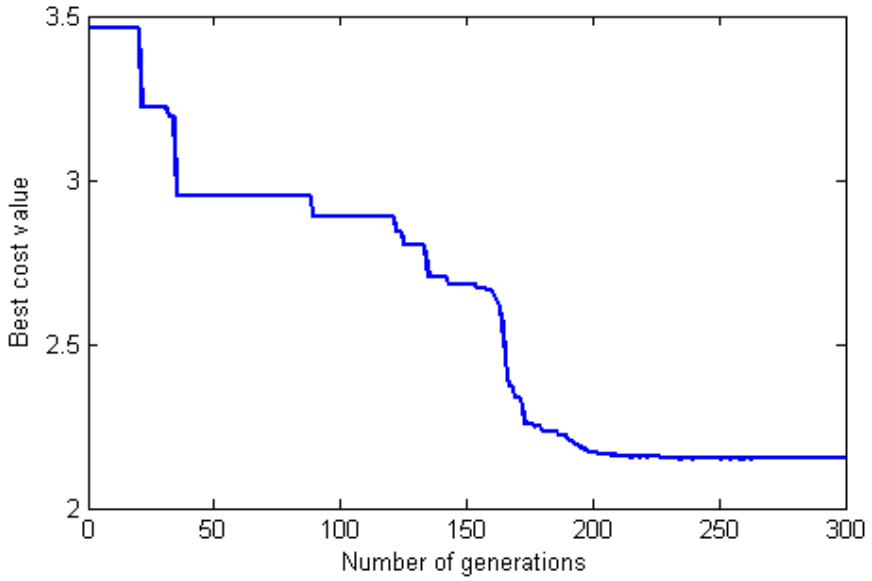

Fig. 7.35. Variation of the best cost value with generations for the triple-band transmission line fed grounded slot antenna

The automated geometry is shown in the figure below:

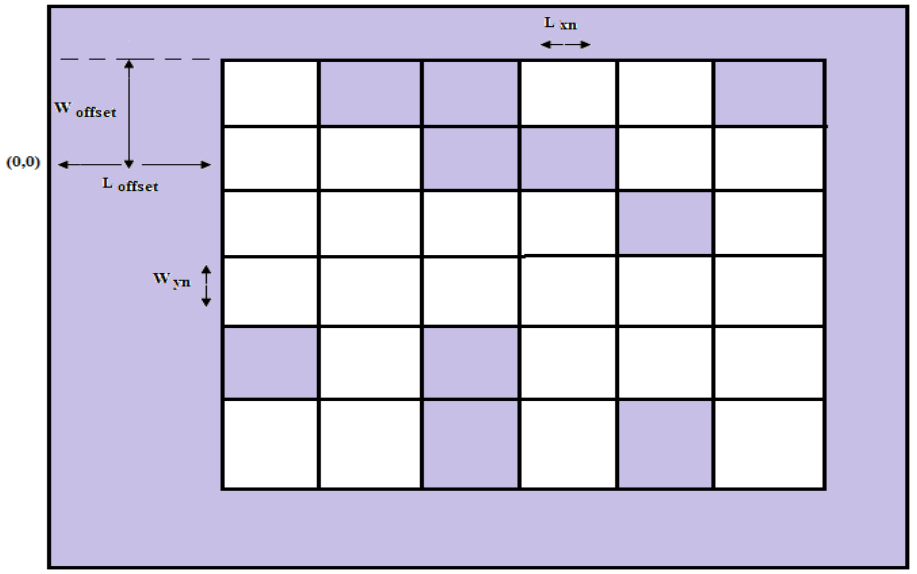

Fig. 7.36(a) Top view of the triple-band transmission line fed grounded slot antenna

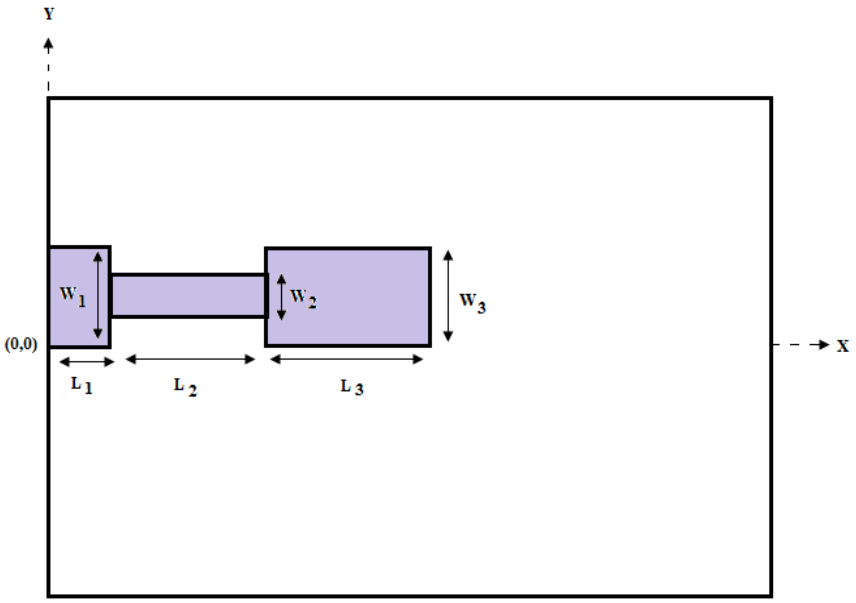

Fig. 7.36(b) Bottom view of the triple-band transmission line fed grounded slot antenna

The optimal dimensions of the antenna are given in Table 7.6.

Table 7.6. Dimensions of the optimal triple-band transmission line fed grounded slot antenna (all dimensions in mm).

L_1	1.000	L_2	7.425	W_1	2.575	W_2	1.575
L_3	6.800	L_{offset}	8.000	W_3	3.375	W_{offset}	7.075
L_{x1}	3.850	L_{x2}	3.525	W_{y1}	3.500	W_{y2}	4.450
L_{x3}	1.925	L_{x4}	3.150	W_{y3}	4.075	W_{y4}	2.800
L_{x5}	5.225	L_{x6}	2.375	W_{y5}	4.075	W_{y6}	4.000

7.7.2 Results and Observations

The antenna is designed assuming a substrate of permittivity 4.3 and thickness 30 mils. The variation of S_{11} with frequency at the triple bands is shown below:

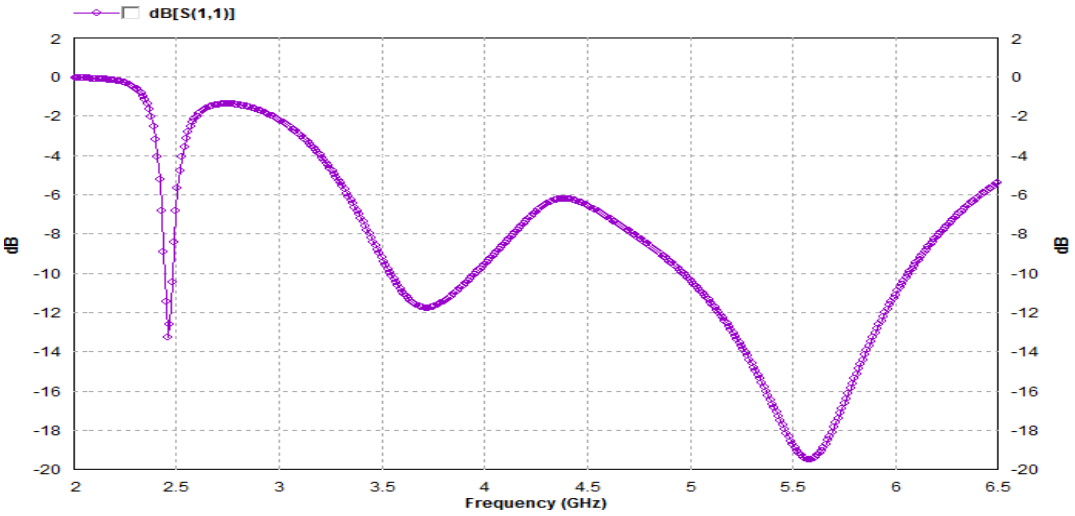

Fig. 7.37 Variation of S_{11} with frequency in the optimal triple-band transmission line fed grounded slot antenna

The variations of gain with frequency at the triple bands are shown below:

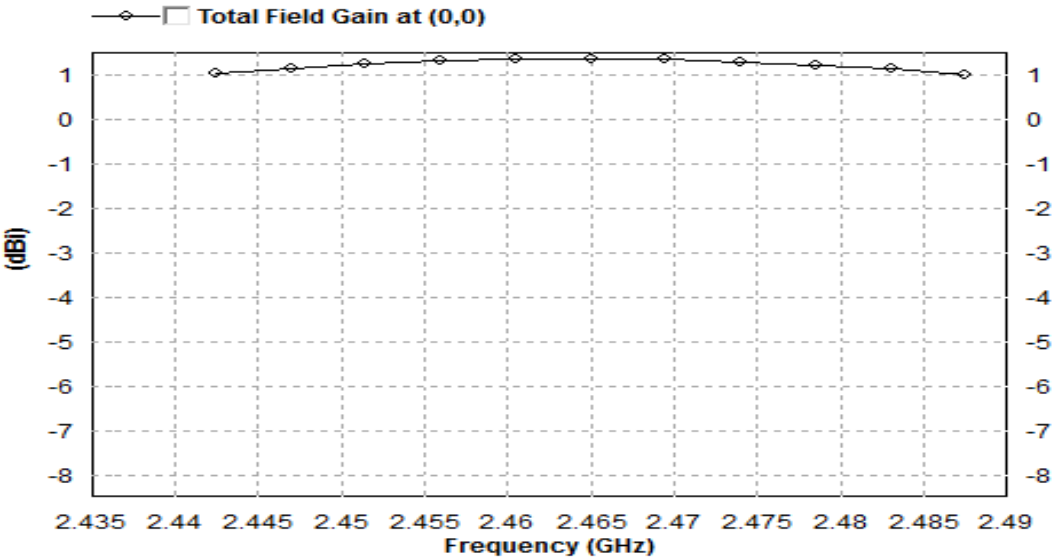

Fig. 7.38 (a) Variation of gain with frequency around 2.46 GHz

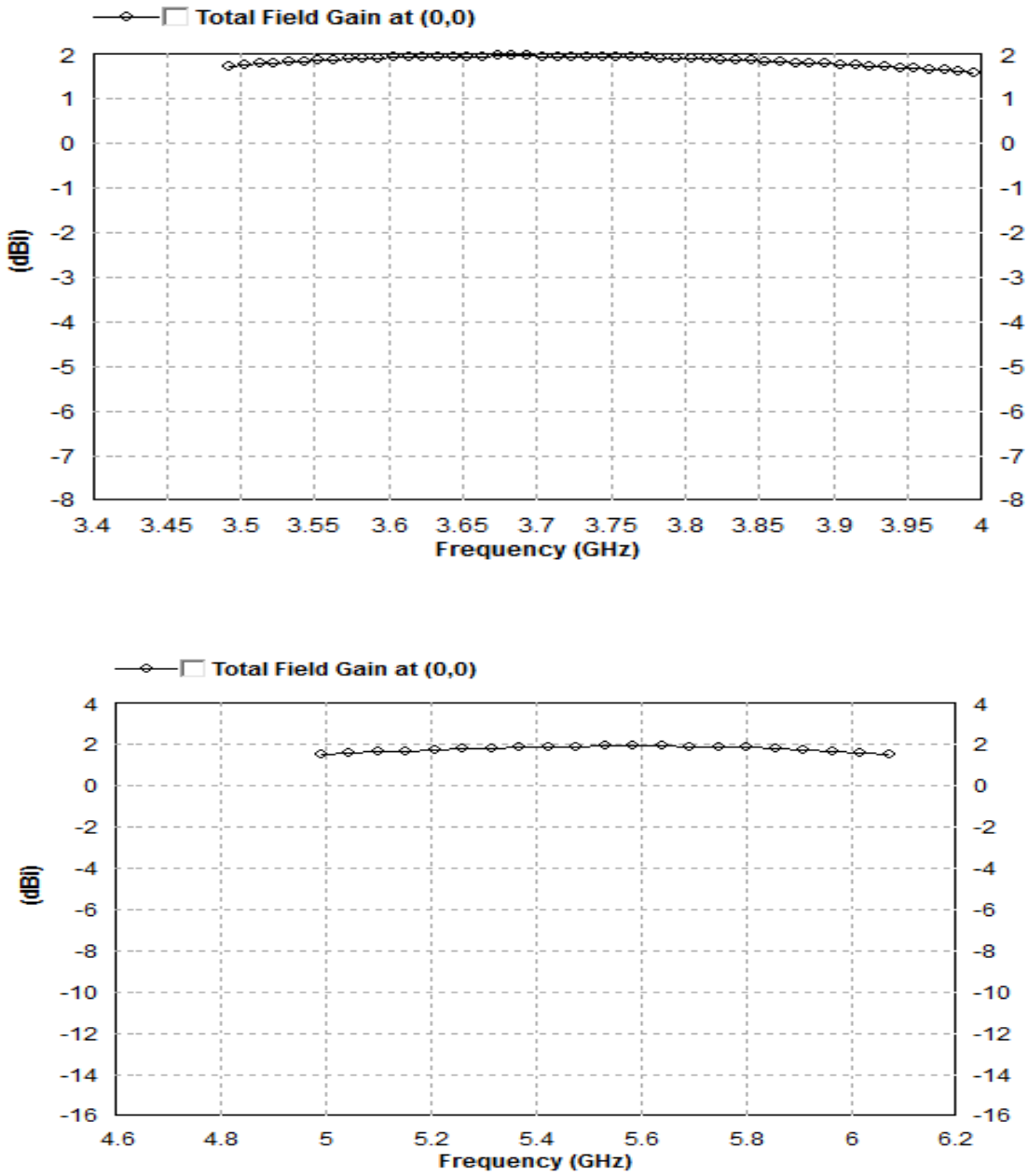

Fig. 7.38 (c) Variation of gain with frequency around 5.85 GHz

The elevation pattern gain plots at the triple frequencies are shown below:

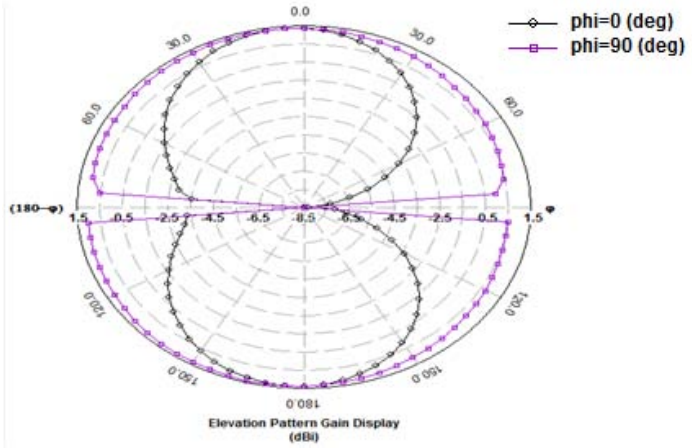

Fig. 7.39 (a) Elevation pattern gain plot at 2.46 GHz

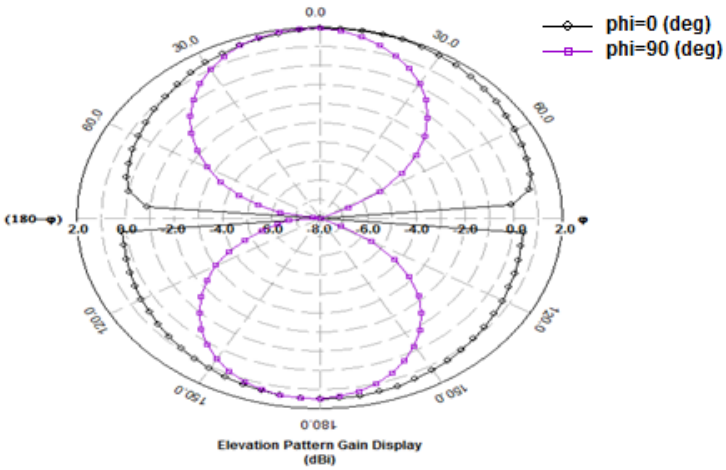

Fig. 7.39 (b) Elevation pattern gain plot at 3.65 GHz

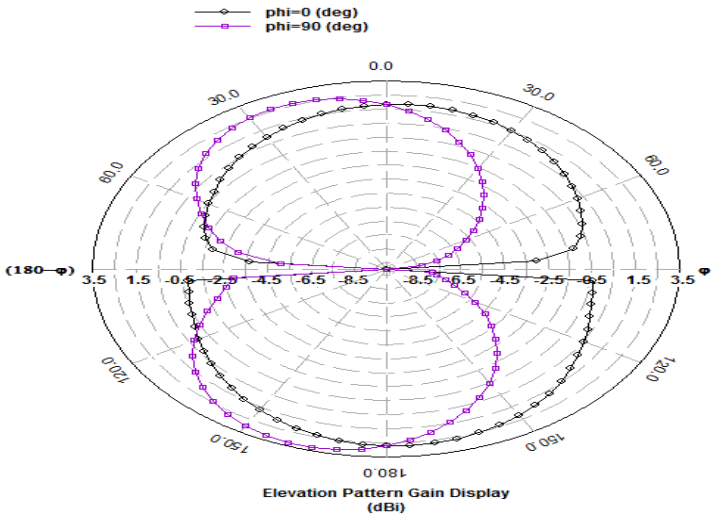

Fig. 7.39 (c) Elevation pattern gain plot at 5.85 GHz

The optimized automated slot antenna geometry exhibited impedance bandwidths of 45 MHz, 502.5 MHz and 1080 MHz at the center frequencies of 2.46 GHz, 3.65 GHz and 5.85 GHz respectively. The broadside gains are 1.348 dBi, 1.930 dBi and 1.870 dBi at the center frequencies of 2.46 GHz, 3.65 GHz and 5.85 GHz respectively.

7.8 Conclusion

Six microstrip antennas have been designed and optimized using suitable versions of differential evolution algorithm in this chapter. The antennas are suitable for WLAN and vehicular communication applications. Some of these antennas are fabricated and their S-parameter measurements are done by Agilent E5071B ENA series vector network analyzer. The first antenna is a simple one employing shorting pin near the probe feed for compactness and designed to operate in the GPS L1 band. This antenna is optimized using the simple DE/rand/1 algorithm and the cost function evaluation is done for the cavity model formulation of the antenna. There are fabrication tolerances associated with the fabricated prototype because of the proximity of the shorting pin and the probe feed resulting in variation between the simulated and the measured S_{11} data of the antenna. The second antenna is a single layer gap coupled microstrip antenna designed to operate in the GPS L1 band and vehicular DSRC band radiating circularly and linearly polarized waves in the bands respectively. The third antenna is a modification of the second antenna radiating right handed circularly polarized and left handed

circularly polarized waves in the GPS L1 band and DSRC band respectively. Both these antennas are optimized using differential evolution algorithm with neighborhood based mutation operator employing suitable cost function, value of which is determined by the method of moment based electromagnetic simulation software IE3D. The prototype of the third antenna is fabricated and its measured characteristics are compared with the simulated ones. A frequency shift is observed in both the lower and higher frequencies, which can be attributed to fabrication tolerances. The fourth antenna is a slotted microstrip antenna with probe feed designed to radiate right handed circularly polarized waves in the broadside direction at dual frequencies. This antenna is optimized using the modified differential evolution algorithm. A prototype of this antenna is fabricated and its measured characteristics are compared with the simulated ones. The fifth antenna is a dual band circularly polarized transmission line fed grounded slot antenna. This antenna is bidirectional in nature and is based on automated geometry generation, optimized using the self-adaptive real-Boolean differential evolution algorithm proposed in the previous chapter. A prototype of this antenna is also fabricated. Comparison of the simulated characteristics with the measured characteristics shows good agreement between them. The sixth antenna is a triple band linearly polarized transmission line fed grounded slot antenna. This antenna is bidirectional in nature and is based on automated geometry generation, optimized using improved real-Boolean differential evolution algorithm proposed in the previous chapter.

Chapter 8

Conclusion

8.1. Concluding Remarks

This research is focused on applying conventional and advanced versions of bio-inspired optimization algorithms and their variants, particularly differential evolution algorithm to the design of single band and multi band circularly polarized microstrip antennas and arrays. The research work has been carried out in four phases.

In the first phase (as reported in chapter 4) of the research work, a set of numerical antenna and array optimization benchmark optimization problems have been defined. Statistical performance comparison of genetic algorithm, particle swarm optimization, differential evolution and some of their advanced schemes (including quantum genetic algorithm, improved genetic algorithm, improved comprehensive learning particle swarm optimization, position mutated hierarchical particle swarm optimization and differential evolution with neighborhood based mutation operator) are carried out with respect to the benchmark problems in this chapter. The optimization objectives for the right handed circularly polarized microstrip antennas (with probe feed, transmission line feed and aperture coupled feed) are to provide improved impedance matching within a predefined frequency range, minimize axial ratio and maximize gain at the centre frequency. All objectives in the cost function are combined using dynamic weights based on fuzzy rules. The control parameters of all algorithms are tuned nearly to their best performance by meta-level optimization algorithms. However the process is computationally expensive requiring huge computation time and memory. The values of the control parameters for different algorithms provided in this chapter may guide the readers to optimally use these algorithms for future designs. Differential evolution (with neighborhood based mutation operator) is adjudged to be the statistically most suited algorithm for all designs of RHCP microstrip antennas reported in this chapter. The optimization objectives for the linear array of unequally spaced isotropic elements are minimization of beam width between first nulls, minimization of maximum side lobe level and minimization of inter-element spacing between the elements to reduce the overall size of the array. Optimization of impedance properties is not carried out since isotropic antenna elements are considered. The statistical performances of the

algorithms are very close in this case. It is found that differential evolution (with neighborhood based mutation operator) has slightly beaten others with its high convergence rate and 100% robustness. Both impedance and pattern properties are optimized in the design of 4-element Yagi-Uda antenna array. The optimization objectives in this case are to minimize the half power beam widths and side lobe levels for both E-plane and H-plane, along with improving the voltage standing wave ratio at the design frequency. In this case also, it is found that differential evolution (with neighborhood based mutation operator) has claimed superiority over other algorithms. Statistical performance comparison of advanced schemes of genetic algorithm, particle swarm optimization and differential evolution optimization strategies are reported for the first time with respect to electromagnetic numerical benchmark problems in this chapter where dynamically weighed cost functions are used.

Since differential evolution algorithms performed well on a general basis over other bio-inspired optimization algorithms in the optimization of numerical benchmark problems in chapter 4, more variants of differential evolution algorithms involving non-adaptive and self-adaptive versions are explored in terms of their applicability to similar numerical benchmark problems in the second phase (as reported in chapter 5). Although the objectives and cost functions are kept same for the optimization of unequally spaced array of isotropic antenna elements and the four element Yagi-Uda antenna array, the optimization objectives are improved in the design of circularly polarized microstrip antenna with different feeding techniques. The optimization objectives in this case are to maximize the axial ratio bandwidth, improve impedance matching within the axial ratio band and maximize the gain at the center frequency. The control parameters of the non-adaptive differential evolution algorithms are tuned using a meta-level differential evolution algorithm with neighborhood based mutation operator. Performances of all differential evolution algorithms varied for the benchmark optimization problems. In case of the circularly polarized probe fed and transmission line fed microstrip antennas, modified differential evolution is adjudged to be the best suited differential evolution algorithm. Also, for cross aperture coupled circularly polarized microstrip antenna, modified differential evolution algorithm is adjudged to be superior to others. In case of optimization of the unequally spaced isotropic linear array and 4-element Yagi-Uda antenna array, differential evolution with individual dependent mechanism and modified differential evolution algorithms are found to be the most suited DE algorithms respectively. The data and study results on the applicability of the different optimization

algorithms for antenna and array optimization problems will help the future researchers to choose the DE optimization algorithm aptly for their design problem. Statistical performance comparison of advanced schemes of differential evolution optimization strategies are reported for the first time again with respect to electromagnetic numerical benchmark problems in this chapter where dynamically weighed cost functions are used.

In the third phase of the research work (as reported in chapter 6), attempt has been made to develop self adaptive real-Boolean differential evolution algorithm and apply it successfully for designs of thinned linear and planar antenna arrays. Despite low population size, statistical performance of the new algorithm is observed to be comparatively better than the original Boolean differential evolution algorithm or real-Boolean differential evolution algorithm. This novel algorithm employs composite trial vector generation strategy, self adaptive scheme for control parameters, population dynamics for maintaining population diversity and a population manager.

In the fourth phase of research work (as reported in chapter 7), several antenna designs for WLAN and vehicular applications are optimized using appropriate differential evolution strategy and electromagnetic simulators. Most of the prototypes based on the optimal designs have been fabricated followed by the measurement of their impedance and radiation characteristics. The optimization of microstrip antenna structures by coupling differential evolution algorithms with electromagnetic simulators for cost function evaluation is time consuming. Hence, one requires using algorithms which can work with low population size, converge fast and exhibit good exploration and exploitation capabilities at the same time. Such differential evolution algorithms are identified and reported in this chapter which can serve as a guide to future antenna designers. Six antennas are designed and optimized using suitable versions of differential evolution algorithm. The first antenna is a simple one employing a shorting pin near the probe feed for compactness and designed to operate in the GPS L1 band. This antenna is optimized using the simple DE/rand/1 algorithm and the cost function evaluation is done using the cavity model formulation of the antenna. There are fabrication tolerances associated with the fabricated prototype because of compact size and the proximity of the shorting pin and the probe feed resulting in variation between the simulated and the measured S_{11} data of the antenna. The second antenna is a single layer gap- coupled microstrip antenna designed to operate in the GPS

L1 band and vehicular DSRC band. It radiates circularly and linearly polarized waves in the two bands respectively. The third antenna is a modification of the second antenna radiating right handed circularly polarized and left handed circularly polarized waves in the GPS L1 band and DSRC band respectively. Both these antennas are optimized using differential evolution algorithm with neighborhood based mutation operator. The prototype of the third antenna is fabricated and its measured characteristics are compared with the simulated ones. A frequency shift is observed in both the lower and higher frequencies, which can be attributed to fabrication tolerances. The fourth microstrip antenna is a slotted microstrip antenna with probe feed designed to radiate right handed circularly polarized waves in the broadside direction at 2.45 GHz and 3.65 GHz respectively. This antenna is optimized using the modified differential evolution algorithm. A prototype of this antenna is fabricated and its measured characteristics are also compared with the simulated ones. However there is some fabrication tolerances associated with this antenna. The fifth antenna is a transmission line fed dual band circularly polarized grounded slot antenna. This antenna is bidirectional in nature and is based on automated geometry generation. It is optimized using the self-adaptive real-Boolean differential evolution algorithm proposed in the previous chapter. A prototype of this antenna is also fabricated. Comparison of the simulated characteristics with the measured characteristics shows very good agreement between them. The sixth antenna is a triple-band grounded slot antenna radiating linearly polarized waves in the broadside direction at 2.46 GHz, 3.65 GHz and 5.85 GHz. This antenna is optimized using improved real-Boolean differential evolution algorithm.

8.2 Major Inferences

- Bio-inspired optimization algorithms which are non adaptive in nature should have their control parameters tuned for optimal performance (pertaining to the optimization problem at hand) using a meta-optimization algorithm. However the process is computationally expensive requiring huge computation time and memory.
- Differential evolution with neighborhood based mutation operator and modified differential evolution algorithm have shown statistically superior performance compared to the other algorithms in the design of probe fed and transmission line fed circularly polarized microstrip antennas and also for the design of 4 element Yagi-Uda antenna array using cost functions with dynamic weights as inferred from the observations made in chapters 4 and 5.

- Differential evolution with neighborhood based mutation operator and modified differential evolution algorithm are adjudged to be superior compared to other algorithms in the design of circularly polarized cross aperture coupled microstrip antenna as inferred from the observations made in chapters 4 and 5.
- Differential evolution with neighborhood based mutation operator and differential evolution with individual dependent mechanism have shown slightly better performance compared to other algorithms in the synthesis of unequally spaced isotropic antenna elements using cost functions with dynamic weights as inferred from the observations made in chapters 4 and 5.
- Self –adaptive real-Boolean differential evolution employing low population size has been proposed and applied successfully to the synthesis of thinned linear and planar antenna arrays in chapter 6. It has exhibited statistically superior performance compared to the conventional real-Boolean differential algorithm for such designs.
- Differential evolution with neighborhood based mutation operator, modified differential evolution and self adaptive real-Boolean differential evolution algorithm have been applied to the design and optimization of several novel dual-band circularly polarized microstrip antennas in chapter 7. These algorithms exhibited capability to work with low population size and moderate convergence rate. These antennas have been fabricated and measurements of their impedance and pattern characteristics are carried out. Slight shift in operating frequencies have been observed between measured and simulated data which can be attributed to fabrication tolerances.

8.3. Future Scope

The investigations reported in the initial phases of the research can be extended in several directions focusing on advancement in the area of bio-inspired optimization algorithms and their applications in antenna designs as indicated below:

- Most of the algorithms need their control parameters to be tuned using a meta-level optimization algorithm. Self adaptive versions of these algorithms can be developed using variable population size so that the computation time and memory requirement can be reduced simultaneously. It is believed that using dynamic population will not only result in faster convergence but also lead to better exploration and exploitation.

- The applicability of the algorithms considered in chapters 4 and 5 is done with respect to only single band circularly polarized antennas using different feeding techniques. This study can be extended for optimization of dual band circularly polarized microstrip antennas with different feeding techniques.
- The self-adaptive real-Boolean differential evolution algorithm can be used for automated design of multi-band antennas (with more than two bands), triple-band, quad-band and wideband circularly polarized slot antennas as well.

References:

[1]. T.S. Rappaport, *Wireless communications principles and practice*, Prentice Hall India, 2009.

[2]. C.A. Balanis, *Antenna theory analysis and design*, John Wiley and Sons, 2005.

[3]. R. Garg, P. Bhartia, I. Bahl, and A. Ittipiboon, *Microstrip antenna design handbook*. Norwood, MA, USA: Artech House, 2001, pp. 495–496.

[4]. G.A. Deschamps, 'Microstrip microwave antennas,' presented at *3rd USAF symposium on Antennas*, 1953.

[5]. H. Gutton and G. Bassionat, 'Flat aerial for ultra high frequencies,'*French patent number 703113*, 1955.

[6]. J.A. McDononough, 'Recent development in the study of microstrip antennas,'*IRE Nat. Conv. Rec. 5Pt1*, pp.173-176, 1957.

[7]. E.J. Dellinger ,'Radiation from microstrip resonators,' *IEEE Transactions on Microwave Theory and Techniques*, vol. 17, pp.235-236, 1969.

[8]. R.E. Munson, 'Conformal Microstrip antennas and microstrip feed arrays,'*IEEE Transactions on Antennas and Propagation*, vol. 22, pp. 74-78, 1974.

[9]. Derneryd ,'A theoretical investigation on rectangular microstrip antenna element,' *IEEE Transactions on Antennas and Propagation*, vol. 26, pp. 532-535, 1978.

[10]. Y.T. Lo, D. Solomon and W. F. Richards ,'Theory and experiments on microstrip antennas,' *IEEE Transactions on Antennas and Propagation*, vol. 27, pp.137-145, 1979.

[11]. K.P. Karver and J.W. Mink ,'Microstrip antenna technology,' *IEEE Transactions on antennas and Propagation*, vol. 29, no. 1, pp. 38-46, 1981.

[12]. W.F. Richards, Y. J. Lo and D.D. Harrison ,'An improved theory of microstrip antennas with applications,' *IEEE Transactions on Antennas and Propagation*, vol. 29, no. 1, pp., pp.38-46, 1981.

[13]. C. Wood, P.S. Hall and J. R. James, 'Design of wideband circularly polarized microstrip antennas and arrays,' *International Conference on Antennas and Propagation*, pp. 312-316, 1978.

[14]. J. Henrikkson, K. Markus and M. Tiuri ,'A circularly polarized travelling wave chain antenna', of the *9th European Microwave conference, Microwave Exhibitions and publishers*, England, pp. 174-178, 1979.

[15]. L. C. Shen,'The elliptical microstrip antenna with circular polarization', *IEEE Transactions on Antennas and Propagation*, vol. 29, pp. 90-94, 1981.

[16]. K. Ito, 'Circularly polarised printed antenna with wide axial-ratio bandwidth using strip dipoles and slots,' *IEE Proceedings*, vol. 130, Pt. H, no. 6, pp. 397-402, 1983.

[17]. S. Nishimura, Y. Sugio and T. Makimoto ,'Crank type circularly polarized microstrip line antenna', *IEEE AP-S International Symposium on Antenna Propagation*, pp. 162-165, 1983.

[18]. P. S. Hall, ' Microstrip linear array with polarization control', *IEE Proceedings*, vol. 130, pt. H, pp.215-224, 1983.

[19]. P. C. Sharma and K. C. Gupta, 'Analysis and optimized design of single feed circularly polarized microstrip antennas,'*IEEE Transactions on Antennas and Propagation*, vol. 31, pp. 949-955, 1984.

[20]. J. Huang, 'A technique for an array to generate circular polarization with linearly polarized elements ,' *IEEE Transactions on Antennas and Propagation*, vol. 32, no. 9, pp. 991-994, 1984.

[21]. P.L. Sullivan and D.H. Schaubert, 'Analysis of an aperture coupled microstrip antenna,'*IEEE Transactions on Antennas and Propagation*, vol. 34, pp. 977-984, 1984.

[22]. D. M. Pozar ,'A microstrip antenna aperture coupled to a microstrip line,'*Electronics Letters*, vol. 21, pp. 49-50, 1985.

[23]. M. Himdi, J.P. Daniel and C. Terret ,'Transmission line analysis of aperture coupled microstrip antenna,' *Electronics Letters*, vol. 25, pp. 1229-1230, 1989.

[24]. M. Himdi, J.P. Daniel and C. Terret ,'Analysis of aperture coupled microstrip antenna using cavity method,' *Electronics Letters*, vol. 25, pp. 391-392, 1989.

[25]. A. Adrian and D. H. Schaubert ,'Dual aperture-coupled microstrip antenna for dual or circular polarization,' *Electronics Letters*, vol. 23, no. 23, pp. 1126-1227,1987.

[26]. M. Haneishi and S. Yoshida, *A design method of circularly polarized rectangular microstrip antenna by one point feed*, Microstrip Antenna Design, K. C. Gupta and A. Benella, Artech House, Norwood, MA, 1988.

[27]. Y. Suzuki, N. Miano and T. Chiba, *Circularly polarized radiation from singly-fed equilateral-triangular microstrip antenna*, in Microstrip Antenna Design, K. C. Gupta and A. Benella, Artech House, Norwood, MA, pp. 338-342, 1988.

[28]. M. Haneishi and Y. Suzuki, 'Circular polarization and bandwidth, '*Handbook of microstrip antennas*, vol. 1, J. R. James and P. S. Hall, Peter Peregrinus, London, UK,1989.

[29]. K. Ito , T. Teshirogi and S. Nishimura ,'Circularly polarized antenna arrays,' in *Handbook of microstrip antennas*, vol. 1, J. R. James and P. S. Hall, Peter Peregrin London, UK, 1989.

[30]. M. Irsadi Aksun, S. L. Chuang and Y. T. Lo ,'On slot coupled microstrip antennas and their applications to CP operation- Theory and Experiment,' *IEEE Transactions on Antennas and Propagation*, vol. 38, no. 8, pp. 1224-1230.

[31]. El. M. Yazidi, M. Himdi and J. P. Daniel ,' Transmission line analysis of non linear slot coupled microstrip antenna,' *Electronics letters*, vol. 28, pp. 1406-1408, 1992.

[32]. S. D. Targonski and D. M. Pozar ,'Design of wideband circularly polarized aperture-coupled microstrip antennas,'*IEEE Transactions on Antennas and Propagation*, vol. 41, no. 2, pp. 214-220, 1993.

[33]. E. Aloni and R. Kastner ,'Analysis of a dual circularly polarized microstrip antenna fed by cross slots,' *IEEE Transactions on Antennas and Propagation*, vol. 32, no.8, pp. 1053-1058, 1994.

[34]. C. Y. Huang, J. Y. Wu and K. L. Wong ,'Slot-coupled microstrip antenna for broadband circular polarization,' *Electronics Letters*, vo. 34, no. 9, pp.835-836, 1998.

[35]. M. A. Saed ,' Efficient method for analysis and design of aperture coupled rectangular microstrip antennas,' *IEEE Transactions on Antennas and Propagation*, vol. 41, pp. 986-988, 1993.

[36]. T. Vlasitis, E. Korolkiewicz and A.Sambell ,'Analysis of cross aperture coupled patch antenna using transmission line model,' *Electronics Letters*, vol. 32, no. 21, pp. 1934-1935, 1996.

[37]. B. Aljibouri, H.Evans, E. Korolkiewicz, E.G.Lim, A. Sambell and T. Vlasitis, 'Cavity model of circularly polarized cross-aperture-coupled microstrip antenna,' *IEE-Proceedings-Microwave and Antenna Propagation*, vol. 148, no. 3, pp. 147-152, June 2001.

[38]. K.L. Wong and Y. F. Lin, 'Circularly polarized microstrip antenna with a tuning stub,' *Electronics Letters*, vol. 34, pp. 831-832,1998.

[39]. K. K. Tsang and R.J. Langley, ' Design of circular patch antennas on ferrite substrates,' *IEE Proceedings, Microwave Antennas and Propagation*, vol. 145, no. 1, pp. 49-55, 1998.

[40]. J. S. Row, 'Design of aperture-coupled annular-ring microstrip antennas for circular polarization,' *IEEE Transactions on Antennas and Propagation*, vol. 53, no. 5, pp.1779-1784, 2005.

[41]. A. Khidre, K.F.Lee, F. Yang and A. Elsherbeni, 'Wideband circularly polarized E-shaped patch antenna for wireless applications,'*IEEE Antennas and Propagation Magazine*, vol. 52, no. 5, pp. 219-229,2010.

[42]. B. Y. Toh, R. Cahill and V. F. Fusco, 'Understanding and measuring circular polarization,'*IEEE Transactions on Education*, vol. 46, no. 3, pp. 313-318, 2003.

[43]. R. Waterhouse, 'Small microstrip patch antenna,' *Electronics Letters*, vol. 31, no. 8, pp. 604-605, 1995.

[44]. R. Porath, 'Theory of miniaturized shorting post microstrip antennas', *IEEE Transactions on, Antennas and Propagation*, vol. AP- 48, pp. 41-47, 2000.

[45]. K. L. Wong and W. S. Chen, 'Compact microstrip antenna with dual frequency operation,'*Electronics Letters*, vol. 33, no. 8, pp. 646-647, 1997.

[46]. K. L. Wong and S. C.Pan, 'Compact triangular microstrip antenna,' *Electronics Letters*, vol. 33, no. 6, pp. 433-434, 1997.

[47]. H. Kan and R. B. Waterhouse, 'Small circularly polarized printed antenna,' *Electronics Letters*, vol. 36, no. 5, pp. 393-394, 2000.

[48]. J. S. Roy, N. Chattoraj, and N. Swain, 'Short circuited microstrip antennas for multi-band wireless communications', *Microwave & Optical Technology Letters*, vol. 48, pp. 2372 –2375, 2006.

[49]. J. George, M. Deepukumar, C. K. Aanandan, P. Mohanan and K. G. Nair, 'New compact microstrip antenna,'*Electronics Letters*, vol. 32, no. 6, pp. 508-509, 1998.

[50]. W. S. Chen, C. K. Wu and K. L.Wong, 'Compact circularly polarized microstrip antenna with bent slots,' *Electronics Letters*, vo. 34, no. 13, pp.1278-1279, 1998.

[51]. X. H. Tang, K. L. Lau, Q. Xue and Y. L. Long, 'Miniature circularly polarized patch antenna,' *Electronics Letters*, vol. 46, no. 6, 2010.

[52]. P. Pourahmadazar and S. Mohammadi, 'Compact circularly polarized slot antennas for UWB applications,' *Electronics Letters*, vol. 47, no. 15. 2011.

[53]. Nasimuddin, X. Qing and Z. N. Chen, 'Compact asymmetric slit microstrip antennas for circular polarization,' *IEEE Transactions on Antennas and Propagation*, vol. 59, no. 1, pp. 285-288, 2011.

[54]. Nasimuddin, Z. N. Chen, and X. Qing, 'A Compact circularly polarised cross shaped slotted microstrip antenna,' *IEEE Transactions on Antennas and Propagation*, vol. 60, no. 3, pp. 1584-1588, 2012.

[55]. K. Ito and N. Goto, 'Dual-frequency circularly polarised printed antenna composed of strips and slots,' *IEE Proceedings*, Vol. 130, Pt. H, no. 2 , pp. 170-174, 1983.

[56]. W. S. Chen, 'Single feed dual frequency rectangular microstrip antenna with square slot,' *Electronics Letters*, vol. 34, no. 3, pp. 231-232, 1998.

[57]. G. P. Srivastava, S. Bhattacharya and S. K. Padhi, 'Dual band tunable microstrip patch antenna,' *Electronics Letters*, vol. 35, no. 17, pp. 1397-1398, 1999.

[58]. M. Deepukumar, J. George, C. K. Aanandan, P. Mohanan and K. G. Nair, 'Broadband dual frequency microstrip antenna,' *Electronics Letters*, vol. 32, no. 17, pp. 1531-1532, 1996.

[59]. S. Maci and G. B.Gentili, 'Dual-frequency patch antennas,' *IEEE Antennas and Propagation Magazine*, vol. 39, no. 6, pp.13-20, 1997.

[60]. K. L. Wong and K. P. Yang, 'Small dual frequency microstrip antenna with cross slot,' *Electronics Letters*, vol. 33, no. 23, pp. 1916-1917, 1997.

[61]. M. A. S. Alkanhal, 'Composite compact triple band microstrip antennas,' *Progress in Electromagnetics Research*, vol. 93, pp. 221-236, 2009.

[62]. D. Sanchez-Hernandez, and I. D. Robertson , 'Analysis and design of a dual-band circularly polarised microstrip patch antenna,' *IEEE Transactions on Antennas and Propagation*, vol. 43, no. 2, pp. 201-205, 1995.

[63]. D. M. Pozar and S. M. Duffy, 'A dual-band circularly polarized aperture-coupled stacked microstrip antenna for global positioning satellite,' *IEEE Transactions on Antennas and Propagation*, vol. 45, pp. 1618-1625, 1997.

[64]. G. B. Hseih, M. H. Chen, and K. L. Wong, 'Single-feed dual-band circularly polarised microstrip antenna,' *Electronics Letters*, vol. 34, no. 12, pp. 1170-1171, 1998.

[65]. K. P. Yang, and K. L. Wong, ' Dual-band circularly-polarised square microstrip antenna,' *IEEE Transactions on Antennas and Propagation*, vol**.** 49, no**.** 3, pp. 377-382, 2001.

[66]. C. Ming Su and K. L. Wong, 'A dual-band GPS microstrip antenna,' *Microwave and Optical Technology Letters*, vol.33, no. 4, 238-240, 2002.

[67]. Y. J. Sun and Y.-S. Kim, 'Circular polarised microstrip patch antennas for broadband and dual band operation,' *Electronics Letters*, vol. 40, no. 9.

[68]. X. F. Peng, S. S. Zhong, S. Q. Xu and Q. Wu, 'Compact dual-band GPS microstrip antenna,' *Microwave and Optical Technology Letters*, vol 44, no. 1, pp. 58-61, 2005.

[69]. F. Ferrero, C. Luxey, G. Jacquemod and R. Staraj, 'Dual-band circularly polarized microstrip antenna for satellite applications,' *IEEE Antennas and Wireless Propagation Letters*, vol. 4, pp. 13-15, 2005.

[70]. L. Zhou, S. Liu, Y. Wei, Y. Chen, and N. Gao, 'Dual-band circularly-polarised antenna based on complementary two turns spiral resonator,' *Electronics Letters*, vol. 46, no. 12, pp. 1-2, 2010.

[71]. Nasimuddin, Z. N. Chen and X. Qing, 'Dual-band circularly polarized S-shaped slotted patch antenna with a small frequency-ratio,'*IEEE Transactions on Antennas and Propagation*, vol. 58, no. 6, 2112-2115, 2010.

[72]. P. Nayeri, K. F. Lee, A. Z. Elsherbeni and F. Yang, 'Dual band circularly polarized antennas using stacked patches with asymmetric U-slots,' *IEEE Antennas and Wireless Propagation Letters*, vol. 10, pp. 492-495, 2011.

[73]. T. N. Chang and J. M. Lin, 'Serial aperture-coupled dual band circularly polarized antenna,' *IEEE Transactions on Antennas and Propagation*, vol. 59, no. 6, pp. 2419-2423, 2011.

[74]. C. H. Chen and E.K.N. Yung, 'A novel unidirectional dual-band circularly polarized patch antenna,' *IEEE Transactions on Antennas and Propagation*, vol. 59, no. 8, pp. 3052-3057, 2011.

[75]. J.H. Holland, 'Genetic algorithms,'*Scientific American*, pp.66-72, July 1992.

[76]. D. E. Goldberg, *Genetic Algorithms in Search, Optimization and Machine Learning*. Reading, MA, USA: Addison-Wesley Reading, pp. 1–214, 1975.

[77]. R L Haupt, 'An introduction to genetic algorithms for electromagnetic,' *IEEE Antennas and Propagation Magazine*, vol. 37, no. 2, pp. 7-15, 1995.

[78]. J. M. Johnson and Y. R. Samii, 'Genetic algorithms in engineering electromagnetics,' *IEEE Antennas Propag. Mag.*, vol. 39, no. 4, pp. 7–21, 1997.

[79]. J. J. Grefenstette, 'Optimization of control parameters for genetic algorithms,' *IEEE Trans. Systems, Man, Cybern.*, vol. smc-16, no. 1, pp. 122–128, 1986.

[80]. R L Haupt, 'Thinned arrays using genetic algorithms,' *IEEE Transactions on Antennas and Propagation*, vol. 42, no. 7, pp. 993-999, 1994.

[81]. O Quevedo-Teruel and E Rajo-Iglesias, 'Ant colony optimization in thinned array synthesis with minimum side lobe level,' *IEEE Antennas and Wireless Propagation Letters*, vol. 5, pp. 349-352, 2006.

[82]. A Farazi and K Forooraghi, 'Thinned arrays using pattern search algorithms,' *Progress in Electromagnetics Research*, vol.78, pp.61-71, 2008.

[83]. B. V. Ha, M. Musetta, P. Pirinoli and R.E. Zich, 'Modified compact genetic algorithm for thinned array synthesis,' *IEEE Antennas and Wireless Propagation Letters*, vol. 15, pp. 1105-1108, 2016.

[84]. E. E. Altshuler and D.S. Linden, 'Wire antenna designs using genetic algorithms,' *IEEE Transactions on Antennas and Propagation* , vol. 39, no. 2, pp. 33-43, 1995.

[85]. D. S. Linden, *Automated design and optimization of wire antennas using genetic algorithms*, Ph.D. dissertation, Dept. Electrical Eng. Comput. Sci., Mass. Inst. of Technol., Cambridge, MA, USA, 1997.

[86]. E. A. Jones and W. T. Joines, 'Design of Yagi-Uda antennas using genetic algorithms,' *IEEE Transactions on Antennas and Propagation*, vol. 45, no. 9, pp. 1386-1392, 1997.

[87]. Y. Kuwahara, 'Multi-objective optimization design of Yagi-Uda antenna,'*IEEE Transactions on Antennas and Propagation*, vol. 53, no. 6, pp. 1984-1992, 2005.

[88]. X. Chen, K. Huang, and X. B. Xu, 'Automated design of a three- dimensional fishbone antenna using parallel genetic algorithm and NEC,' *IEEE Antennas and Wireless Propagation Letters*, vol. 4, pp. 425-428, 2005.

[89]. S. N. Sorokin, V. V. Savelyev, E. V. Evanchenko and M. P. Oleynik, 'Fitness function calculation technique in Yagi-Uda antennas evolutionary design,' *IX-th International Conference on Mathematical Methods in Electromagnetic Theory*, pp. 452-454, 2002, Kiev, Ukraine.

[90]. D. Eclercy, A. Reinix and B. Jecko, 'FDTD genetic algorithm for antenna optimization,' *Microwave and Optical Technology Letters*, vol. 16, no. 2, pp. 72-74, 1997.

[91]. H. Choo and H. Ling, 'Design of multiband microstrip antennas using a genetic algorithm,' *IEEE Microwave and Wireless Components Letters*, vol. 12, no. 9, pp. 345-347, 2002.

[92]. L. A. Griffiths, C. Furse and Y. C. Chung, 'Broadband and multiband antenna design using the genetic algorithm to create amorphous shapes using ellipses,' *IEEE Transactions on Antennas and Propagation*, vol. 54, no. 10, pp. 2776-2782, 2006.

[93]. D. Arnoud-Cormos, R. Loison and R. Gillard, 'Fast multistructure method of moments combined with a genetic algorithm (MSMoM/GA) for efficient optimization of printed antennas,' *IEEE Antennas and Wireless Propagation Letters*, vol. 6, pp.172-174, 2007.

[94]. P. Mukherjee and Bhaskar Gupta, 'Genetic algorithm based design optimization of aperture coupled rectangular microstrip antenna,'*Defence Science Journal*,vol. 55, No 4, Oct 2005, pp. 487-492, 2005.

[95]. N. Chattoraj and J. S. Roy, 'Application of genetic algorithm to the optimization of microstrip antennas with and without superstrate,' *Microwave Review*, vol.12, pp, 32-35, 2006.

[96]. N. Chattoraj and J. S. Roy, 'Application of genetic algorithm to the optimization of gain of magnetized ferrite microstrip antenna,' *Engineering Letters*, 14:2 , pp. 1-6, 2007.

[97]. R. Ghatak, D. R. Poddar and R. K. Mishra, 'Design of Sierpinski gasket fractal microstrip antenna using real coded genetic algorithm,' *IET Microwaves, Antennas and Propagation*, vol. 3, no. 7, pp. 1133-1140, 2009.

[98]. D. Zhou, R. A. Abd-Alhameed, C. H. See, M. S. Bin Melha, Z. B. Zainal Abdin, and P. Excell, 'New antenna designs for wideband harmonic suppression using adaptive surface meshing and genetic algorithms,' *IET Microw. Antennas Propag.*, vol. 5, no. 9, pp. 1054–1061, 2011.

[99]. I. Bhattacharyya, A. K. Bandypopadhyay, B. Gupta, A. Chattopadhyay, R. Chattopadhyay and K. Yasumoto, ' Vector GA - A novel enhancement of genetic algorithms for efficient multi-variable or multi-dimensional search,' *ACM Software Engineering Notes*, Vol.34, No. 6, pp.1-5, 2009.

[100]. X. H. Shi, Y. C. Liang, H. P. Lee, C. Lu, and L. M.Wang, 'An improved GA and a novel PSO-GA-based hybrid algorithm,' *Inf. Process. Lett.* , vol. 93, no. 5, pp. 2764–2775, 2005.

[101]. A. Narayan and M. Moore, 'Quantum inspired genetic algorithms,' *Proc. IEEE International Conference on Evolutionary Computation*, pp.61-66, 1996.

[102]. H. Ma and W. Wang, 'The application of improved quantum genetic algorithm to beam forming of adaptive array of smart antennas,' in *Proc. 2nd Int. Conf. Mechan. Autom. Control Eng. (MACE)*, 2011, pp. 1723–1727.

[103]. L. Cen, Z. Liang Yu, W. Ser, and W. Cen, 'Linear aperiodic array synthesis using an improved genetic algorithm,' *IEEE Trans. Antennas Propag.*, vol. 60, no. 2, pp. 895–902, 2012.

[104]. E. R. Schlosser, M.V.T. Heckler, R. Machado, and A. F. T. Salazar, 'Synthesis and implementation aspects of linear antenna arrays with shaped radiation pattern for mobile communications,' *IET Microwaves, Antennas and Propagation*, vol. 10, no. 4, pp. 442-452,2016.

[105]. J. Kennedy and R. Eberhart,'Particle Swarm Optimization,'*Proceedings of IEEE International Conference on Neural Networks*, vol. 4, pp. 1942-1948, Australia , 1995.

[106]. R. Poli, J. Kennedy and T. Blackwell, 'Particle swarm optimization: an overview,'*Swarm Intelligence*, vol. 1, no. 1, pp. 33-57, 2007.

[107]. J. Robinson and Y. Rahmat Samii, 'Particle swarm optimization in electromagnetics,' *IEEE Trans. Antennas Propag.*, vol. 52, no. 2, pp. 397–407, 2004.

[108]. S. Xu and Y. R. Samii, 'Boundary conditions in particle swarm optimization revisited,' *IEEE Trans. Antennas Propag.*, vol. 55, no. 3, pp. 760–765, 2007.

[109]. N. Jin and Y. Rahmat Samii, 'Particle swarm optimization for antenna designs in engineering electromagnetic,' *Journal of Artificial Evolution and Applications*, vol. 2008, pp. 1-10, 2008.

[110]. J. Robinson, S. Sinton, and Y. Rahmat Samii, 'Particle swarm optimization, genetic algorithm and their hybrids: Optimization of a profile corrugated horn antenna,' in *Proc. Antennas Propag. Soc. Int. Symp.*, 2002, vol. 1, pp. 314–317.

[111]. D. W. Boeringer and D. H. Werner, 'Particle swarm optimization versus genetic algorithms for phased array synthesis,' *IEEE Trans. Antennas Propag.*, vol. 52, no. 3, pp. 771–779, 2004.

[112]. N. Jin and Y. Rahmat Samii, 'Advances in particle swarm optimization for antenna designs: real number, binary, single-objective and multi-objective implementations,' *IEEE Trans. Antennas Propag.*, vol. 55, no. 3, pp. 556-567, 2007.

[113]. N. Pathak, G. K. Mahanti, S. K. Singh, J. K. Mishra and A. Chakraborty, 'Synthesis of thinned planar circular array antenna,' *Progress in Electromagnetics Research Letters*, vol. 12, pp. 87-97, 2009.

[114]. D. Cao, A. Modiri, G. Sureka, and K. Kiasaleh, 'DSP Implementation of the particle swarm and genetic algorithms for real time design of thinned array antennas,' *IEEE Antennas Wireless Propag. Lett.*, vol. 11, pp. 1170–1173, 2012.

[115]. W B Wang, Q Y Feng and D Liu, 'Synthesis of thinned linear and planar antenna arrays using Binary PSO algorithm,' *Progress in Electromagnetics Research*, vol. 127, pp. 371-387, 2012.

[116]. Z. G. Byraktor, P. L. Werner and D. H. Werner, 'The design of miniature three-element stochastic Yagi-Uda arrays in particle swarms optimization,' *IEEE Antennas and Wireless Propagation Letters*, vol. 5, pp. 22-26, 2006.

[117]. M. F. Pantoja, A. R. Bretones, F.G. Ruiz, S. G. Garcia and R. G. Martin, 'Particle swarm optimization in antenna design: Optimization of log periodic dipole arrays,' *IEEE Antennas and Propagation Magazine*, vol. 49, no. 4, pp. 34-47, 2007.

[118]. X. H. Shi, Y. C. Liang, H. P. Lee, C. Lu, and L. M.Wang, 'An improved GA and a novel PSO-GA-based hybrid algorithm,' *Inf. Process. Lett.* , vol. 93, no. 5, pp. 2764–2775, 2005.

[119]. N. Jin and Y. Rahmat Samii, 'Particle swarm optimization and finite difference time domain algorithm for multiband and wide band patch antenna designs,' *IEEE Trans. Antennas Propag.*, vol. 53, no. 11, pp. 3459–3468, 2005.

[120]. R. Azaro, L. Debiasi, E. Zani, M. Benedetti, P. Rocca, and A. Massa, 'A hybrid pre-fractal three-band antenna for multi-standard mobile wireless applications,' *IEEE Antennas Wireless Propag. Lett.*, vol. 8, pp. 905–908, 2009.

[121]. L. Lizzi, F.Viani, R.Azaro, and A.Massa, 'A PSO-driven spline-based shaping approach for ultrawideband (UWB) antenna synthesis,' *IEEE Trans. Antennas Propag.*, vol. 56, no. 8, pp. 2613–2621, 2011.

[122]. J. J. Liang, A. K. Qin, P. N. Suganthan, and S. Baskar, 'Comprehensive learning particle swarm optimizer for global optimization of multimodal functions,' *IEEE Trans. Evol. Comput.*, vol. 10, no. 3, pp. 281–295, 2006.

[123]. H. Wu, J. Geng, R. Jin, J. Qiu, W. Liu, J. Chen, and S. Liu, 'An improved comprehensive learning particle swarm optimization and its application to the semiautomatic design of antennas,' *IEEE Trans. Antennas Propag.*, vol. 57, no. 10, pp. 3018–3028, 2009.

[124]. S. M. Mikki and A. A. Kishk, 'Quantum particle swarm optimization for electromagnetics,' *IEEE Trans. Antennas Propag.*, vol. 54, no. 10, pp. 2764–2775, 2006.

[125]. S. Das, A. Abraham, and A. Konar, 'Particle swarm optimization and differential evolution algorithms: Technical analysis, application and hybridization perspectives,' *Studies in Comput. Intell. (SCI)*, vol. 116, pp. 1–38, 2008.

[126]. M. Afshinmanesh, A. Marandi, and M. Shahabadi, 'Design of a single-feed dual-band dual-polarized printed microstrip antenna using a Boolean particle swarm optimization,' *IEEE Trans. Antennas Propag.*, vol. 56, no. 7, pp. 1845–1852, 2008.

[127]. N. Jin and Y. Rahmat Samii, 'Hybrid real-binary particle swarm optimization (HPSO) in engineering electromagnetic,' *IEEE Transactions on Antennas and Propagation*, vol. 58, no. 12, pp. 3786-3794, 2010.

[128]. R. Bhattacharya, T. K. Bhattacharya, and R. Garg, 'Position mutated hierarchical particle swarm optimization and its application in synthesis of unequally spaced antenna arrays,' *IEEE Trans. Antennas Propag.*, vol. 60, no. 7, pp. 3174–3181, 2012.

[129]. R. Storn and K. Price, 'Differential evolution-a simple and efficient heuristic for global optimization over continuous spaces,' *J. Global Optim.*, vol. 11, pp. 341–359, 1997.

[130]. J. Vesterstrom and R. Thomsen, 'A comparative study of differential evolution, particle swarm optimization and evolutionary algorithms over numerical benchmark problems,' in *Proc. Congr. Evol. Comput.*, vol. 2, pp. 1980–1987, 2004.

[131]. R.Gamperle, S. D. Muller and A. Koumoutsakos, 'Parameter study for differential evolution,' in *Proc. WSEAS NNA-FSFS-EC 2002,*Interlaken, Switzerland, pp.293-298, 2002.

[132]. D. Karaboga and S.Okdem, 'A simple and global optimization algorithm for engineering problems: differential evolution algorithm,' *Turkish Journal of Electrical Engineering and Computer Sciences*, vol. 12, pp. 53-60, 2004.

[133]. A. Qing and C.K. Lee, *Differential Evolution in Electromagnetics*, Springer, pp. 1-235, 2010.

[134]. M. A. Panduro and C. A. Brizuela, 'A comparative analysis of the performance of GA, PSO and DE for circular antenna arrays,' in *Proc. Antennas Propag. Soc. Int. Symp.*, pp. 1–4, 2009.

[135]. J. Li and Y.Y. Kwi, 'Design of folded wire loaded antennas using bi-swarm differential evolution,' *Progress in Electromagnetics Research Letters*, vol. 24, pp. 91-98, 2011.

[136]. J. Guo and X. Li, 'Design of a wide beam wire antenna by differential evolution,' *International Conference on Mechatronic Sciences, Electric engineering and Computer*, Dec .20-22, 2013, China.

[137]. U.K. Chakraborty, *Advances in differential Eevolution*, Springer, Studies in computational Intelligence, vol. 143, pp. 1-334, 2008.

[138]. A. K. Qin and P.N. Suganthan, 'Self adaptive differential evolution algorithm for numerical optimization,' *IEEE Proceedings of the Congress of Evolutionary Computation*, vol. 2, pp. 1785-1791, 2005.

[139]. J. Brest, S. Greiner, B. Boskovic, M. Mernik and V. Zumer, 'Self adapting control parameters in differential evolution : A comparative study on numerical benchmark problems,' *IEEE Transactions on Evolutionary Computation*, vol. 10, no. 6, pp. 646-657, 2006.

[140]. Z Jingqiao and A C Sanderson, 'JADE: Adaptive differential evolution with optional external archive,' *IEEE Transactions on Evolutionary Computation*, vol. 13, no. 5, pp. 945-958, 2009.

[141]. S. Goudos, K. Siakavera, T. Samaras, E. Vafiadis and J. Sahalos, 'Self adaptive differential evolution applied to real valued antenna and microwave design problems,' *IEEE Transactions on Antennas and Propagation*, vol.59, no. 4, pp. 1286-1298, 2011.

[142]. S. Das, A. Abraham, U. K. Chakraborty, and A. Konar, 'Differential evolution with neighborhood based mutation operator,' *IEEE Trans. Evol. Comput.*, vol. 13, no. 3, pp. 526–553, 2009.

[143]. P. Ghosh and S. Das, 'Synthesis of thinned planar concentric circular antenna arrays-differential evolutionary approach,' *Progr. electromagn. Res. B*, vol. 29, pp. 63–82, 2011.

[144]. D. Simon, 'Biogeography-based optimization,' *IEEE Transactions on Evolutionary Computation*, vol. 12, no. 6, pp. 702-713, 2008.

[145]. A. Bhattacharya and P.K. Chattopadhyay, 'Hybrid differential evolution with biogeography-based optimization for solution of economic load dispatch,' *IEEE Transactions on Power systems*, vol. 25, no. 4, 2010.

[146]. U Singh and T S Kamal, 'Optimal synthesis of thinned arrays using biogeography based optimization,' *Progress in Electromagnetics Research M*, vol. 24, pp. 141-155, 2012.

[147]. L Zhang, Y C Jiao, Z B Weng and F S Zhang, ' Design of planar thinned arrays using a Boolean differential evolution algorithm,' *IET Microwaves , Antennas and Propagation*, vol. 4, no. 12, pp. 2172-2178,2010.

[148]. L. Zhang, Y. C. Jiao, B. Chen and F.S. Zhang, 'Synthesis of linear aperiodic arrays using a self adaptive hybrid differential evolution algorithm,' *IET Microwaves, Antennas and Propagation*, vol. 5, no. 12, pp. 1524-1528, 2010.

[149]. R.Li, L. Wu, X.-W.-Shi, N. Zhang Z.-Q Lv, 'Improved differential evolution strategy for antenna array pattern synthesis problems,' *Progress in Electromagnetics Research*, vol. 113, pp. 429-441, 2011.

[150]. P. Rocca, G. Oliveri, and A. Massa, 'Differential evolution as applied to electromagnetics,' *IEEE Antennas Propag. Mag.*, vol. 53, no. 1, pp. 38–49, 2011.

[151]. Y. Wang, Z.Cai and Q. Zhang, 'Differential evolution with composite trial vector generation strategies and control parameters,' *IEEE Transactions on Evolutionary Computation*, vol. 15, no. 1, pp. 55-66, 2011.

[152]. Sk. M. Islam, S. Das, S. Ghosh, S. Roy and P. N. Suganthan, 'An adaptive differential evolution algorithm with novel mutation and crossover strategies for global numerical optimization,' *IEEE Transactions on systems, man and cybernetics-part B cybernetics*, vol. 42, no. 2, 2012.

[153]. W. Yu and J. Zhang, 'Adaptive differential evolution with optimization state estimation,' *GECCO'12*, pp. 1285-1291, Philadelphia, USA, 2012.

[154]. L. Xie and Y. C. Jiao, 'Hybrid real-binary differential evolution algorithm applied to antenna optimization,' *Microwave and Optical Technology Letters*, vol. 54, no. 6, pp. 1460-1463, 2012.

[155]. D Li, F S Zhang and J H Ren, 'A compact tri-band antenna design using Boolean differential evolution algorithm,' *Progress in Electromagnetics Research C*, vol. 32, pp. 139-149, 2012.

[156]. F. Zhang, W. Zia, and M. Yao, 'Linear aperiodic array synthesis using differential evolution algorithm,' *IEEE Antennas and Wireless Propagation Letters*, vol. 13, pp. 797-800,2013.

[157]. M. Mahdavi, M. Fesanghary and E. Damangir, 'An improved harmonic search algorithm for solving optimization problems,' *Applied Math. Comput.*, Vol. 188, pp. 1576-1579, 2007.

[158]. X. Li, W. Li, X. Shi, J. Yang and J.Yu, 'Modified differential evolution algorithm for pattern synthesis of antenna arrays,' *Progress in Electromagnetics Research*, vol. 137 pp. 371-388,2013.

[159]. L. Tang, Y. Dong and J. Liu, 'Differential evolution with an individual dependent mechanism,' *IEEE Transactions on Evolutionary Computation*, vol. 19, no. 4, pp. 560-574, 2015.

[160]. R.A. Sarker, S. M. Elsayed and T. Ray, 'Differential evolution with dynamic parameters selection for optimization problems,' IEEE *Transactions on Evolutionary Computation*, vol. 18, no. 5, pp. 689-707, 2014.

[161]. M Yang, C Li, Z Cai and J Guan, 'Differential evolution with auto enhanced population diversity,' *IEEE Transactions on Cybernetics*, vol. 45, no. 2, pp. 302-315, 2015.

[162]. Y-F. Ge, W-J. Yu and J. Zhang, 'Diversity-based multi-population differential evolution for large scale evolution,' *Proceedings of the Annual Conference on Genetic and Evolutionary Computation*, pp. 31-32, Colorado, 2016.